AFFDL-TR-70-146

PARAFOIL WIND TUNNEL TESTS

JOHN D. NICOLAIDES

UNIVERSITY OF NOTRE DAME

TECHNICAL REPORT AFFDL-TR-70-146

JUNE 1971

AIR FORCE FLIGHT DYNAMICS LABORATORY
AIR FORCE SYSTEMS COMMAND
WRIGHT-PATTERSON AIR FORCE BASE, OHIO

UNCLASSIFIED

Security Classification

DOCUMENT CONTROL DATA - R & D

(Security classification of title, body of abstract and indexing annotation must be entered when the overall report is classified)

1 ORIGINATING ACTIVITY (Corporate author) University of Notre Dame Notre Dame, Indiana	2a. REPORT SECURITY CLASSIFICATION UNCLASSIFIED 2b GROUP N/A

3 REPORT TITLE

PARAFOIL WIND TUNNEL TESTS

4 DESCRIPTIVE NOTES (Type of report and inclusive dates)

Final Report

5 AUTHOR(S) (First name, middle initial, last name)

John D. Nicolaides

6 REPORT DATE June 1971	7a TOTAL NO OF PAGES 201	7b NO OF REFS 18
8a CONTRACT OR GRANT NO AF33615-67-C-1670 b PROJECT NO 6065 c 606501 d 606501007	9a ORIGINATOR'S REPORT NUMBER(S) AFFDL-TR-70-146 9b OTHER REPORT NO(S) (Any other numbers that may be assigned this report)	

10 DISTRIBUTION STATEMENT

This document is subject to special export controls and each transmittal to foreign governments or foreign nations may be made only with prior approval of the Air Force Flight Dynamics Laboratory/FER, Wright Patterson AFB, Ohio.

11 SUPPLEMENTARY NOTES N/A	12 SPONSORING MILITARY ACTIVITY Air Force Flight Dynamics Laboratory Wright-Patterson AFB, Ohio 45433

13 ABSTRACT

Extensive Parafoil wind tunnel tests have been carried out by the University of Notre Dame in its 2 ft x 2 ft tunnel and in the NASA Langley 30 ft x 60 ft tunnel. Parafoil model sizes ranged from .09 ft^2 to 147 ft^2 and Parafoil aspect ratios ranged from .5 to 3.0. The wind tunnel test velocities ranged from approximately 20 ft per second to over 60 ft per second. The aerodynamic stability coefficients, C_L, C_D, C_M, $C_{M_q} + C_{M_{\dot{\alpha}}}$, C_y, C_n, and C_l, were measured. The Parafoil remained self inflated and rigid over a range of angle of attack from -10^o to 80^o and revealed no stall characteristics. Maximum lift coefficients from 0.751 to 1.005 were measured for Parafoils of different aspect ratio. Maximum lift to drag ratios ranging from 1.83 to 6.40 were measured for the various Parafoil designs. The various wind tunnel tests confirm both the static and the dynamic stability of the Parafoil in pitch, yaw, and roll. The results of these investigations are consolidated in this report by summary plots and special presentations.

Details of illustrations in this document may be better studied on microfiche

DD FORM 1473

UNCLASSIFIED

Security Classification

NOTICES

When Government drawings, specifications, or other data are used for any purpose other than in connection with a definitely related Government procurement operation, the United States Government thereby incurs no responsibility nor any obligations whatsoever; and the fact that the Government may have formulated, furnished, or in any way supplied the said drawings, specifications, or other data, is not to be regarded by implication or otherwise as in any manner licensing the holder or any other person or corporation, or conveying any rights or permission to manufacture, use, or sell any patented invention that may in any way be related thereto.

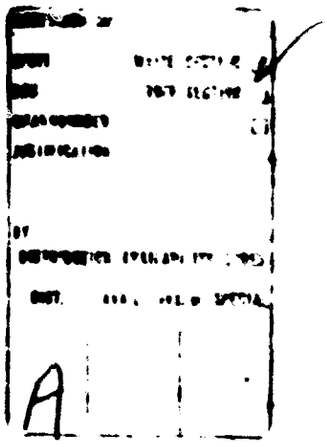

Copies of this report should not be returned unless return is required by security considerations, contractual obligations, or notice on a specific document.

*U.S. Government Printing Office: 1971 — 799-077/870

14 KEY WORDS	LINK A		LINK B		LINK C	
	ROLE	WT	ROLE	WT	ROLE	WT
Paraloft						
Para-Foil						
Steerable Parachute						
Flexible Wing						
Hi-Glide Canopy						
Parachute						
Guiding Parachute						
Maneuverable Parachute						
Parachute Wind Tunnel Tests						

PARAFOIL WIND TUNNEL TESTS

JOHN D. NICOLAIDES

FOREWORD

This report was prepared by the University of Notre Dame, Notre Dame, Indiana, under U.S. Air Force Contract AF33615-67-C-1670. This contract was initiated under Project 6065, "Performance and Design of Deployable Aerodynamic Decelerators", Task 606501, "Terminal Descent Deceleration Concepts". The work was administered under the direction of the Recovery and Crew Station Branch of the Air Force Flight Dynamics Laboratory at Wright-Patterson Air Force Base, Ohio. Mr. R. Walker and Mr. R. Speelman served as successive project engineers during the duration of the effort.

The author, of the University of Notre Dame Aerospace and Mechanical Engineering Department was J. D. Nicolaides, Professor. Contributing students of the University of Notre Dame Aerospace and Mechanical Engineering Department were James Greco, Barney Goren, Charles Lorenzen, Steve Cuspard, Michael Tragarz, Michael Higgins and Patrick Sullivan.

The University of Notre Dame wishes to acknowledge the contributions of Mr. James Hassell, Jr. of NASA (Langley) in conducting the wind tunnel program, and in particular would like to acknowledge the extraordinary contributions of Mr. Ralph Speelman.

The contractor's number for this report is F33615-67-C-1670.

The manuscript for this report was released by the author in February 1971 for publication as an AFFDL technical report.

Publication of this report does not constitute Air Force approval of the report's findings or conclusions. It is published only for the exchange and stimulation of ideas

GEORGE A. SOLT, JR.
Chief, Recovery and Crew Station Branch
Vehicle Equipment Division
AF Flight Dynamics Laboratory

ABSTRACT

The first wind tunnel tests on the Parafoil were carried out at the University of Notre Dame beginning in 1964. Numerous designs were studied. Certain of these Parafoil configurations were of interest to the U. S. Air Force Flight Dynamics Laboratory, who sponsored the University in carrying out additional wind tunnel tests both at Notre Dame and at NASA Langley. The results obtained from these special wind tunnel tests, and from some of the original Parafoil tests are presented in this summary report. All of the Parafoil wind tunnel models tested in this program had a rectangular planform with aspect ratios ranging from .5 to 3.0 and with areas ranging from .09 ft^2 to 147 ft^2. The wind tunnel test velocities ranged from approximately 20 ft per second to over 60 ft per second. The wind tunnel tests also included studies of (1) numerous variations in the basic Parafoil configurations, (2) various flap deflections, (3) completely non-rigid models, (4) rigid models, (5) semi-rigid models, and (6) various rigging configurations. The lift and drag coefficients, C_L and C_D, were measured. The aerodynamic moment coefficient, C_m, was determined by both static and dynamic testing techniques. Also, the aerodynamic side force coefficient, Cy, the yaw moment, C_n, and the roll moment coefficient, C_l, were measured. The aerodynamic pitch damping moment coefficients, $C_{mq} + C_{m\dot{\alpha}}$, were measured by a unique dynamic testing technique. The wind tunnel tests results showed that the Parafoil is able to remain self inflated and rigid over a large range of angles of attack from -10^o to 80^o (maximum angle tested in the wind tunnel). The tests revealed that the lift curve slope was approximately linear over a large range of angles of attack, depending on the aspect ratio. None of the non-rigid Parafoil designs had the usual abrupt stall characteristics of the classical rigid airfoil. Also, the Parafoils retained a high lift coefficient over a very large range of angles of attack. Maximum lift coefficients from 0.751 to 1.005 are measured (no flap deflection). Maximum lift to drag ratios ranging from 1.83 to 6.40 were measured for various Parafoil designs. The various wind tunnel tests confirm both the static and the dynamic stability of the Parafoil in pitch, yaw, and roll.

The results of these investigations are consolidated in this report by summary plots and special presentations.

CONTENTS

CONTENTS (continued)

CONTENTS (continued)

ILLUSTRATIONS

ILLUSTRATIONS (continued)

ILLUSTRATIONS (continued)

ILLUSTRATIONS (continued)

ILLUSTRATIONS (continued)

ILLUSTRATIONS (continued)

ILLUSTRATIONS (continued)

ILLUSTRATIONS (continued)

NOMENCLATURE

a	Resultant force moment arm about quarter-chord reference
AR	Aspect ratio, (=b/c)
b	Parafoil span
c	Parafoil Chord: The distance along the bottom surface from the upper leading edge (projected down) to the trailing edge (Figure 6)
C_A	Axial force coefficient, $\frac{\text{Axial Force}}{qS}$
C_D	Drag coefficient of wing based on planform area, $\frac{\text{Drag}}{qS}$
C_{D_w}	Drag coefficient of lines based on line area, $\frac{\text{Drag}}{qS_{\text{line}}}$
C_{D_S}	Drag coefficient of lines based on wing planform area, $\frac{\text{Drag}}{qS}$
C_L	Lift coefficient, $\frac{\text{Lift}}{qS}$
C_{L_α}	Lift-curve slope, $\partial C_L/\partial\alpha$ per degree
C_l	Rolling-moment coefficient, $\frac{\text{Rolling Moment}}{q\,S_{\text{side}}\,b}$
C_{l_β}	Lateral stability parameter, $\partial C_l/\partial\beta$ per degree
C_m	Pitching moment coefficient, $\frac{\text{Pitching Moment}}{qSc}$
C_{m_α}	Pitching stability parameter, $\partial C_m/\partial\alpha$ per degree
$C_{m_q}+C_{m_{\dot\alpha}}$	Aerodynamic pitch damping moment coefficients, $\frac{\text{Pitch Damping Moment} + \text{Lag Moment}}{qS\,c}$

C_N	Normal force coefficient, $\frac{\text{Normal Force}}{qS}$
C_n	Yawing-moment coefficient, $\frac{\text{Yawing Moment}}{qS_{side}\,b}$
$C_{n\beta}$	Directional stability parameter, $\partial C_n/\partial\beta$ per degree
C_R	Resultant force coefficient, $\frac{\text{Resultant Force}}{qS}$
C_y	Side force coefficient, $\frac{\text{Side Force}}{qS_{side}}$
D	Drag force
d	Distance parallel to Parafoil chord from lower leading edge to CPT
dia	Line diameter
FPS	Feet per second (fps)
ft	Feet
h	Vertical distance from platform to A-flare tip
I	Moment of inertia about Y axis (Pitch moment of inertia)
in	Inches
L	Lift force
$\underline{L}$	Length of A-suspension line from A-flare tip to attachment riser
l	Length from A-flare tip to extended platform line
L/D	Lift to drag ratio
M	Moment about pitch axis

mph	Miles per hour
n	Integer (number of ...)
q	Free-stream dynamic pressure
RN	Reynolds number
S, S_{wing}	Parafoil planform area, bc
S_{line}	Total line frontal area
t	Time (seconds)
V	Free-stream velocity
XYZ	Body axes (Figure I-1)
x	In longitudinal stability analysis: normal force moment arm about CPT
x	In tether line drag analysis: projected length along platform from CPT to A-suspension line
$\bar{x}$	Distance parallel to Parafoil chord from CPT to reference
x_{CP}	Distance parallel to Parafoil chord from reference to center of pressure
$\bar{z}$	Distance perpendicular to Parafoil chord, from CPT to Parafoil chord
α	Angle of attack of Parafoil chord line, lower surface of Parafoil, in degrees
α_s	Angle of attack determined by strut position
α_T	Trim angle of attack (Mean of the two extreme points of minimum amplitude)

α_v	Angle of attack determined by visual means
β	Angle of sideslip, in degrees
δ_f	Flap deflection parameter, positive when trailing edge is down
γ_l	Glide angle, arctan (C_D/C_L)
γ	Angle between Parafoil chord line and suspension bars
θ_R	Angle of rigging, arctan (d/z)
ξ	Length from Parafoil trailing edge to ring
f	Vertical distance from floor to strain gauge mount

SUBSCRIPTS

CPT	Confluence point
max	Maximum
NT	Nose taped
NNT	Nose not taped
REF	Reference point (also ref.)
sus	Suspension lines
cont	Control lines
guide	Guide lines
100	100 pound test line
375	375 pound test line
550	550 pound test line

MISCELLANEOUS

ND 1.67 (75)	Notre Dame Parafoil of aspect ratio 1.67 and with an area of 75 ft^2

INTRODUCTION

The Parafoil* is a true flying wing made entirely of nylon cloth and has absolutely no rigid members, Fig. 1. Like the aeroplane wing it has both an upper surface and a lower surface, and also an airfoil section. However the leading edge is open to permit self inflation due to ram air pressure. The Parafoil is composed of numerous airfoil shaped cells which give this cloth wing its unique rigid shape in flight. It is fabricated of a low porosity nylon cloth and can be packed and deployed in a manner similar to a conventional parachute. Flares or pennants are distributed along the bottom surface to which the various suspension lines are attached. These pennants serve three purposes: 1) they distribute the aerodynamic forces to the suspension lines, 2) they partially channel the flow into a two dimensional flow pattern which reduces tip losses and improves the aerodynamic efficiency and, 3) they provide side area which aids in obtaining directional flight stability.

The first wind tunnel tests on the Parafoil were carried out by Nicolaides[1,2] in the unique flow visualization wind tunnels at the University of Notre Dame beginning in December of 1964, Fig. 2-4. Numerous Parafoil designs were studied which had variations in aspect ratio, airfoil section, planform, leading edge opening, trailing edge opening, pennant size-form-location, rigging, dihedral, wash-in, wash-out, et al. The data from these various wind tunnel tests revealed that the Parafoil had the same excellent aerodynamic characteristics as the classical rigid wing of aviation. This important finding was documented.[16]

Wind tunnel tests on the Parafoil carried out under the direction or cognizance of the University of Notre Dame include**:

1) Wind Tunnel tests at Notre Dame***
2) Wind Tunnel tests at NASA (Langley) Series 1.****
3) Wind Tunnel tests at NASA (Langley) Series 2.***

The results of all of these wind tunnel tests will be presented in this report together with some of the results from the original wind tunnel program.

---

*The Parafoil is a design and development of Dr. John D. Nicolaides (patent pending), and is based on the multi-cell ram airfoil Patent No. 3285546 held by SRRC, Inc., Florida.

**Professor J. D. Nicolaides, Principal Investigator.

***Supported by the Flight Dynamics Laboratory, U.S. Air Force, Wright Field.

****Supported by NASA (Langley). Two Parafoils furnished by Notre Dame.

Primary emphasis was placed on detern ining the static aerodynamic force coefficients, C_L and C_D, for various Parafoil configurations. The static aerodynamic moment coefficients, C_m, C_n, and C_l were also measured. The static side force coefficient, C_y, was measured. Of particular importance was the measurement of the damping and lag moment coefficients, $C_{m_q} + C_{m_{\dot{\alpha}}}$, and the measurement of the static moment coefficient, C_{m_α}, from unique dynamic wind tunnel tests on a Parafoil model oscillating and damping in free pitching motion.

Numerous Parafoil configurations were tested which included variations in aspect ratio, airfoil thickness, airfoil shape, pennant design, leading edge opening, control surface deflections et al. Also, the tests were carried out for a wide range in Parafoil size, wind tunnel velocity, and rigging. The various data from these wind tunnel test programs will be presented. In order to assist the reader, special summary curves are presented which allow a definitization of Parafoil aerodynamics.

In the sections which follow the wind tunnel facilities and testing techniques will be reviewed, the various wind tunnel test results will bc presented, and the general findings will be summarized.

TESTING FACILITIES AND TECHNIQUES

Wind Tunnel Facilities

Notre Dame Wind Tunnel

The University of Notre Dame wind tunnel is a low speed, indraft, and open circuit tunnel which has the characteristics summarized in Table I. Also see Figures 3 and 4. A series of anti-turbulence screens reduces the turbulence level of the air. A smoke generator provides white smoke when flow visualization is desired. Wind tunnel models 1-4 (Table II) were tested in the Notre Dame tunnel.

NASA (Langley) Full Scale Wind Tunnel

All NASA tests (series one and two) were carried out in the Langley Full-Scale Wind Tunnel, Langley, Virginia. The Langley Full-Scale Wind Tunnel is a low speed, double return and open test section wind tunnel with the characteristics given in the Table I. The tunnel and test section is illustrated in Figure 5. Models 5-13 were tested in the Langley tunnel (Table II).

Description of Models

Notre Dame Models

Model 1 (Table II) is one of the numerous original nylon fabric Parafoil scale models tested in the Notre Dame wind tunnels in the spring of 1965. The airfoil shape and dimensions are given in Figure 6.[1,2]

Model 2, which was tested in the spring of 1966, is a rigid Parafoil model that was a replica of Parafoil number 125.* The dimensions of this model which was constructed in the Aero-Space Engineering Department of Notre Dame is given in Table II. Figure 7 gives the airfoil coordinates. The skin or covering of the model was 24 gauge aluminum sheet metal fastened to plexiglass ribs with an epoxy glue. The pennants were also made from 24 gauge aluminum sheet metal. In order to simulate the full-scale Parafoil a nylon cloth was laid over the aluminum upper surface.[6]

*Parafoil number 125 denotes a particular Parafoil known as "Notre Dame 2", which has an aspect ratio ($AR = \frac{b}{c}$) of 1.77 and a chord of 6 ft. 10 inches.

Table I

WIND TUNNELS

	Notre Dame	NASA (Langley)
V_{max} :	90 fps	120 mph
Turbulence Level :	0.01%	1.1%
Test Section Shape :	2x2 ft (sq.)	30x60 ft (elliptic)
Test Section Length :	6 ft.	55.8 ft.
Contraction Ratio :	25:1	4.93:1
Horsepower :	15	8000

TABLE II

MODEL DESCRIPTION AND DIMENSIONS

Model Number	Description	AR	Area	Chord	Maximum Thickness
1	ND fabric scale model (Nicolaides-Knapp)	0.83	93.6 in^2	10.4 in.	.127C
2	ND rigid scale model (Nathe)	1.77	63.6 in^2	6 in.	0.19C @ 0.25C
3	ND semi-rigid model (Kang 1967)	3.0	75 in^2	5 in.	0.179C @ 0.21C
		2.5	62.5		"
		2.0	50		"
		1.5	37.5		"
		1.0	25		"
		0.5	12.5		"
4	ND semi-rigid model (Kang 1968) (Walker)	3.0	75	5 in.	"
		2.5	62.5		"
		2.0	50		"
5	Fabric model	0.64	31.7 ft^2	7.04 ft	0.201C @ 0.25C
6	Langley Series One)	0.78	26.1	5.79	0.126C @ 0.25C
7		0.94	40.2	6.56	0.184C @ 0.25C
8	Fabric model	1.0	147 ft^2	12.12 ft	0.179C @ 0.20C
9	(Langley Series Two)	1.5	"	9.90	"
10	"	2.0	"	8.57	"
11	"	2.5	"	7.67	"
12	"	3.0	"	7.00	"
13	Fabric model	3.0	"	7.0	"
		2.5	123	7.0	"
	(Langley Series Two variable AR)	2.0	98	7.0	"
		1.5	73.5	7.0	"
		1.0	49	7.0	"

Models 3-4 are semi-rigid scale models constructed at the University of Notre Dame. The pennants and rib sections were made of galvanized iron (0.19 inches thick). The rib-only sections were made of aluminum shim stock of 0.01 inch thickness. The upper and lower surfaces were made of non-porous nylon cloth which was attached to the ribs with glue. Different aspect ratio models were formed by cutting off the end of the model at the rib-flare locations. Hence, these models can be referred to as the Notre Dame variable aspect ratio models. Model 3 yielded aspect ratios of 3.0, 2.5, 2.0, 1.5, 1.0, and 0.5 while model 4 resulted in aspect ratios 3.0, 2.5, and 2.0*. This latter aspect ratio of model 4 served as the test model for the dynamic test program.[6] A schematic assembly of models 3 and 4 is given in Figure 8, while Figure 9 contains the airfoil coordinates.[7,8]

NASA Langley Models**

Nine Parafoil models were tested, all employing a rectangular planform and a truncated airfoil shape with flat undersurface***. The airfoil section and dimensions of models 5-7 (series one) are given in Figures 10-12. The configuration and dimensions of models 8-13 (series two) are given in Figure 13. Model dimensions are given in Figures 14 - 16 for models 5-7; Figures 17-21 for models 8-13.

Structurally each model is composed of individual "air" cells sewn together. Each cell consists of a top cambered surface, a flat bottom surface, and airfoil section sides. Attached to the bottom surface are triangular shaped pennants to which the suspension lines are attached. The suspension lines are joined together at a confluence point located beneath the Parafoil. The position of the confluence point is determined from the desired trim angle and stability requirements for the Parafoil.

The confluence points of models 8-13 were determined to be 1.5 spans below the bottom surface and a distance forward determined by the testing mount arrangement.

Models 5-7 were made of approximately 2.0 oz. per square yard low porosity acrylic-coated, rip stop nylon. The suspension lines employed were of 375 pound test and 550 pound test braided nylon cord. The diameters of the lines were determined under tension to average approximately 0.125 inches (550 line) and 0.050 inches (375 line).

*Model 3 was tested in 1967; model 4 in 1968 under AFFDL contract.
**The NASA (Langley) Parafoil models were designed by Nicolaides and were constructed under the direction of the University of Notre Dame.
***Models 5-7 were tested in the Spring of 1966. Models 8-13 were tested in March of 1968.

Model 13 was initially an aspect ratio three design with the same dimensions as model 12, however, in the test program side panels were subsequently cut off from each end reducing the aspect ratio in increments of 0.5, also affecting a reduction in planform area. Hence in the remainder of this analysis this model will be referred to as the Langley variable aspect ratio model.

Model 5 was procurred from the Space Recovery and Research Center, Incorporated and models 6-7 were supplied by Nicolaides.[3] Models 8-13 were supplied by the University of Notre Dame under contract to the Air Force.* The Dutron Corporation of South Bend fabricated the models.

Testing Techniques

Notre Dame

The Notre Dame static test models were supported vertically on a force balance system, located atop the test section as shown in Figure 22. This system uses a strain gauge balance to measure the lift and drag forces. The determination of the force coefficients from the strain gauge system will be treated in the section on data reduction. The angle of attack was recorded from a calibrated degree dial attached to the support sting atop the test section.[1,6,7] In the early Notre Dame tests, a conventional rigid wing was tested, affecting a comparison between the Parafoil and the rigid airfoil. Since a Parafoil is made from nylon cloth and has pennants. attached to its bottom surface, it was desired to establish the effects of these factors on aerodynamic performance. The conventional wing model (rigid airfoil) and the rigid Parafoil model were therefore each tested in the following manner:[6]

(1) rigid model
(2) rigid model plus pennants (flares)
(3) rigid model plus nylon cloth
(4) rigid model plus pennants plus nylon cloth

The pitching moment stability coefficient, C_{m_α}, and the pitch damping moment stability coefficient, $C_{m_q} + C_{m_{\dot{\alpha}}}$, were measured by dynamic testing techniques in the Notre Dame tunnel.[8] The techniques used consisted of photographing a pointer which was mounted to the supporting strut outside the top of the wind tunnel section as shown in Figure 23. The pointer oscillated with the same angular motion experienced by the Parafoil. The data points were read directly in degrees from the calibrated disk (referred to hereafter as the angle indicator) mounted under the pointer.

*Air Force Flight Dynamics Laboratory, Wright-Patterson Air Force Base, Contract No. F33615-67-C-1670, P002-P003.

The Parafoil was suspended from the axis of rotation by two steel bars as shown in Figure 24. These bars serve to simulate, in a completely rigid manner, the suspension lines of a Parafoil system in free flight. The suspension bars also allow for selecting various trim angles as well as various positions of the model above the axis of rotation.

The supporting strut was a 3/8 inch diameter steel rod, twenty-seven inches long with a needle point (7/16 inches) mounted on one end and separable into two sections to allow ease of installation and model position changes. A pointer was attached to that portion of the supporting strut which protruded outside and above the wind tunnel section. Figure 23 shows the pointer and angle indicator, which when photographed as it oscillates, provides support strut rotation in degrees.

The mounting arrangement for the support strut consisted of a low friction jewel bearing* in which the needle point rotated and two roller bearings prevented translation of the strut. The mounting system which contained these bearings was permanently attached to the door section of the wind tunnel as shown in Figure 25. This allowed ease of assembly and disassembly prior to and following each test sequence.

The Parafoil model was mounted in a four square foot working section (Sec.#8) as shown in Figure 23. Notice that the model is mounted in what is commonly referred to as the yaw plane.** Because the Parafoil was mounted in this fashion a glass bottom working section was used and each trim position as well as the angle between the suspension bars and the Parafoil chordline were obtained from a photograph taken through the bottom of the section as shown in Figure 26. A graphflex, still picture camera with polaroid attachment was used to take pictures of the Parafoil trim positions. From each picture the trim angle, α_T, and suspension bar chordline angle, γ, were obtained as also shown in Figure 26.

A 16mm high speed motion picture camera was mounted as shown in Figure 23. This camera ran at a film speed of 128 frames per second and photographed the pointer and angle indicator. The angular motions of the Parafoil were then read directly from the developed 16mm high-speed film.

The procedure used in acquiring the desired data after the test apparatus was assembled consisted of arbitrarily selecting a Parafoil trim position.

*The use of jewel bearings in this investigation reduces the friction to a negligible quantity. Any bearing friction in the support equipment would effect the damping moment coefficients, $C_{m_q} + C_{m_{\dot{\alpha}}}$, but does not normally affect the frequency of oscillation and therefore does not affect the pitching moment coefficient, C_{m_α}.

**By mounting the model in this manner a gravity moment is not introduced when the trim angle of the model is changed.

This was achieved by fixing the angle between the suspension bars and the chordline after which the Parafoil assumed a trimmed condition (i.e. there were no moments about the pivot point). At this point a polaroid picture of the Parafoil was taken through the glass bottom of the test section. The Parafoil was then disturbed from its trim position by manually rotating the support strut (i.e. twisting by hand that portion of the strut which protruded through the top of the working section). Normally the Parafoil was displaced from its trim position approximately 8-10 degrees.

The support strut was then released at which time the high speed camera began photographing the pointer oscillations until they appeared to be completely damped. The time for the oscillations to damp varied from 8 to 15 seconds. Having completed these data acquisition requirements the entire procedure was repeated after selecting another trim angle which in effect simulated a different rigging of the Parafoil. Once a series of tests were completed for various trim angles, the Parafoil suspension system was disassembled and a change was made in the suspension bar length. This was accomplished by cutting the bars to a shorter length; thereby, simulating "different rigging" of the Parafoil by a method other than changing trim angle. With the shorter suspension bar the same procedure was used in obtaining the dynamics of the Parafoil at various trim positions. The Parafoil dynamics at three different suspension bar lengths were analyzed.

Following each test series and prior to shortening the suspension bars, the Moment of Inertia for that particular configuration was obtained.[8]

NASA Langley (Series One)

Four test set-ups[3] were used in this technique in obtaining the aerodynamic data of models 5-7 . The forces and moments acting on the Parafoils were measured by an externally mounted six-component strain gauge balance system. Reference 3 gives a detailed description of each technique incorporated.

Force tests were made over an angle of attack* range from as low as 0^{o} to as high as 70^{o} to determine the static longitudinal stability characteristics of the models. The static lateral stability characteristics were measured over an angle of sideslip range from -10^{o} to $+10^{o}$ and for angles of attack between 0^{o} and 70^{o}. Test wind tunnel velocities measured 20 to 40 feet per second.[3]

NASA Langley (Series Two)

The models were tested with two different mounting systems hereby referred to as (1) the Tether Testing Phase, and (2) the Strut Testing Phase. Figures 27 and 28 show photographs of the models as they appeared in each testing arrangement. The Tether Testing Phase yielded only the lift and drag coefficients of models tested, whereas the Strut Testing Phase provided the

*See Nomenclature.

primary means for data acquisition of all the force and moment coefficients ($C_L, C_D, C_m, C_y, C_n, C_l$).

Tether Test Phase. Figures 29a and 29b illustrate the test set-up. The models were tested with its effective confluence point constrained. Since all suspension lines did not join at one point, the confluence point was considered to be the point where all the "front" lines were joined (effective confluence point). A strain gauge balance was mounted at this constraint measuring the lift and drag forces. The strain gauge-constraint was attached to a vertical I-beam and varied according to the aspect ratio model tested. This enabled the Parafoil to fly at the centerline of the tunnel. Table II-1 in Appendix II depicts the mount position per aspect ratio.

All the A-flare* suspension lines were brough together to a connector link, as were B, C, and D-flare suspension lines each to a connector link (Figure 29b). The four connector lines were then attached to four adjustable (web) risers. The risers were attached to a metal bar with connector links, with the bar attached to the strain gauge balance system.

The Parafoil model to be tested was raised into position by pulling upward on two "guide" lines (375# cord) attached to the forward outboard flare on each side. Once the model was elevated, the tunnel was turned on and gradually brought to the desired test speed. The two "guide" lines remained attached to the Parafoil and secured above the tunnel exit, but allowed slack so as to affect no additional constraint on the model. Control was maintained by employing an individual to operate the two control lines near the strain gauge balance. When the model appeared to be steady, the controller relaxed the controls and a data point was recorded. Simultaneously the angle of attack was obtained from the side by two techniques: (1) photographing the near side chord line and (2) visual inspection of the near side chord line, incorporating a window-mounted protractor in a plane parallel to the Parafoil chord line.

The angle of attack was varied by adjusting the position of the bar relative to the strain gauge mount, and, when necessary, the Parafoil profile was maintained by adjusting the risers. Due to limitations in the mounting system and the available wind tunnel area, the angles of attack ranged from 0^{o} to 20^{o}.

Tests were performed at tunnel speeds of 30, 40, 50 and 60 feet per second for models 9-12; tunnel speeds of 30, 40 and 50 feet per second for model 8; and speeds of 30 and 40 feet per second for the variable aspect ratio (Model 13). Each variable aspect ratio model was tested with its open leading edge taped 33%** (Figure 17a) closed and with a lighter line (100# test) replacing 75% of the heavier suspension lines (Figures 17-21). The variable aspect ratio 1.0 model was also tested with its nose untaped (to afford a comparison to the taped condition) and with the standard distribution of heavier line (Figure 17).

*Flare A is the leading edge flare, successive letters indicate successive flares proceeding toward the trailing edge of the canopy.

** A 1" width tape was placed in the center of each cell running from the top surface to the lower surface. The normal cell opening height defined the 100% tape length. Therefore the 33% length represented a cell decreased by 1/3.

Flap deflection* tests were performed for the basic models (8-13) at a speed of 40 feet per second. Flap deflection conditions were defined as zero, one-third, two-third, and full. No precise measurements were made as to the exact angle of flap deflection. However, a zero flap condition corresponds to maintaining the Parafoil chord line straight, a full flap condition is indicative of a flap deflection of about 75° with the horizontal, one-third, about 25°, and two thirds about 50°.

The tests yielded lift and drag data versus angle of attack.

Strut Testing Phase. The Strut Testing set-up is given in Figures 28 and 30. The suspension lines were cut a distance approximately 33.9" from the flares to permit the Parafoil to fly essentially at the tunnel center-line. These lines were then attached to a metal grid framework. The grid was attached to a strut mounting system extending from the groundboard. Two strain gauge balances were positioned on the bottom surface of the Parafoil at the quarter-chord locations on each side, in addition to various gauges located beneath the groundboard which yielded all the force and moment coefficients. The groundboard was mounted on a turntable, which could be rotated for data acquisition as the model was yawed.

Unlike the tether testing phase, the model control lines were attached to the grid, and could be adjusted according to flap deflections desired. Tufts of wool were attached to the top cambered surface to assist visual analysis of the flow field (Figure 31).

The grid and mounting arrangement for each model was first "tested" with the Parafoil removed. By recording the force and moment effects due to the mounting apparatus, this effect was then removed from the wing-line data. As a data point was recorded the angle of attack was measured by two methods: (1) by photographing the main strut support (this support was attached perpendicular to the Parafoil chord line at the models mid-span); and (2) by visually observing the near-side Parafoil chord line. The angle of attack was varied mechanically by rotating the strut grid. Hence an angle of attack range from -10° to 80° was achieved.

Parafoil models 8, 10, and 12 (AR 1.0, 2.0, 3.0) were tested extensively at a tunnel speed of 40 feet per second yielding the longitudinal coefficients C_L, C_D, and C_m, and the lateral-directional coefficients: C_Y, C_n, and C_l. Longitudinal data only was recorded for model 9 (AR 1.5) at tunnel speeds of 30, 40, 50 and 60 feet per second. Model 11 (AR 2.5) was tested at 40 feet per second yielding longitudinal data. Models 8, 10, and 12 were tested at various flap deflection conditions defined as zero, one-half, and full. A zero flap condition corresponds to maintaining a straight Parafoil chord line, a full flap condition corresponds to a flap deflected about 75° with the horizontal and a half flap condition, about 37.5°.

*The rear 25% of the wing area is deflected by pulling in the control lines across the entire span.

Data Reduction

Notre Dame

Static Tests. The Notre Dame static model configurations yielded the lift and drag forces measured by the balance system. The signals from the strain gauge were channeled to potentiometers where the lift and drag forces were read independently of each other. This technique involved a calibration and balancing of circuits, and a conversion of milli-volt readings to pounds. The drag measured by the balance included the drag of the metal sting on which the model was mounted. This drag contribution was then subtracted from the total drag, yielding the aerodynamic force of the wing itself. The angle of attack was measured by means of a protractor dial and correlated with the lift and drag measurements.[6,7]

Dynamic Tests. The reduction of data obtained through dynamic tests was accomplished in the following manner. A polaroid picture representing one trim position of the Parafoil model was analyzed to determine (1) the angle of trim, α_T*, and (2) the angle, γ, as shown in Figure 26. This information was tabulated for that specific test run to later compare with the results of the dynamic analysis.

The 16mm high speed film documenting the oscillatory motion of the Parafoil was processed to a negative print from which the Parafoil motion in degrees was read directly. By using a stop-frame projector, the pointer position in each frame of the film was read in angular degrees to within an accuracy of .25 degrees. The change in the pitch angle, θ, with time was determined by utilizing the camera film speed (128 frames/sec).

The zero position of the angle indicator was aligned with the x-axis in the wind tunnel thereby permitting the direct determination of the angle of attack from the position of the pointer.

Now that the motion has been reduced to a set of angles at known increments of time this data was then fitted to the following equation:[9]

$$\alpha = Ke^{\lambda t} \cos(\omega t + \delta) + \alpha_T$$

Writing the above equation in symbolic form,

$$\alpha = f(\alpha_T, t, K, \lambda, \omega, \delta)$$

---

* $\alpha_T = K_3, \theta \quad \alpha_o$

This equation consists of two variables (angle of attack and time) and four undetermined constants which are

K - maximum amplitude
λ - damping rate
ω - angular frequency
δ - phase angle

By using the Method of Differential Corrections and obtaining the initial approximation for the four constants from the plotted data, the constants are determined.

The first approximations for the various constants were determined in the following manner from the plotted data (θ vs time).

(1) α_T was determined as the mean of the two extreme points of minimum amplitude.

(2) $\omega = \frac{(n-1)\pi}{t_n}$

where n is the number of extreme points and t_n is the time interval between the first and last of the extreme points.

(3) δ is determined as $\delta = \omega t_o$ where t_o is the time interval between the normalized time zero (middle point of sections of data being fitted) and the preceding positive maximum.

(4) K is determined as the distance from the α_T line to the intercept at normalized time zero of the envelope of positive maximum points.

(5) $\lambda = 0$

An example of the oscillatory motion of a typical test run is presented in Figure 32 with the first approximations shown.

The "WOBBLE PROGRAM",[9] was used to extract representative values for K, λ, ω and α_T as functions of time from the pitching motion of the Parafoil. Using these computed values along with the lateral moment of inertia, I, of the Parafoil and suspension system, the wind velocity, and the Parafoil characteristic length and area, the stability coefficients C_{m_α} and $C_{m_q} + C_{m_{\dot{\alpha}}}$ were determined as functions of time from the following equations.

$$C_{m_\alpha} = -2\omega^2 I / \rho V^2 Sc$$

$$C_{m_q} + C_{m_{\dot{\alpha}}} = {}^{8\lambda I}/_{\rho V S c^2}$$

By employing overlapping sectional fits in the data reduction technique, a means of investigating the non-linearities of the stability coefficients with angle of attack is provided.

NASA Langley (Series One)

The data obtained through this test program was taken from reference 3, and represents the forces and moments characteristics of the Parafoil systems. For comparison purposes the force data was referred to the basic Parafoil by removing the suspension line drag as explained in Appendix II.

NASA Langley (Series Two)

Langley presented the data obtained to the University of Notre Dame for analysis in tabular coefficient form representing the system as tested, uncorrected for unexposed suspension lines. Because the mounting technique resulted in a percentage of the suspension lines being unexposed to the airstream, (tether phase) or a percentage being cut off (strut phase), the entire drag force was not measured. Hence this data was corrected according to two different approaches dictated by the analysis desired.

The first approach considered the removal of the drag due to the suspension line lengths exposed to the airstream. Hence the corrected data resulted in the drag of the Parafoil alone and serves as an excellent method of comparing the aerodynamic characteristics of the Parafoils to one another. The procedure was to determine the length and number of suspension lines exposed to the airstream. Knowing the diameter of the lines (under tension), the projected frontal area was computed. Assuming a drag coefficient of 1.0 based on the line frontal area,[10] the drag coefficient based on wing area was determined. This line drag coefficient was then subtracted from the given test drag coefficient, and resulted in the drag coefficient of the Parafoil itself. For a more detailed treatment refer to Appendix II.

The second approach considered the addition of the drag due to the suspension line lengths not exposed to the air flow. The procedure is very much similar to the former case but results in the drag of the total system - Parafoil and suspension lines. For a more concise treatment of this approach refer to Appendix III.

Wind tunnel data from all of the test programs was punched onto IBM computer cards and programmed for various operations on the University of Notre Dame Univac digital computer, Model 1107. Thus, the results could then be plotted by the computer in any desired manner.

ANALYSIS OF RESULTS

Early Notre Dame Tests

The first wind tunnel tests were carried out on a completely fabric model of an original Parafoil kite modified for wind tunnel testing. The unit was placed in the wind tunnel with flow visualization made possible by the use of smoke streamlines. The flow field over the Parafoil was observed. Special attention was given to the location of the stagnation points, separation of the flow, three dimensional effects due to the flares, general rigidity, and stability characteristics. Figures 2 and 33 show some of these smoke flow pictures.

Following these flow visualization tests the first Parafoil wind tunnel model was constructed and tested. This wind tunnel model is described in the section on the model description (Model 1). Summary curves of the aerodynamic data for the flexible unit is given in Figures 34 and 35 as the AR 0.83 traces.

Extensive wind tunnel tests were also carried out on all rigid models of the Parafoil.[6] Results for the all rigid model wind tunnel tests were compared with data obtained on a rigid airfoil model (no openings in the leading edge). Wind tunnel tests were also carried out where fabric cloth was placed over the rigid model and also used as flares. Summary curves for this rigid Parafoil model (Model 2) are given in Figures 34 and 35 as the AR 1.77 traces.

A summary of the effects of the rigid airfoil and its model variations is presented inFigure 36*. A summary of the effects of the rigid Parafoil and its model variation is presented in Figure 37.*-** In addition, Figure 37 also shows the C_L curve of the Parafoil plus flares plus nylon cloth corrected to a RN of 3,000,000, corresponding to a velocity of 70 ft/sec. on a Parafoil having a chord length of 6'10".

Comparing the effects of the flares alone on the rigid airfoil and the rigid Parafoil shows that on both models they increased the slope of the lift curve, decreased $C_{L_{max}}$, and increased the drag slightly.

*Figures 36 and 37 show C_L data appearing like a stall. This reduction in lift is not a true stall phenomenon but is rather characteristic of testing a small model (c=5") in a low speed wind tunnel. In this case a laminar separation occurs which may be extrapolated to higher R_N by using the standard methods[4].

**Due to mounting, the data from the rigid Parafoil had to be shifted 2^o to the left.

The effect of the nylon cloth alone on the rigid airfoil and the rigid Parafoil was to increase the slope of the lift curve, and increase the drag.

The effect of the flares and the nylon cloth together was to increase the slope of the lift curve, and, increase the drag.

A comparison of the Parafoil Airfoil section and the conventional airfoil section showed that the Parafoil airfoil section decreased the slope of the lift curve, and increased the drag.

The rigid airfoil model variations produced an L/D range of 4.43 to 5.15. The rigid Parafoil model variations produced an L/D range of 3.90 to 5.0 .

There is a small reduction in the aerodynamic performance (L/D ratio) of the rigid Parafoil as compared to the rigid airfoil as evidenced by the increase in drag on the rigid Parafoil, and the decreased slope of the lift curve.

Data obtained from free flight tests carried out at the University confirmed Parafoil performance estimates based on the early wind tunnel data and also demonstrated lift to drag ratios in excess of four.[2,17,18]

The success of these early tests suggested that more extensive wind tunnel tests should be carried out on selected Parafoil designs.

Early NASA Tests

On the recommendation of Nicolaides, NASA obtained an original Parafoil kite[3] (Model 5) from Space Recovery Research Center, Inc., and undertook wind tunnel tests in the Langley 30 x 60 full scale wind tunnel in 1965. Some difficulty was experienced in rigging these models. The University was pleased to assist NASA in the rigging, and also loaned two of its Parafoil designs[3] (Models 6 and 7) for testing. The result of the NASA tests[3] are given in Ref. 3 and are also summarized in Figures 38 through 41. (Line drag removed)

Good agreement was obtained between the early Notre Dame wind tunnel tests[1] and the early NASA tests[3] on lift coefficient, drag coefficient and lift to drag ratio when line drag was removed from the Langley data, Fig. 69 and 82. In addition the Langley tests revealed that the Parafoil was statically stable over the entire range of test angles of attack from 0^{o} to 70^{o}.

Notre Dame Wind Tunnel Tests

Notre Dame/Air Force Wind Tunnel Tests

Static. The early wind tunnel tests and flight tests of the Parafoil led to a systematic wind tunnel test program of various Parafoil designs, ranging in aspect ratio from .5 to 3. This program was carried out for the U. S. Air Force Flight Dynamics Laboratory at the University of Notre Dame.

Wind tunnel models 3 and 4 were constructed of aluminum ribs and flares and the top and bottom surface of the model was composed of nylon cloth.* No rigging lines were used. The wind tunnel data from these tests is provided in Ref. 7.

Figure 42 provides a summary of the lift and drag coefficient data obtained on the variable aspect ratio Parafoil model 3. The data demonstrates the normal improvement in lift curve slope resulting from increasing aspect ratio. A summary of lift to drag ratios obtained from the various models is given in Figure 43. Again the improvement of lift to drag ratio with increasing aspect ratio is observed. Repeat tests are given in Figures 44 and 45 on Wind Tunnel Model 4. Summary curves on flap deflection are given in Figure 46.

Dynamic. Dynamic wind tunnel tests were carried out as described in an earlier section. The data from these tests are given in Ref. 8.

*Model 3 tested in 1967; model 4 tested in 1968.

A summary of results for the static pitching moment stability coefficient, C_{m_α}, is given in Figure 47 as a function of different trim angles of attack and for 3 locations of the confluence point below the Parafoil. A summary of the pitch damping moment stability coefficient ($C_{m_q} + C_{m_{\dot{\alpha}}}$) is given in Figure 48 for various trim angles of attack and for 3 locations of the confluence point.

The static and dynamic stability of the Parafoil is demonstrated by these unique wind tunnel tests.

NASA Langley Tests

During the period from 1964 through 1967 extensive flight tests of the Parafoil were carried out in order to obtain performance data to supplement the aerodynamic data from the wind tunnel testing program.[1,17] The results from both the wind tunnel tests and the full scale free flight tests led to a program of full scale Parafoil wind tunnel tests in the 30' x 60' NASA (Langley) full scale wind tunnel. This program was carried out by Notre Dame under the direction of the Air Force Flight Dynamics Laboratory commencing in the spring of 1968. The all fabric wind tunnel models 8 through 13 were designed by Nicolaides and were constructed under University supervision by the Dutron Corporation.

All of this data was transferred to IBM cards which were used in various computer programs. The various computer programs permitted the preparation of numerous plots. In this way data of different test conditions could be compared. Also, the various aerodynamic coefficients could be computed both with and without rigging line drag for comparison with previous wind tunnel tests. In addition special summary curves were prepared. For example, a summary plot of the wind tunnel data obtained on the aspect ratio 1 Parafoil at wind tunnel speeds of 30, 40 and 50 per second is given in Figure 49. Similar summary curves for the other aspect ratio models are given in Figures 50-53. Summary curves showing the effect of aspect ratio on lift coefficient and on lift to drag ratio are given in Figure 54 at a wind tunnel speed of 40 ft per second. An examination of this data suggests that some effects of speed or wing loading are indicated. Summary data for the various flap deflection effects is given in Figure 55 where it is noted that increases in the lift coefficient are obtained with increasing flap deflection as expected for basic wing theory. Figures 49-55 are prepared with line drag removed.

In order to improve Parafoil performance the leading edge opening was*

*Wind tunnel and flight tests at Notre Dame revealed better flight performance due to improved nose flow as observed in smoke photographs.

decreased by using 1" tape. The data resulting from this change in configuration is given in figures 56 through 59 for the aspect ratio 1 and the aspect ratio 3 models.

The strut tests enable determination of a restoring moment. A summary of the moment data is given in figure 62 and 109. The static pitching moment about the confluence point is plotted in figure 63 for confluence points located 1.5 span lengths below the Parafoil. Appendix I presents the method of performing this transformation of moments. See summary curves 60-61.

A summary of lift curve slope vs aspect ratio is provided in figure 64. The static yaw moment coefficient for aspect ratio 1,2,3 models is given in figure 65 which shows good stability. The static roll moment coefficient for side slip is given in figure 66 for 3 aspect ratio Parafoils. Again stabilizing moments are observed.

Qualitative

In addition to the aerodynamic force and moment coefficient data presented in the preceding paragraphs, numerous valuable visual observations were made. Of particular interest was the rigidity and self-inflation of the Parafoil over a large range of angles of attack. In the tether tests the Parafoil remained fully rigid and inflated over the entire range of test angles of attack, from -5^{o} to 70^{o}.

Any particular Parafoil is designed and rigged for a specific flight trim angle of attack. This design trim angle is generally near $+5^{o}$. When forced out of that trim angle by deflecting tether (Tether Tests) or by rotating strut (Strut Tests), the pennants and their lines will become slack and will flap, thereby causing unnecessary drag. The observations revealed that as the angle of attack is decreased below the design trim, the D lines first flap and then the C, and B.

At the large angles of attack the D lines first and then the C lines again flap. In a special test the D lines were disconnected and their pennants taped up. It was found that the Parafoil flew quite well with no flight stability or rigidity problems.

In the series of tests where the aspect ratio three Parafoil was cut off at the tips to yield lower aspect ratio units, the outside rib sections had their rib air passage vents exposed to the airflow, thus reducing the fabric internal pressure constraint. It was found that no change in inflation or stability resulted, and that the reduced AR sizes were as stable as the models with the complete non-porous outboard rib sections.

An investigation of the flow characteristics around the Parafoil was

made by taping wool tufts six inches in length on the upper surface of the Parafoil models at varied locations on the upper surface (Figure 31a). At low angles of attack the flow was clearly attached to the upper surface from leading edge of trailing edge. The flow remained attached until about $\alpha = 7.5^{0}$ (Fig. 31b). Between $\alpha = 7.5^{0}$ and $\alpha = 15^{0}$ the flow field changed significantly and is definitely unattached on the latter half of the upper surface.

Comparison of Tether and Strut Data Considerable differences are evident in comparing the L/D data obtained from the tethered tests (Fig. 54) with the data obtained from the strut tests (Fig. 61). In order to understand these and other differences in the Langley tests it is helpful to review some of the visual observations which were made during the runs.

Tether . During the tether tests the Parafoil models did not fly absolutely steady due to the gustiness of the tunnel flow, and the mount location in the rear of the tunnel. The tether mount system was located downstream in the test section where greater flow disturbances were prevalent. It was necessary, therefore to hand control the Parafoils with control lines attached to the rear. This controllability effect gave rise to residual motions resulting from the necessity to control the model so as to obtain a steady condition for the recording of a data point. Because of the multiplicity of data points recorded at a given angle of attack, all points at the same angle of attack were averaged to yield one representative data point per α. The angle of attack of the Parafoil was assumed to be the same as the right wing tip which was measured from side view photographs. The angle was noted to vary by as much as $\pm 3^{0}$ at a given test condition. In addition, the models were not trimmed to optimum performance conditions at each angle of attack. Hence, it is believed that all of these factors account for the scatter and inconsistencies apparent in the tether results.

The tether technique was employed to check general Parafoil rigidity and performance (e.g. flight stability, trim, trim change, yaw and roll control, etc...). It should not, however, be used in a quantitative manner but rather as confirmation of general Parafoil aerodynamics.

The tether tests, through visual observations and movies, clearly confirmed controllability in yaw, roll, and pitch. The static and dynamic stability of the Parafoils was observed for numerous pitch trim positions and for numerous yaw and roll trim positions.

Strut. In the strut tests the angle of attack of the Parafoil was measured by two means: (1) by photographing the right wing tip (α_V), and (2) by photographing the main bar support (which was positioned so as to always be perpendicular to the mid-span chord line), (α_S). For angles of attack between 11^O and 20^O, α_S and α_V are in good agreement. Figures 67-68 illustrate the shifting of the lift curve and the lift to drag curve as a result of the angle of attack measurement technique. However, for angles of attack less than 11^O, $\alpha_V > \alpha_S$, and for angles of attack greater than 20^O, $\alpha_V < \alpha_S$. The method of strut support utilized rigid tie bars which were attached to the Parafoil at its mid-area. Because of this rigid attachment the Parafoil was not completely free to move to the proper trim angle when the strut angle of attack was changed. As a result the Parafoil was physically distorted and thus its angle of attack distribution was distorted. It was observed that when the model was pitched at a negative angle of attack, the angle of attack of the outboard wing tips was greater than the angle of attack of the mid-span. When the model was pitched to a high angle of attack, the angle of attack of the outboard wing tips was less than that of the mid span. Although this phenomenon might be attributed to the flow field around a non-rigid body such as the Parafoil, it was observed from test film that this was a characteristic resulting from the strut mount arrangement. As previously discussed a given Parafoil is designed for a particular trim angle of attack. That is to say the pennant design and the rigging lines are related to a certain confluence point which is determined by the design trim angle of attack. Once the Parafoil is constructed there is nothing which can be done to change this optimum design. The use of a rigging platform, as employed in the strut tests, simply simulates the design confluence point and thus permits the Parafoil to fit in the available wind tunnel test section area. Any movement of the Parafoil to an angle of attack other than the design trim angle results in an off design condition and results in a forced distortion of the Parafoil from its desired flight position. This distortion was readily obeerved during the tests and could be seen in the test film. Therefore the strut data is highly suspect at the low angles of attack ($\alpha < 5^O$) tested. All strut data unless otherwise specified was plotted versus α_V and each data point represents a recorded data point, that is, no averaging technique was incorporated for values at the same angle of attack.

WIND TUNNEL TEST SUMMARY

Summary curves of wind tunnel data as obtained from the various tests conducted at both the University of Notre Dame, and at NASA have been presented. However, the data from these various programs are not in complete agreement. As a result, general summary curves representing aerodynamic performance of the Parafoil are now given.

Lift Summary

Figures 69 and 70 give a complete summary of all the lift coefficient data. Figures 71 through 81 present the supporting data for the summary curves, and the representative lines used.

Lift to Drag Ratio Summary*

A general summary of the lift to drag ratio data without line drag is given in Figure 82. The supporting data for determining the representative curve data is given in Figures 83 through 93. Figures 107 and 108 present a general summary of this data with line drag effects included.

Drag Summary*

The general summary of wing alone drag data is given in Figure 94, and the supporting curves are given in Figures 95 through 105. Figure 106 presents a general summary of this data including line drag effects.

Moment Summary

The static moment of the wing alone over the full range of angles of attack is shown in Figure 109. Supporting curves are given in Figures 110-114. The same data transferred to a confluence point 1.5 spans** below the Parafoil is illustrated in Figure 63. Supporting curves are given in Figures 115-119.

---

*Parafoil models used in the tests conducted at Notre Dame contained proturbences which produce a drag component not taken into consideration in these lift to drag or drag data presentations. Appendix IV includes an analysis of the effects of correcting the data to reflect removal of this additional drag.

**Flight Parafoils now utilize a 1.0 span confluence point. Also the lines are of reduced number and diameter. Accordingly, all Parafoils of any aspect ratio are able to achieve static stability over their entire range of angles of attack.

PARAFOIL FLIGHT SYSTEMS

Incorporation of the Parafoil into a flight system requires consideration of line and payload drag created by the configuration of the intended system. Appendix V illustrates incorporation of line drag data for a personnel size Parafoil.

CONCLUDING REMARKS

A summary of Parafoil wind tunnel data has been presented. Data from the various wind tunnel testing programs ha been reduced to a common basis and numerous comparison plots have been prepared which illustrate the effects of aspect ratio, velocity, trim angle, control deflection and configuration.

The aerodynamic data confirms that the Parafoil is similar to the airplane wing. The Parafoil has positive lift at zero angle of attack. Figures show lift down to about -5^{o}. The lift curve is quite linear with angle of attack. Increasing the aspect ratio increases the lift curve slope and improves the lift to drag ratio. The Parafoil has static and dynamic stability in all modes of flight, pitch, yaw, and roll.

The Parafoil, because of its configuration and flexibility, does not exhibit the stall characteristics of the aeroplane wing at large angles of attack. Instead the lift falls off gently and thus the Parafoil may also be safely flown at very large angles of attack ($70^{o}+$).

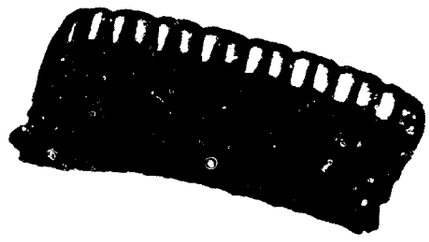

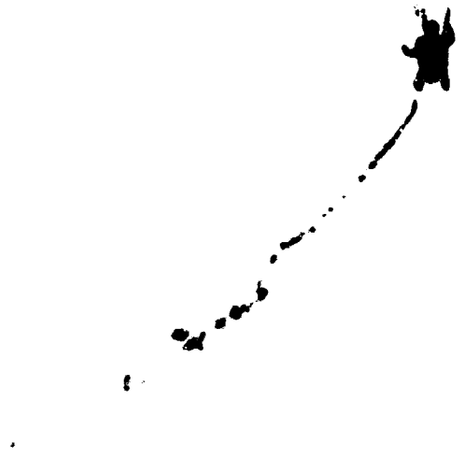

Figure 1a. Parafoil in Gliding Flight.

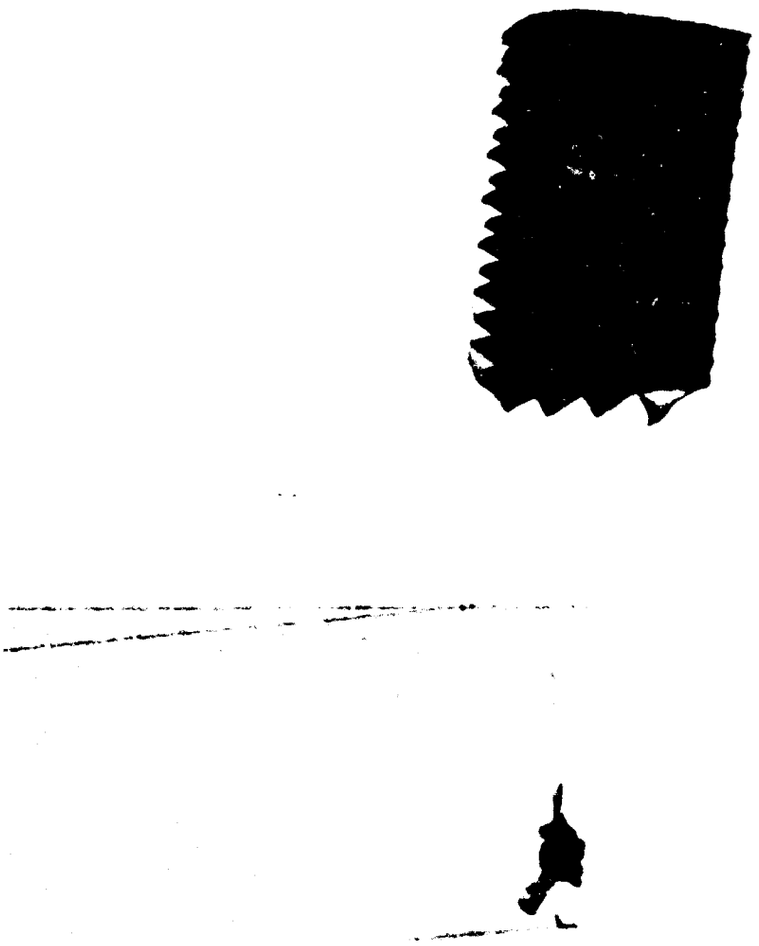

Figure 1b. Parafoil in Gliding Flight.

Figure 2. Smoke Visualization in Notre Dame Wind Tunnel

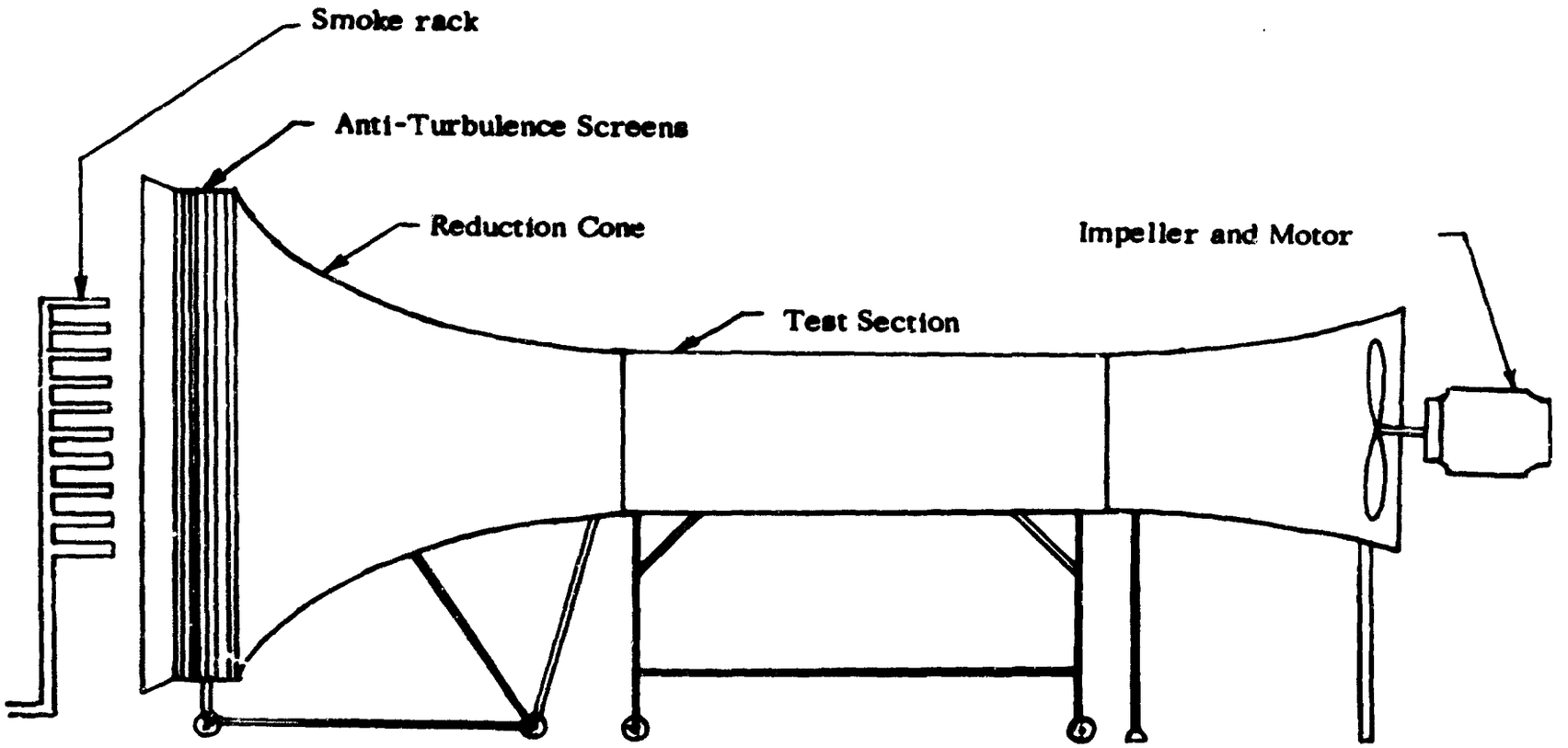

Figure 3. Schematic of Notre Dame Wind Tunnel

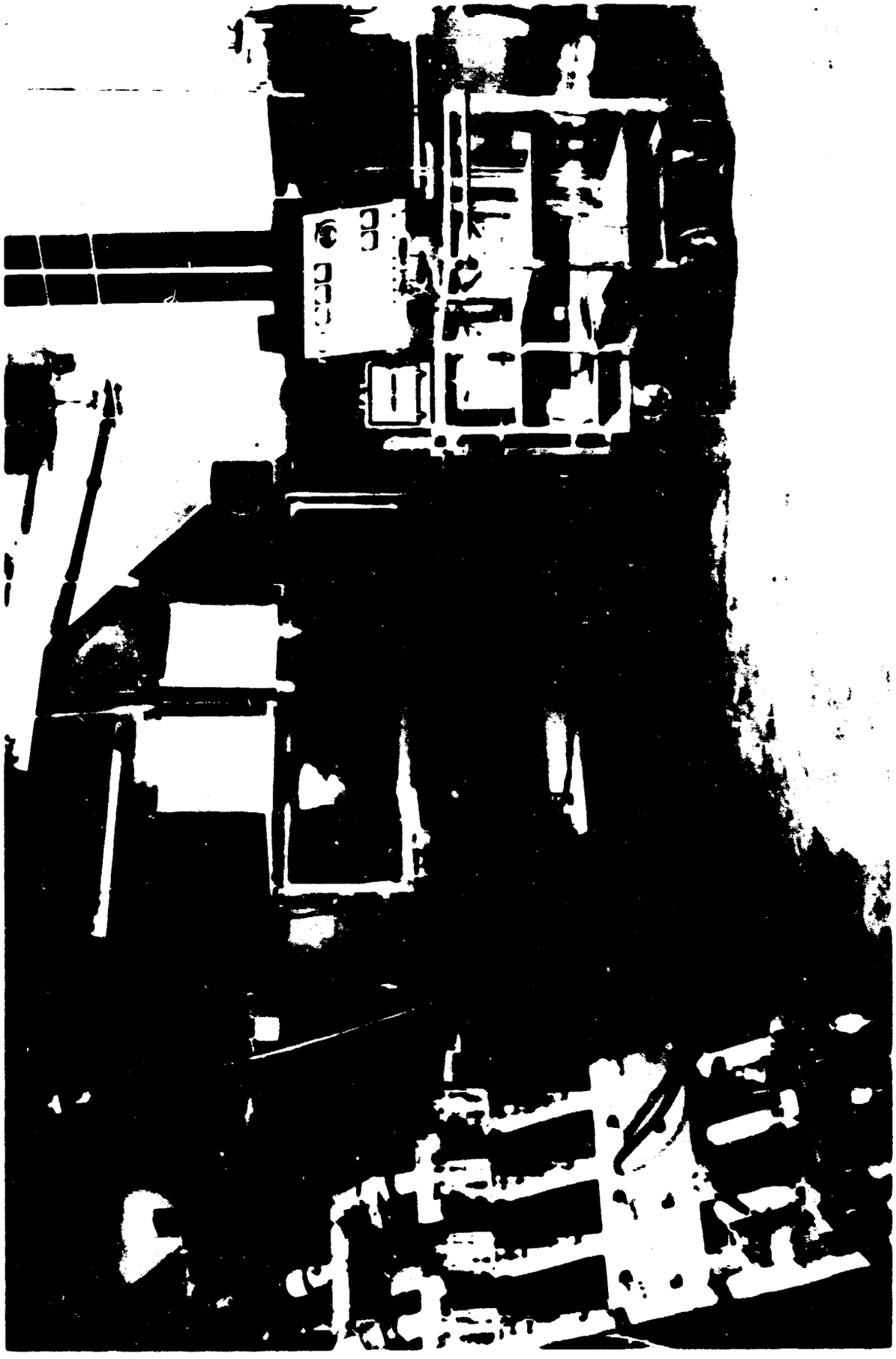

Figure 4. Notre Dame Wind Tunnel

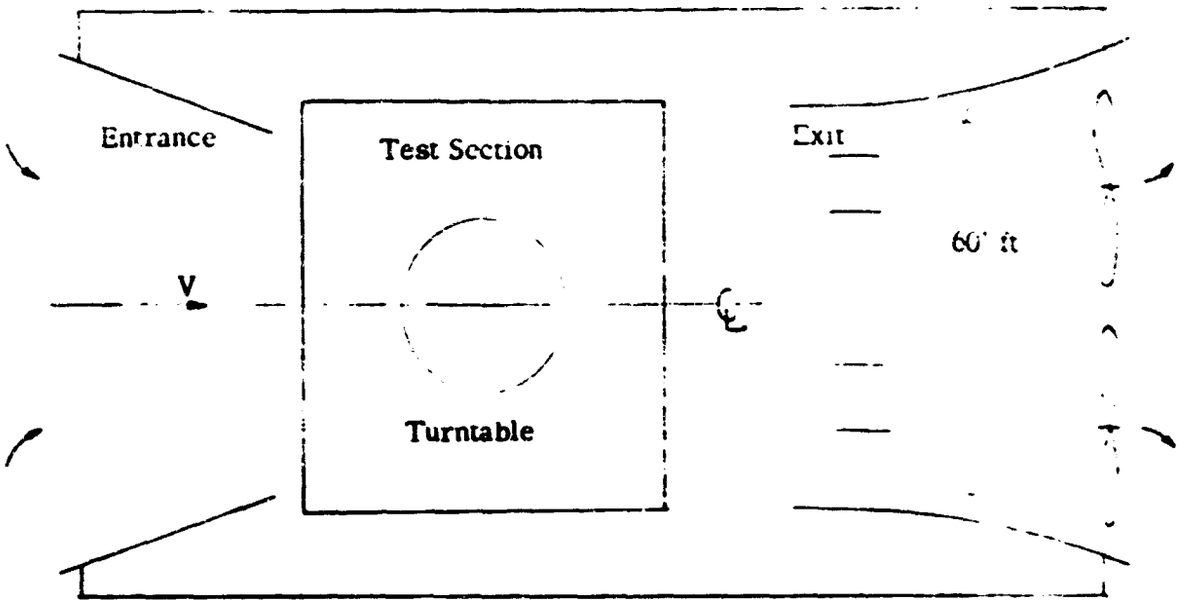

(a) Top Profile

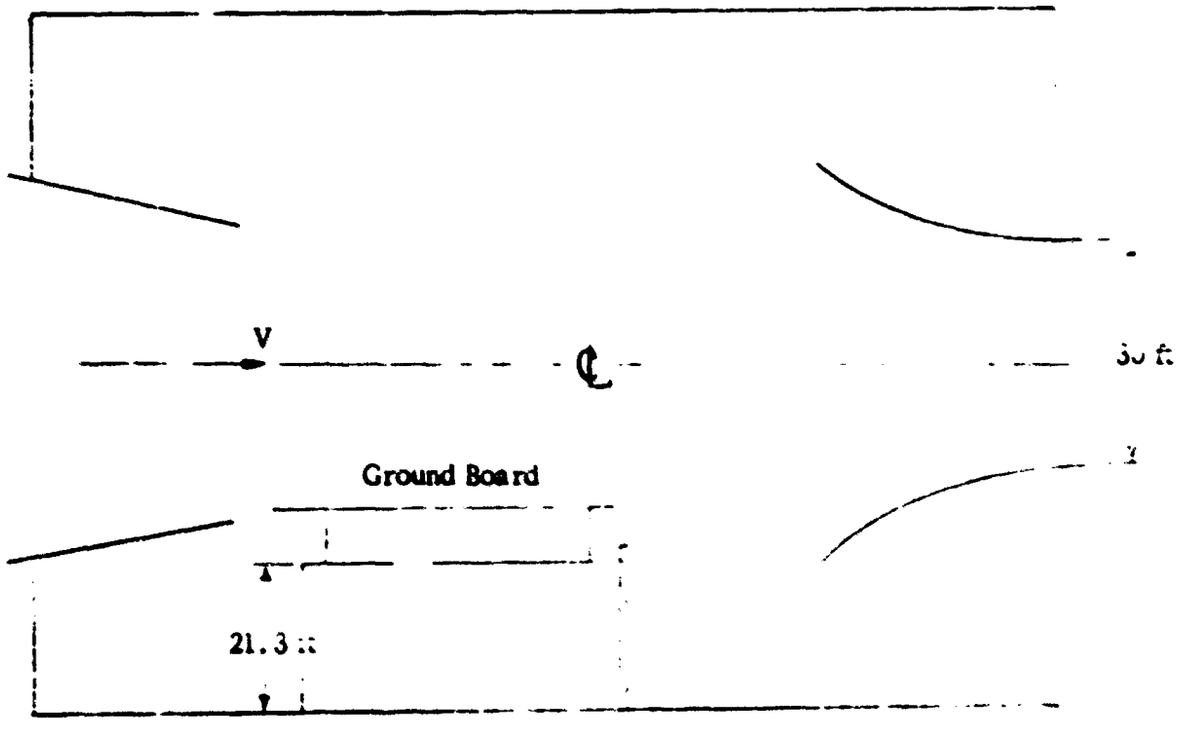

(b) Side Profile

Figure 5. Langley Full-Scale Tunnel

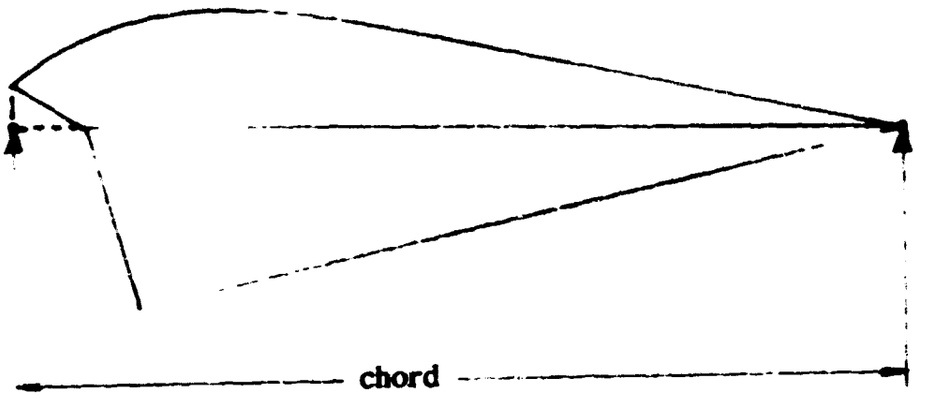

AIRFOIL	
Station	Ordinate
0.0000	0.0481
.0481	.0769
.0769	.0962
.0962	.1106
.1442	.1202
.1731	.1250
.1923	.1269
.2404	.1202
.2885	.1144
.3365	.1077
.3846	.1010
.4327	.0981
.4808	.0962
.5288	.0913
.5769	.0865
.6250	.0750
.0731	.0673
1.0000	.0000

Figure 6. Parafoil Model 1 Airfoil Section and Dimensions (in fraction of chord).

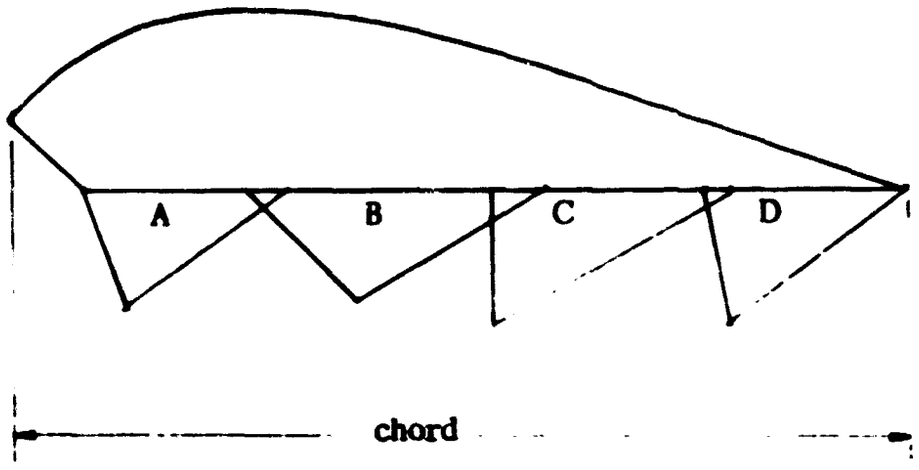

AIRFOIL	
Station	Ordinate
.0000	.0677
.0322	.1048
.0645	.1322
.0806	.1455
.1290	.1661
.1612	.1774
.2258	.1887
.2580	.1919
.2903	.1887
.3225	.1854
.4032	.1774
.4838	.1629
.5645	.1435
.6451	.1209
.7258	.0983
.8064	.0725
.8870	.0435
1.0000	.0000

Figure 7. Parafoil Model 2 Airfoil Section and Dimensions (in fraction of chord)

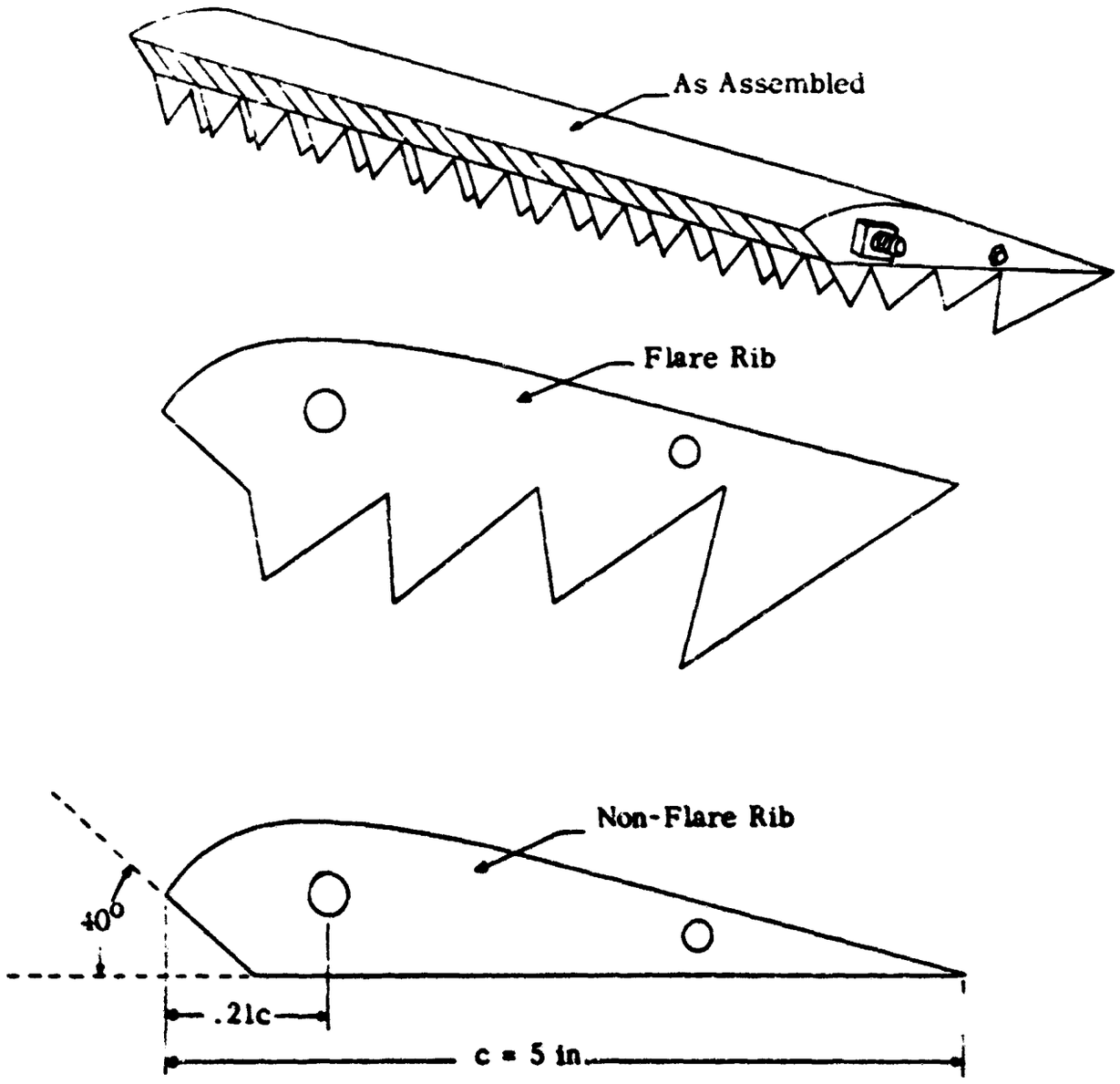

Figure 8. Para-Foil Model Assembly (Models 3 and 4)

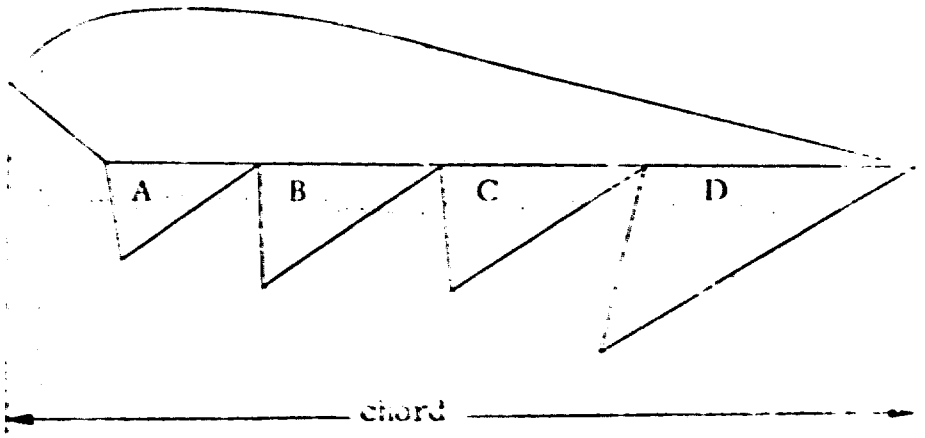

AIRFOIL	
Station	Ordinates
0.	0.0886
.0200	.1206
.0400	.1392
.0600	.1518
.0800	.1616
.1000	.1688
.1056	.0000
.1200	.1730
.1400	.1756
.1600	.1780
.1800	.1784
.2000	.1790
.2200	.1790
.2400	.1768
.2600	.1752
.2800	.1730
.3000	.1705
.3200	.1676
.3400	.1646
.3600	.1606
.3800	.1562
.4000	.1524
.4200	.1476
.4400	.1426
1.0000	0.0000

Figure 9. Parafoil Models 3 and 4 Airfoil Section and Dimensions (in fraction of chord)

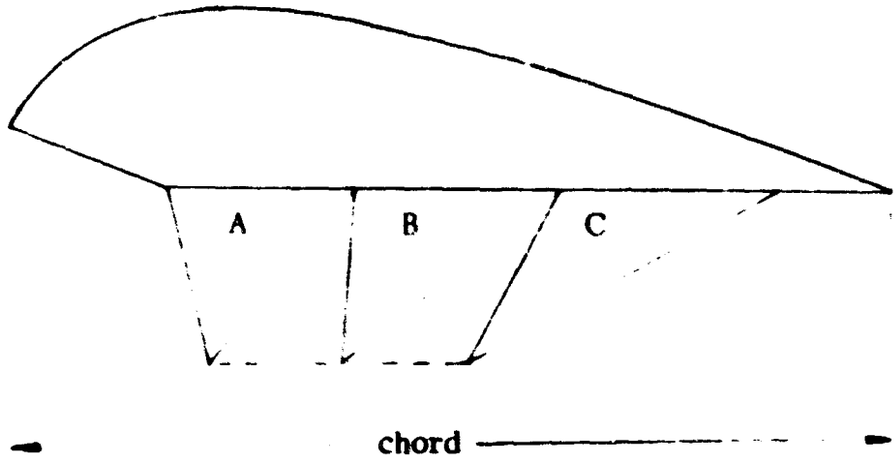

AIRFOIL	
Station	Ordinate
0.0000	0.0606
.0125	.0888
.0250	.1095
.0500	.1331
.0750	.1539
.1000	.1642
.1500	.1805
.2000	.1953
.2500	.2012
.3000	.1953
.4000	.1805
.5000	.1539
.6000	.1317
.7000	.1065
.8000	.0740
.9000	.0385
1.0000	.0000

Figure 10. Parafoil Model 5 airfoil Section and Dimensions (in fraction of chord)

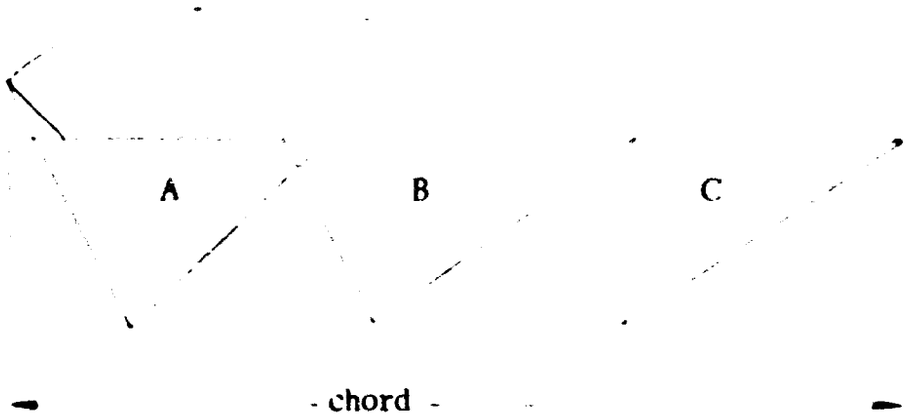

AIRFOIL	
Station	Ordinate
0.0000	0.0594
.0125	.0648
.0250	.0777
.0500	.0899
.0750	.1007
.1000	.1079
.1500	.1169
.2000	.1223
.2500	.1259
.3000	.1259
.4000	.1223
.5000	.1133
.6000	.0950
.7000	.0763
.8000	.0504
.9000	.0288
1.0000	.0000

Figure 11. Parafoil Model 6 Airfoil Section and Dimensions (in fraction of chord)

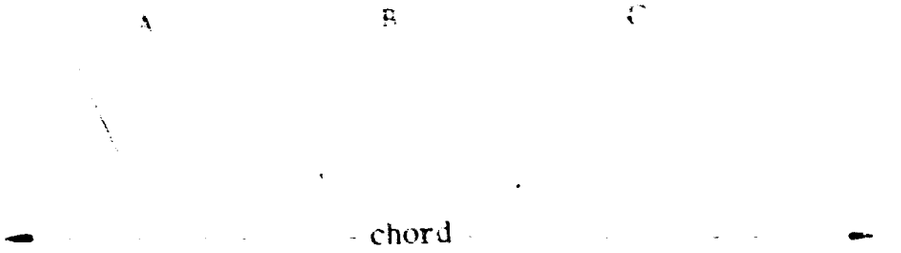

AIRFOIL	
Station	Ordinate
0.0000	0.0811
.0125	.1081
.0250	.1208
.0500	.1399
.0750	.1526
.1000	.1622
.1500	.1749
.2000	.1813
.2500	.1844
.3000	.1812
.4000	.1653
.5000	.1437
.6000	.1208
.7000	.0916
.8000	.0604
.9000	.0286
1.0000	.0000

Figure 12. Parafoil Model 7 Airfoil Section and Dimensions (in fraction of chord)

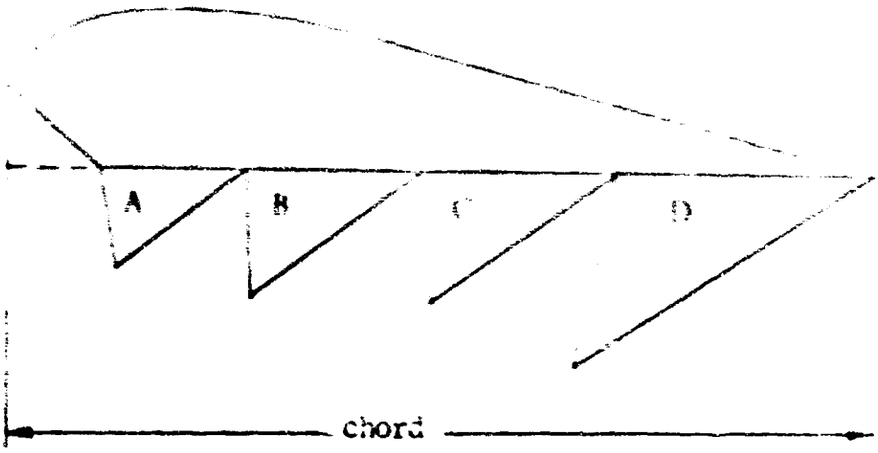

AIRFOIL	
Station	Ordinates
0.	0.0886
.0200	.1206
.0400	.1392
.0600	.1518
.0800	.1616
.1000	.1688
.1056	.0000
.1200	.1730
.1400	.1756
.1600	.1780
.1800	.1784
.2000	.1790
.2200	.1790
.2400	.1768
.2600	.1752
.2800	.1730
.3000	.1708
.3200	.1676
.3400	.1646
.3600	.1606
.3800	.1562
.4000	.1524
.4200	.1476
.4400	.1426
1.0000	0.0000

Figure 13. Parafoil Models 8-13 Airfoil Section and Dimensions (in fraction of chord)

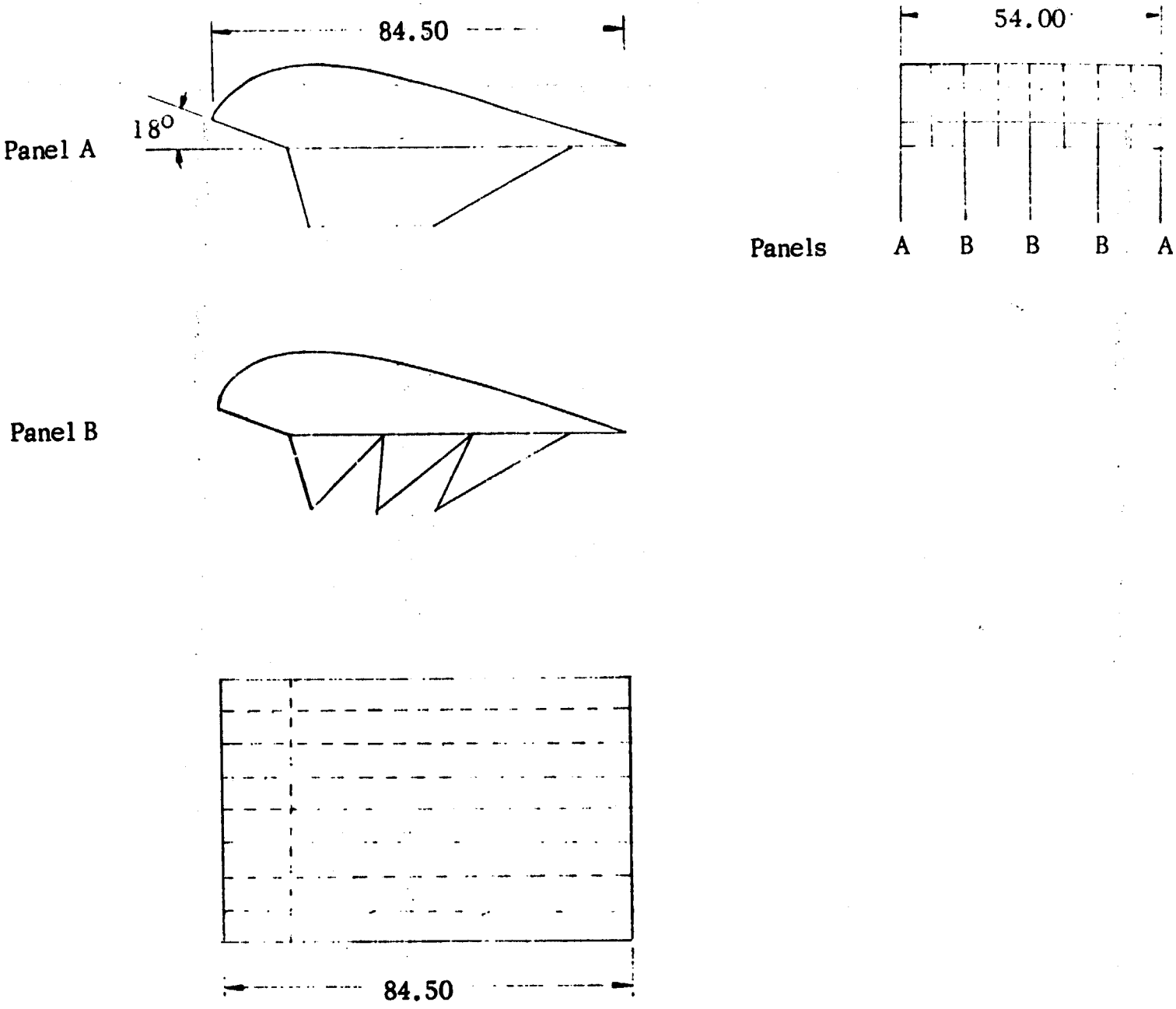

Figure 14. Para-Foil Model 5. Dimensions in inches

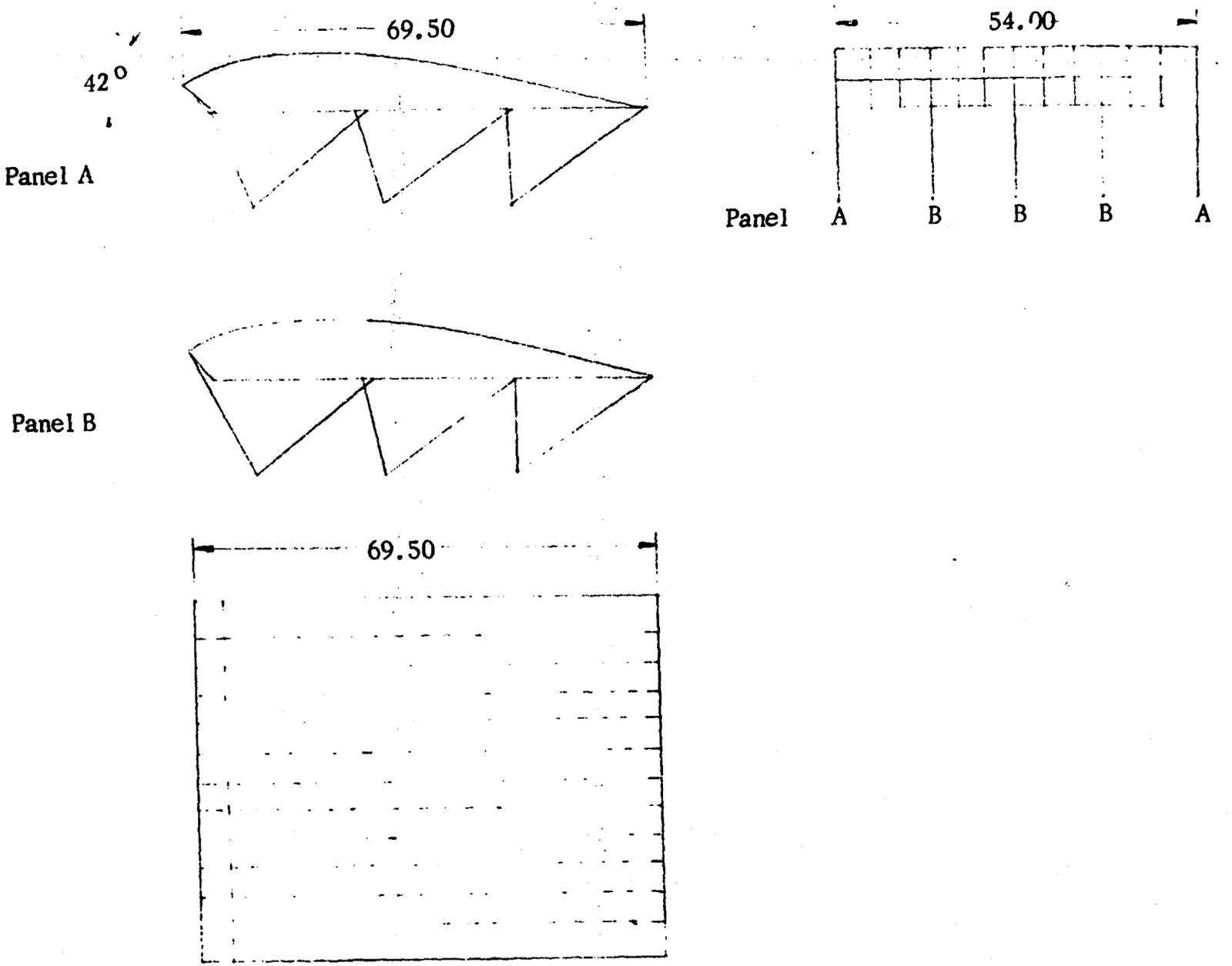

Figure 15. Para-Foil Model 6. Dimensions (in inches)

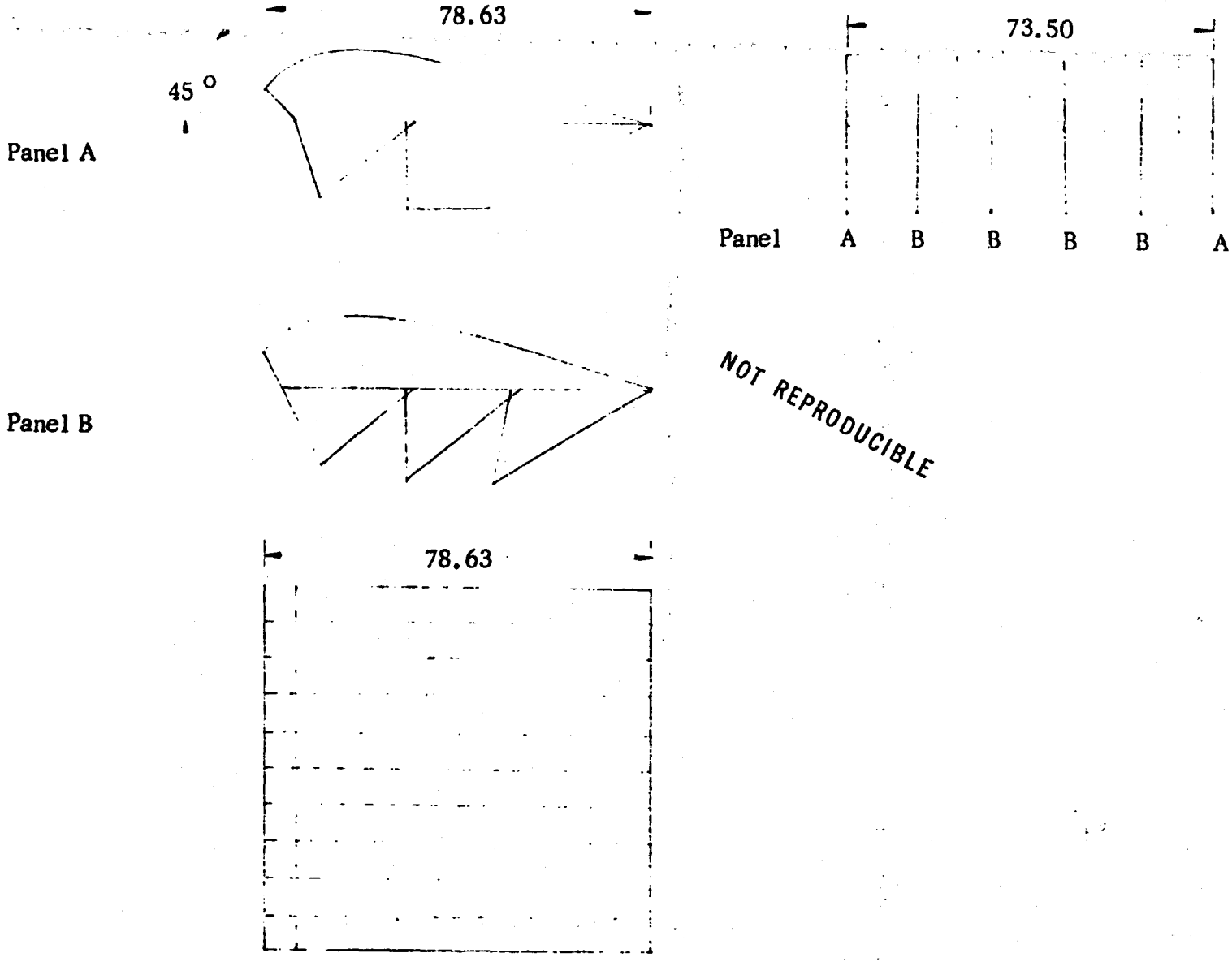

Figure 16. Para-Foil Model 7. Dimensions (in inches)

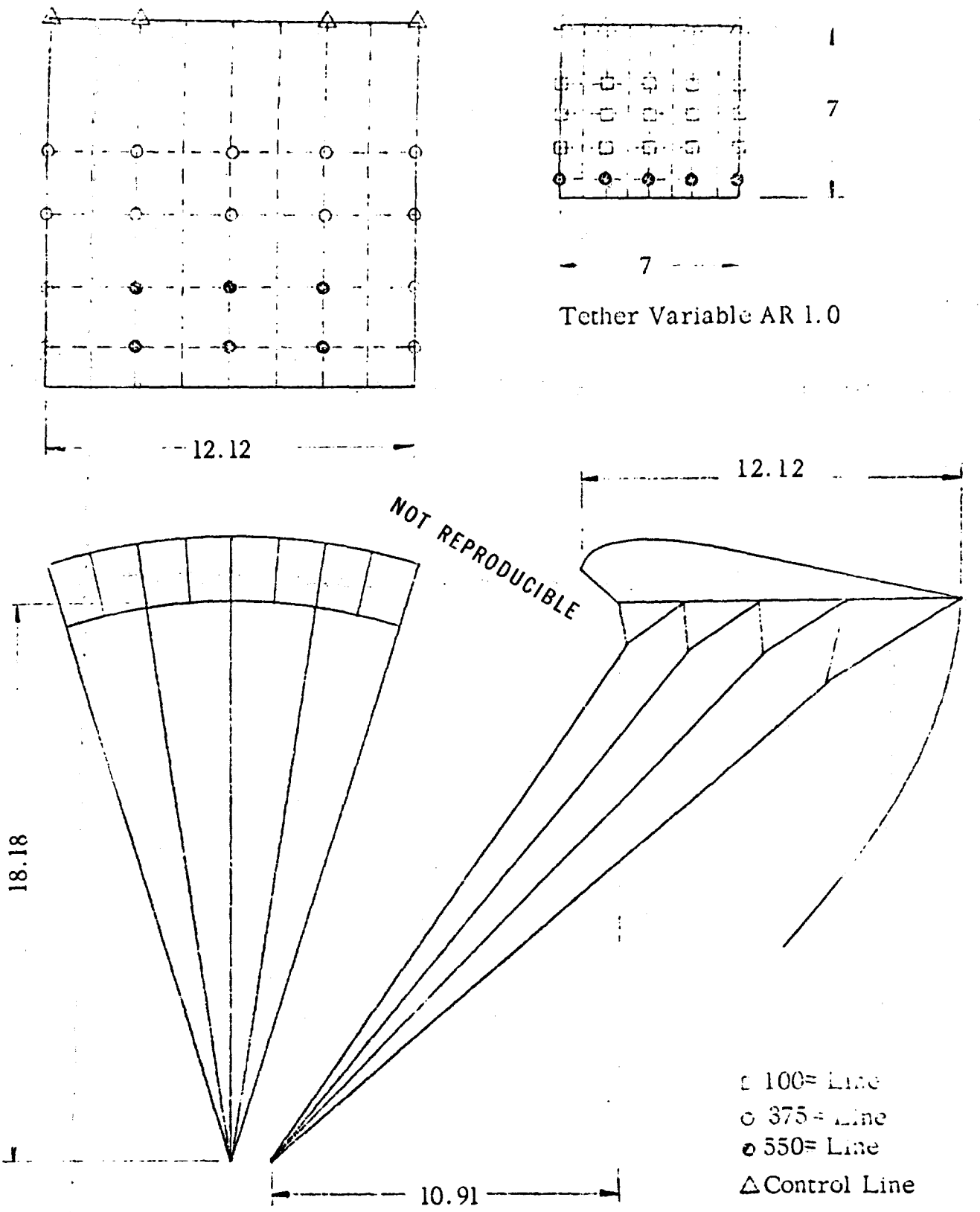

Figure 17. Model 8 : AR 1.0 (Dimensions in feet)

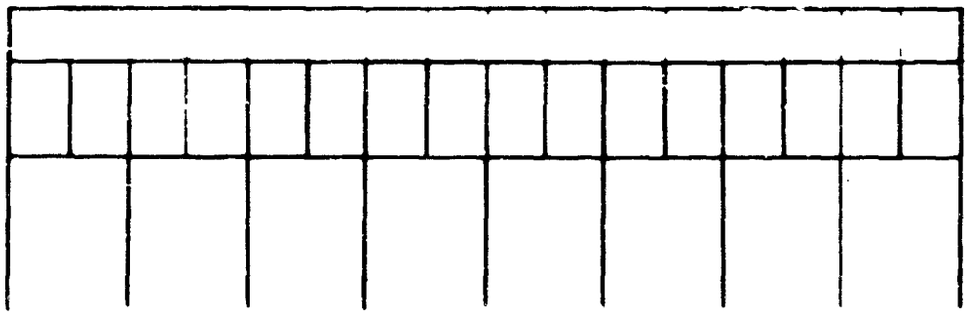

1.) Not Taped

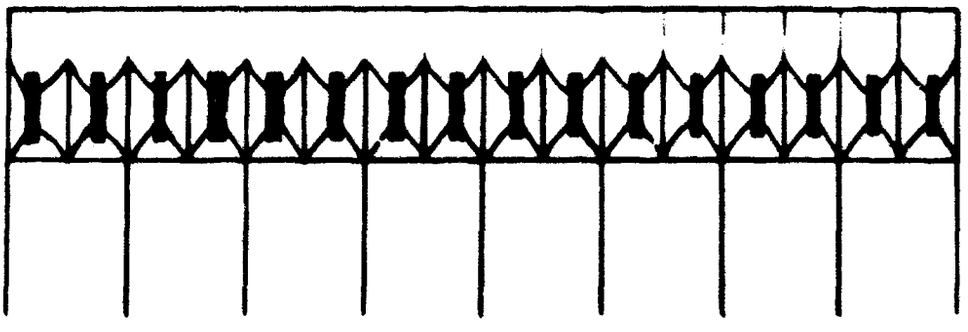

2.) Leading edge taped 33% closed

Figure 17a. Tape on Leading Edge.

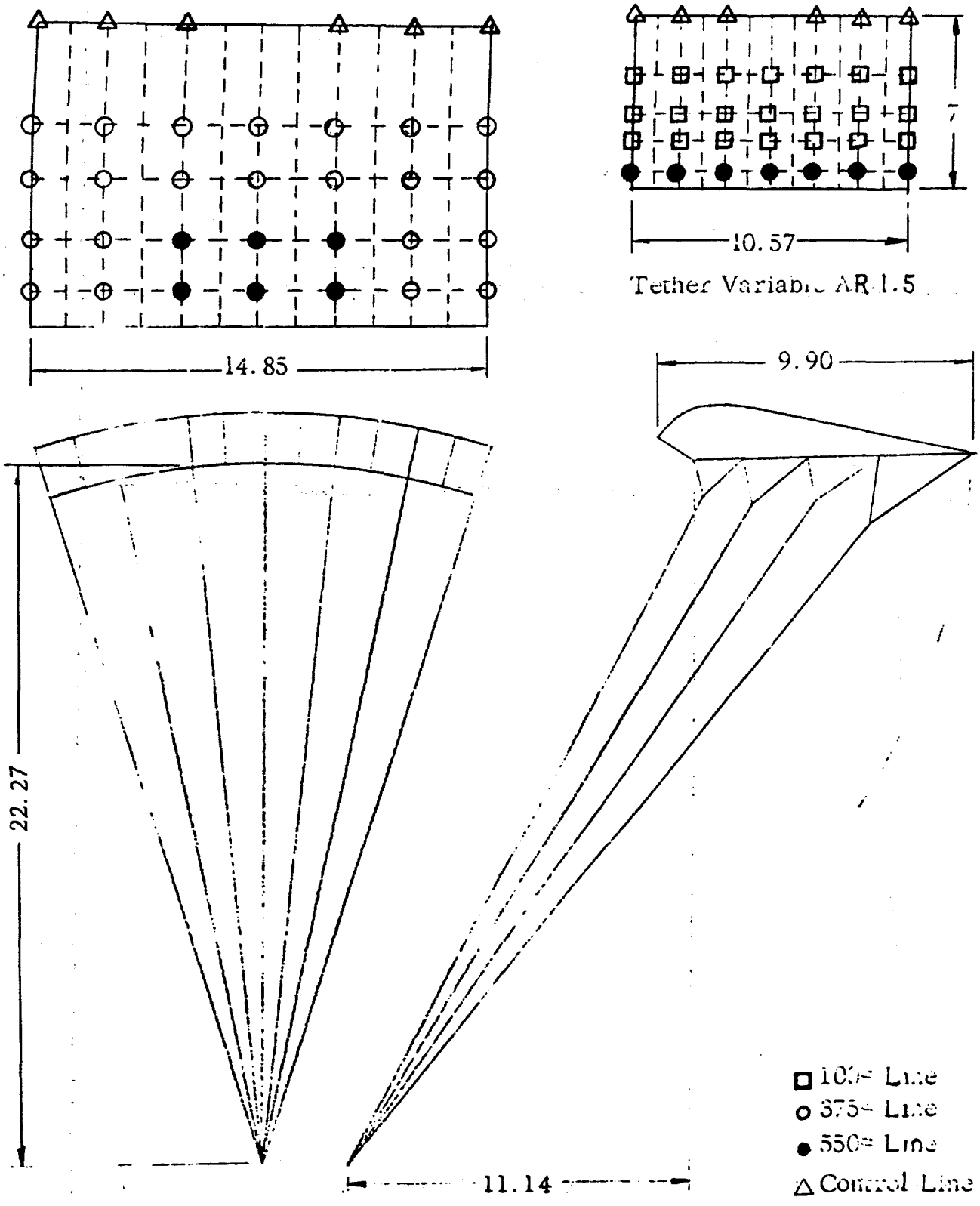

Figure 18. Model 9 : AR 1.5 (Dimensions in feet)

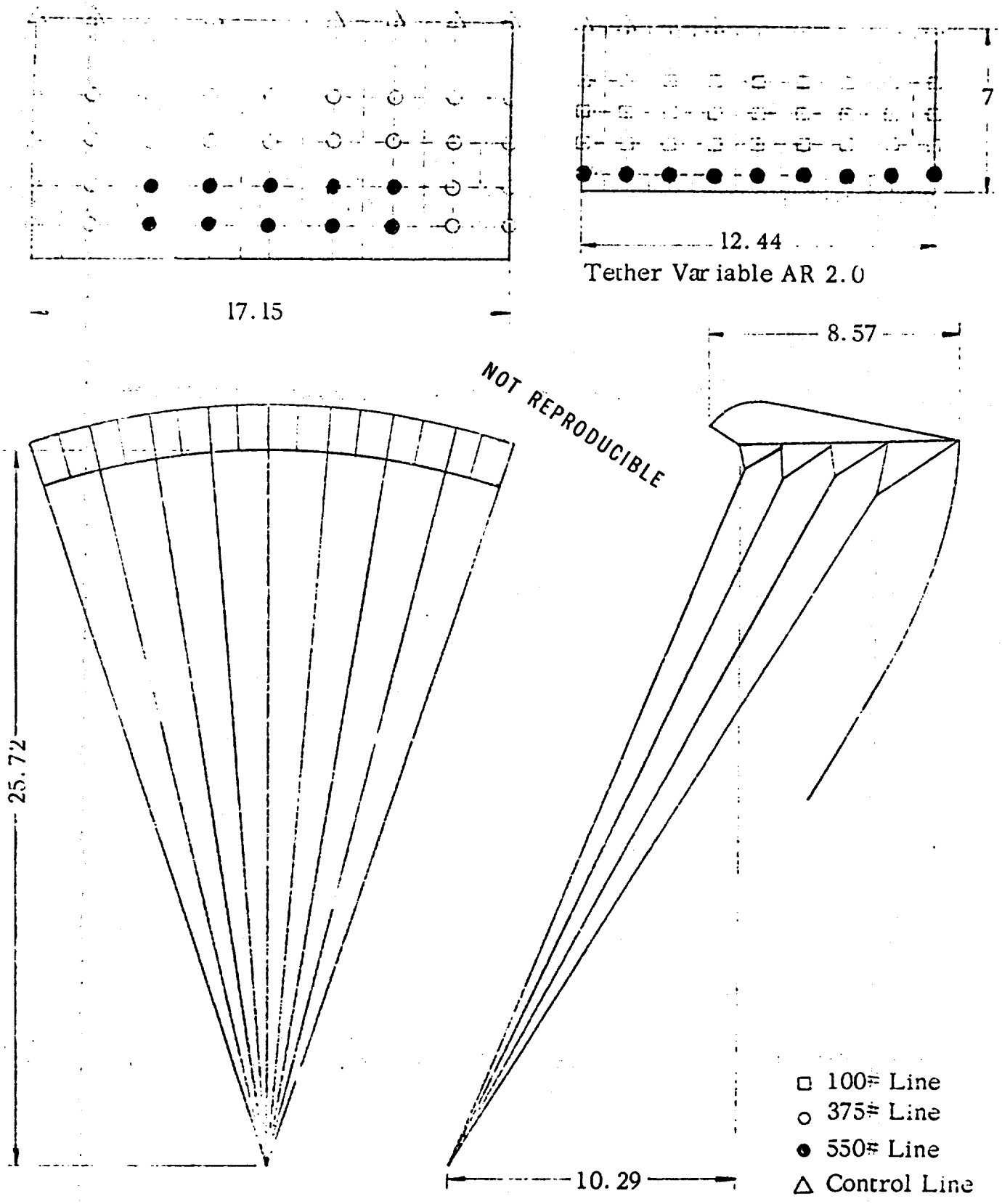

Figure 19. Model 10 : AR 2.0 (Dimensions in feet)

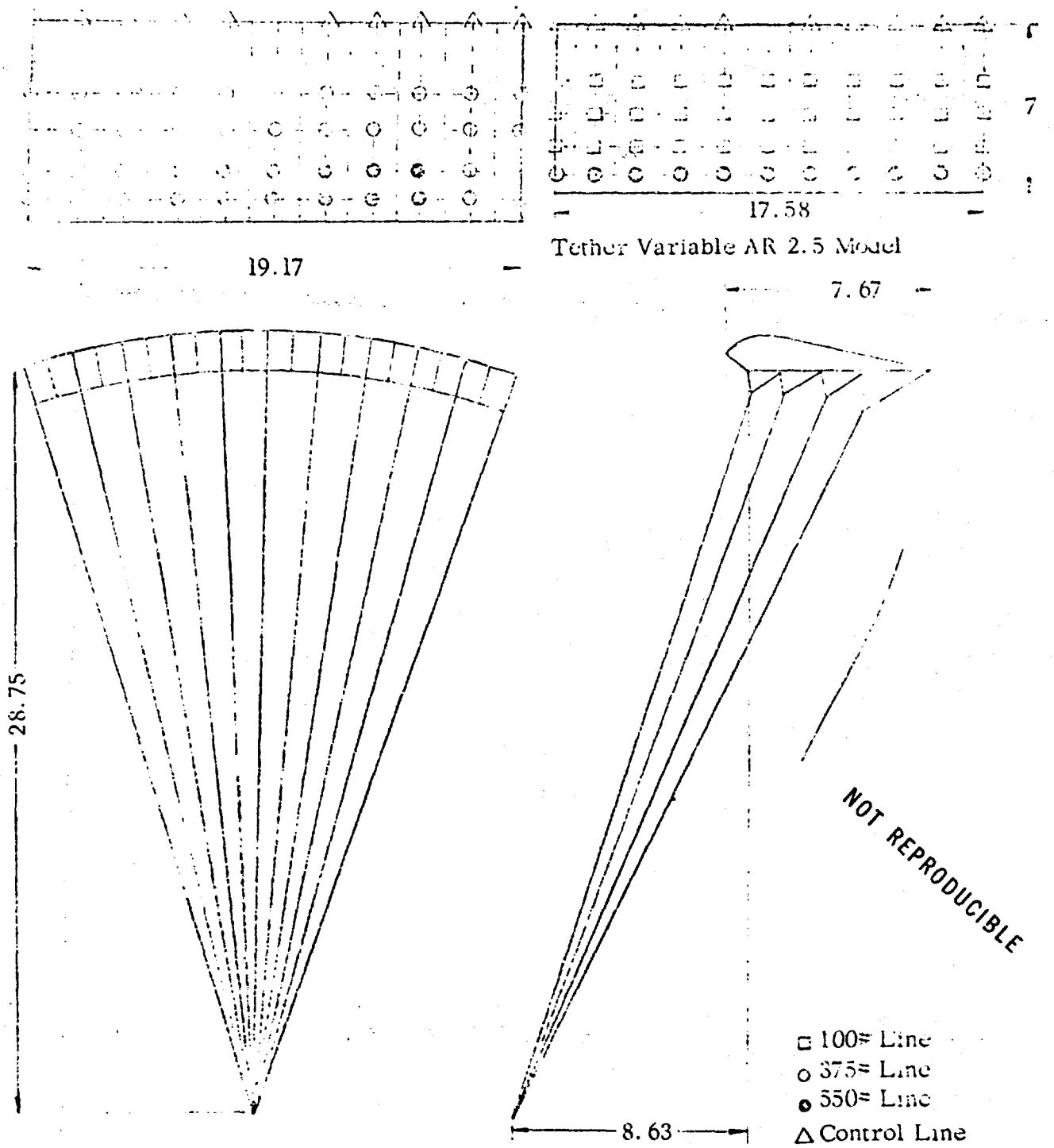

Figure 20. Model 11 : AR 2.5 (Dimensions in feet)

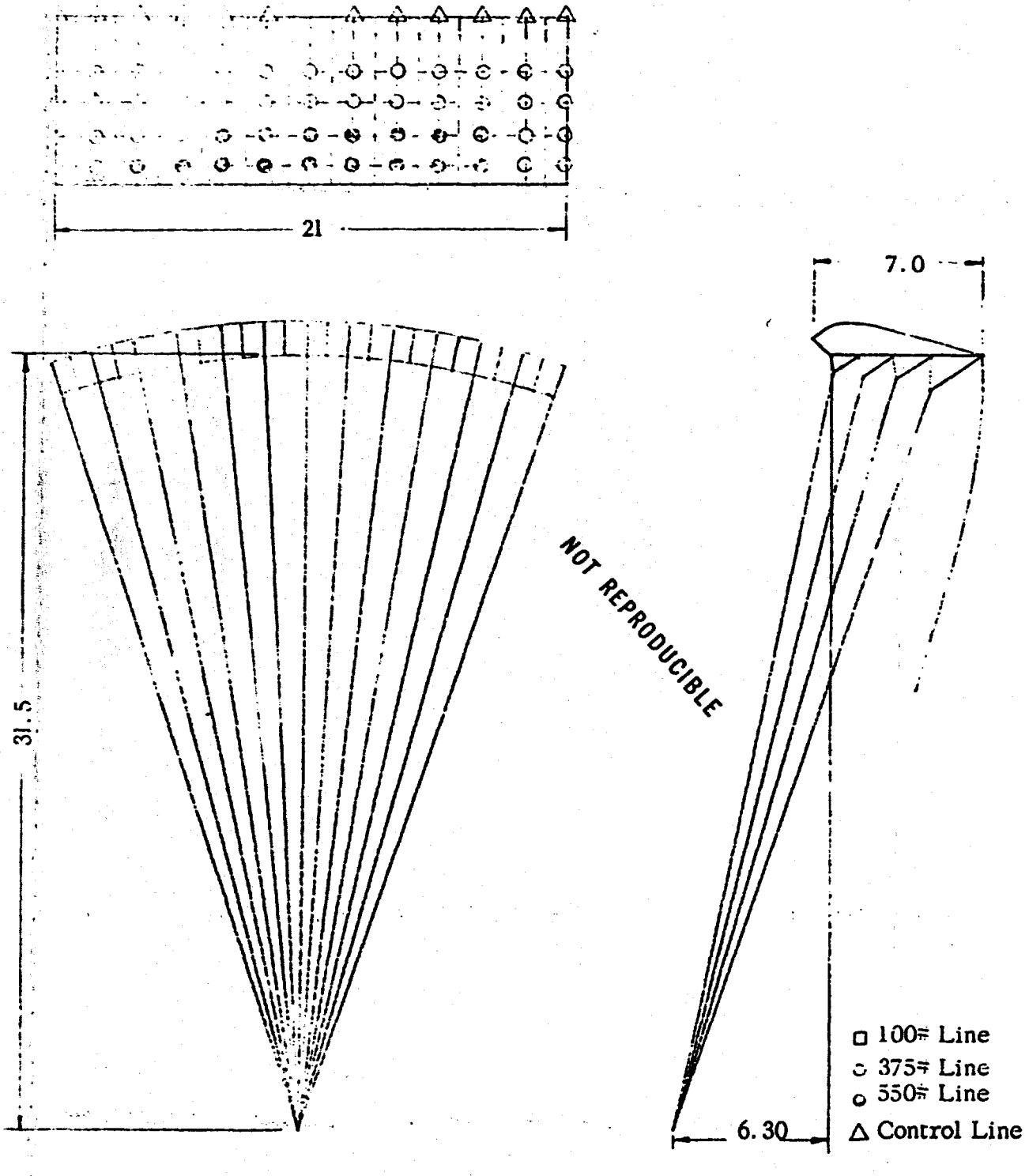

Figure 21 . Models 12 and 13 : AR 3.0 (Dimensions in feet)

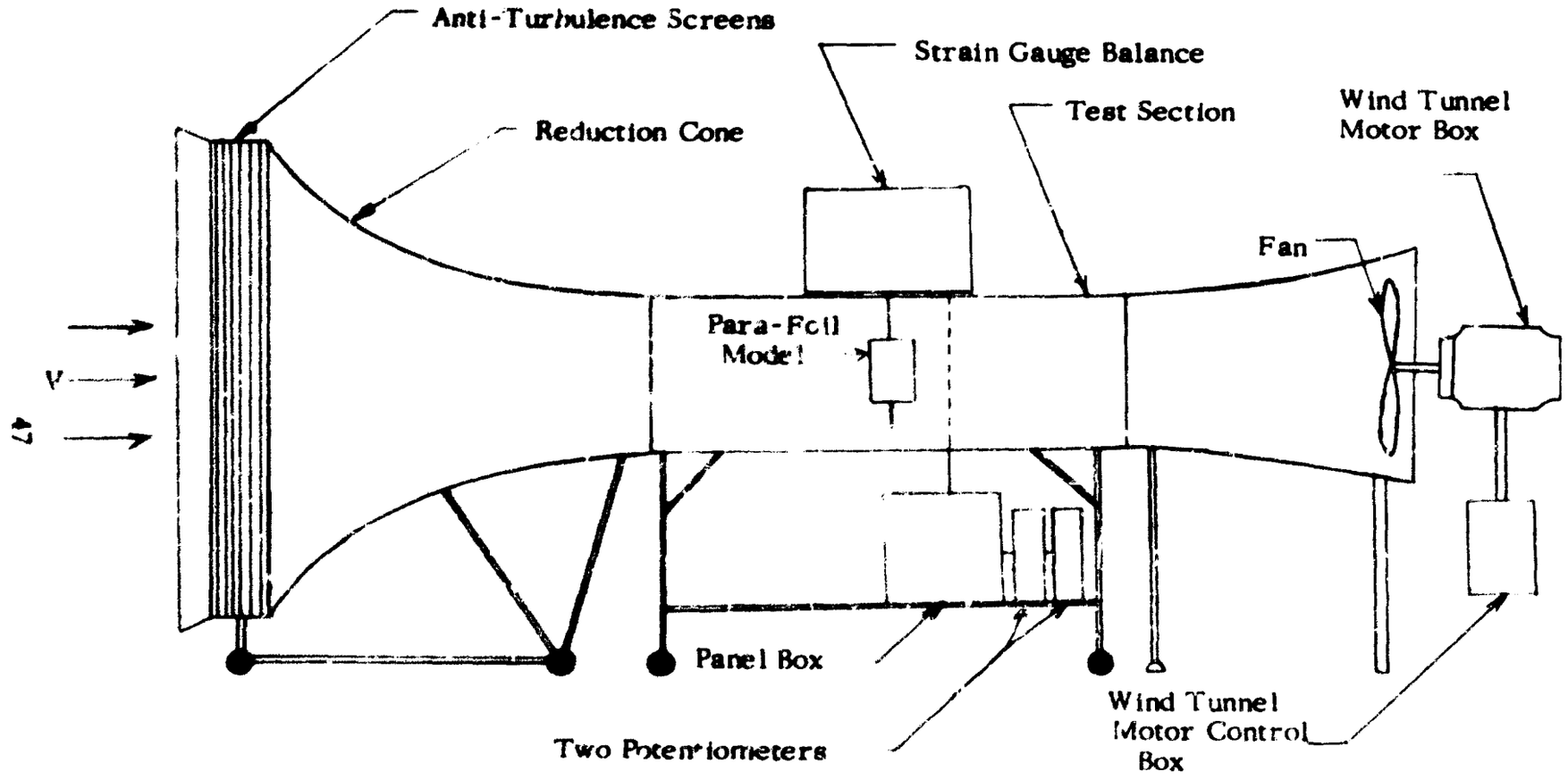

Figure 22. Notre Dame Wind Tunnel with Static Test Mount Configuration

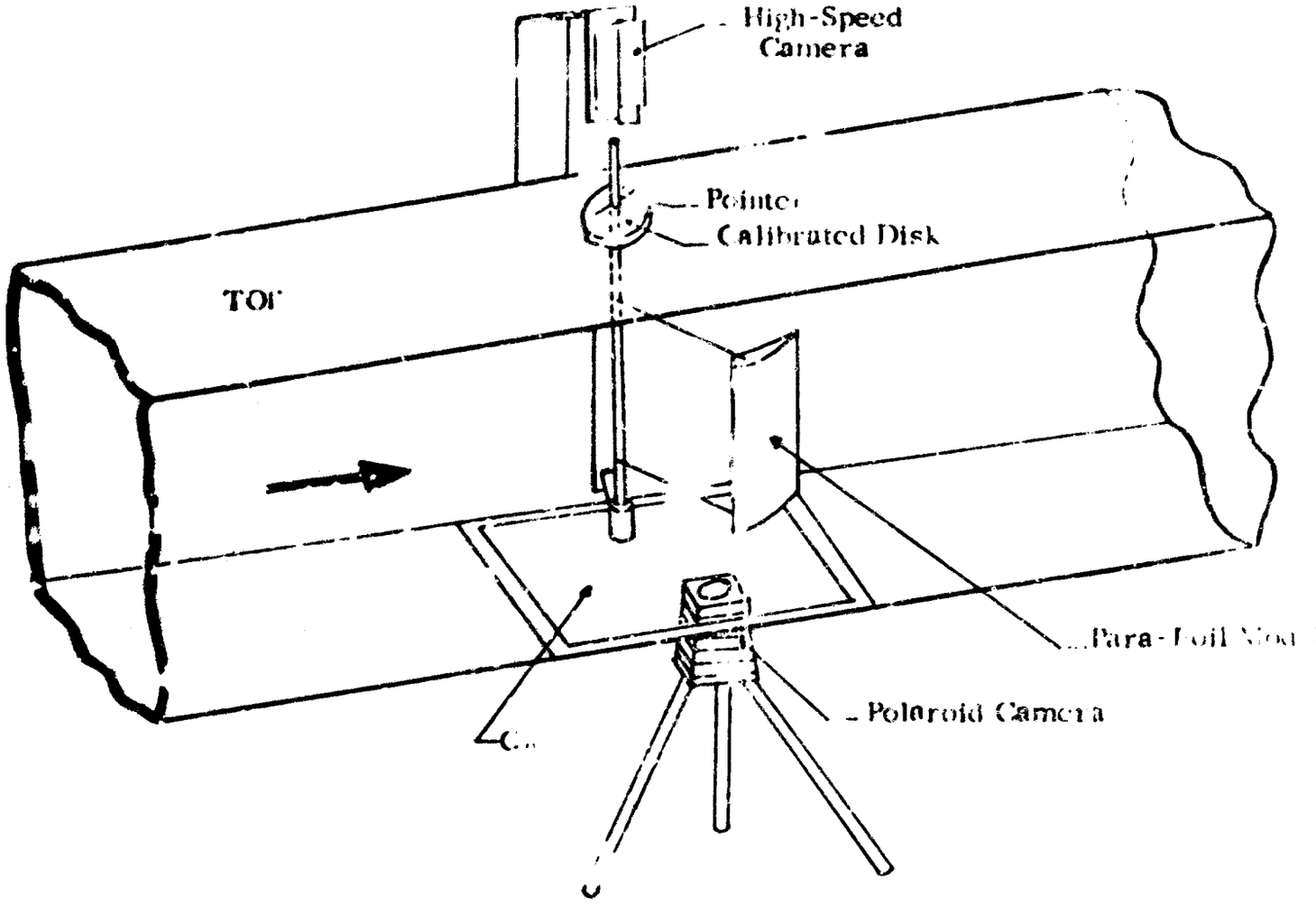

Fig. 23 Para-Foil Mock-Up with Support Equipment as Mounted in Wind Tunnel Test Section.

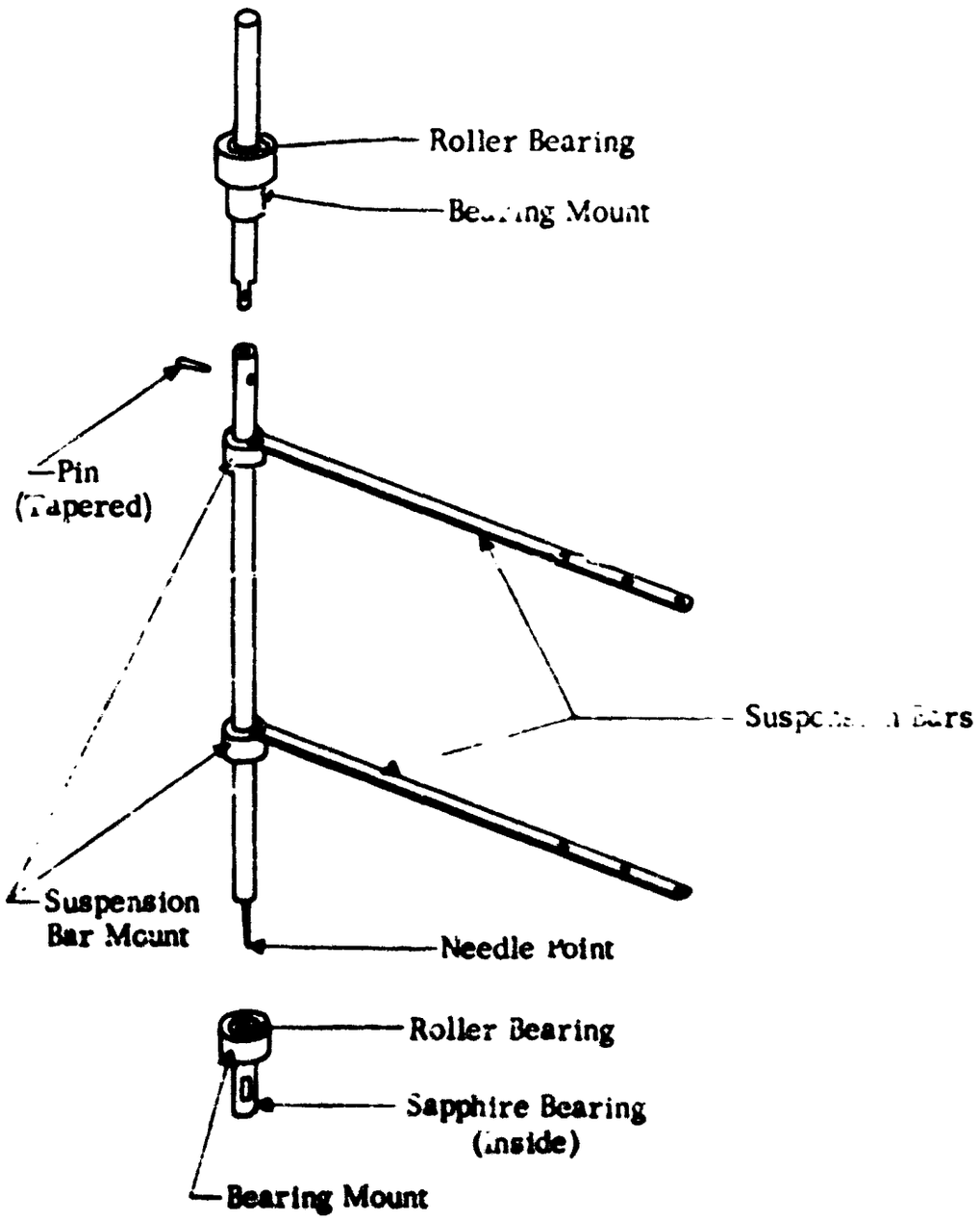

Fig.24 Suspension System Components

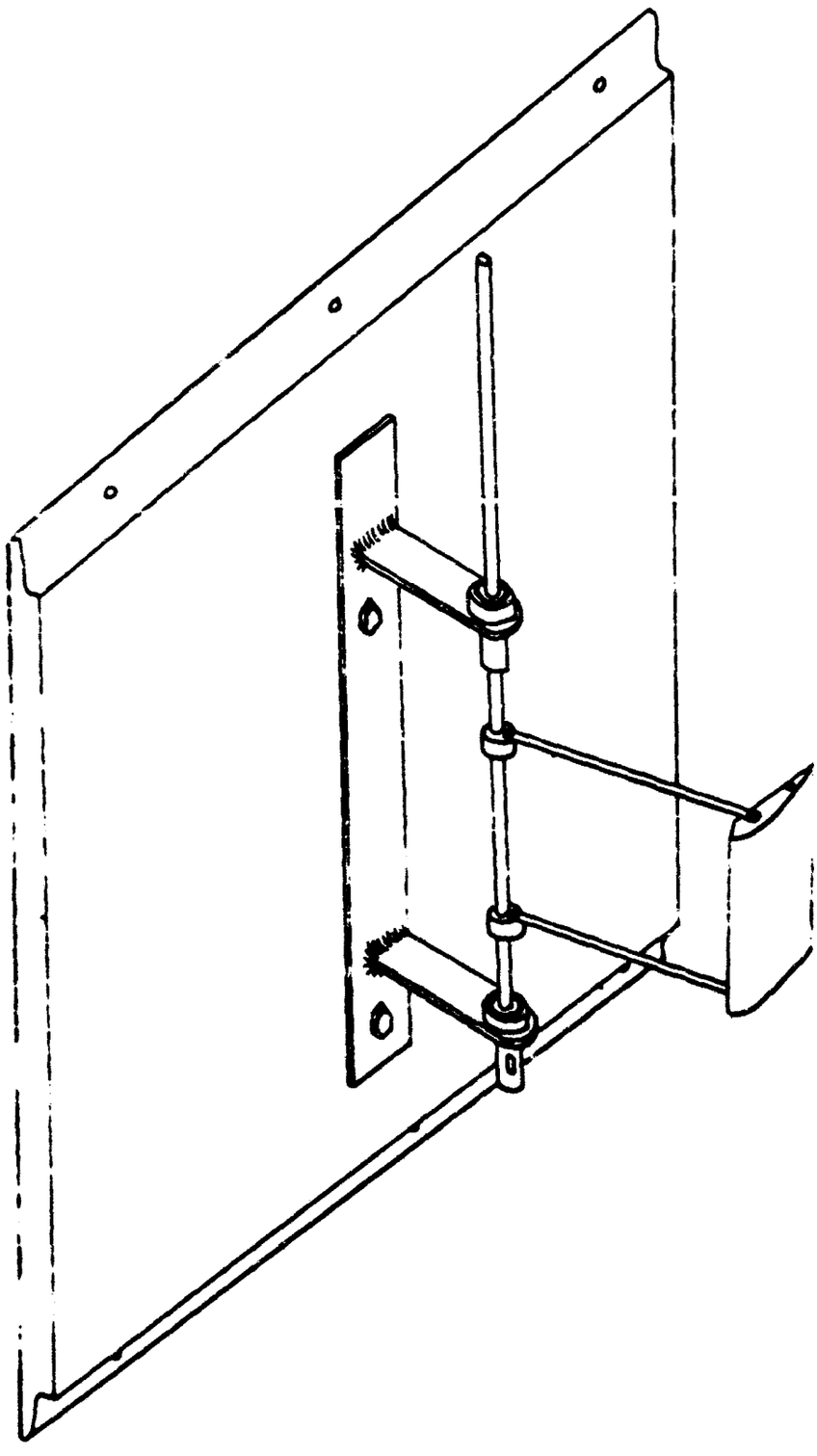

Fig. 25 Suspension System and Model Mounted on Wind Tunnel Door

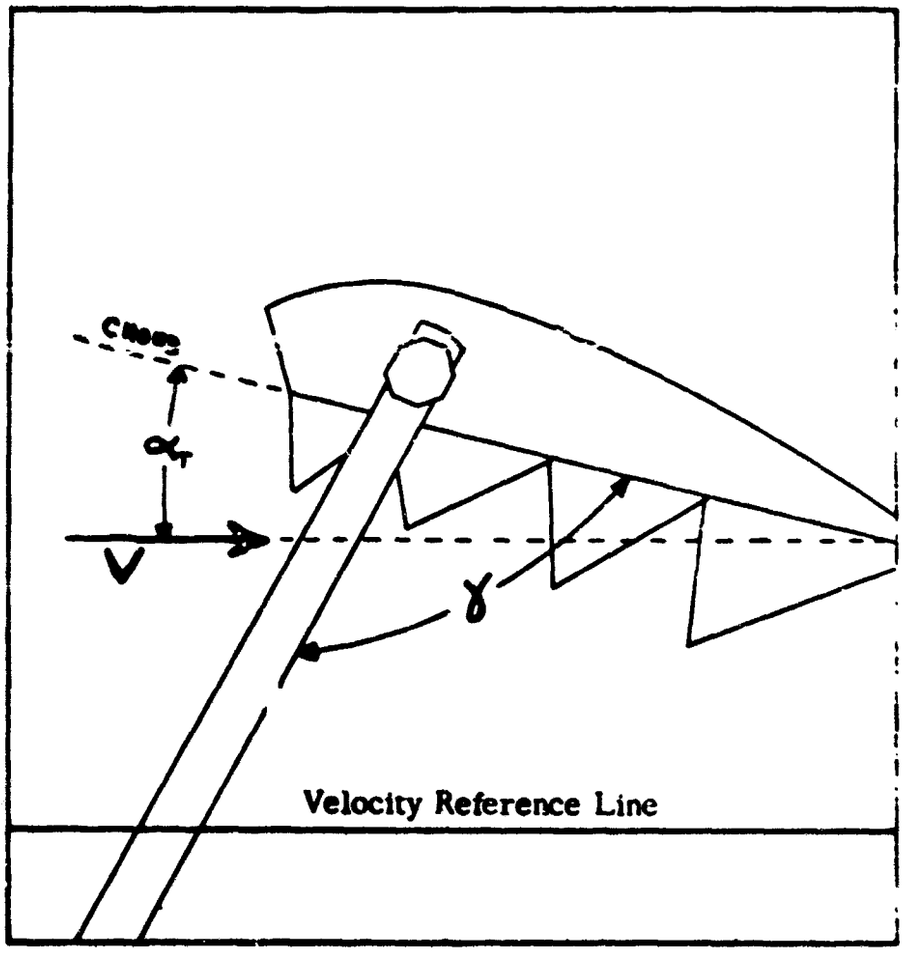

Fig. 26 Schematic of Polaroid Picture Showing α_T and γ

Figure 27. Tether Testing Phase

Figure 28. Strut Testing Phase

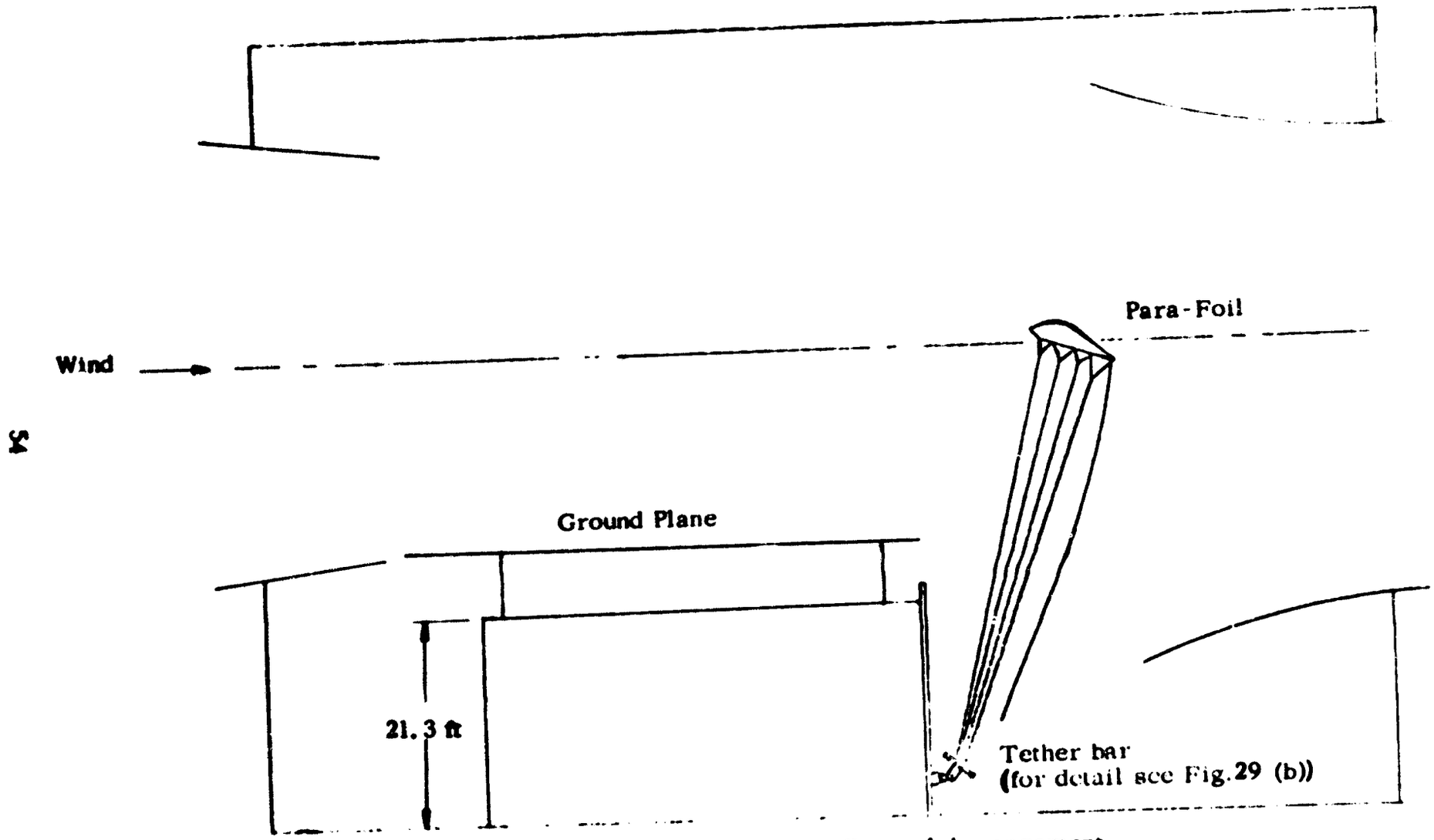

Figure 29 a. Tether Test Set-up- General Arrangement

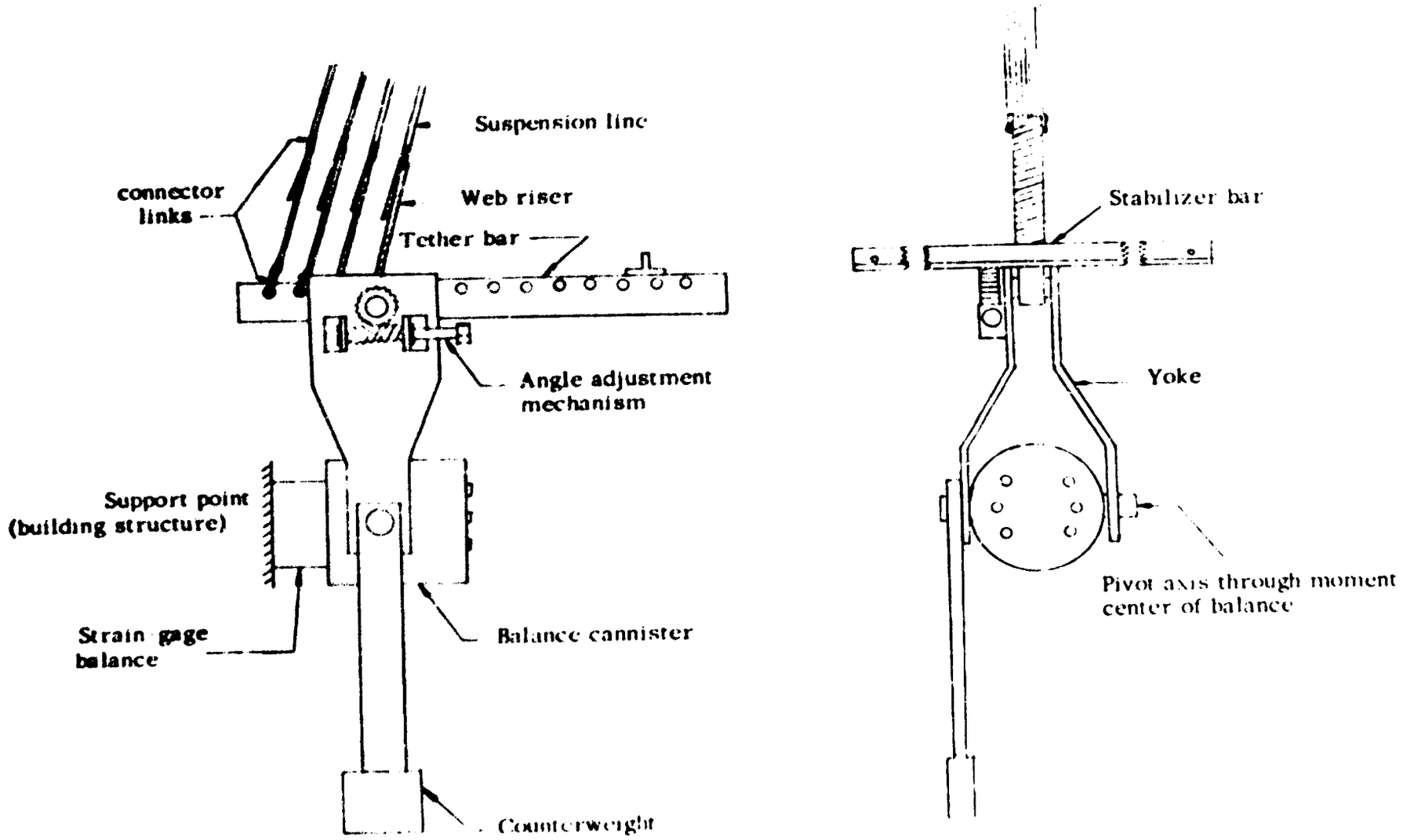

Figure 29 b. Tether Test Set up Mount Assembly

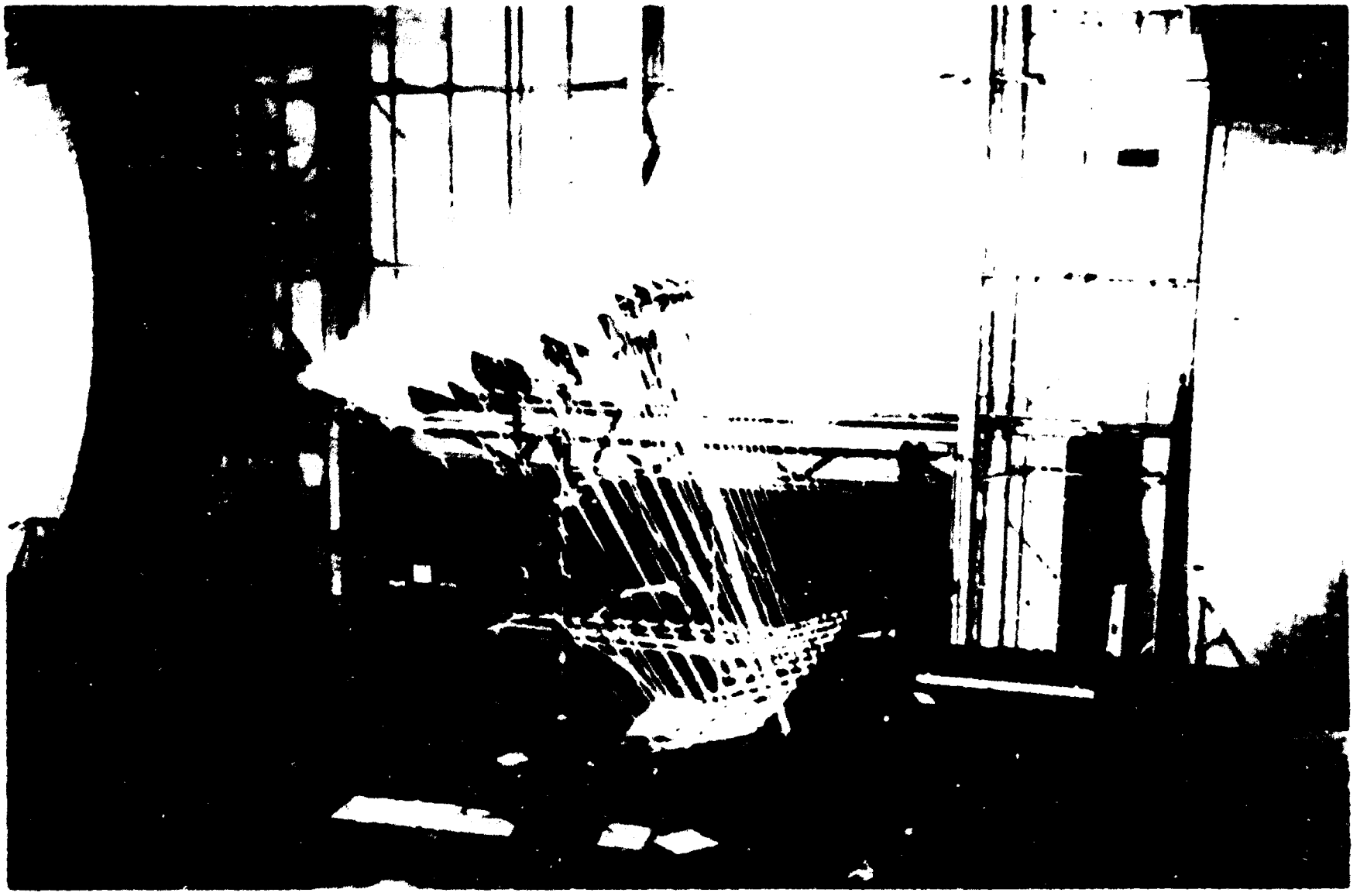

Figure 30. Strut Testing Phase

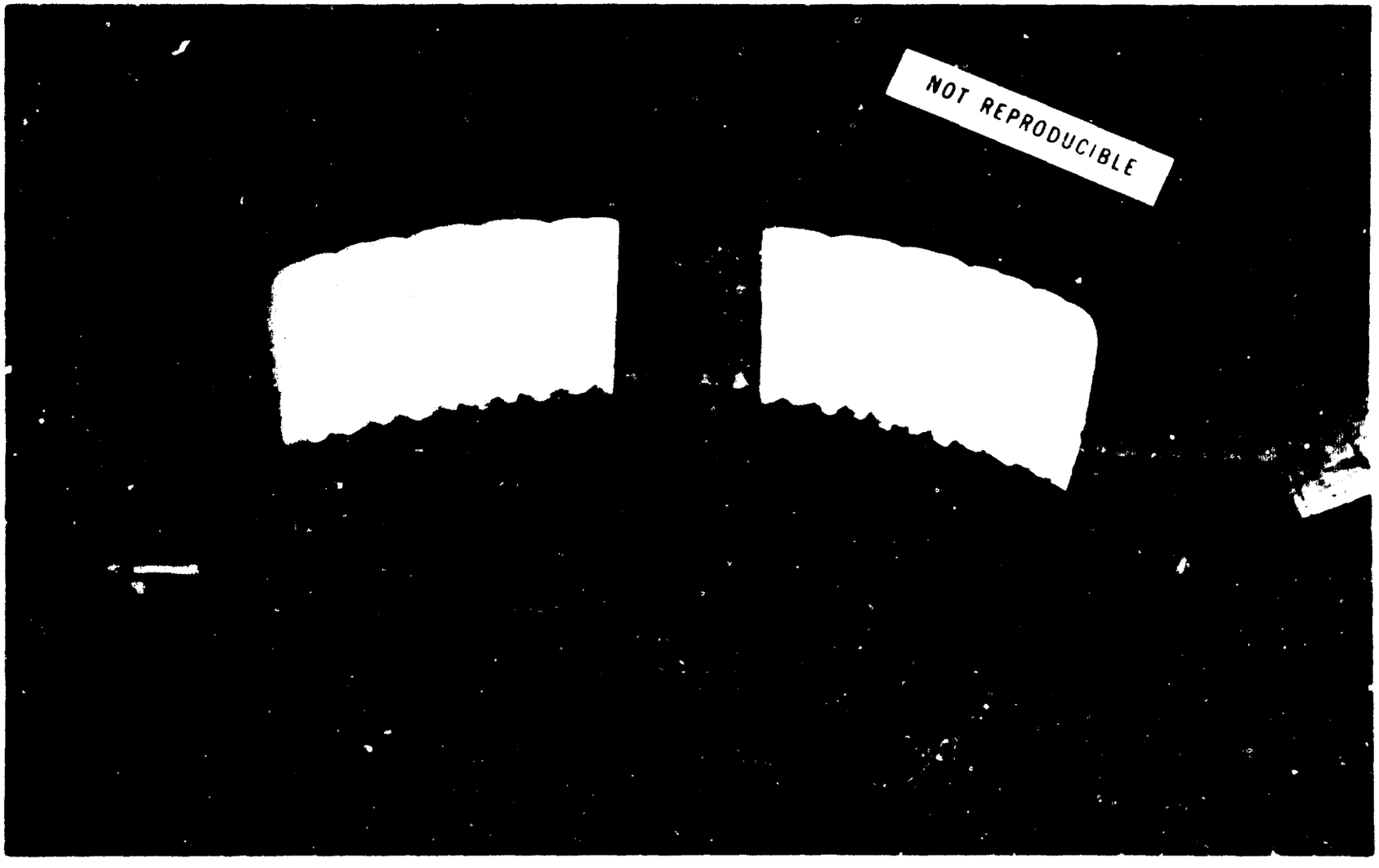

Figure 31 a. : Strut AR 3.0 Model, α = - 5°

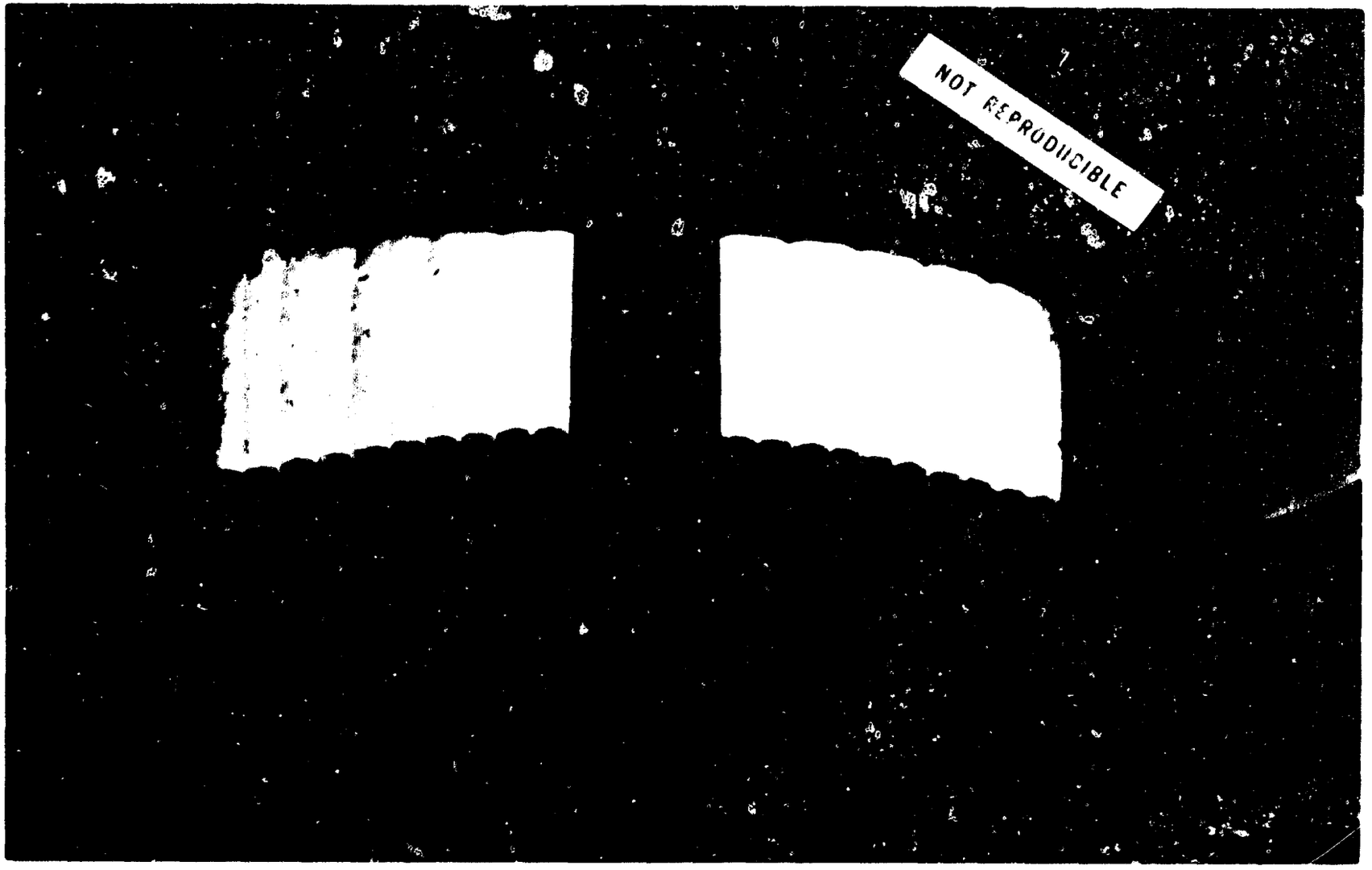

Figure 31 b : Strut AR 3.0 Model. α = 7.5°

Figure 31 c : Strut AR 3.0 Model. $\alpha = 17.5^{o}$

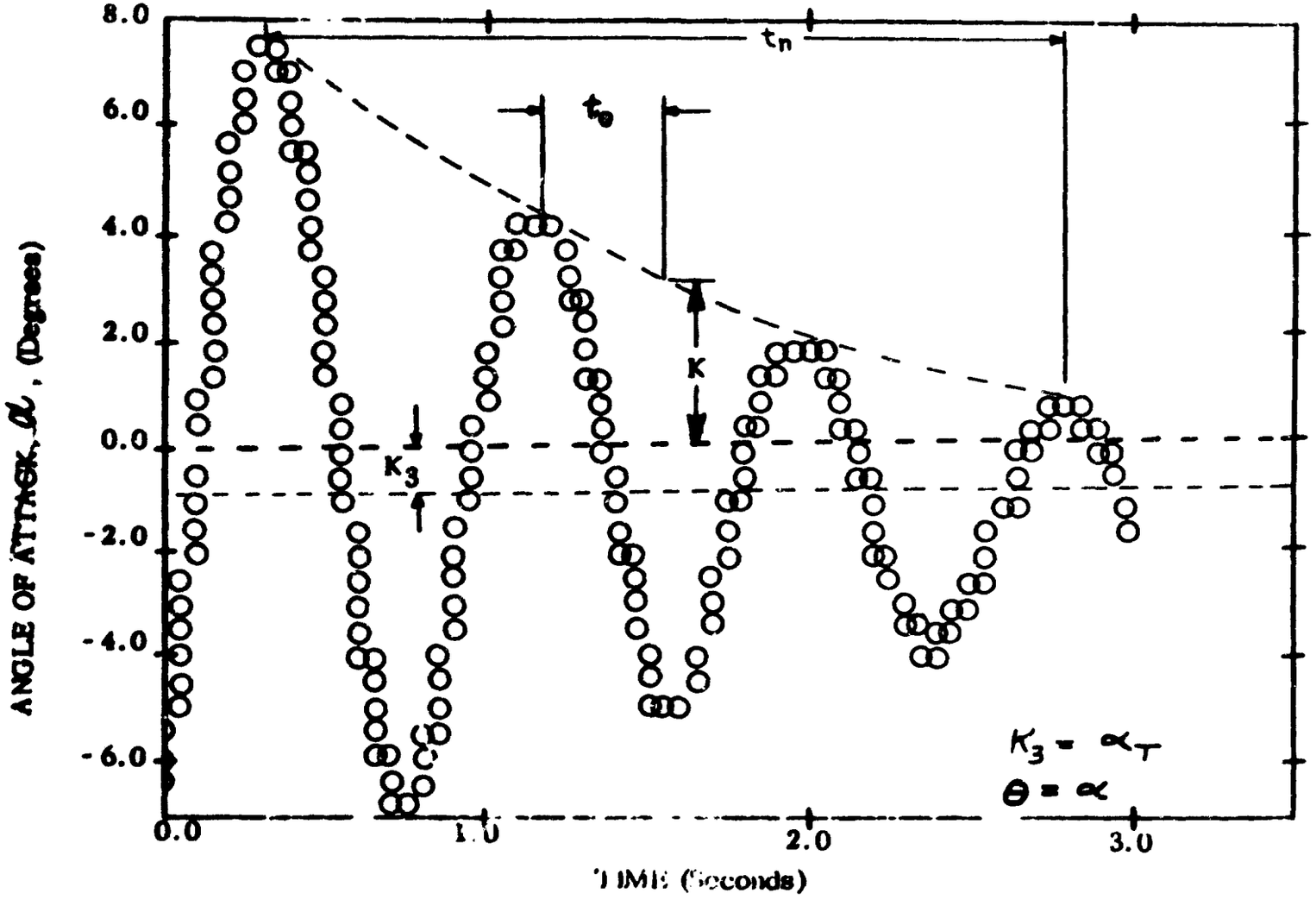

Fig. 32 Data Plot (Test No. 28)

Fig. 33 Para-Flow Flow Visualization in Notre Dame Smoke Tunnel

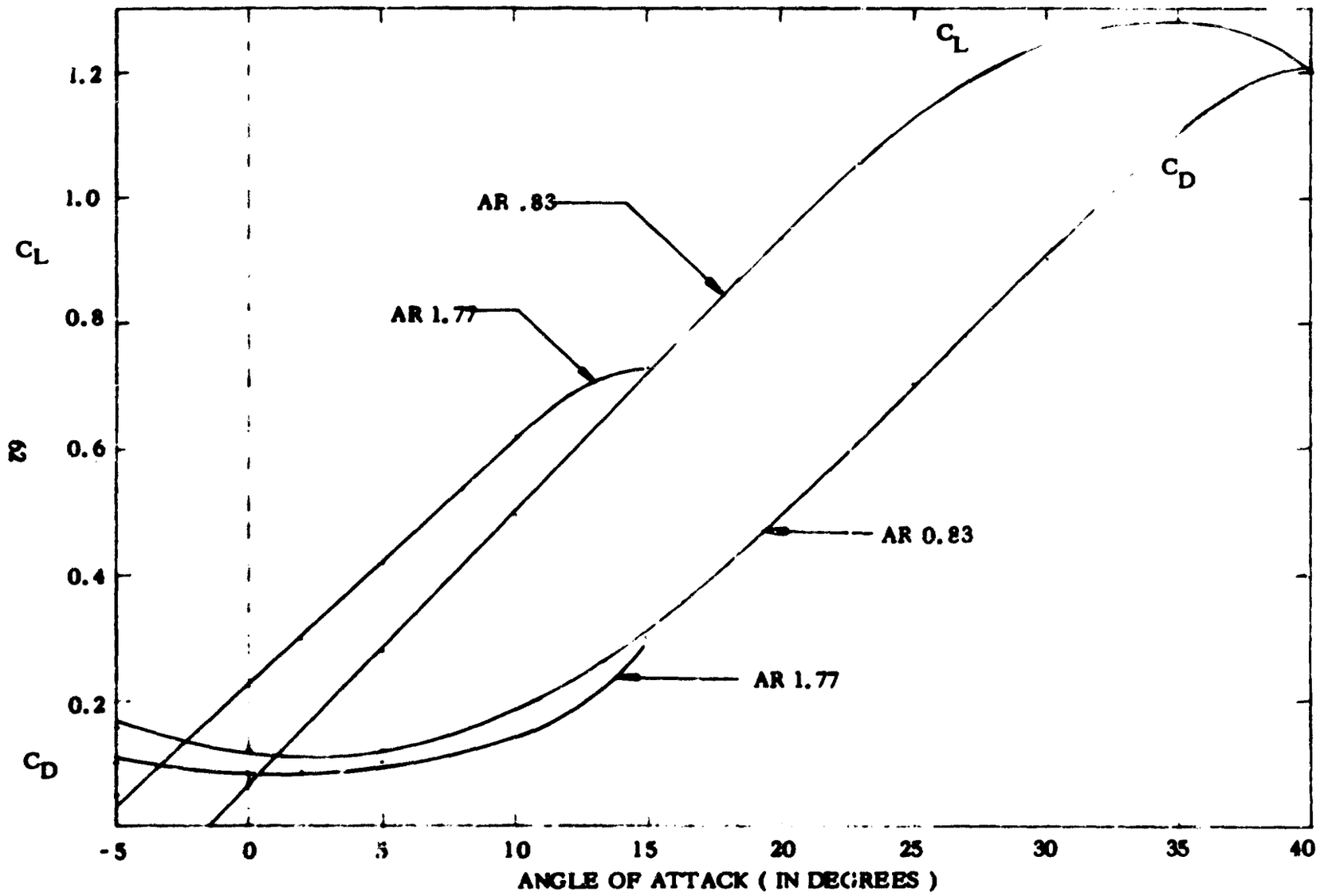

Figure 34. Early Notre Dame Tests : Summary Lift and Drag

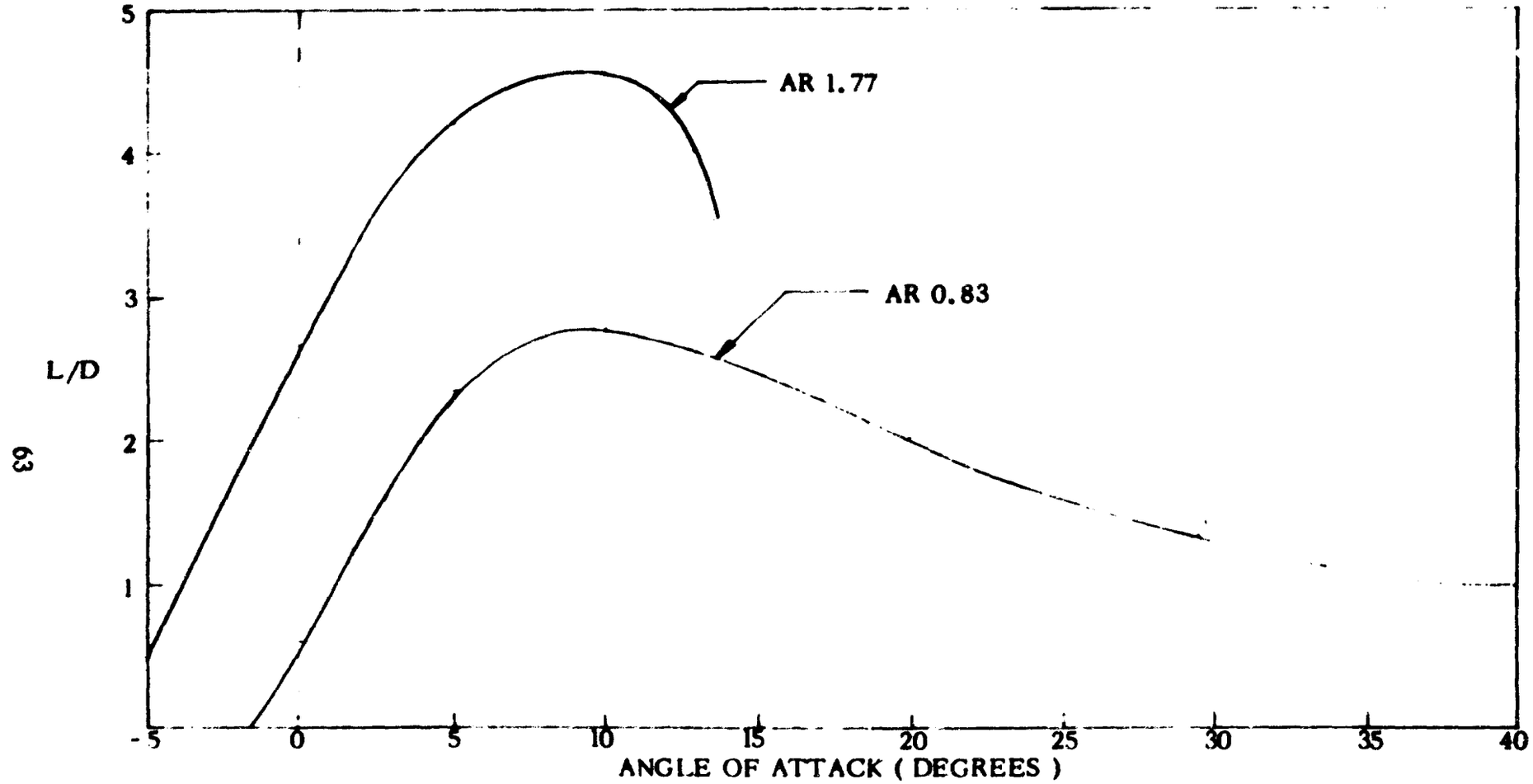

Figure 35. Early Notre Dame Tests : Summary Lift to Drag Ratio

	Rigid Airfoil	Rigid Airfoil plus Flares	Rigid Airfoil plus Nylon Cloth	Rigid Airfoil plus Flares plus Nylon Cloth
Symbols:	+ ———	× ———	▲ ———	o ———
$C_{L\alpha}$:	.0500/deg	.0508/deg	.0530/deg	.0510/deg
$C_{L_{max}}$:	.98 @ 17.5	.93 @ 17.5°	1.12 @ 19.5°	1.20 @ 21.5°
Stall :	17.5°	17.5°	19.5°	21.5°
Drag :	(Basis)	Approx. same	Greater	Slightly greater
L/D_{max} :	5.0 @ 10°	5.15 @ 11°	4.43 @ 11°	4.81 @ 11.5°

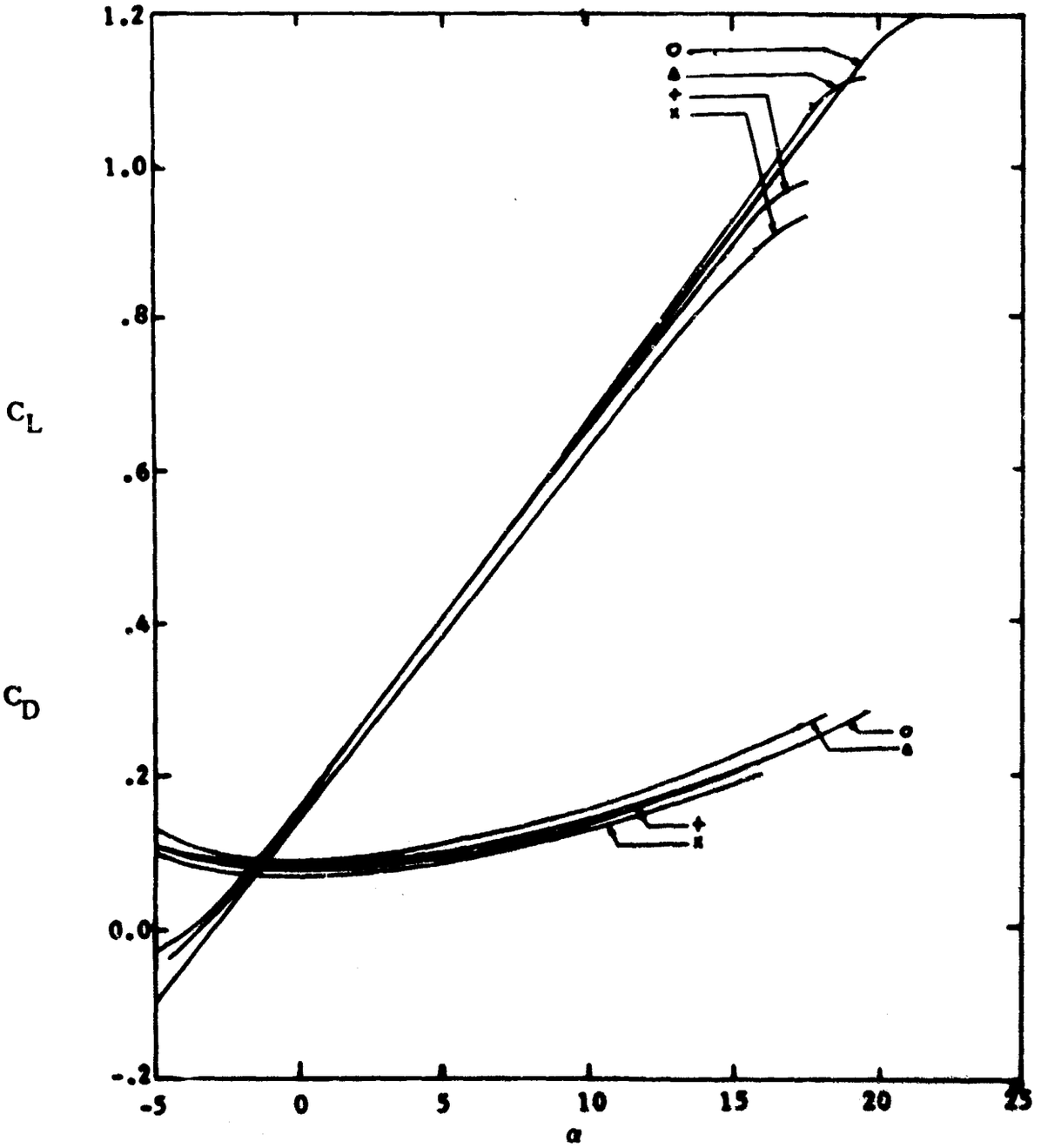

Figure 36. Rigid Airfoil with Model Variations

	Rigid Parafoil	Rigid Parafoil plus Flares	Rigid Parafoil plus Nylon Cloth	Rigid Parafoil plus Flares plus Nylon Cloth
Symbols :	+ ———	x ———	△ ———	o ———
C_{L_α} :	.0400/deg	.0408/deg	.0440/deg	.0410/deg
$C_{L_{max}}$:	.66 @ 11.5°	.58 @ 9.5°	.74 @ 11.5°	.72 @ 13.5°
Stall :	11.5°	9.5°	11.5°	13.5°
Drag :	(Basis)	Slightly Greater	Greater	Slightly Greater
L/D_{max} :	5.0 @ 7.5°	4.0 @ 6.5°	3.9 @ 8°	4.6 @ 10°

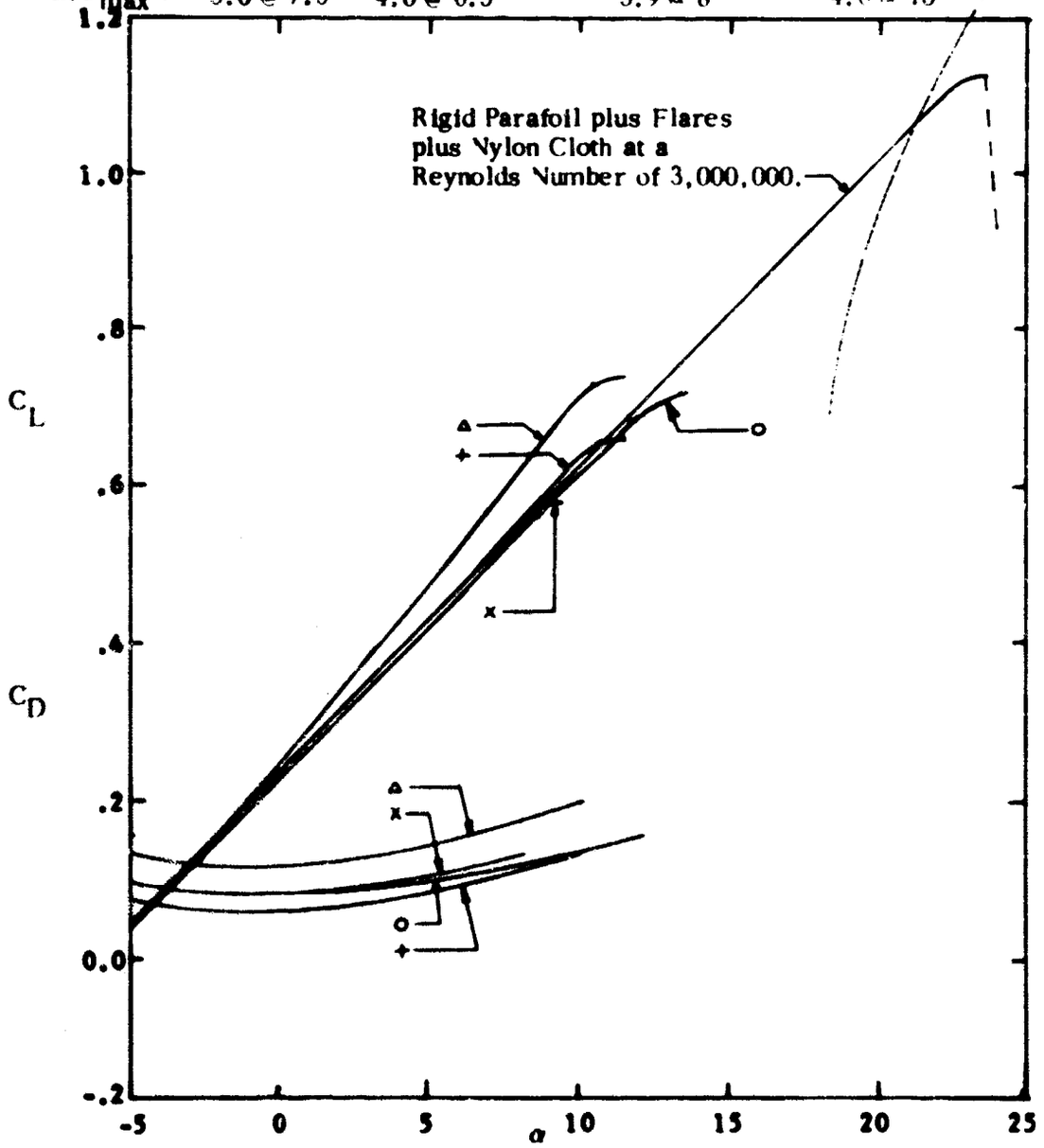

Figure 37. Rigid Parafoil with Model Variations

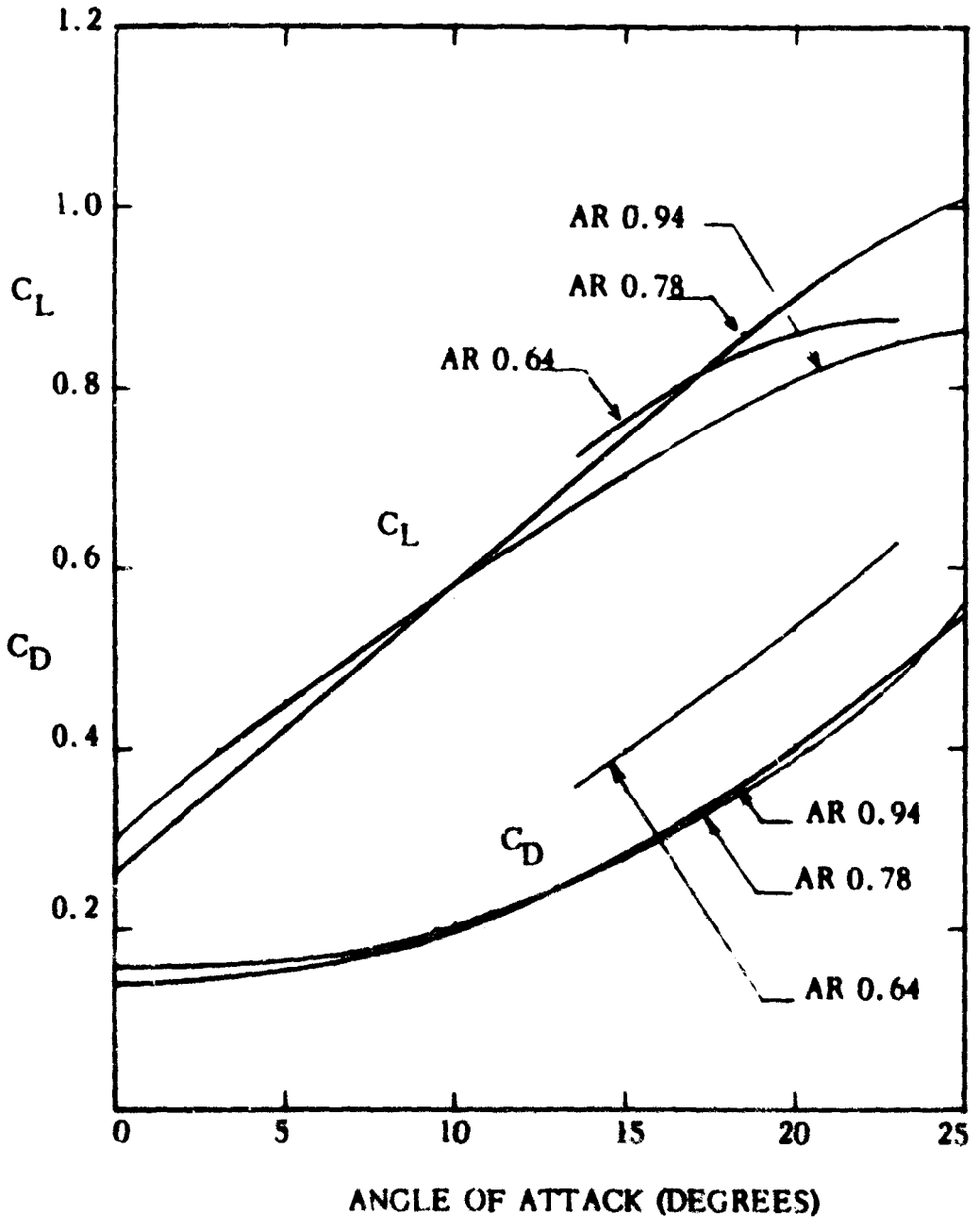

Figure 38. Early NASA Tests: Lift and Drag Summary

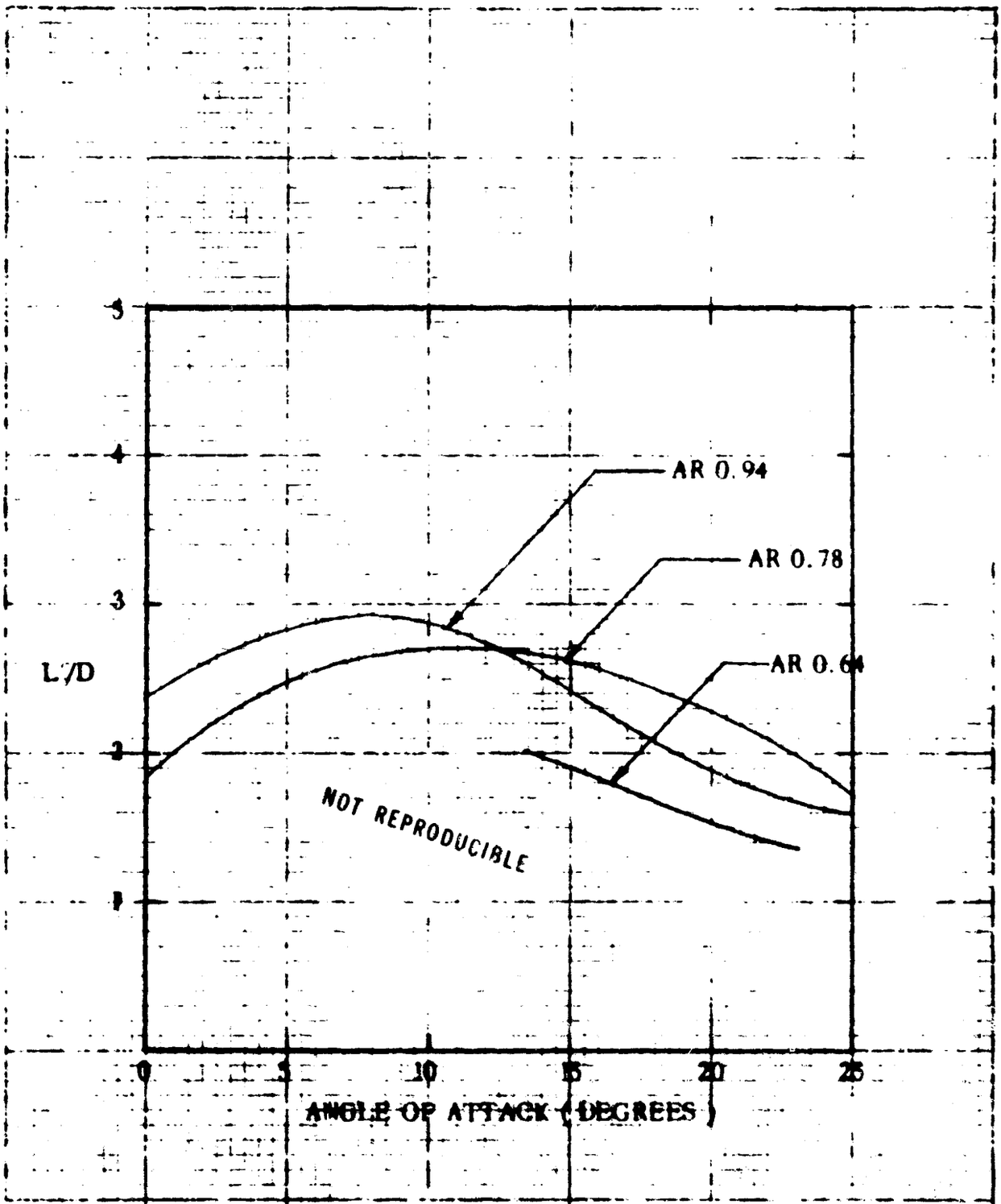

Figure 39. Early NASA Tests: Summary Lift to Drag Ratio

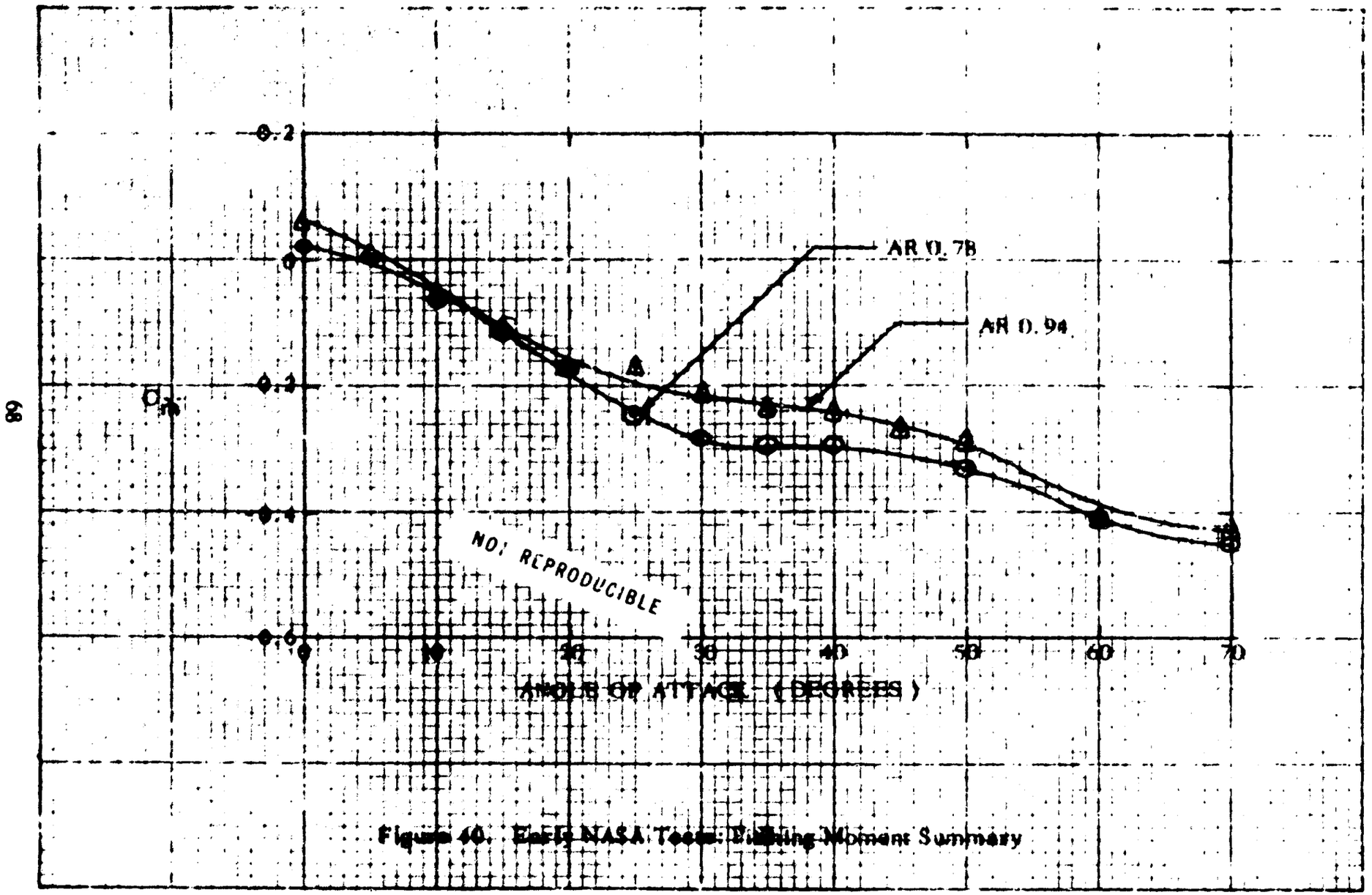

Figure 40. Earle NASA Tests: Pitching Moment Summary

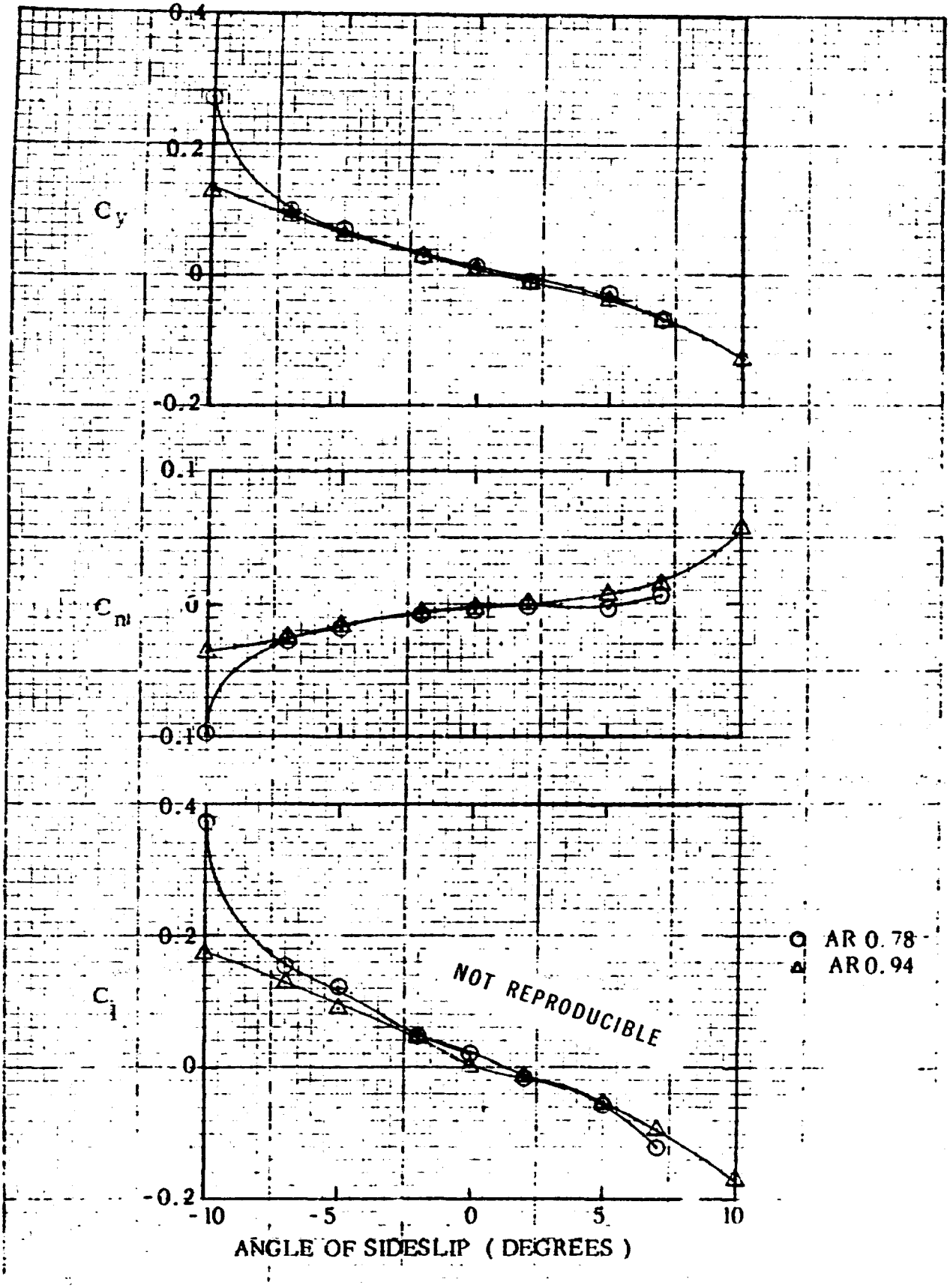

Figure 41. Early NASA Tests: Lateral - Directional Moment Summary

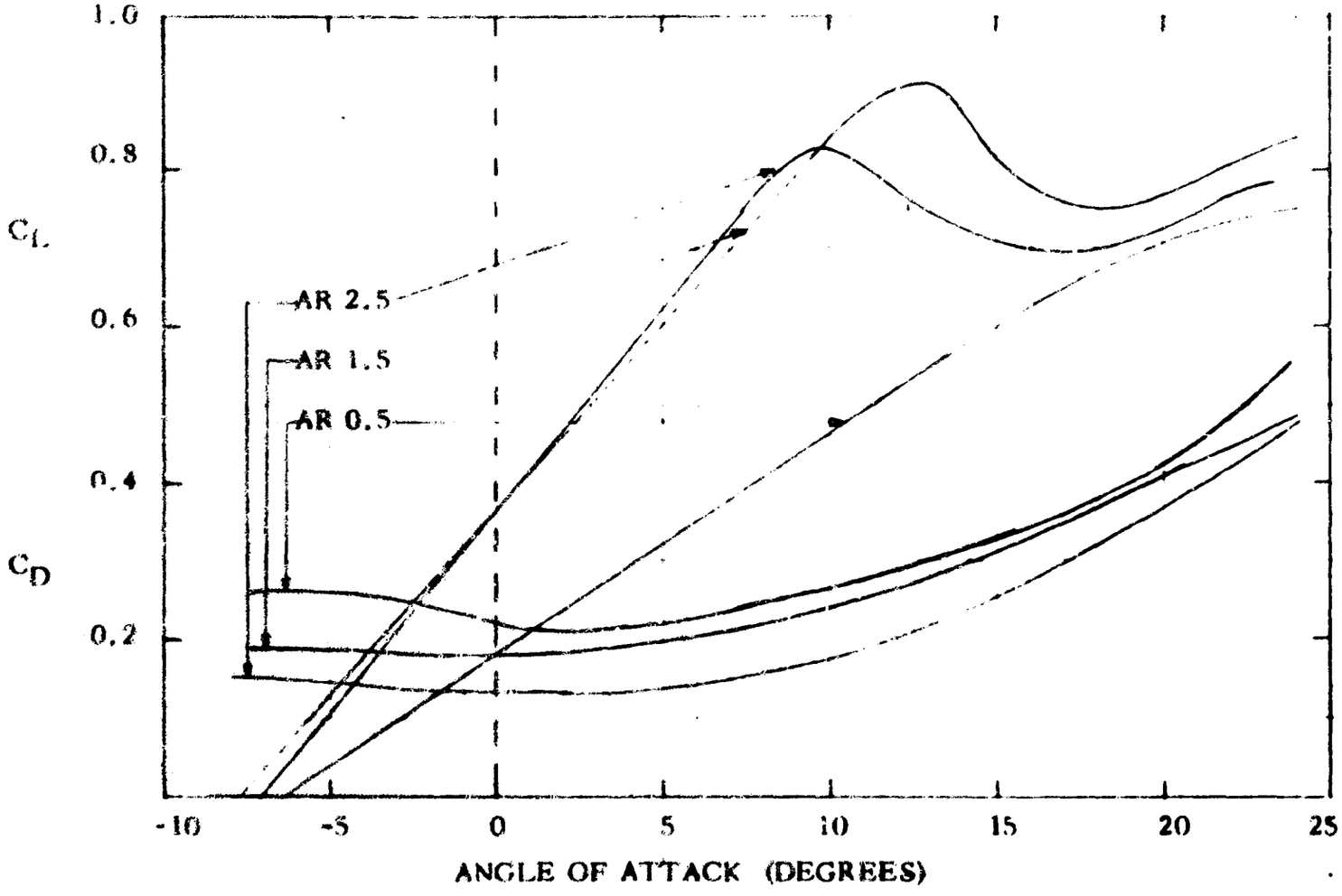

Figure 42a. Notre Dame 1967 Tests: Lift to Drag Summary Curves

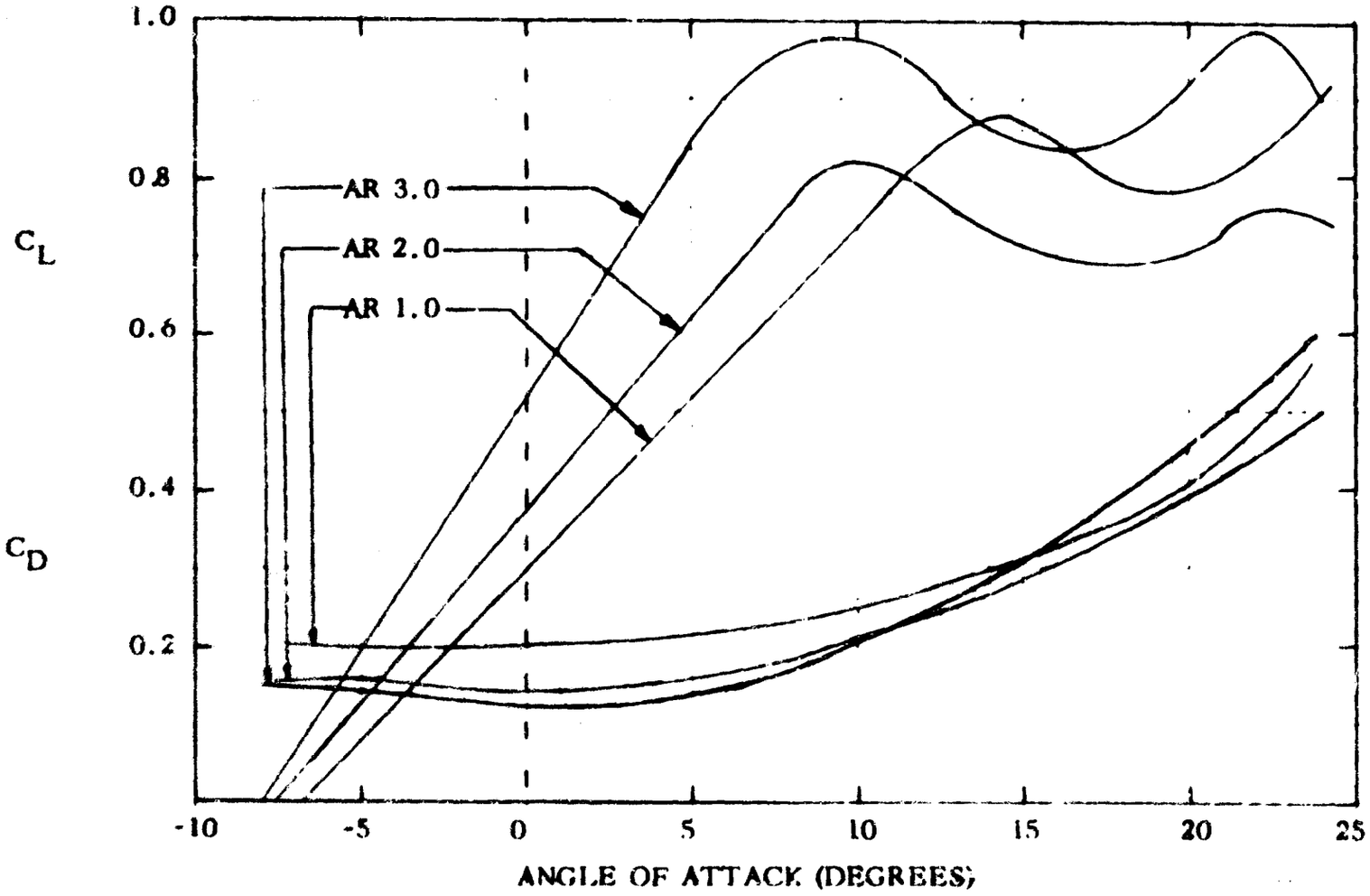

Figure 42b. Notre Dame 1967 Tests: Lift to Drag Summary Curves

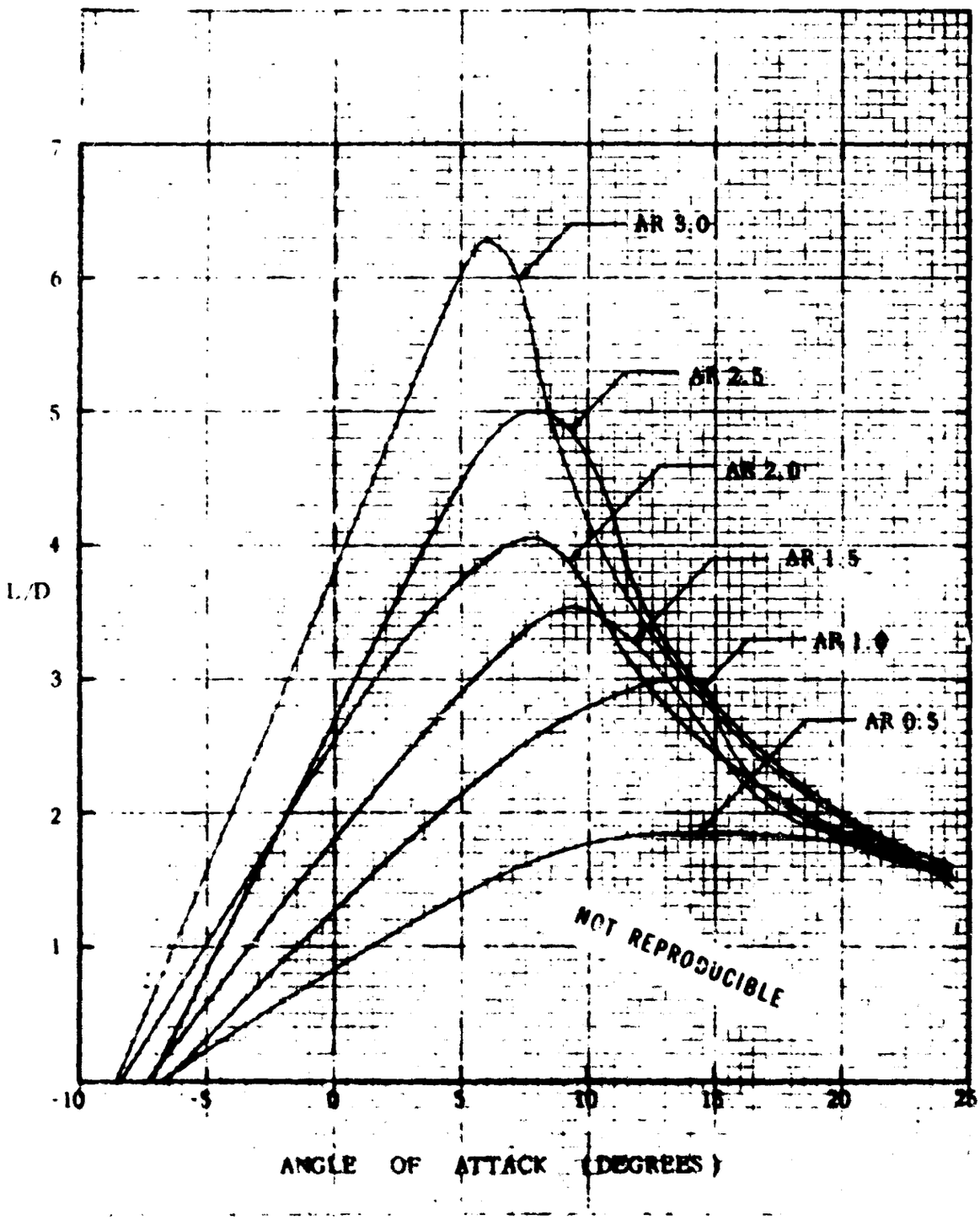

Figure 43. Notre Dame 1967 Tests: Lift to Drag Ratio Summary Curves

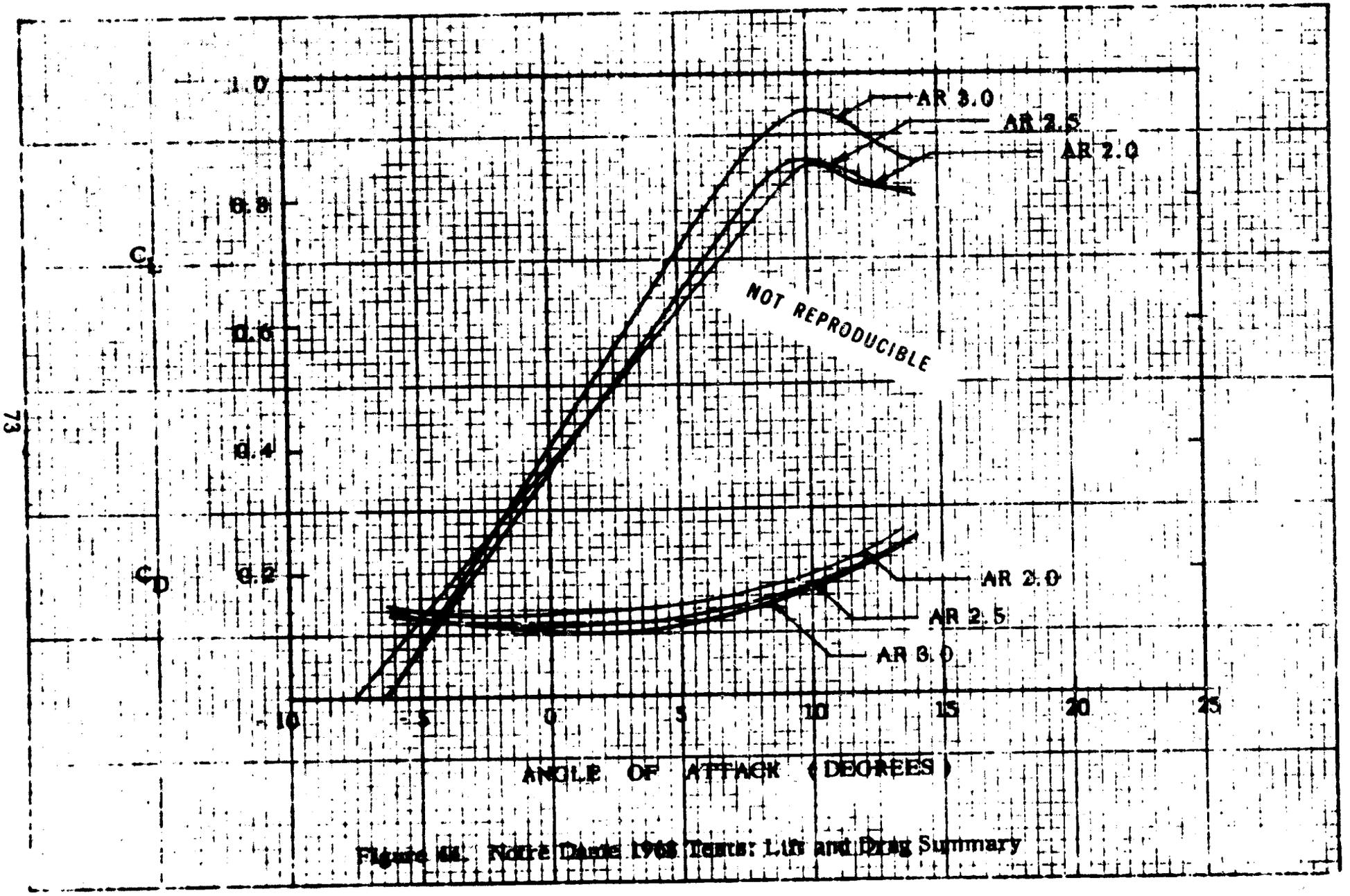

Figure 48. Notre Dame 1968 Tests: Lift and Drag Summary

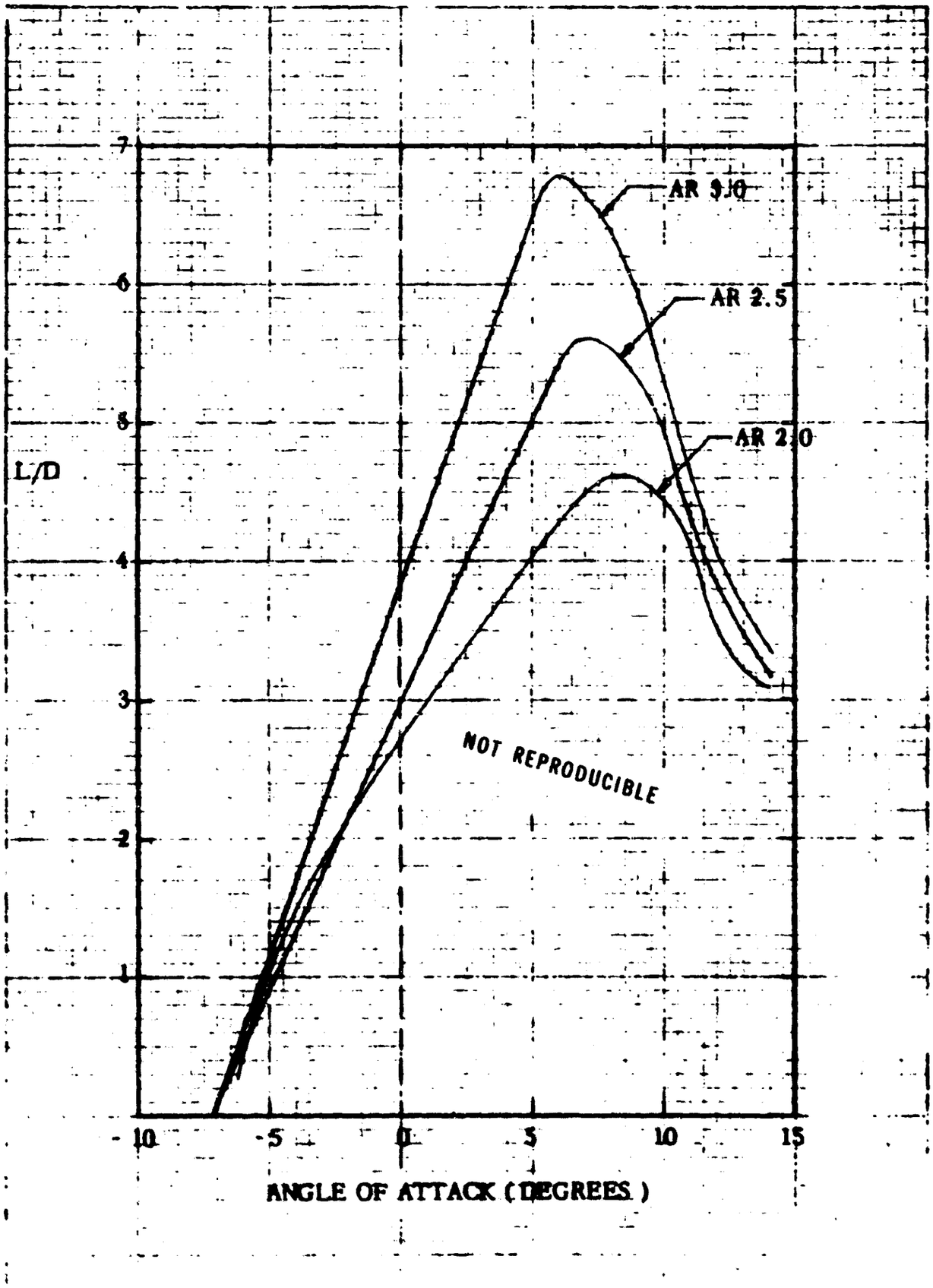

Figure 45. Notre Dame 1968 Tests: Summary Lift to Drag Ratio

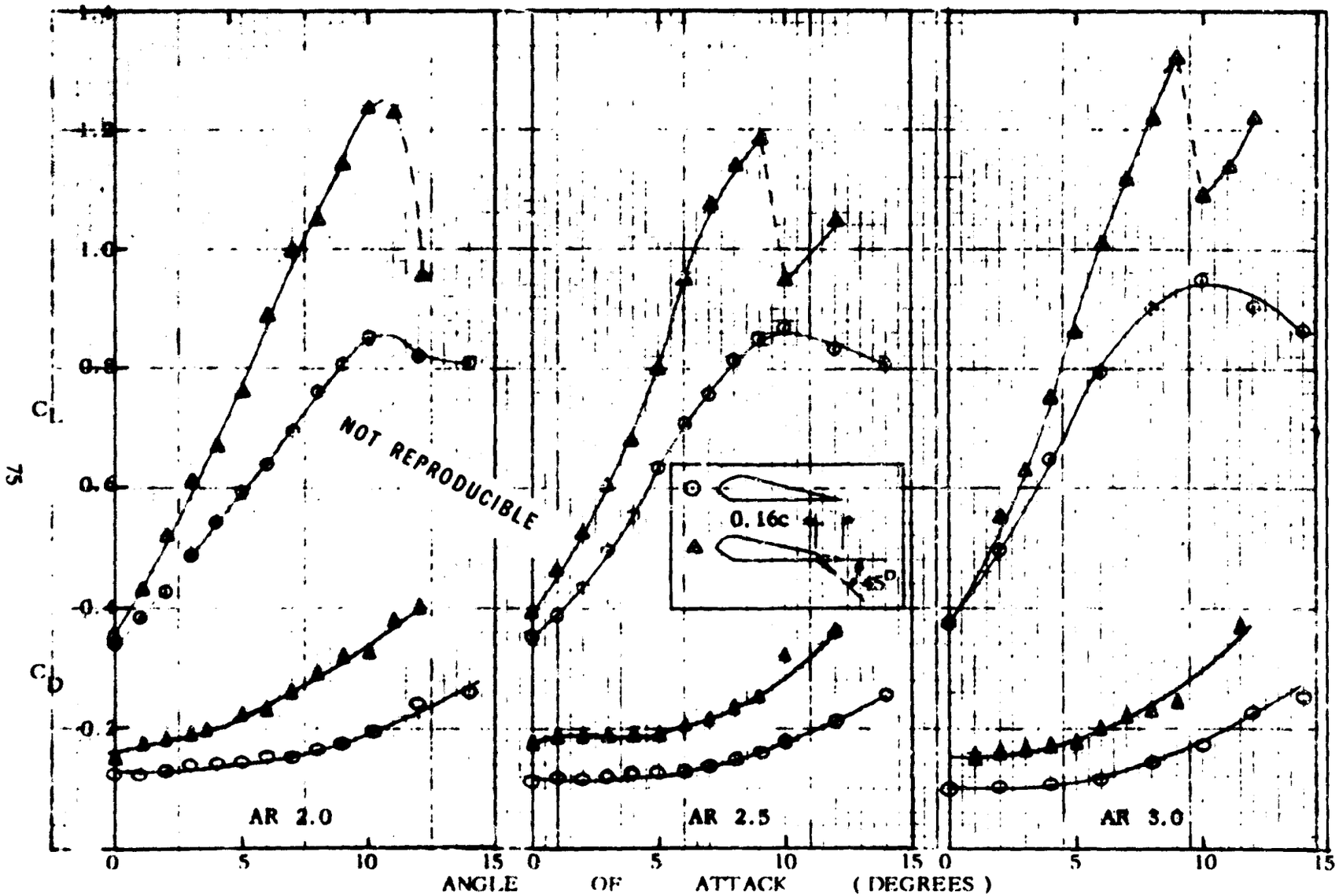

Figure 40. Notre Dame 1968 Tests: Flap Deflection Summary Lift Curves

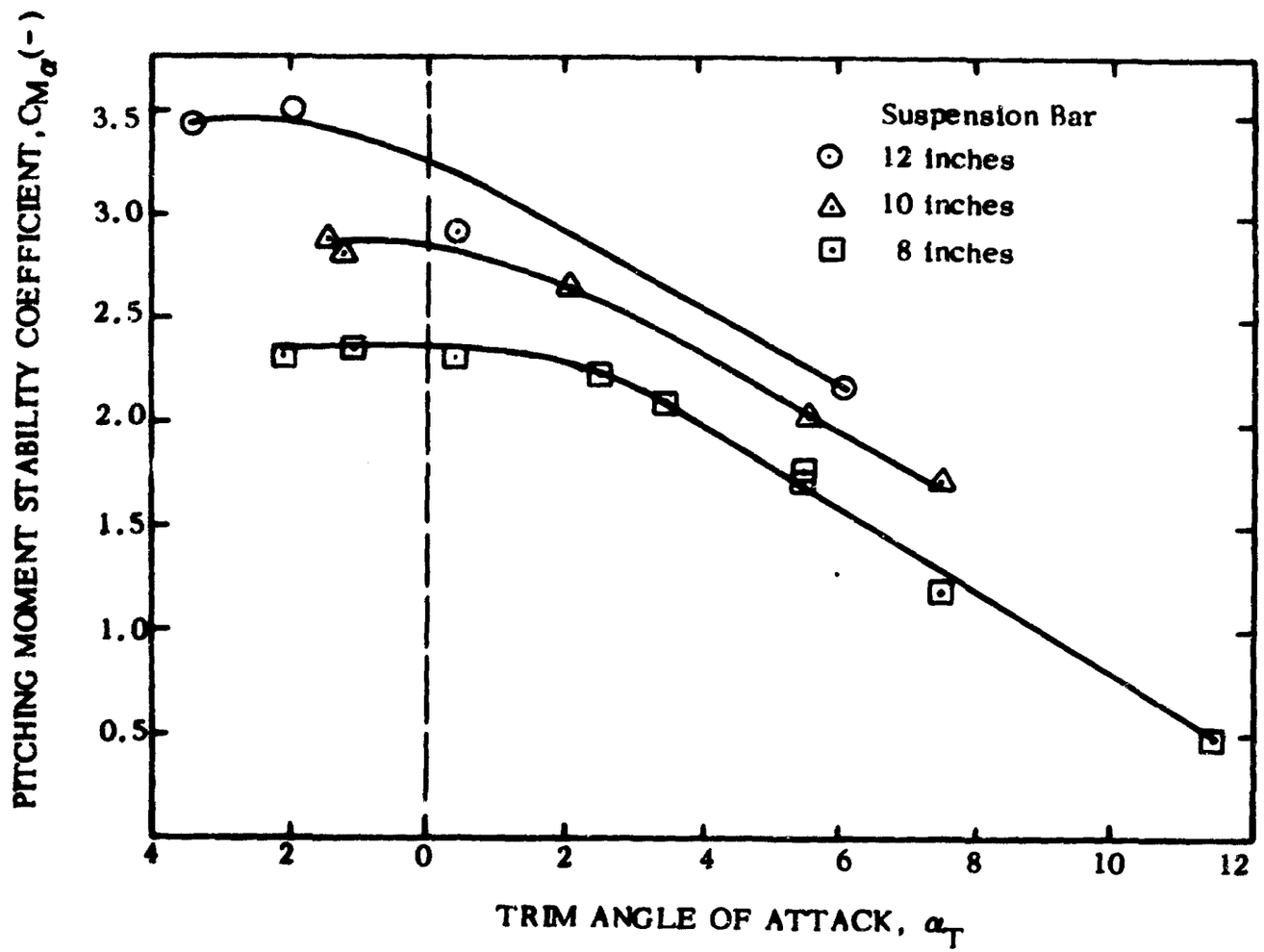

Fig. 47a. Variation of the Pitching Moment Stability Coefficient with Trim Angle.

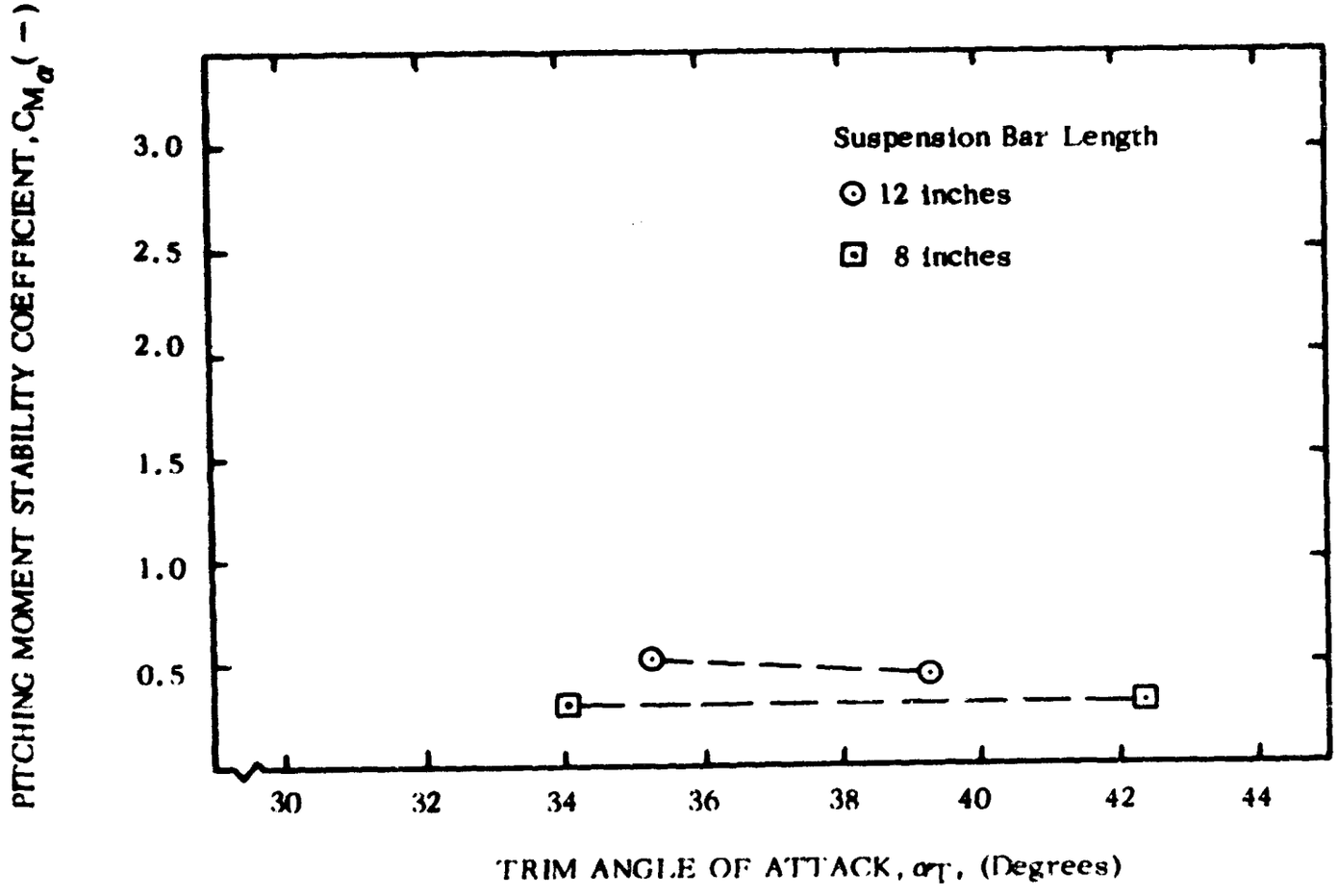

Figure 47b. Variation of Pitching Moment Stability Coefficient with Trim Angle.

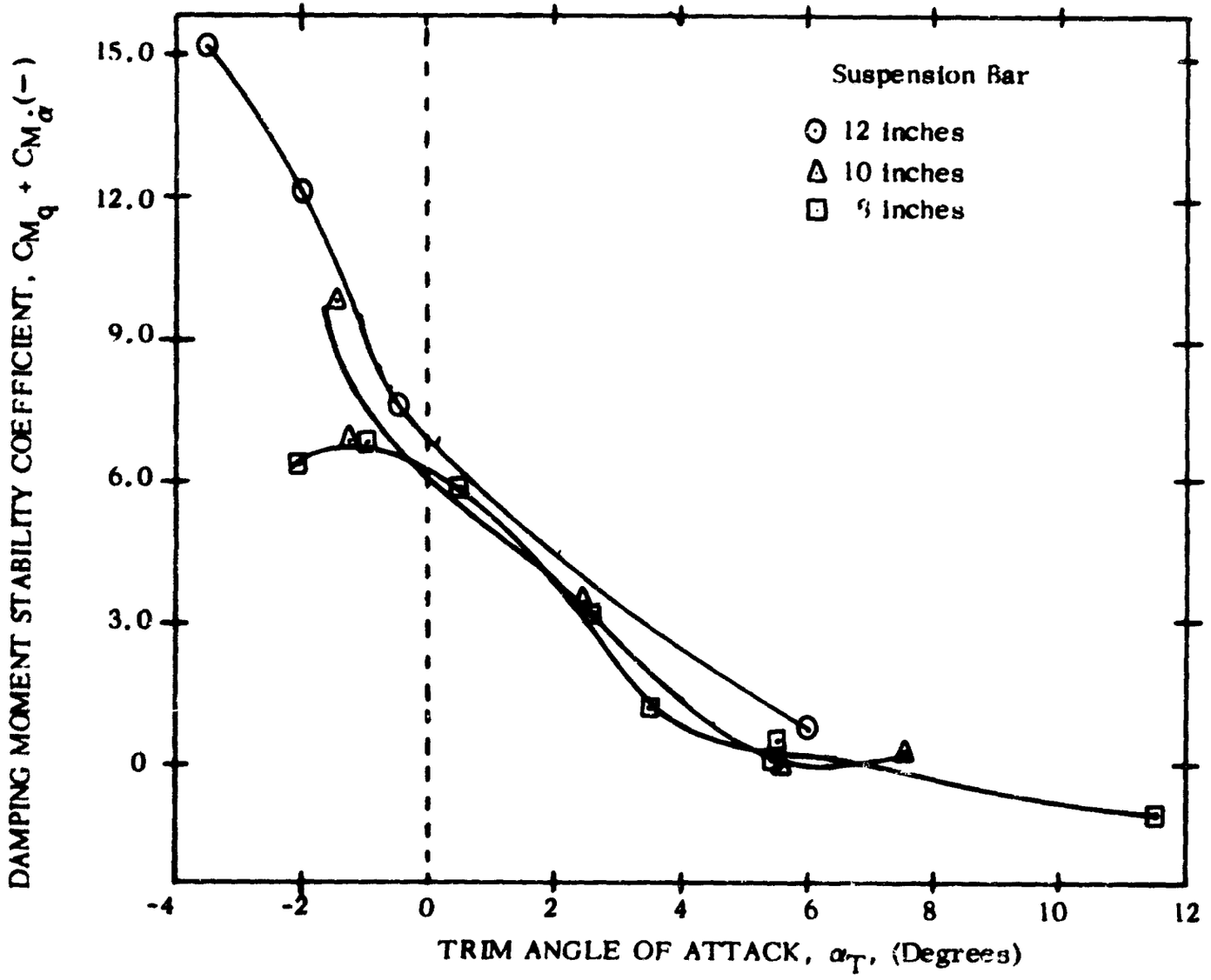

Figure 48a. Variation of Damping Moment Stability Coefficient with Trim Angle

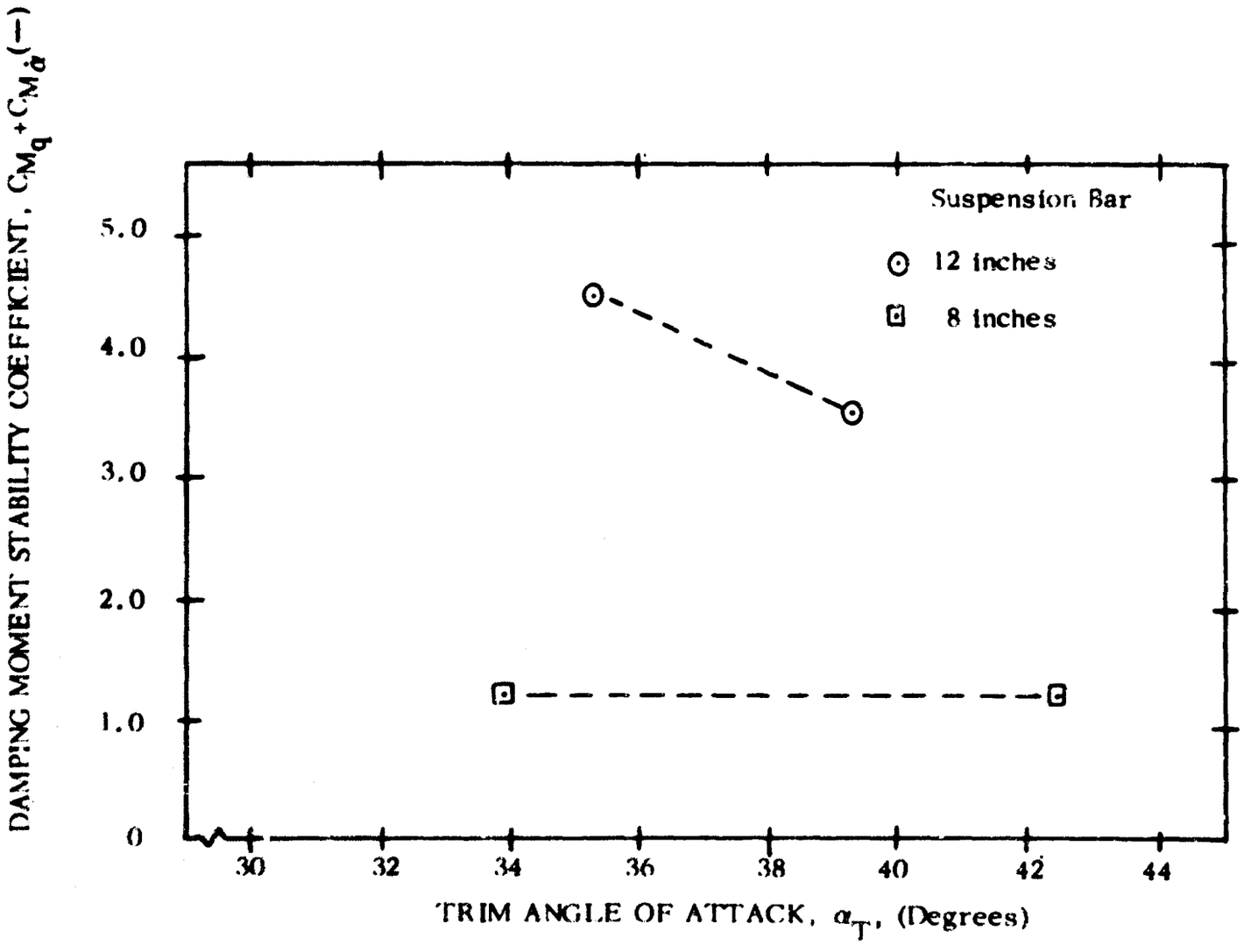

Figure 48b. Variation of Damping Moment Stability Coefficient with Trim Angle

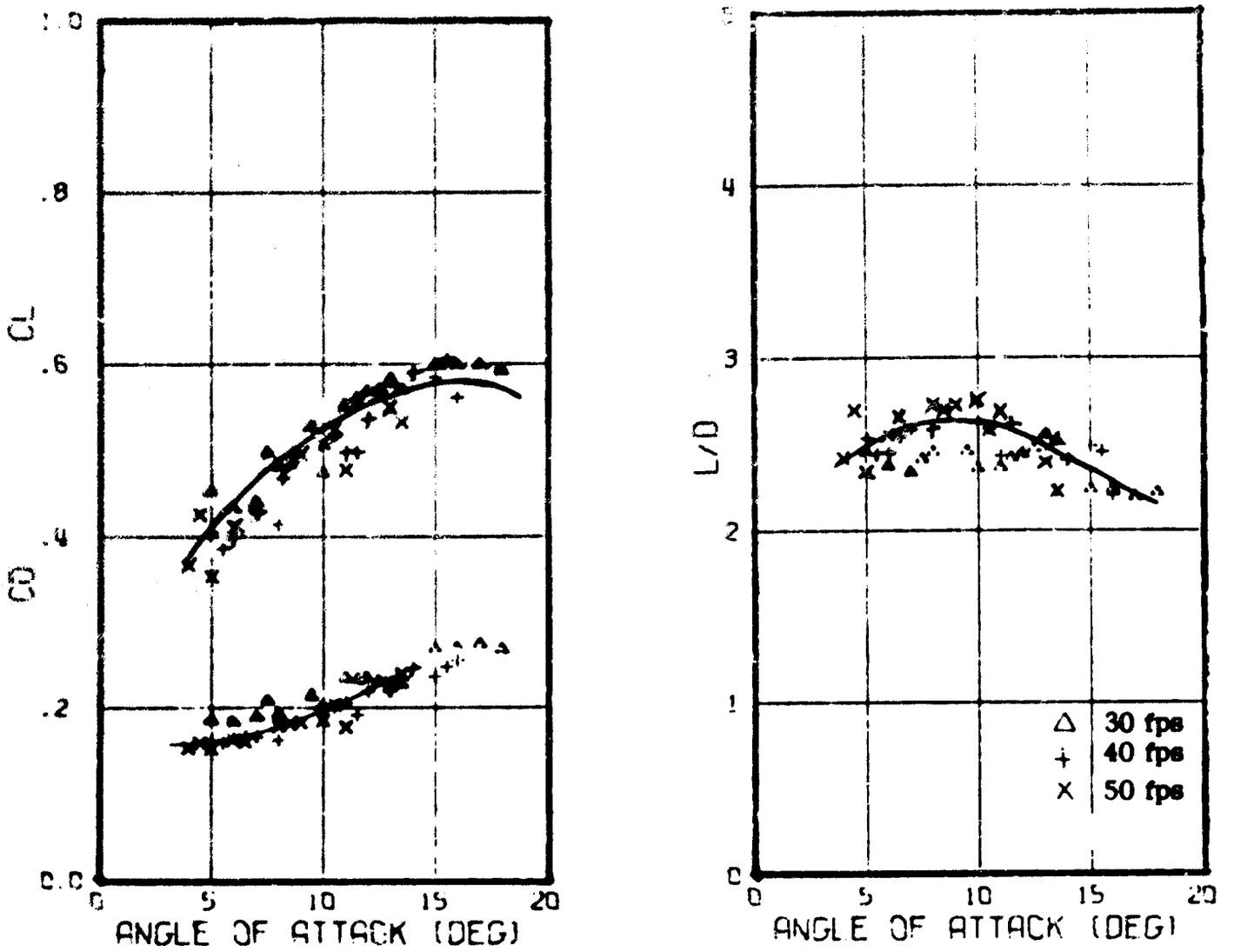

Figure 49. NASA Tether Tests: AR 1.0 Speed Summary

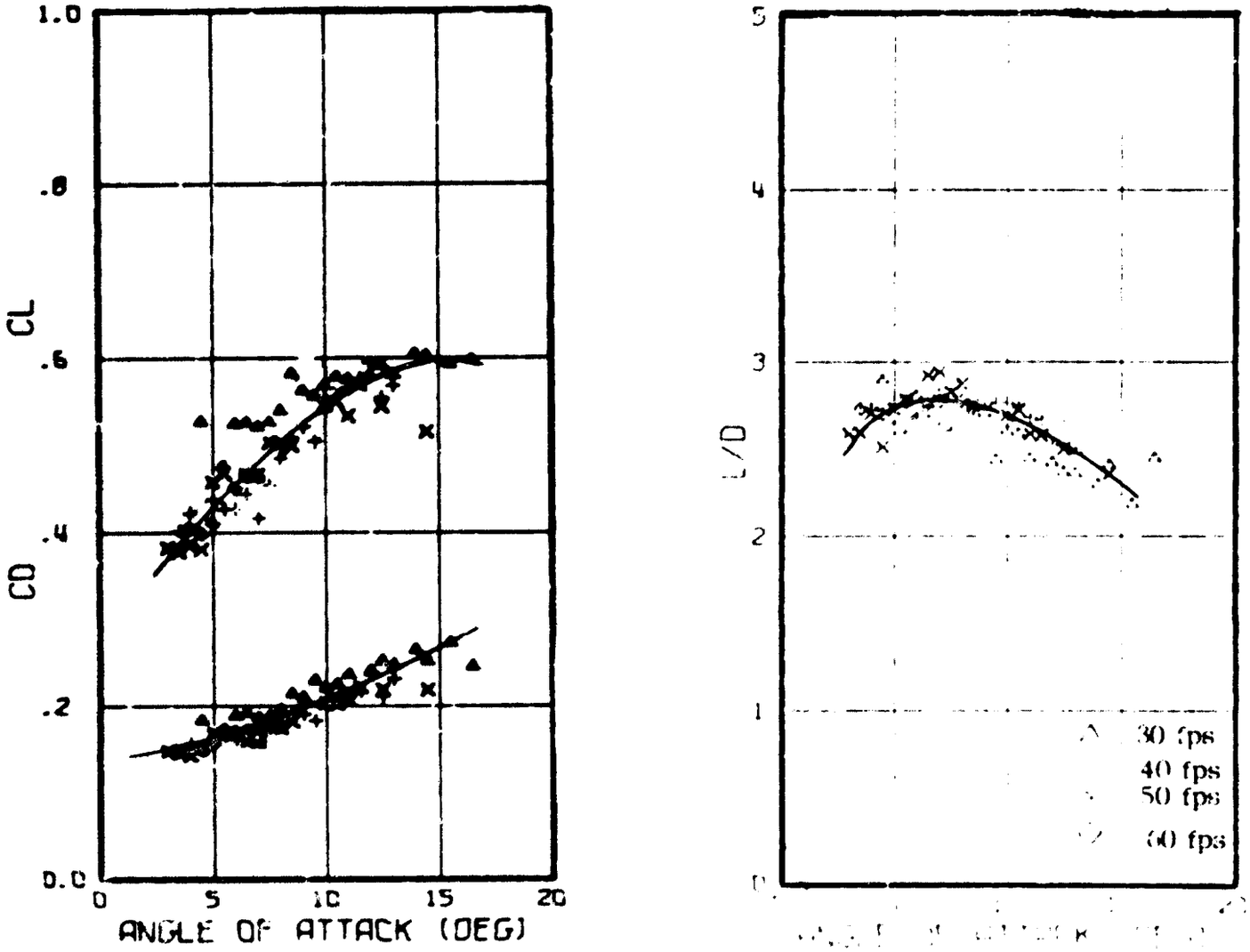

Figure 50. NASA Tether Tests: AR 1.5 Speed Summary

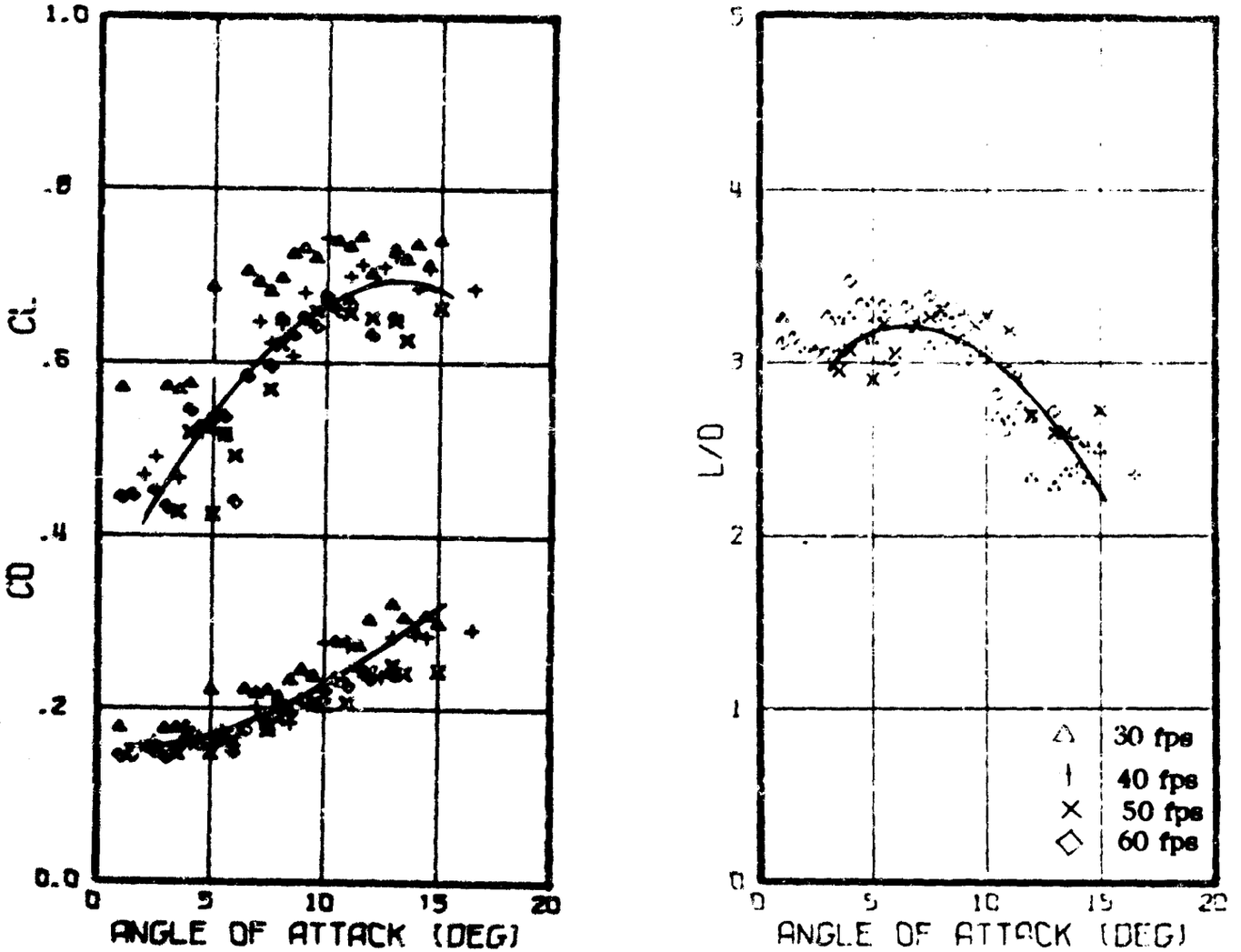

Figure 51. NASA Tether Teats: AR 2.0 Speed Summary

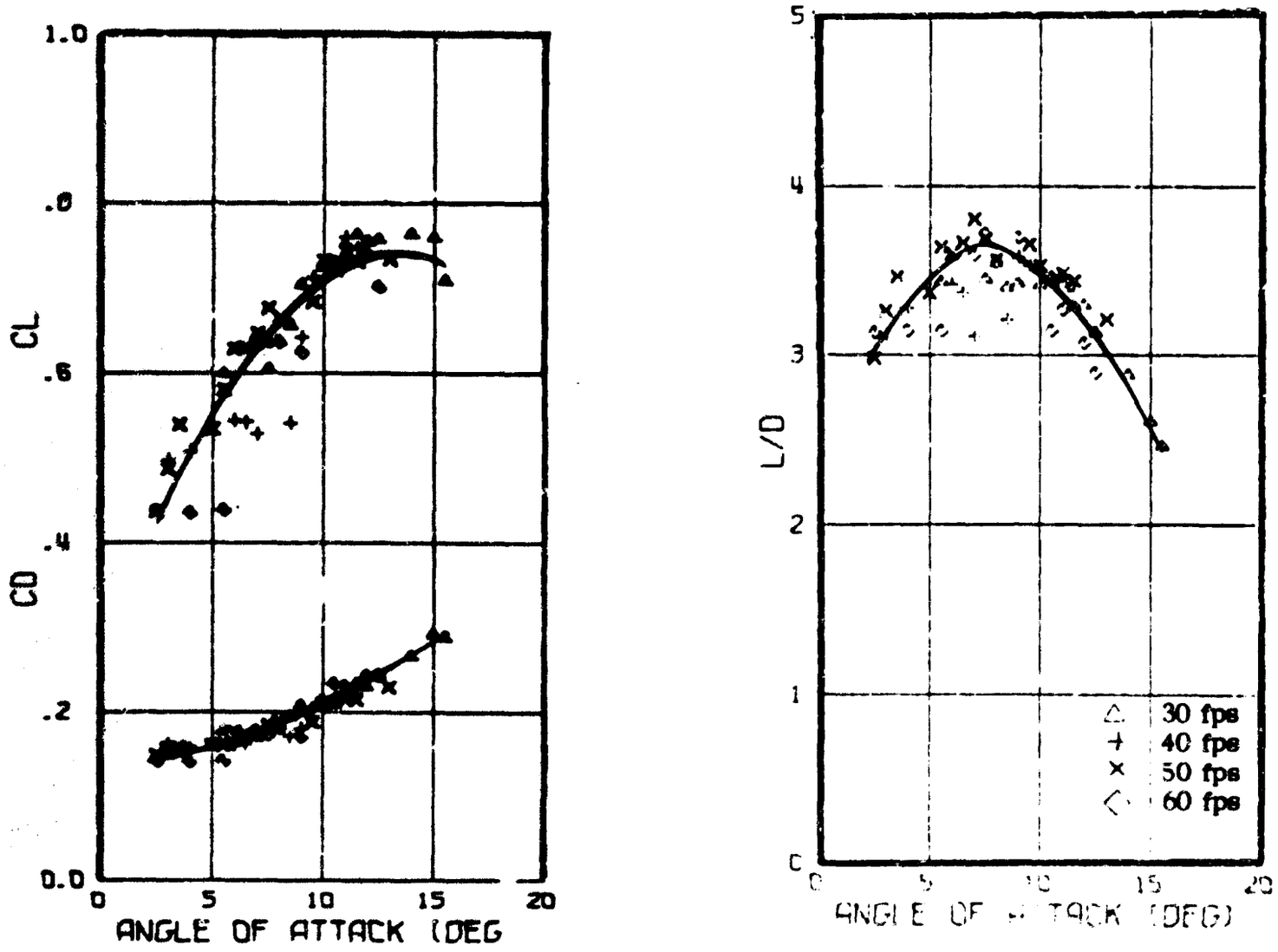

Figure 52. NASA Tether Tests: AR 2.5 Speed Summary

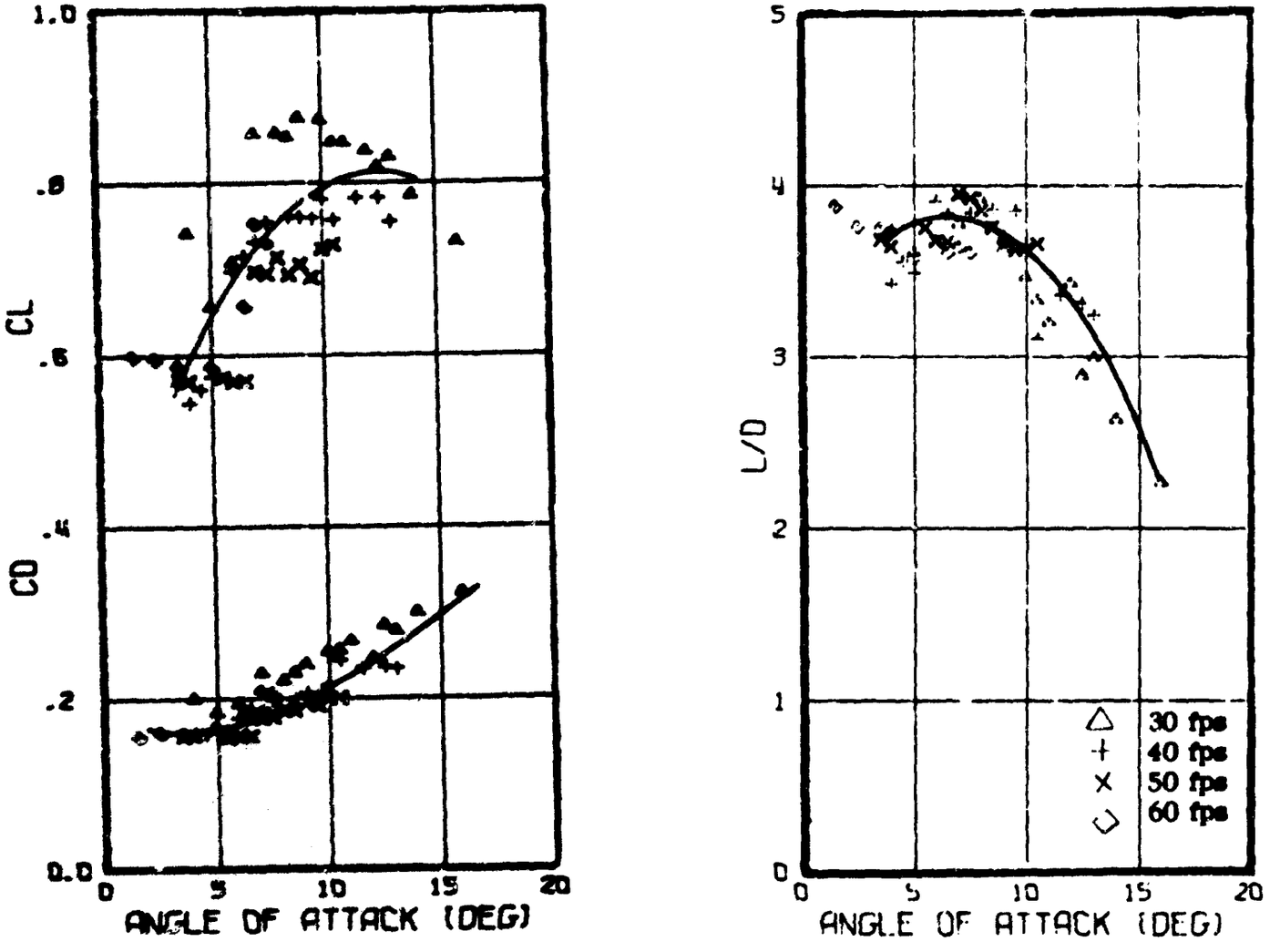

Figure 53. NASA Tether Tests: AR 3.0 Speed Summary

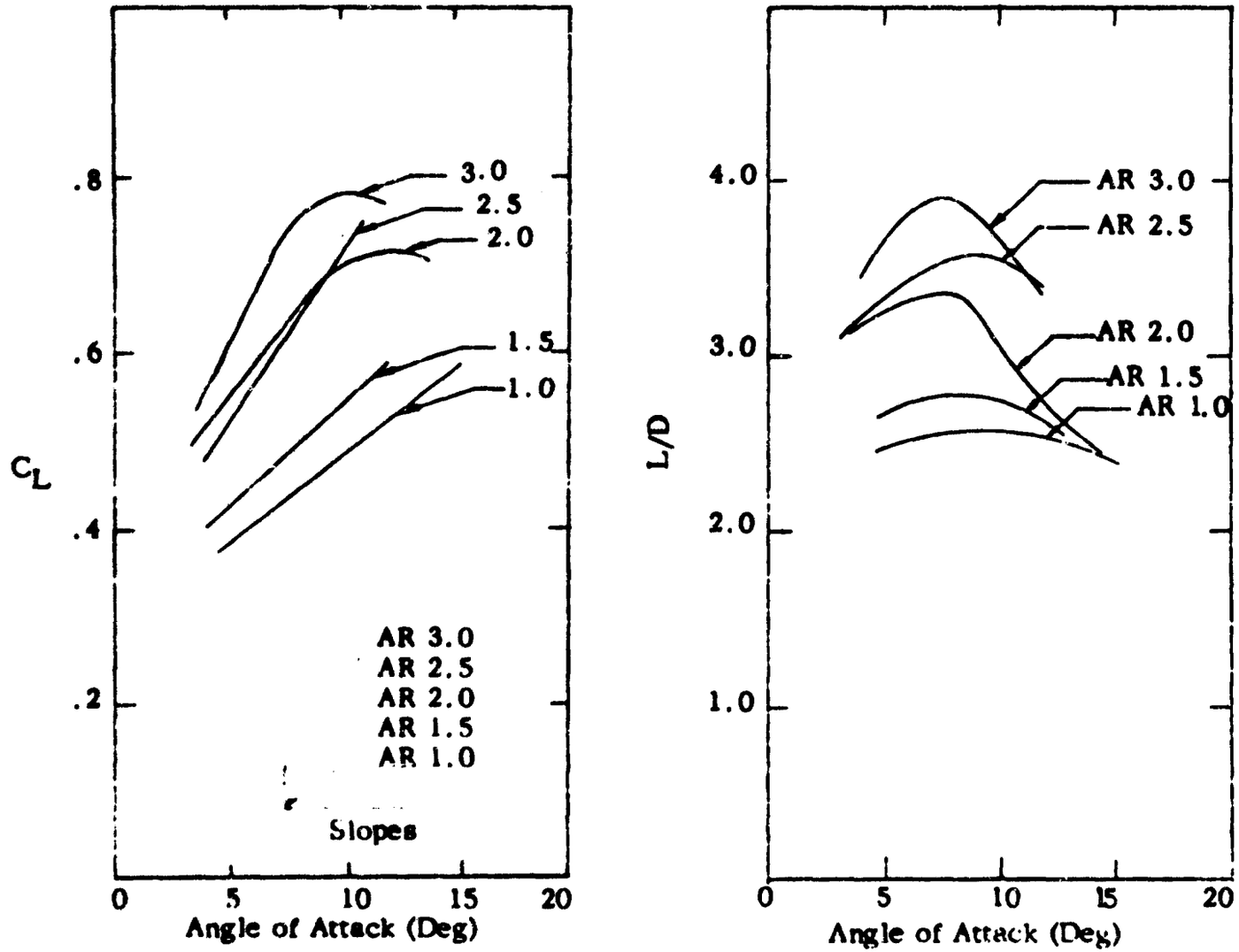

Figure 54. NASA Tether Tests: AR Summary at 40 feet per second

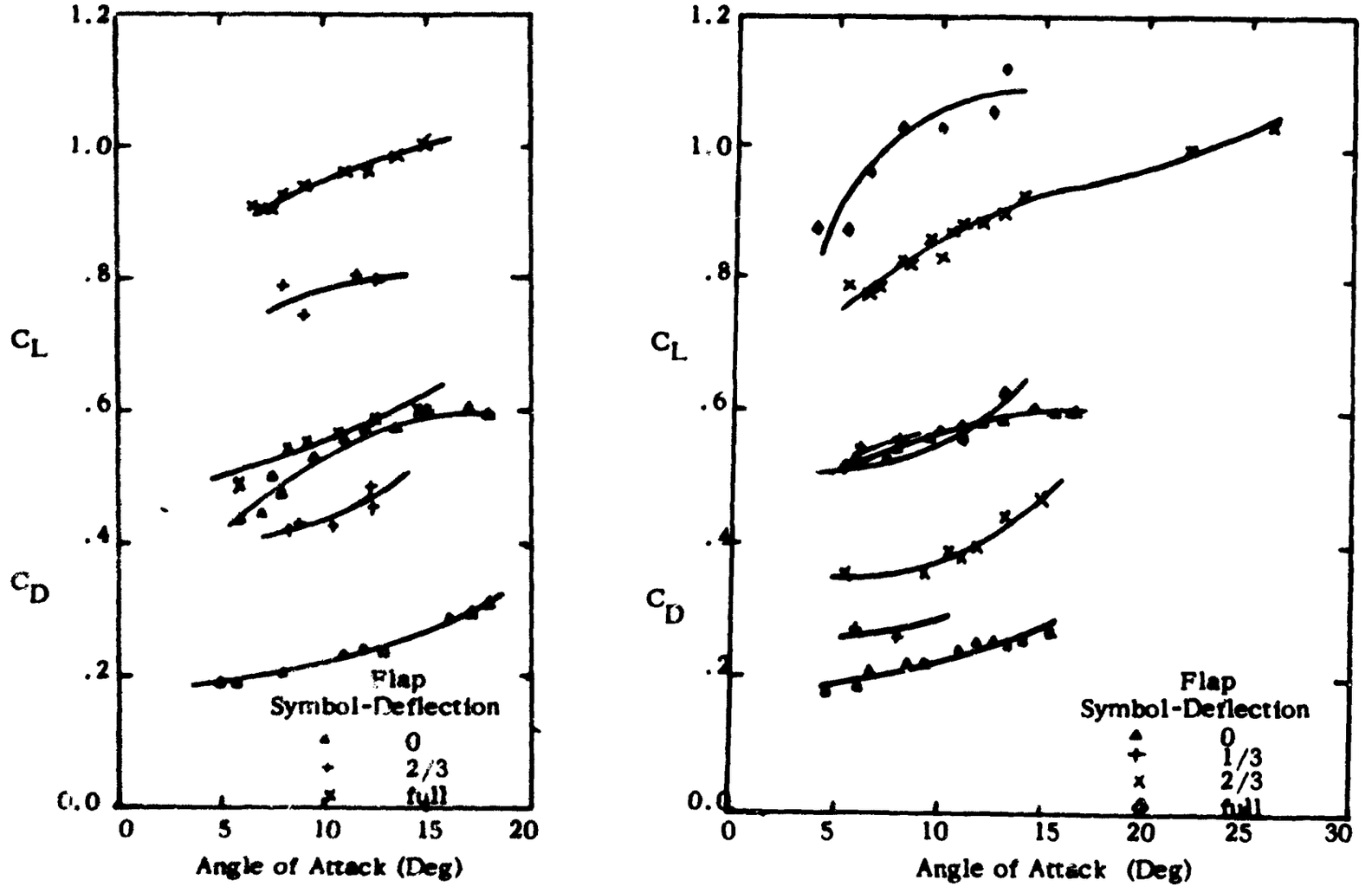

Figure 55. C_L and C_D vs α. Tether Flap Deflection at 30 fps.

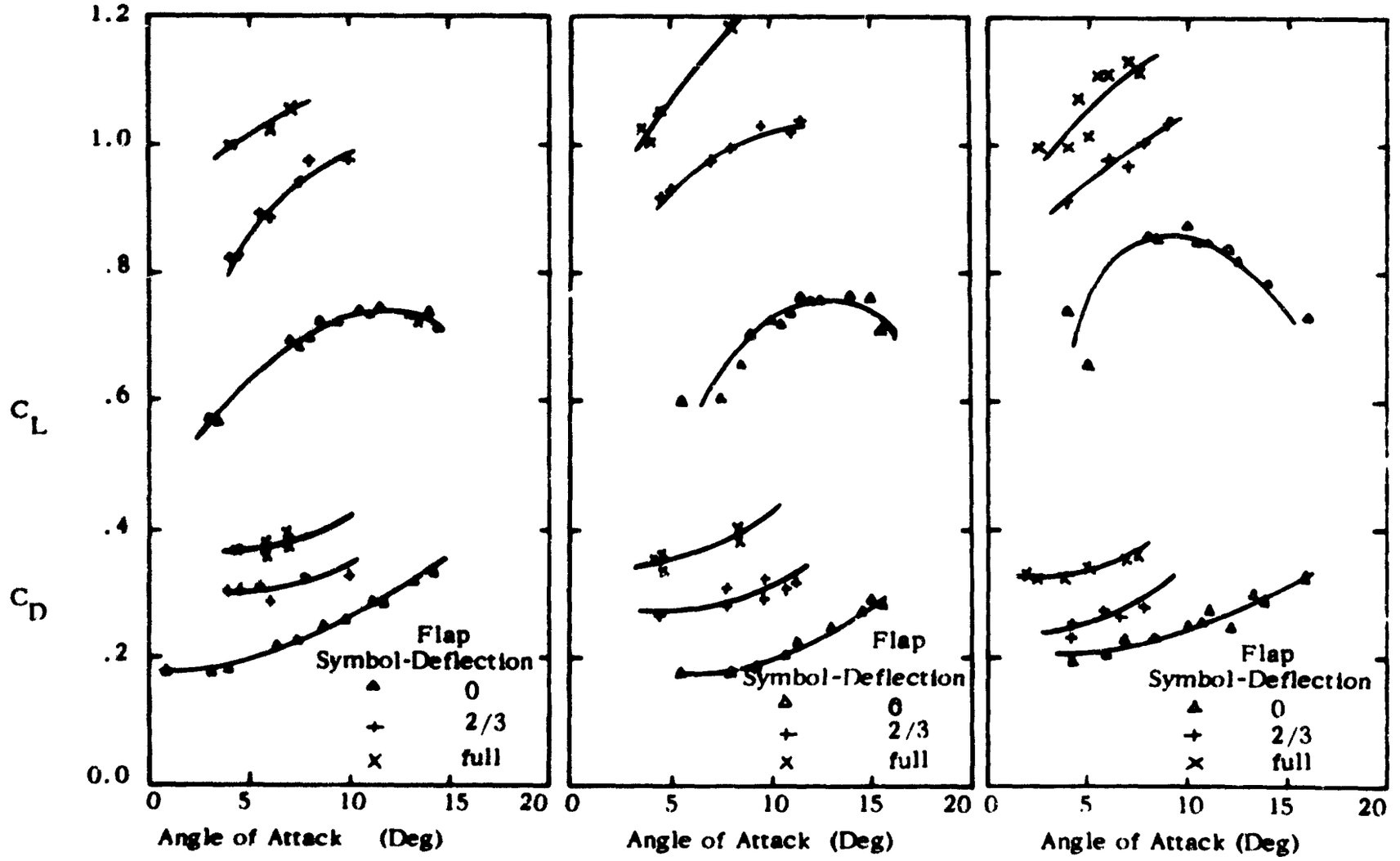

Figure 55 (continued). C_L and C_D vs α. Tether Flap Deflection at 30 fps.

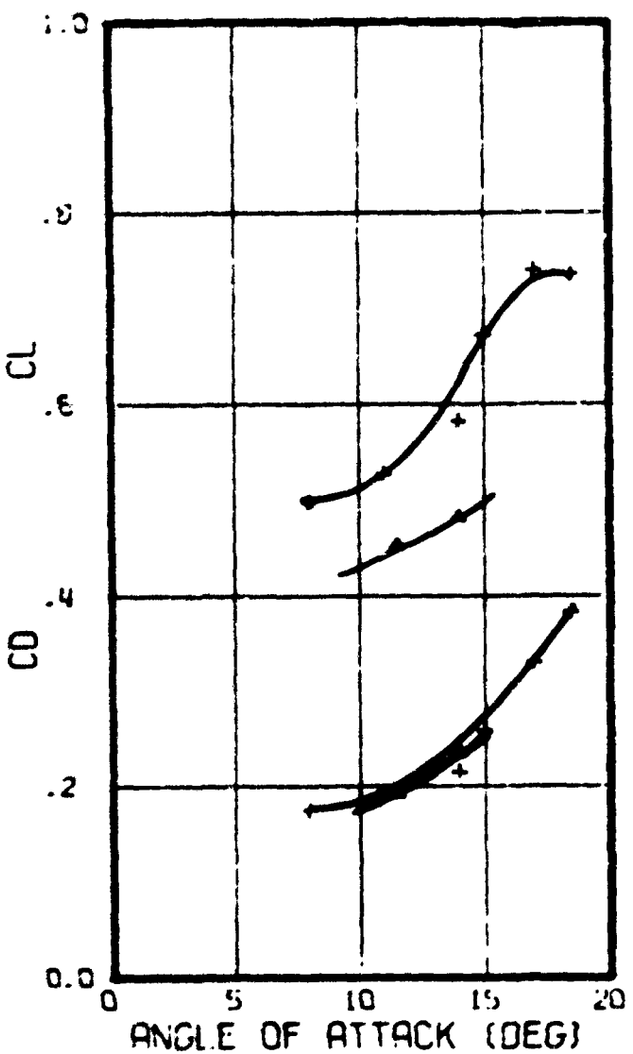

(a) V = 30 fps

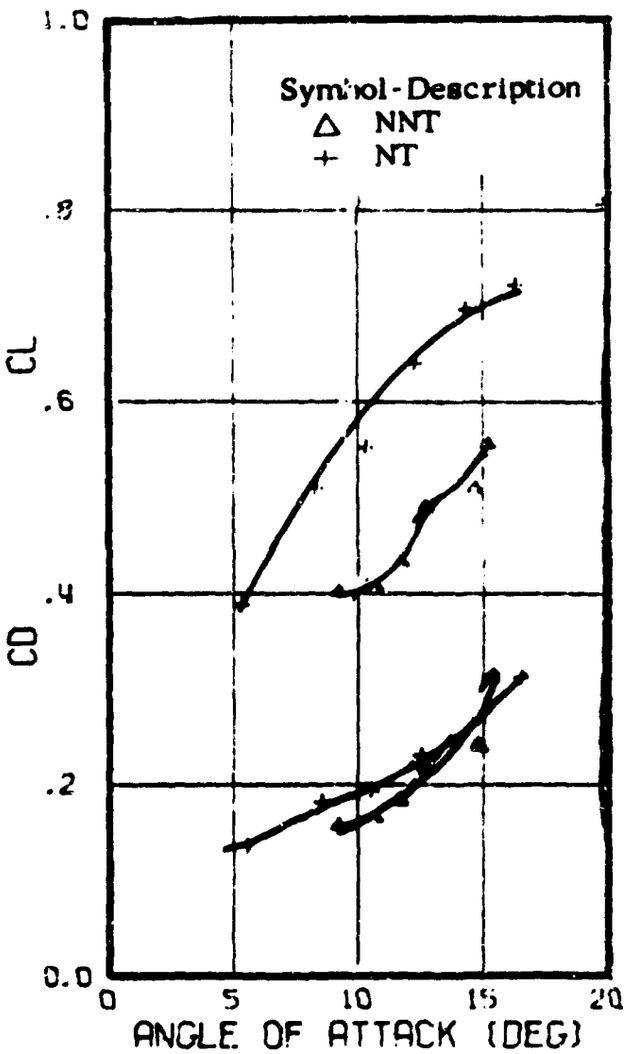

(b) V = 40 fps

Figure 56. C_D & C_L vs α, Tether AR Model 1.0 with Leading Edge Opening Changed (without line drag)

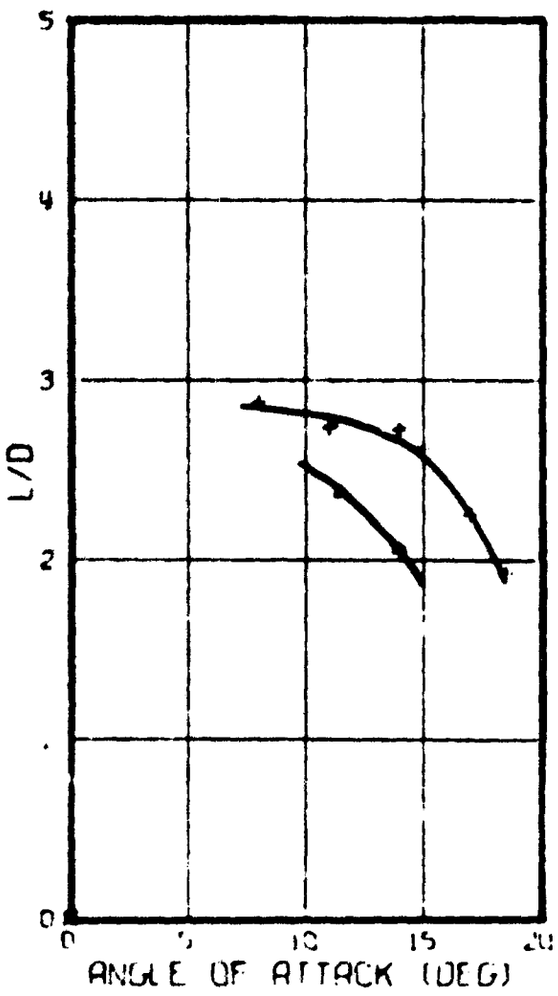

(a) V = 30 fps

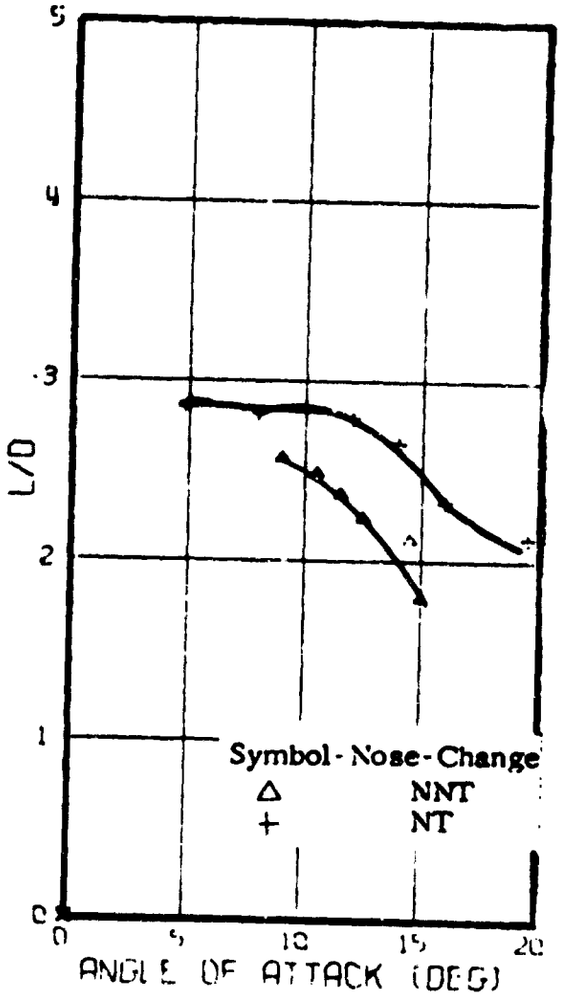

(b) V = 40 fps

Figure 57. L/D vs α. Tether AR 1.0 Model with Leading Edge Opening Changed (without line drag)

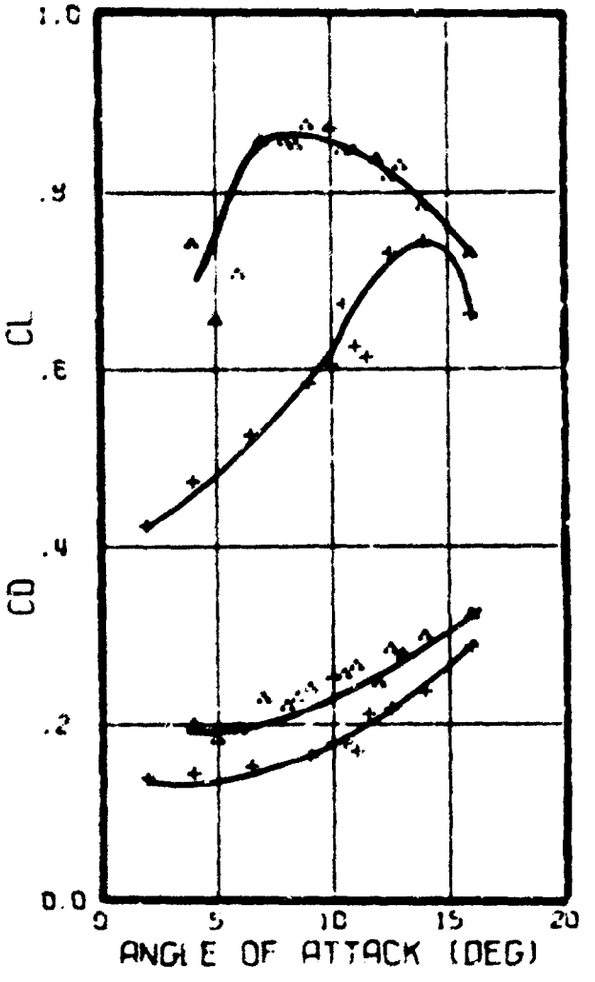

(a) 30 fps

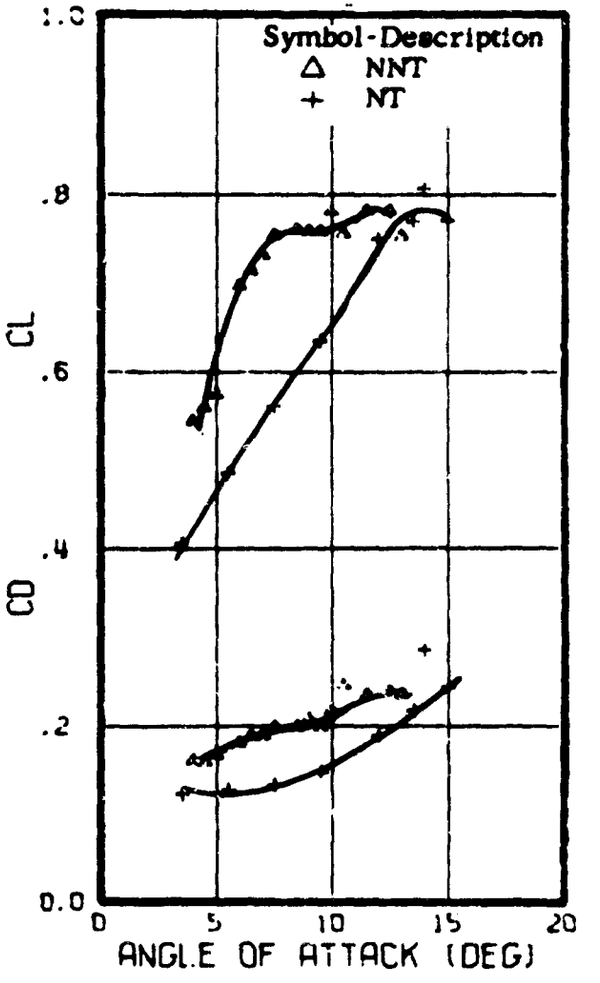

(b) 40 fps

Figure 58. C_D & C_L vs α . Tether AR 3.0 Model w/Leading Edge Opening Changed without line drag

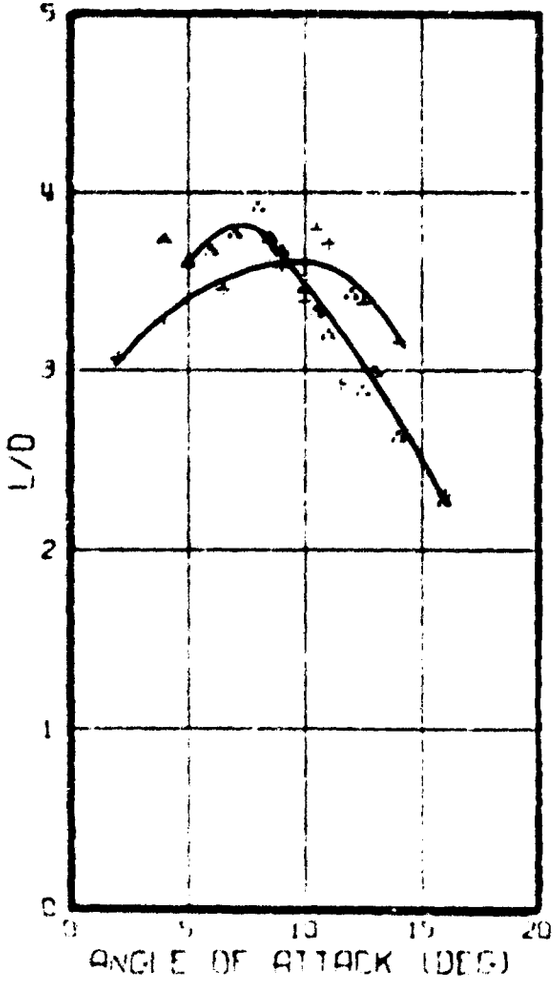

(a) 30 fps

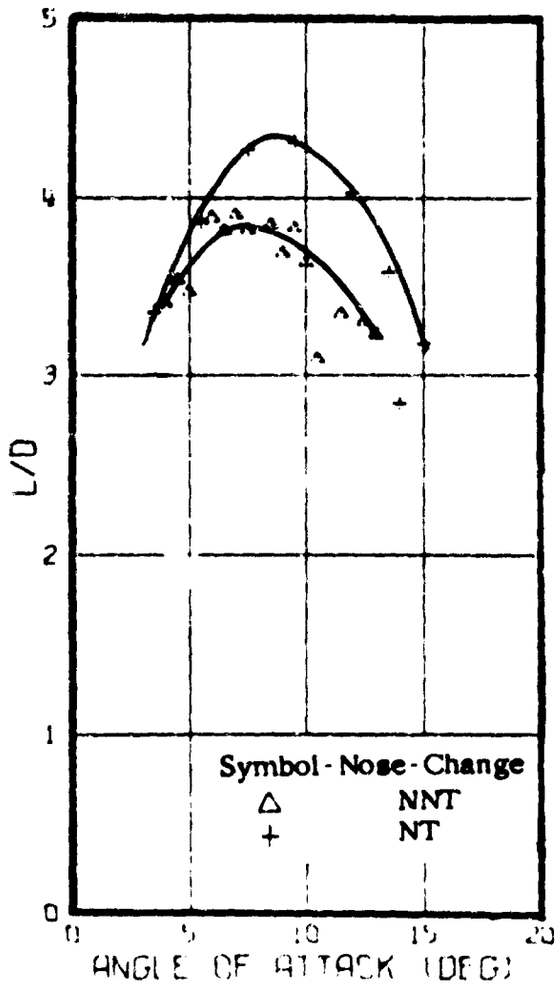

(b) 40 fps

Figure 59. L/D vs α. Tether AR 3.0 Model with Leading Edge Opening Changed (without line drag)

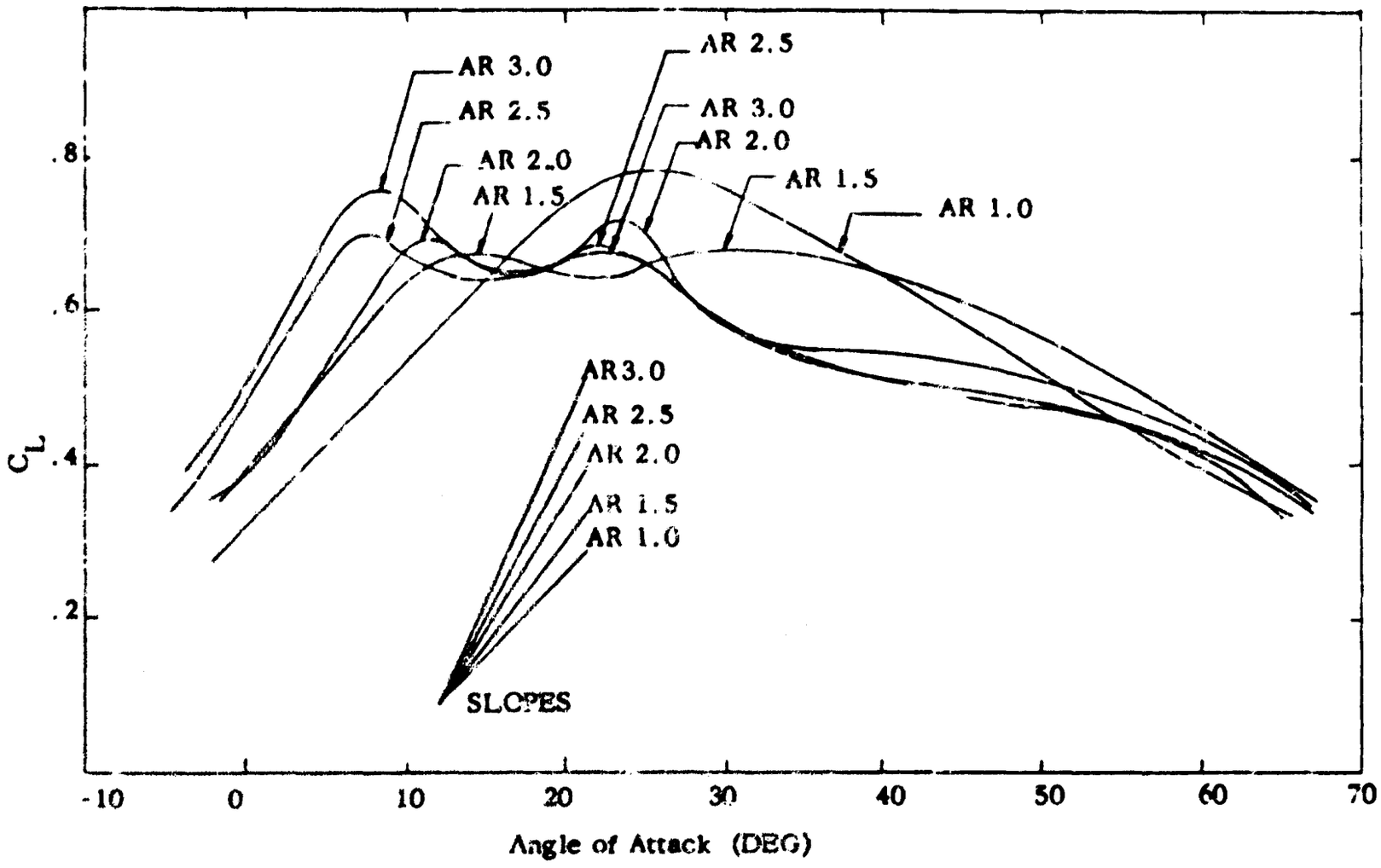

Figure 60. C_L vs α . Strut AR Summary at 40 fps.

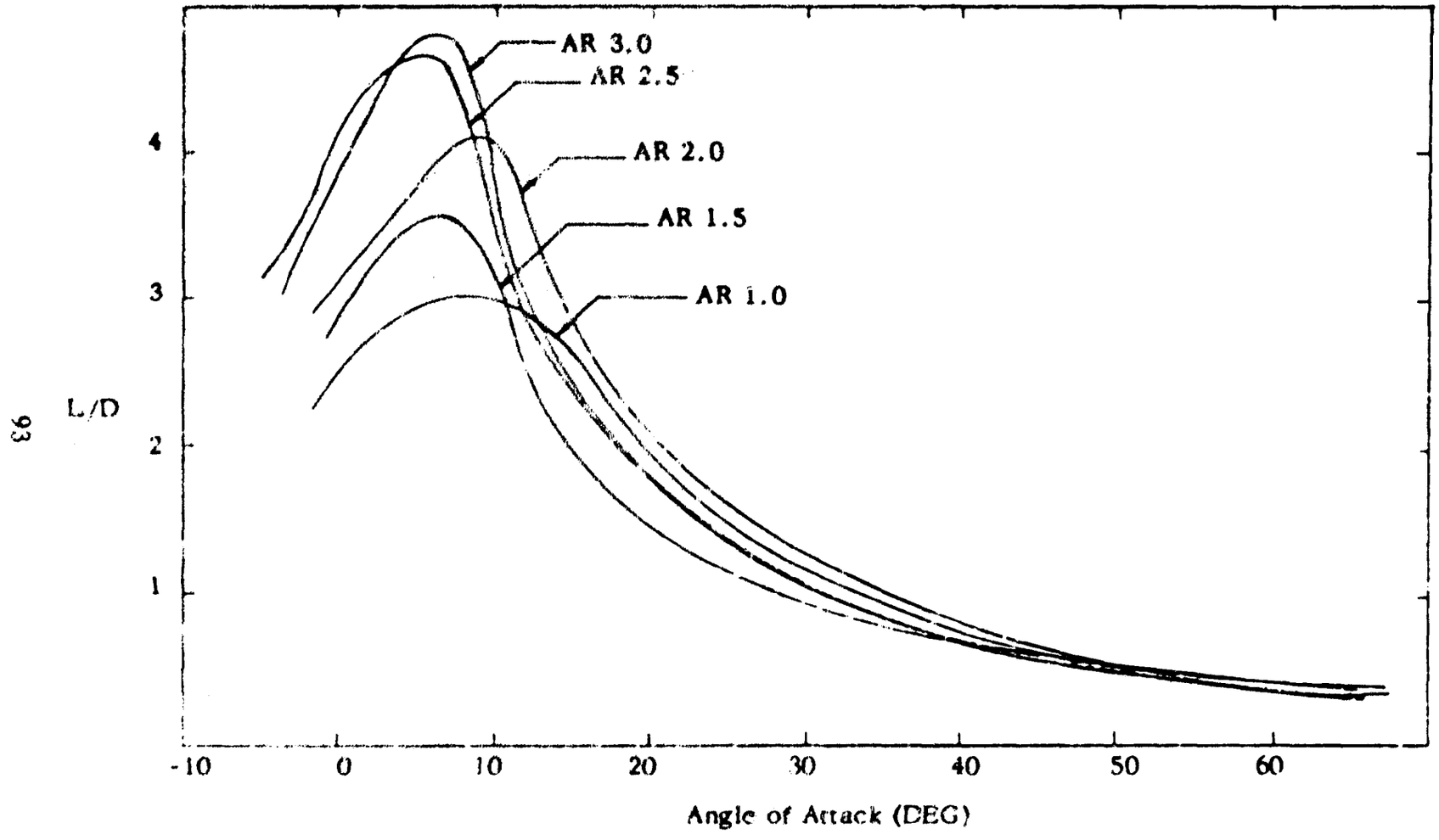

Figure 61. L/D vs α. Strut AR Summary without line drag at 40 fps.

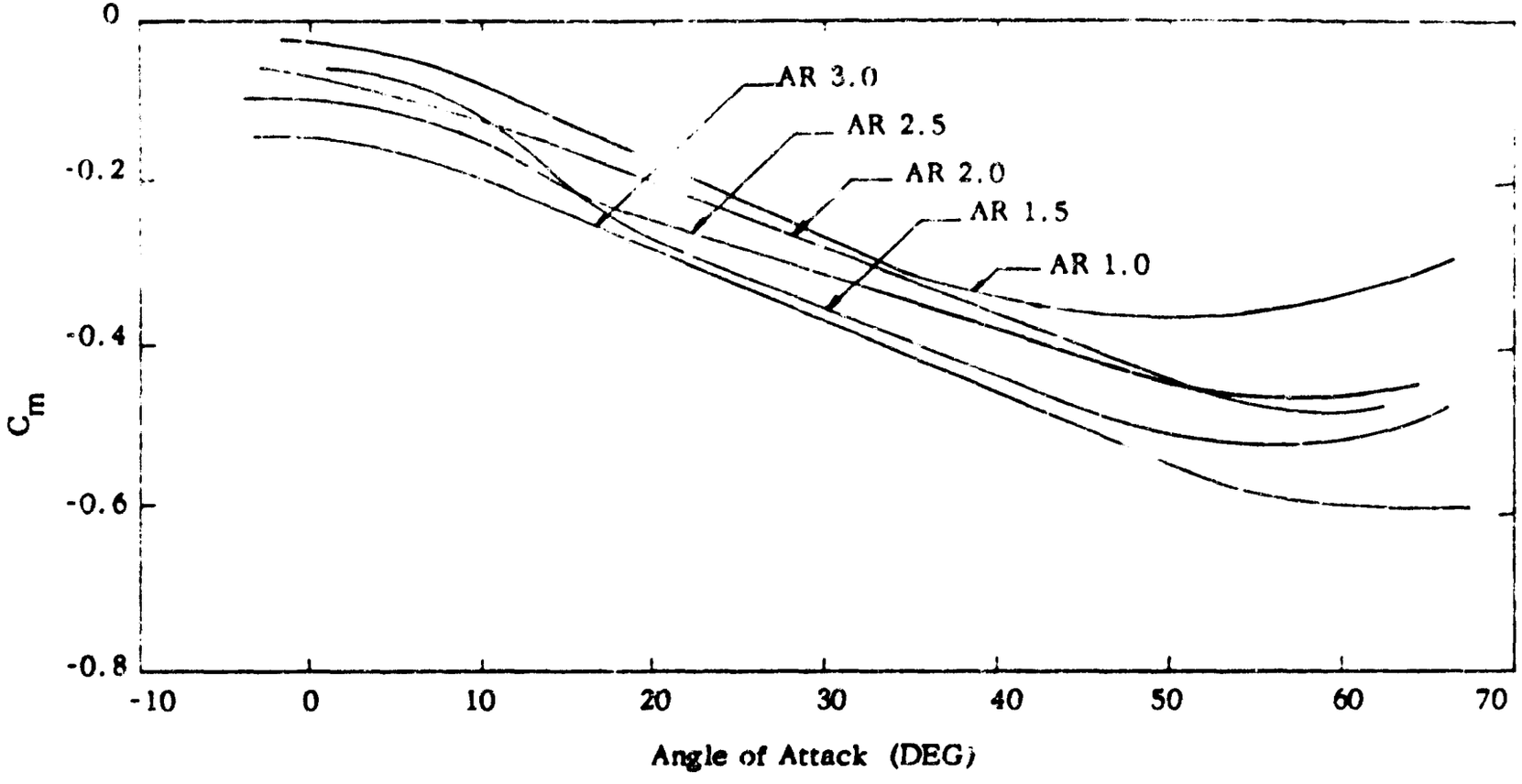

Figure 62. C_m vs α . Strut AR Summary at 50 fps

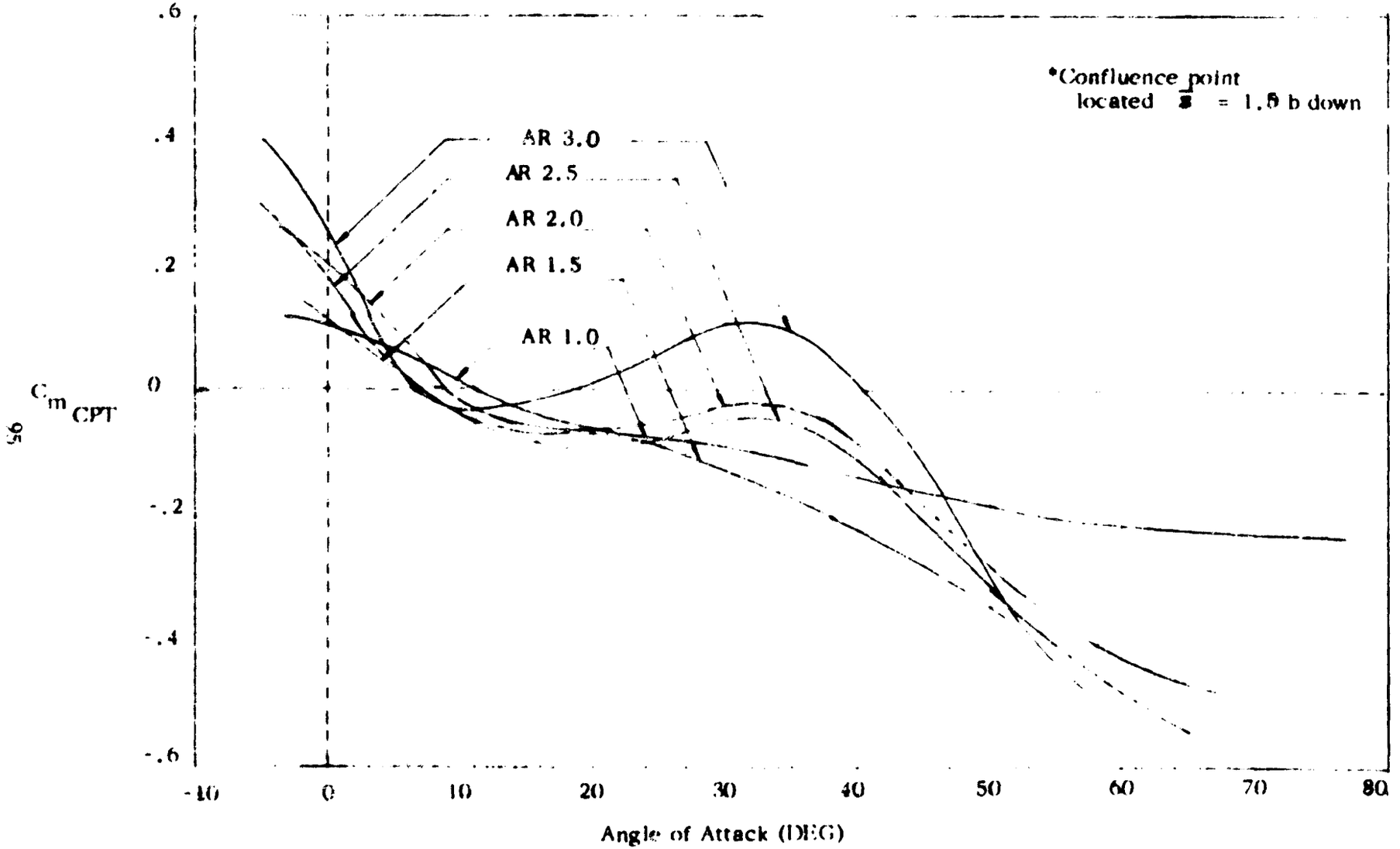

Figure 63. AR Summary. Pitching Moment about the Confluence point*

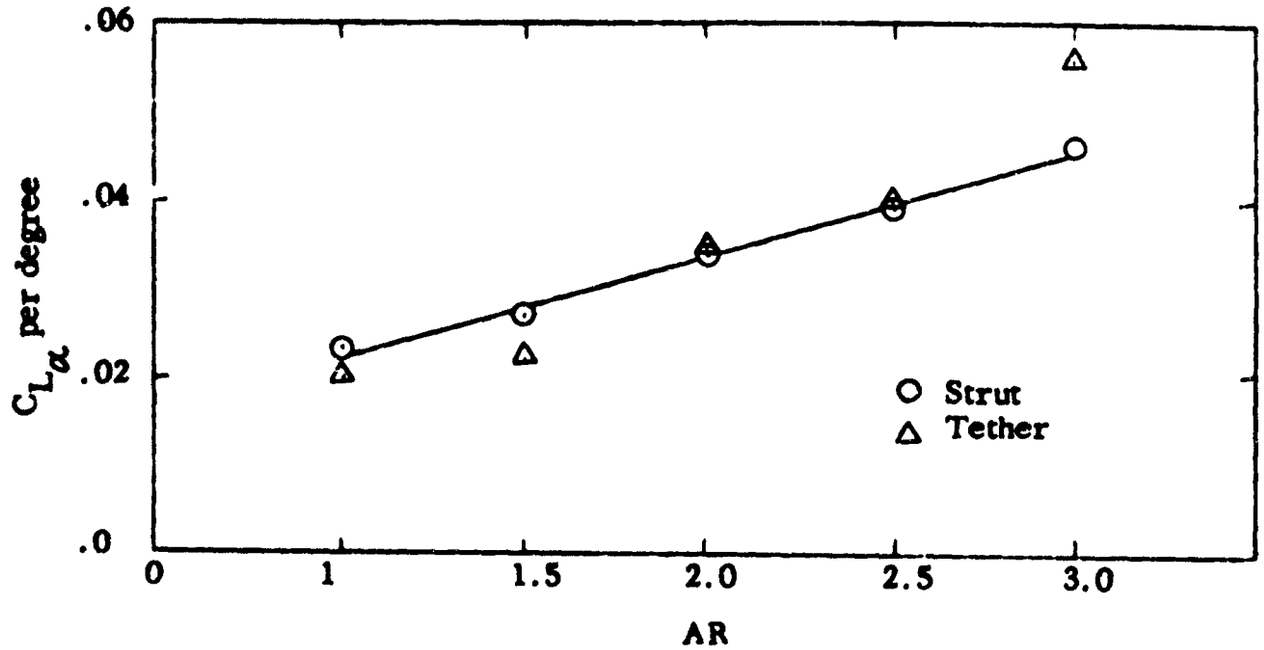

Figure 64. C_{L_α} per degree vs AR

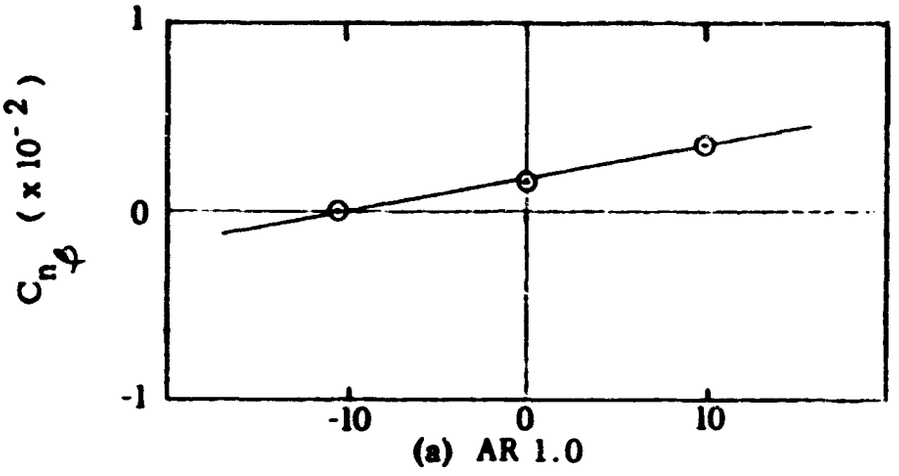

(a) AR 1.0

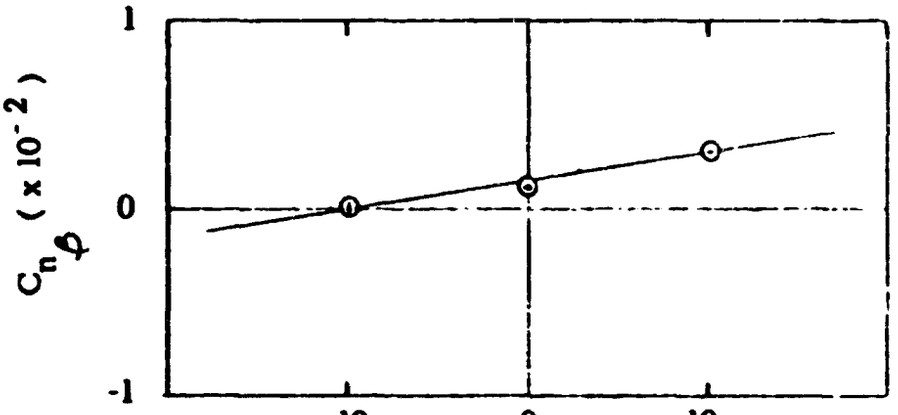

(b) AR 2.0

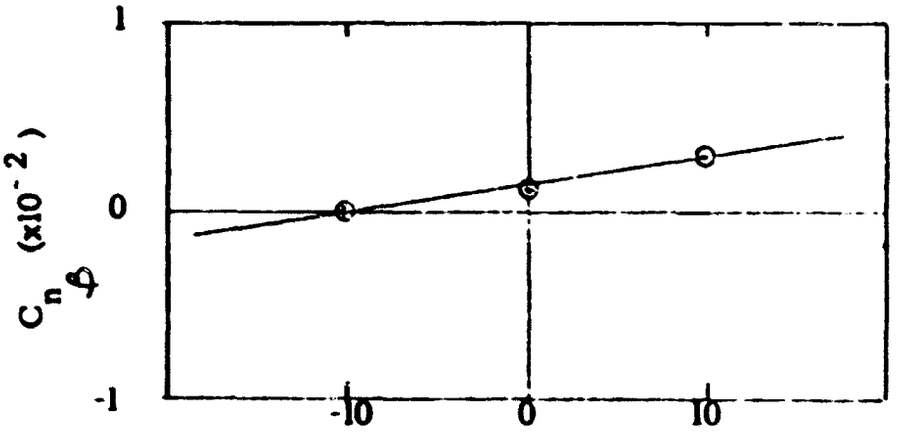

(c) AR 3.0

Figure 65. C_{n_β} vs α . Strut Models at 40 fps.

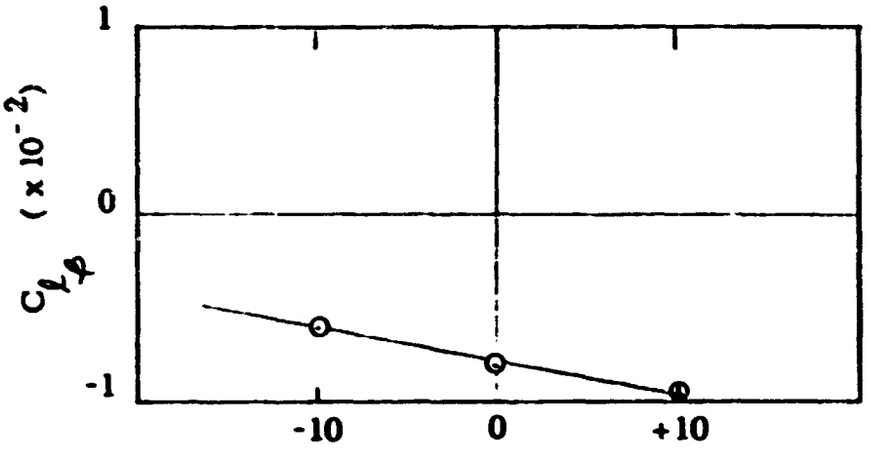

(a) AR 1.0

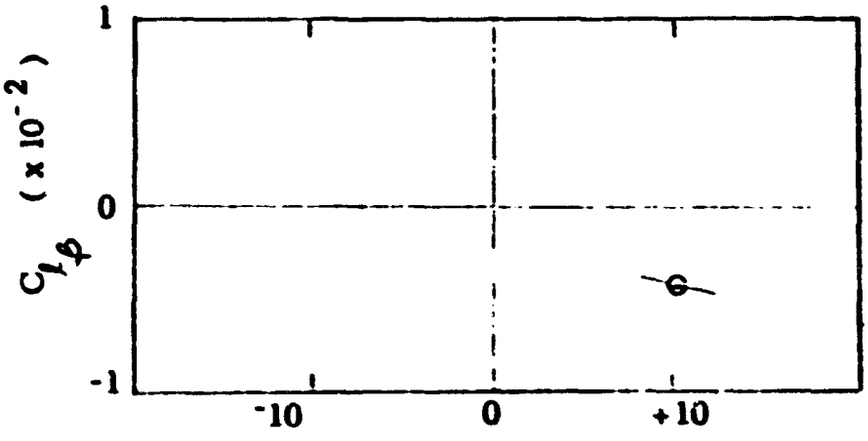

(b) AR 2.0

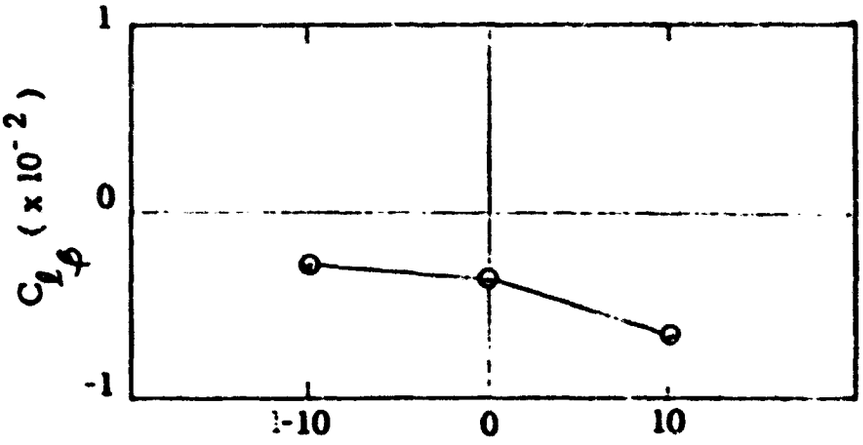

(c) AR 3.0

Figure 66. C_{l_β} vs α . Strut Models at 40 fps.

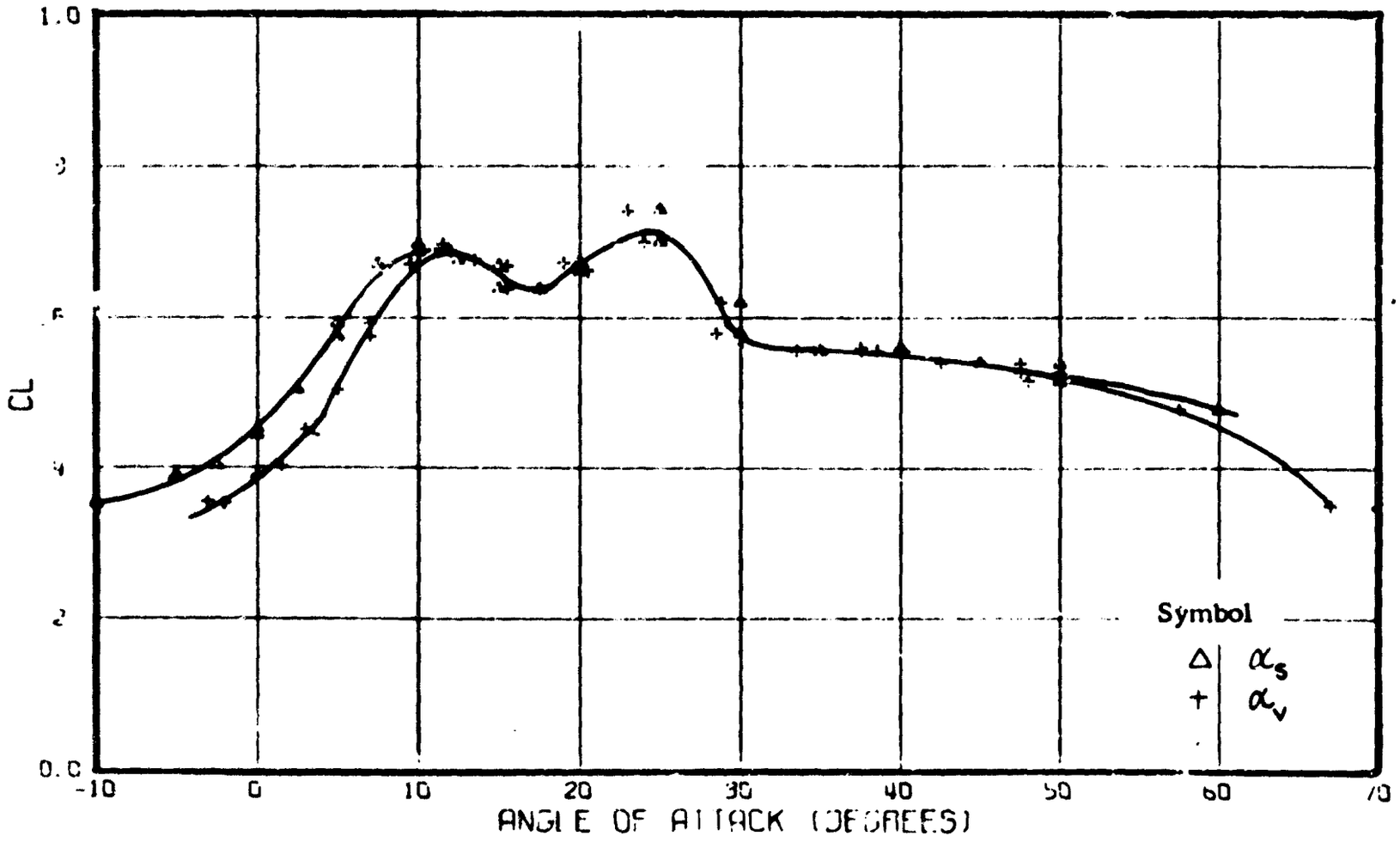

Figure 67. C_L vs α_s, α_v, Strut AR 2.0 Model

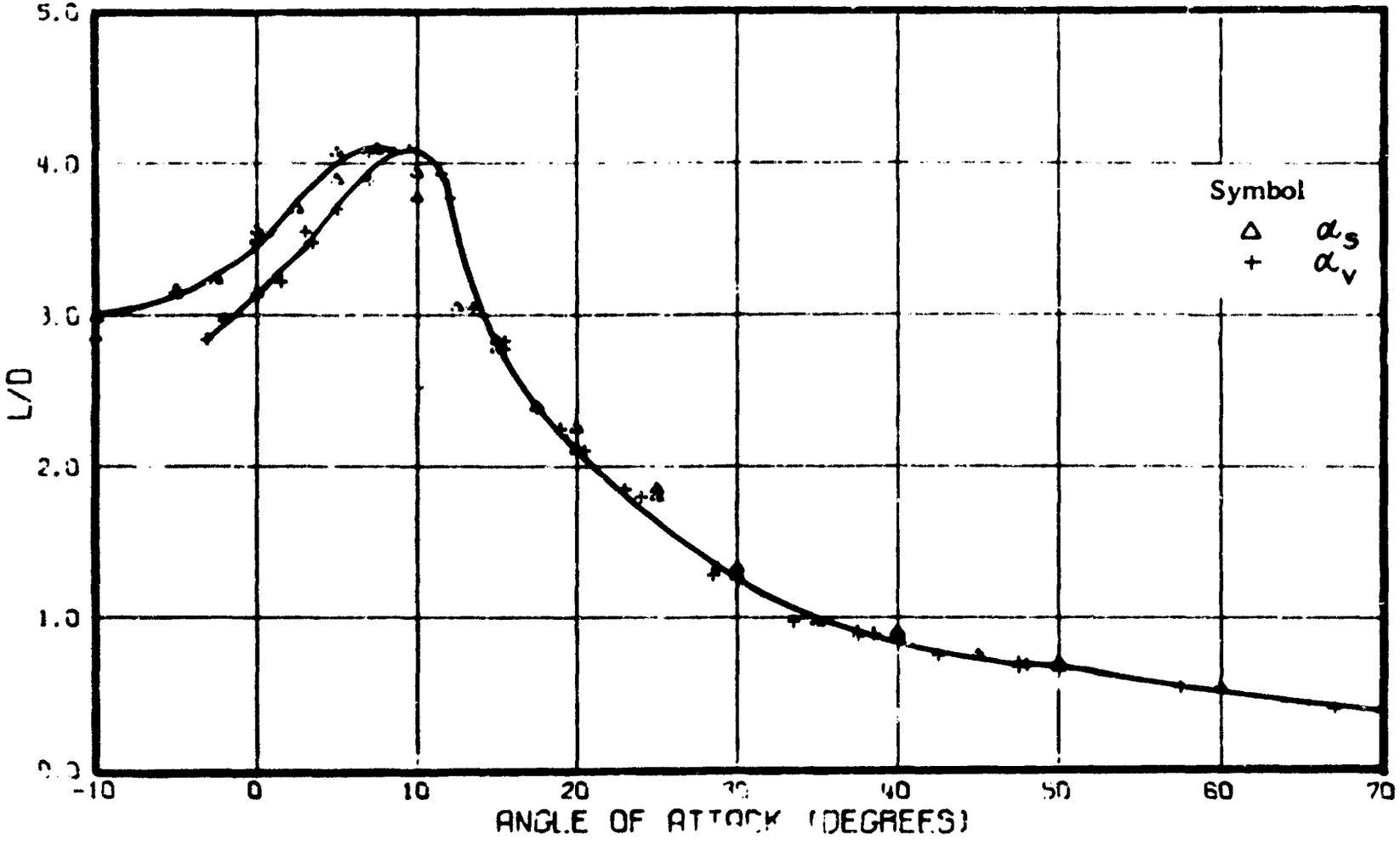

Figure 68. L/D vs α_s, α_v. Strut AR 2.0 Model

General Summary

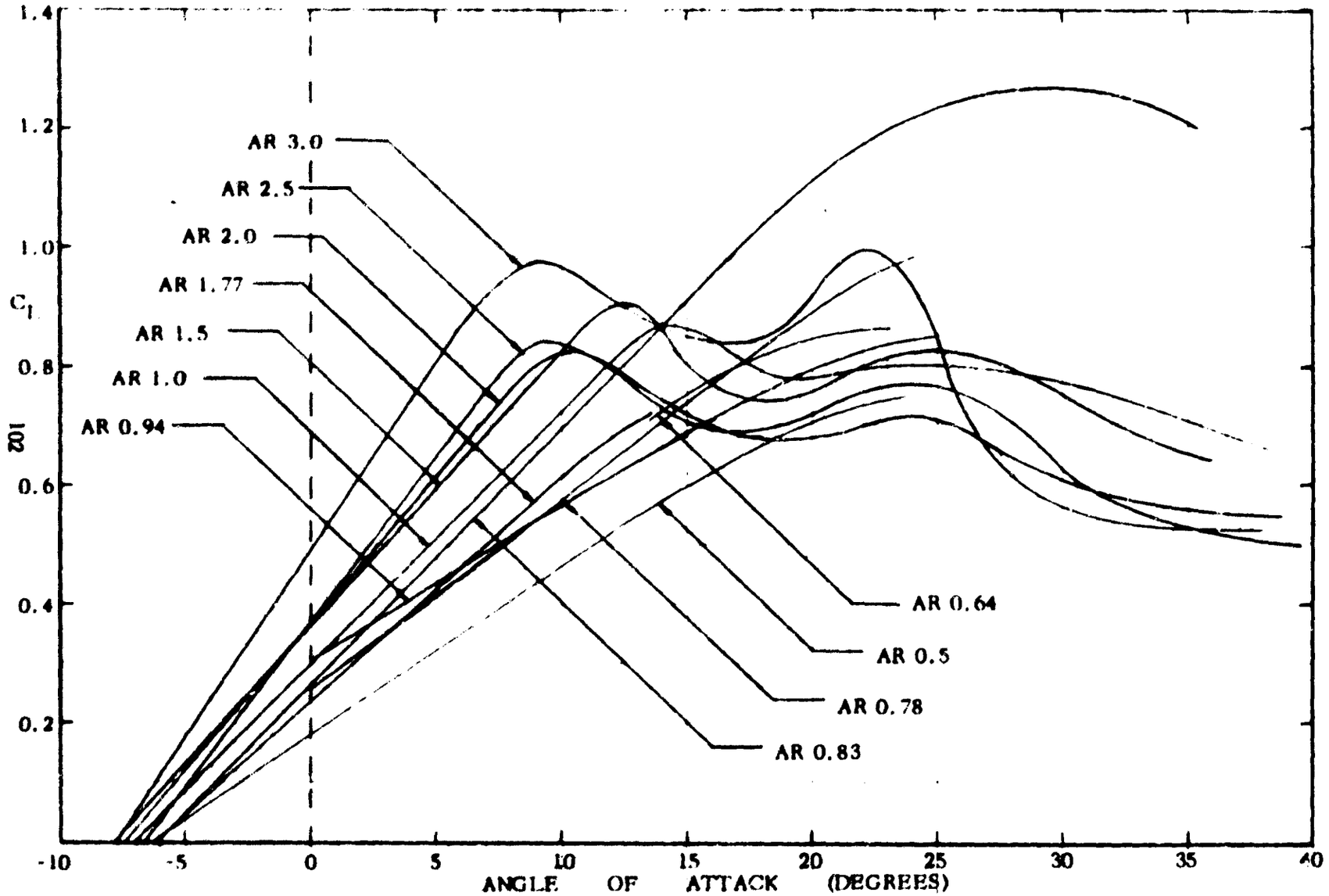

Figure 69. Lift Coefficient : AR Summary

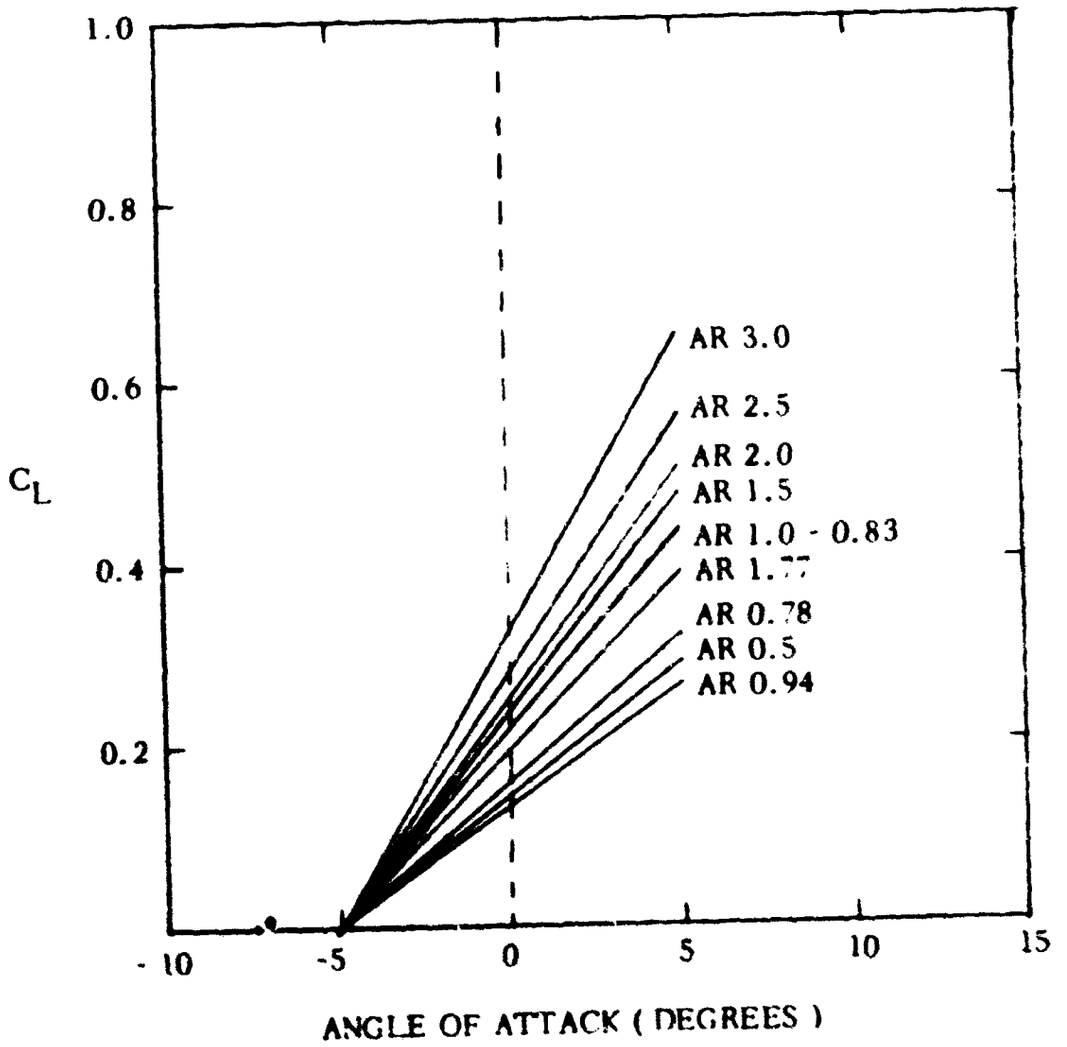

Figure 70. Lift Curve Slope Summary. Lift curve slopes brought through common intercept at $\alpha = -5.6$

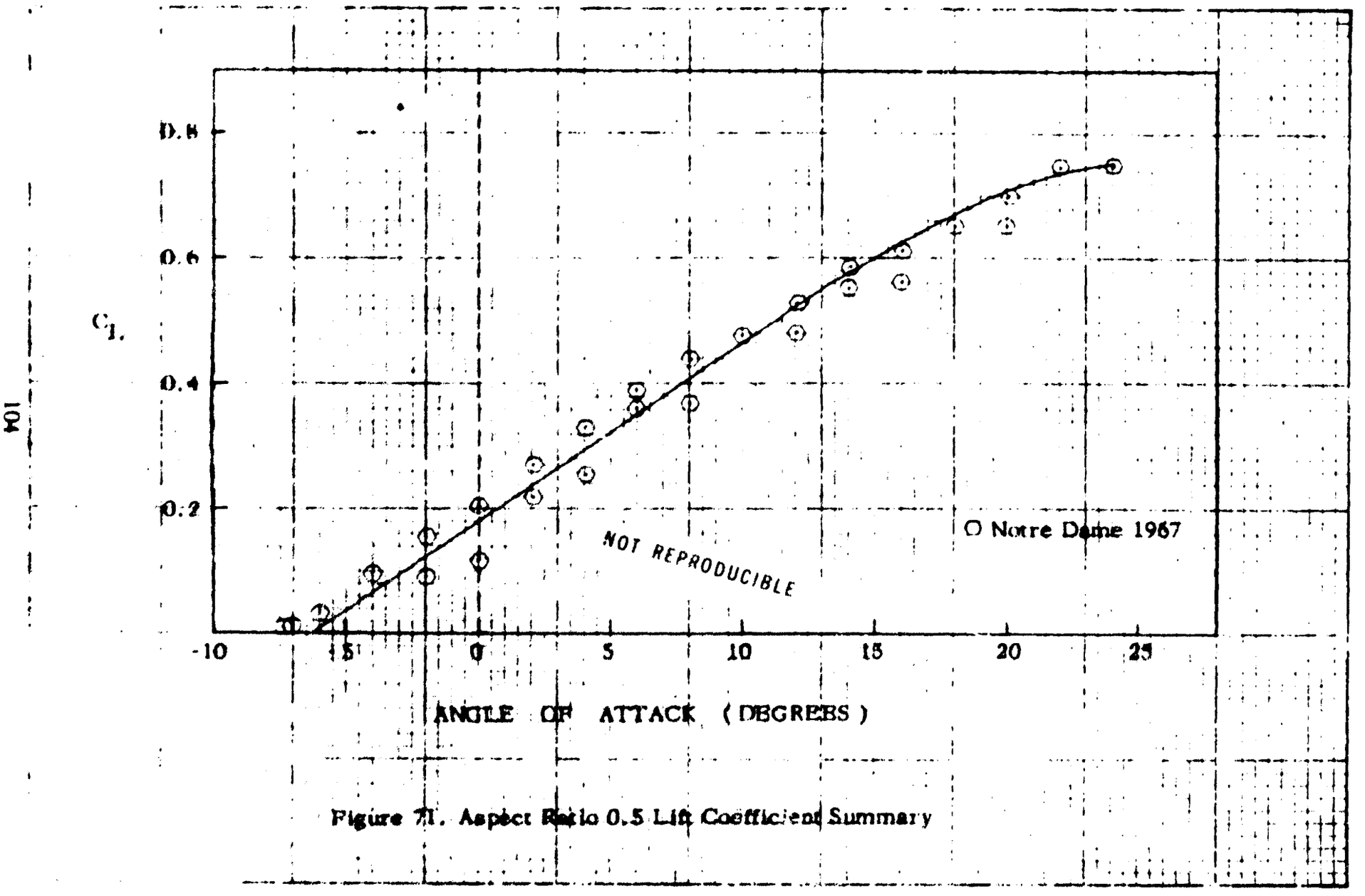

Figure 71. Aspect Ratio 0.5 Lift Coefficient Summary

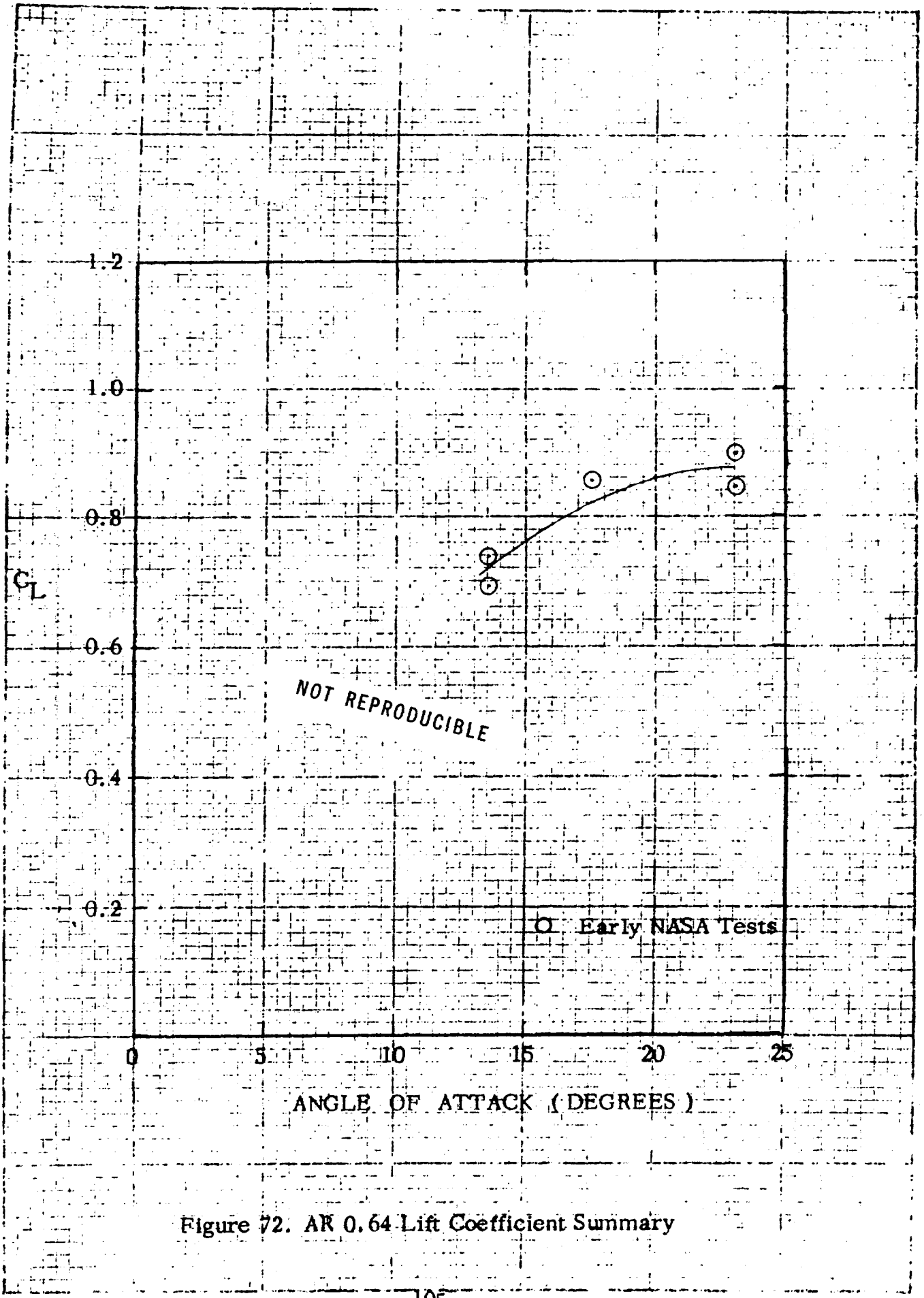

Figure 72. AR 0.64 Lift Coefficient Summary

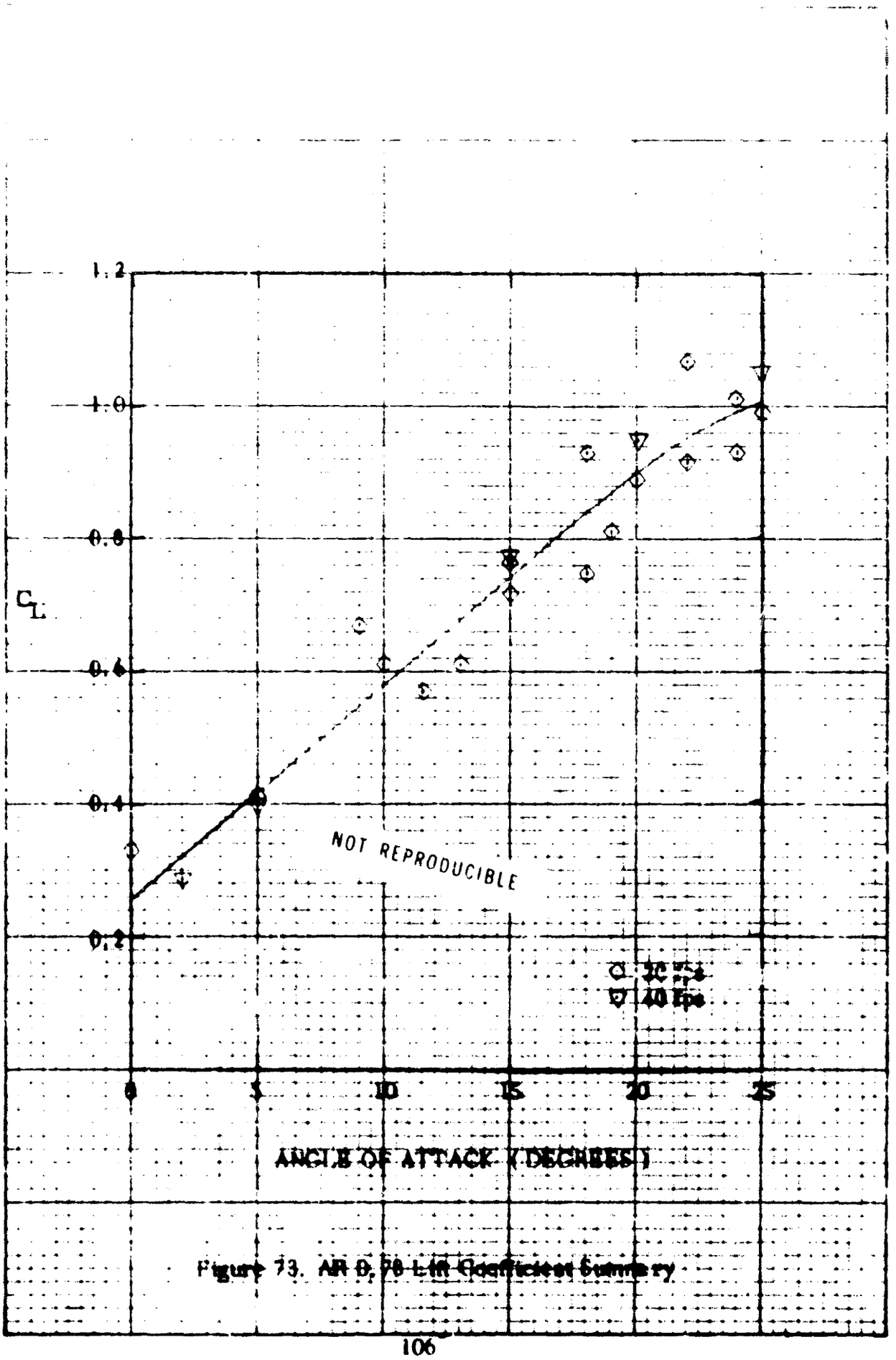

Figure 73. AR 8, 70 Lift Coefficient Summary

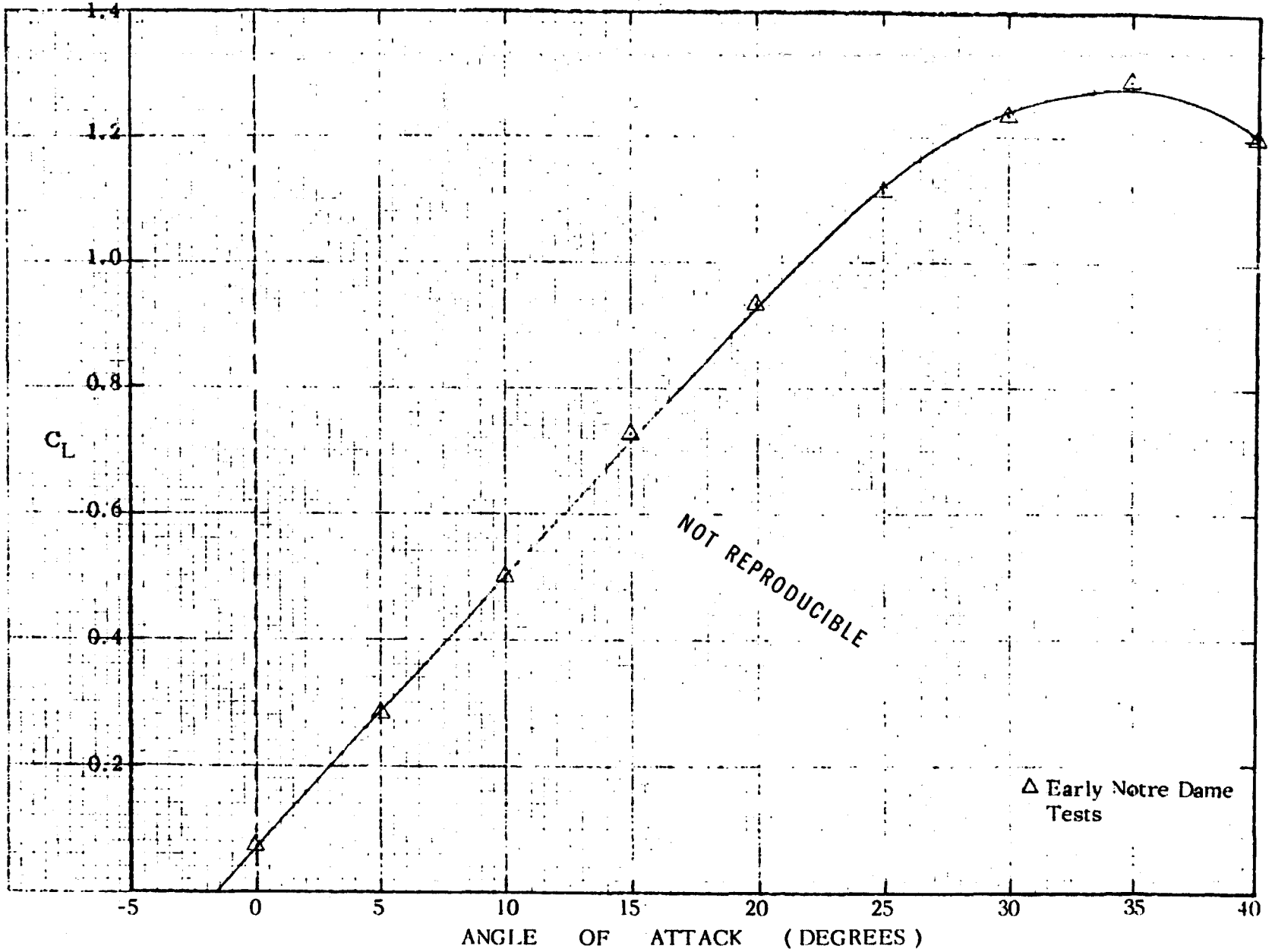

Figure 74. AR 0.83 Lift Coefficient Summary

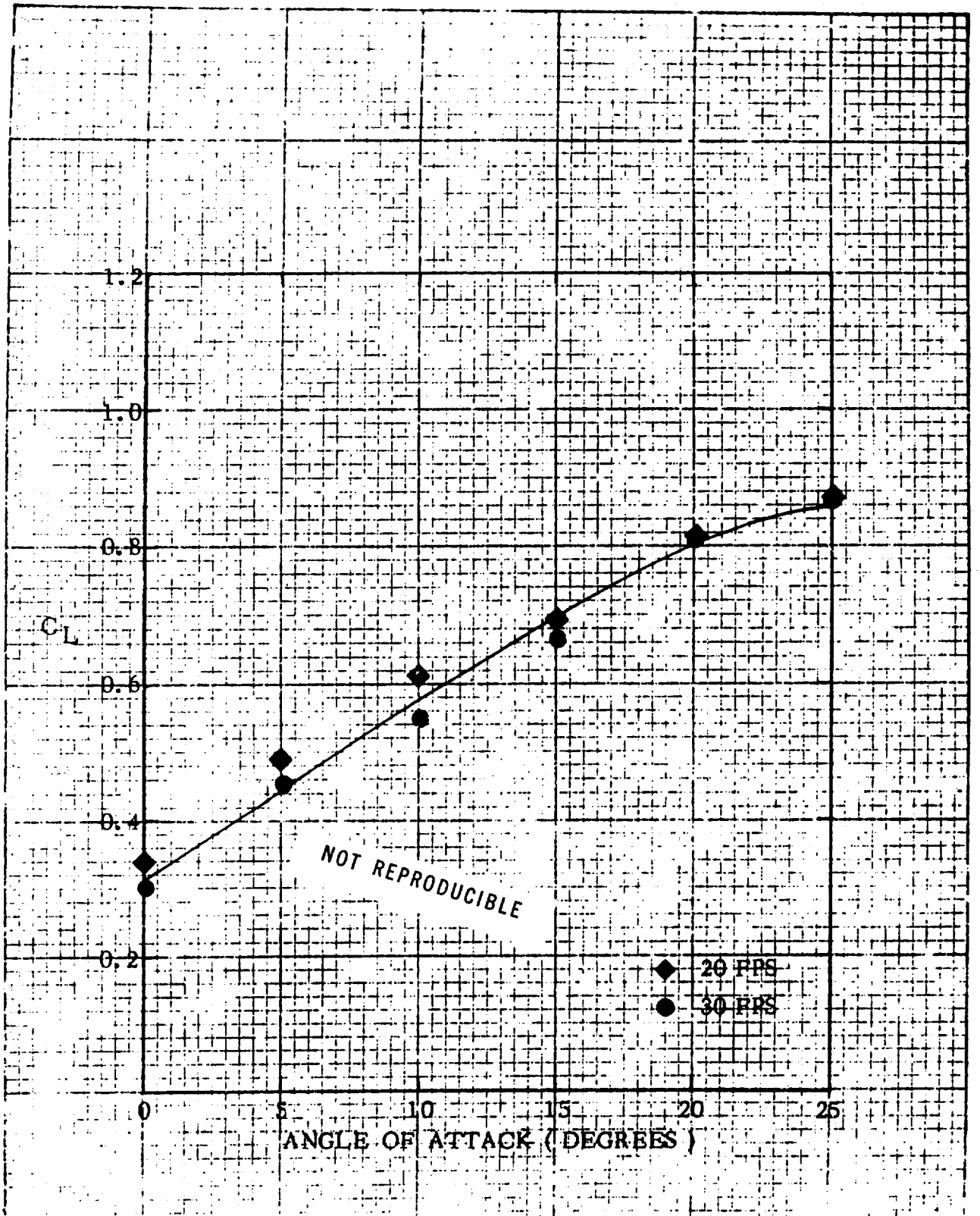

Figure 75. AR 0.94 Lift Coefficient Summary
(Early NASA Tests)

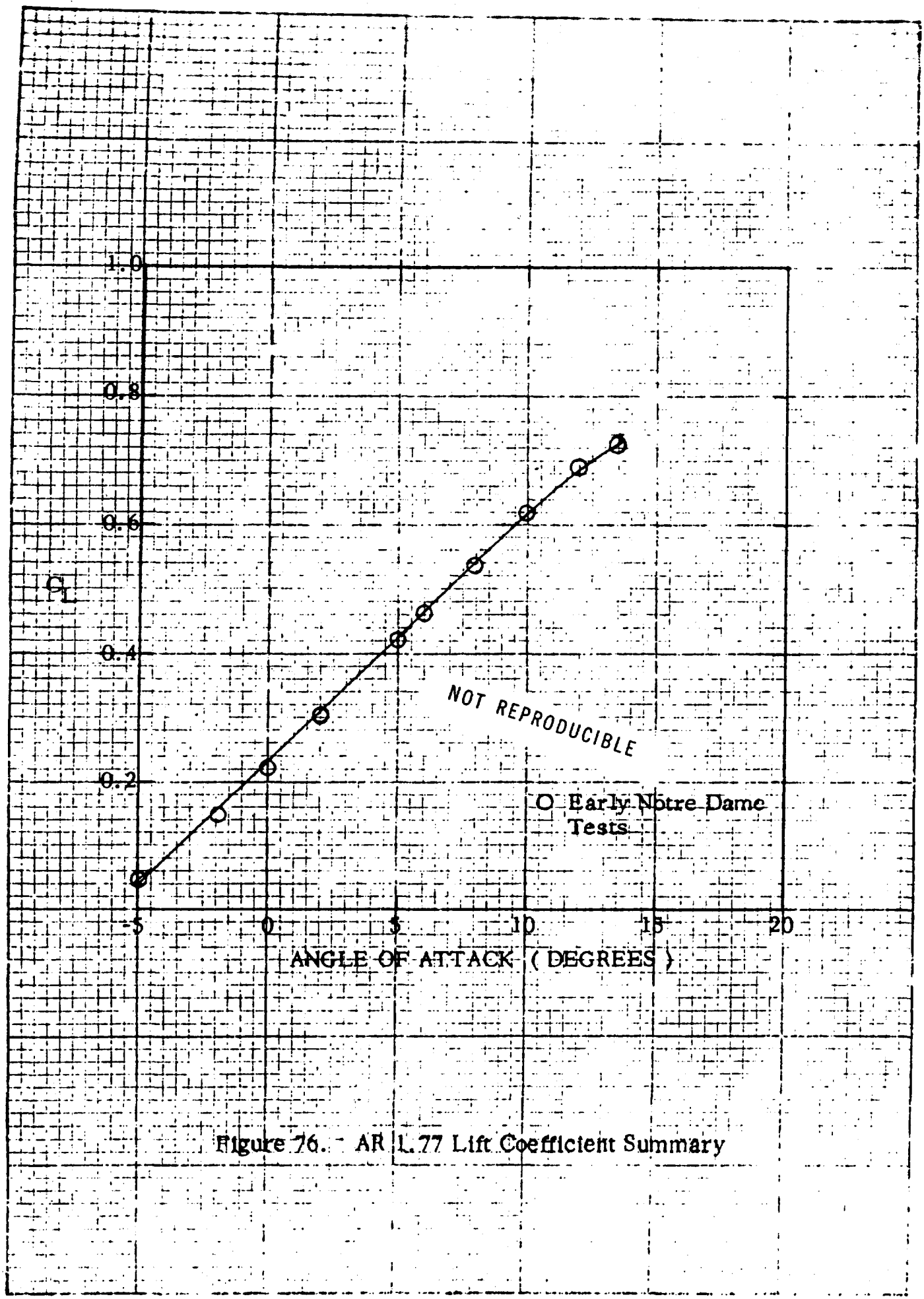

Figure 76. - AR 1.77 Lift Coefficient Summary

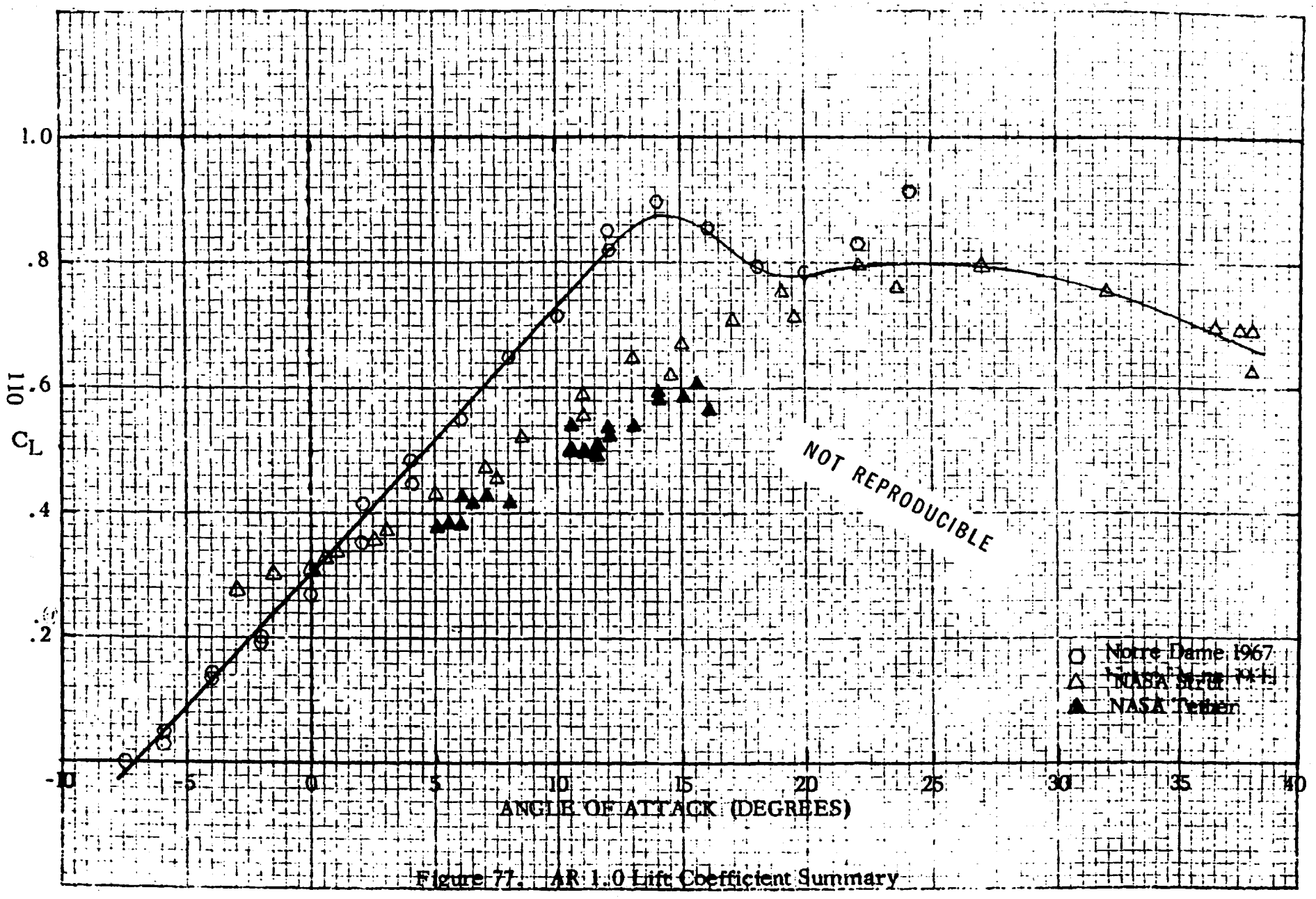

Figure 77. AR 1.0 Lift Coefficient Summary

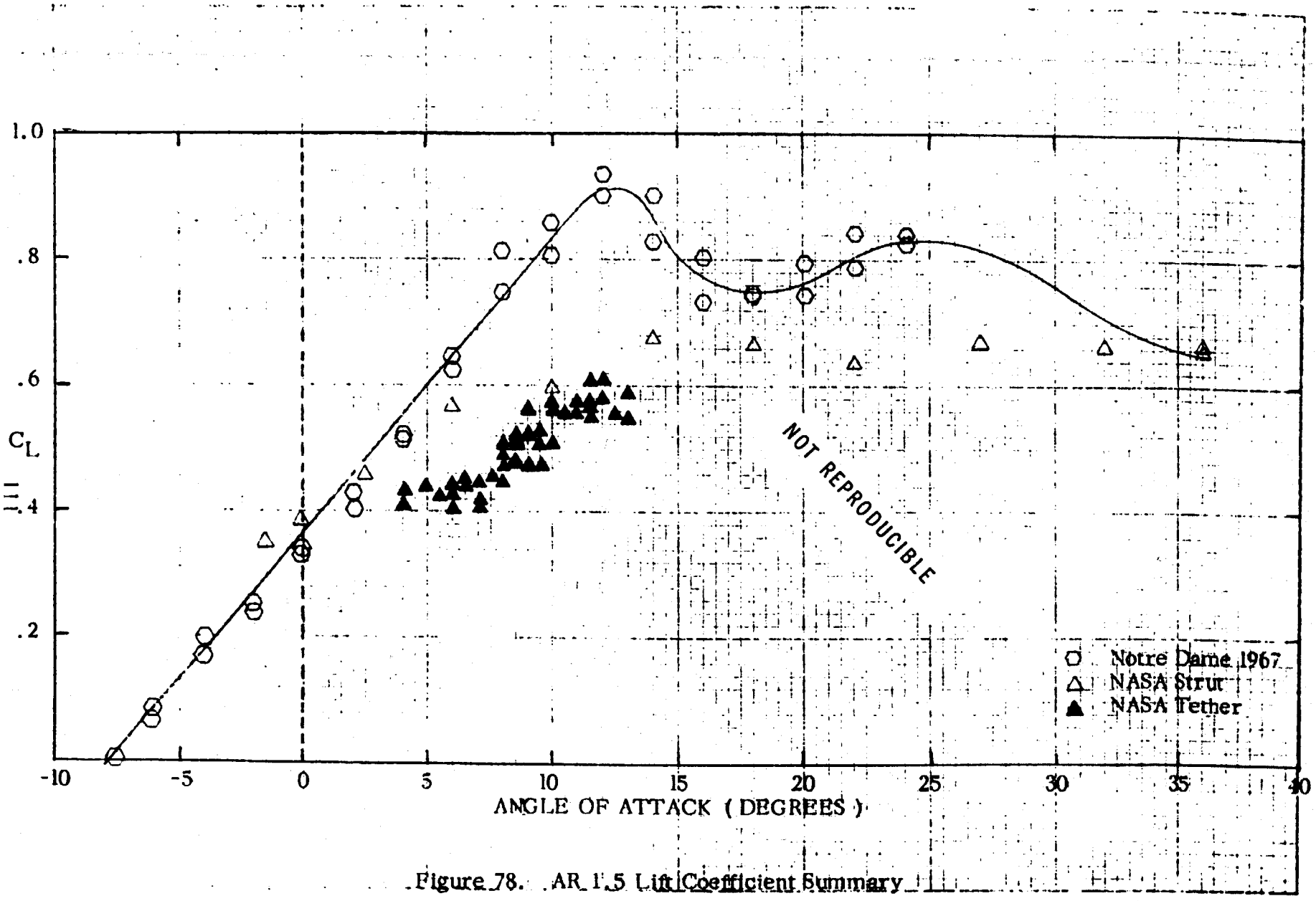

Figure 78. AR 1.5 Lift Coefficient Summary

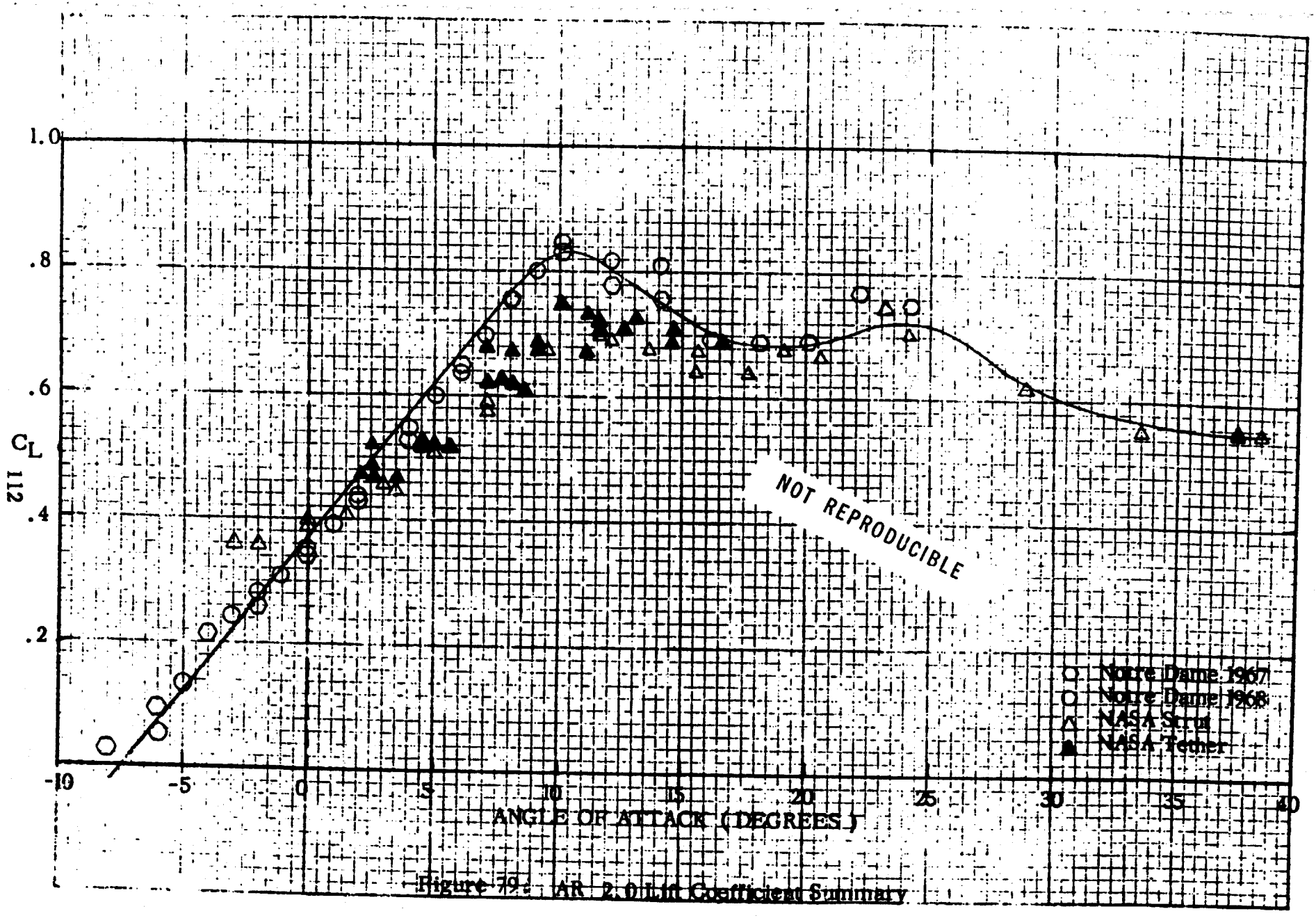

Figure 79. AR 2.0 Lift Coefficient Summary

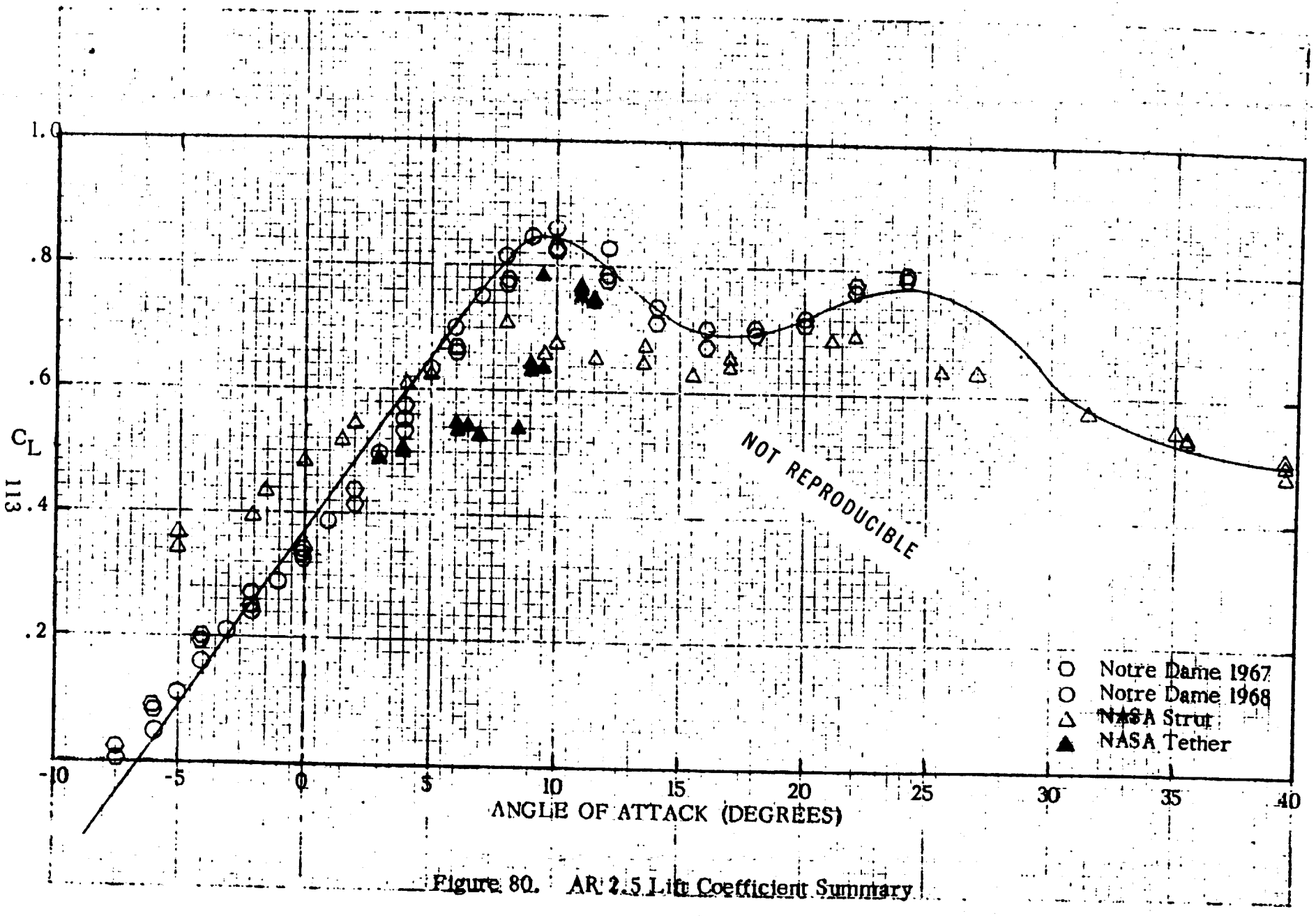

Figure 80. AR 2.5 Lift Coefficient Summary

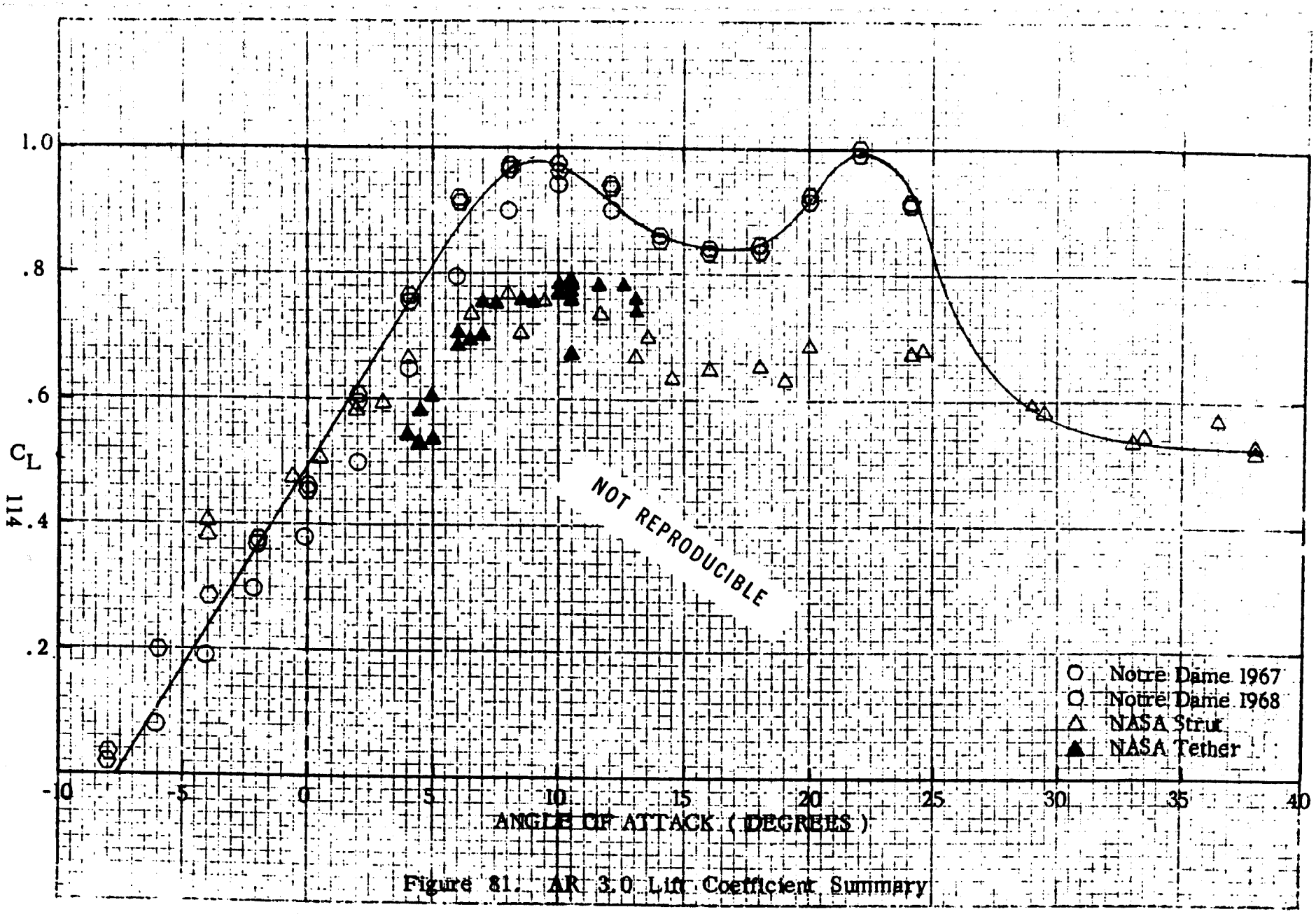

Figure 81. AR 3.0 Lift Coefficient Summary

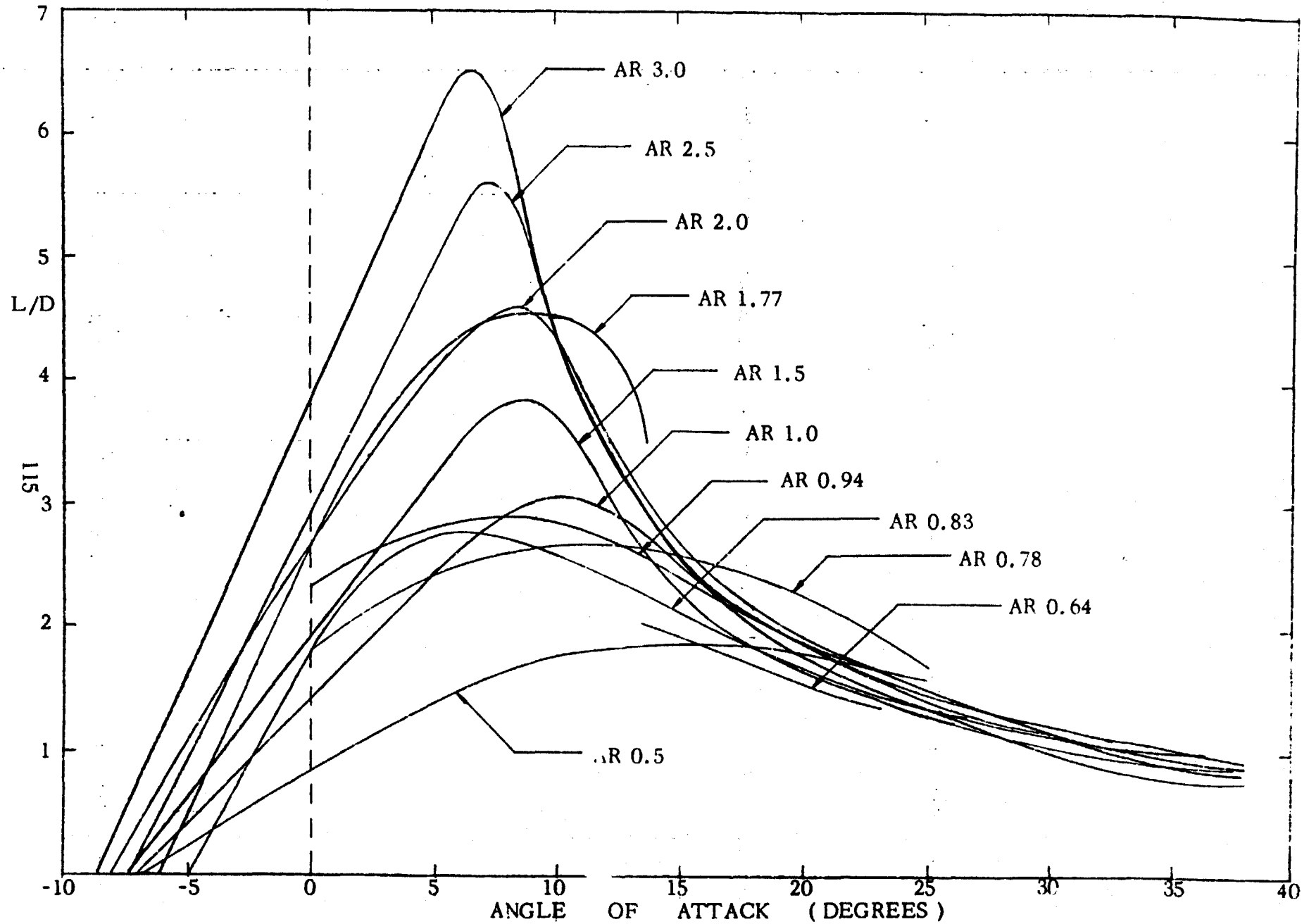

Figure 82. Lift to Drag Ratio : AR Summary

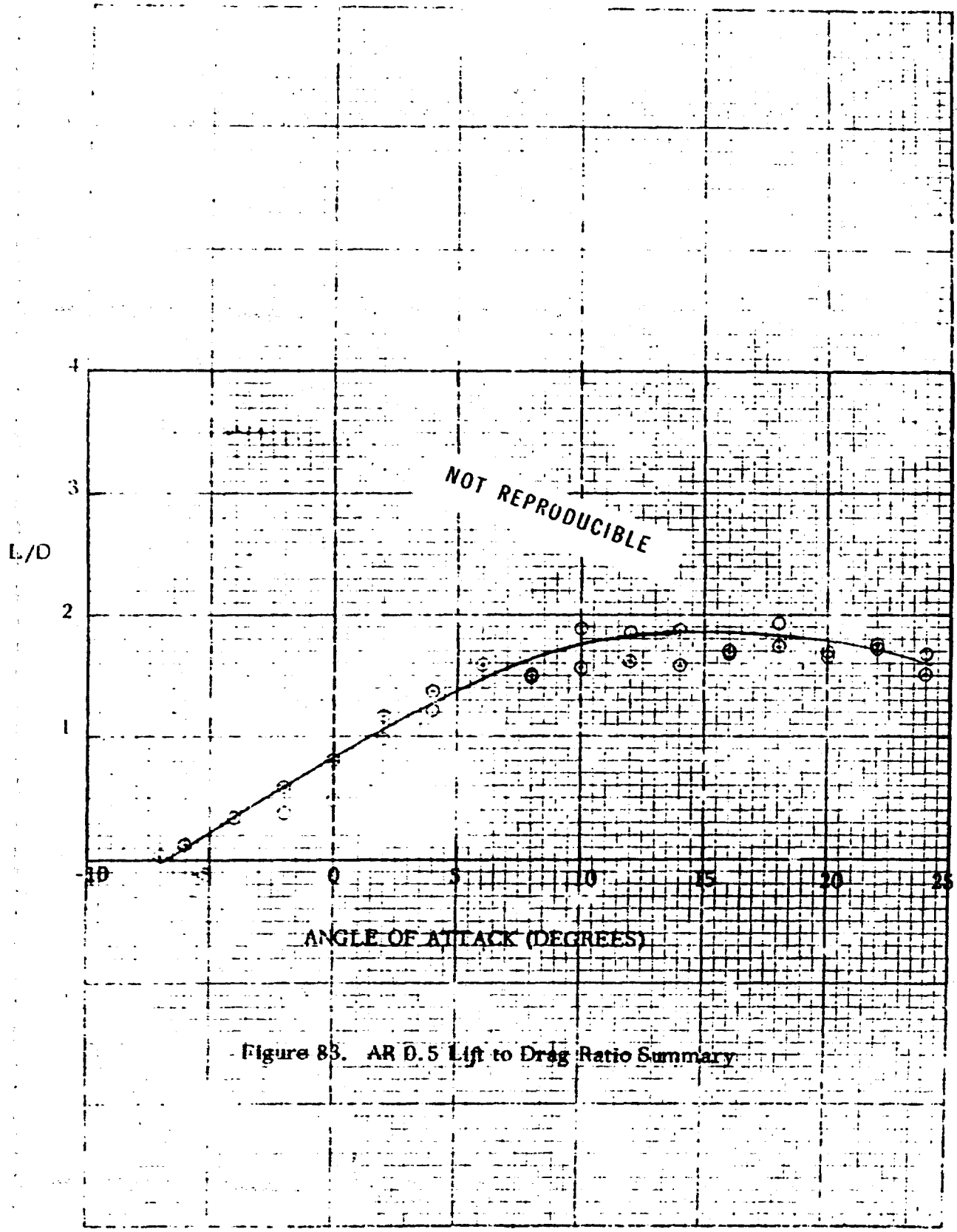

Figure 83. AR 0.5 Lift to Drag Ratio Summary

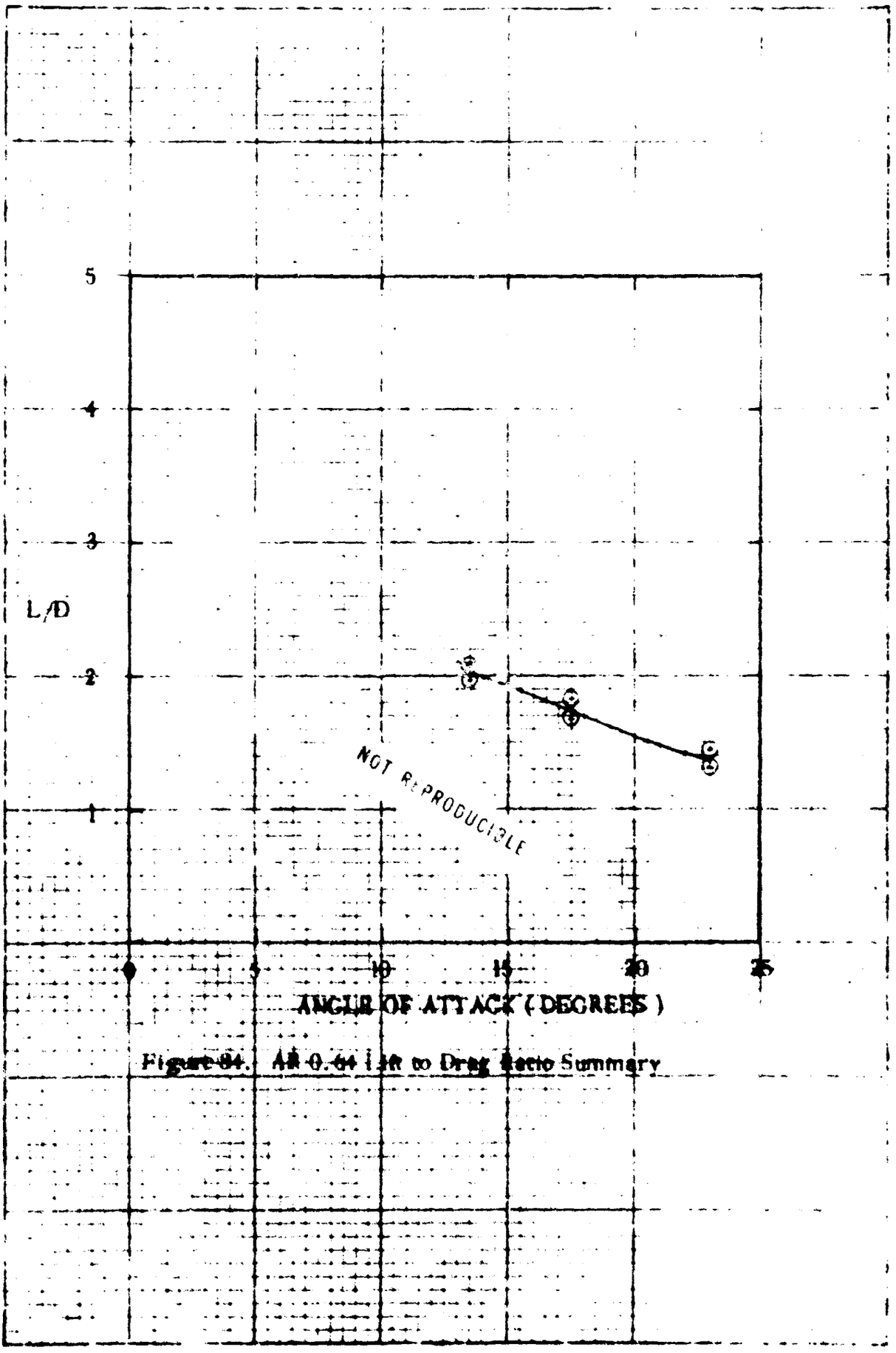

Figure 84. Alt 0.64 Lift to Drag Ratio Summary

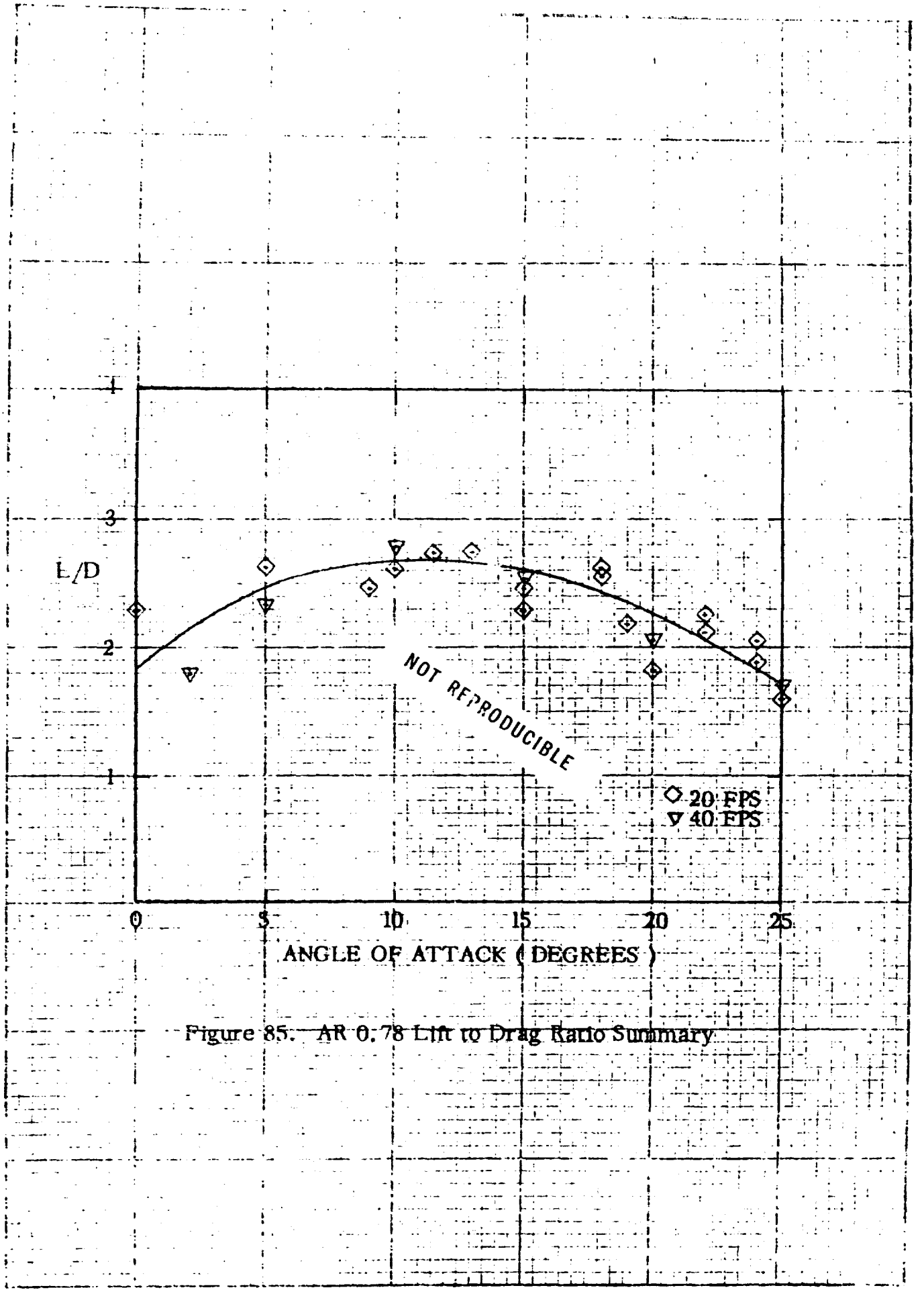

Figure 85. AR 0.78 Lift to Drag Ratio Summary

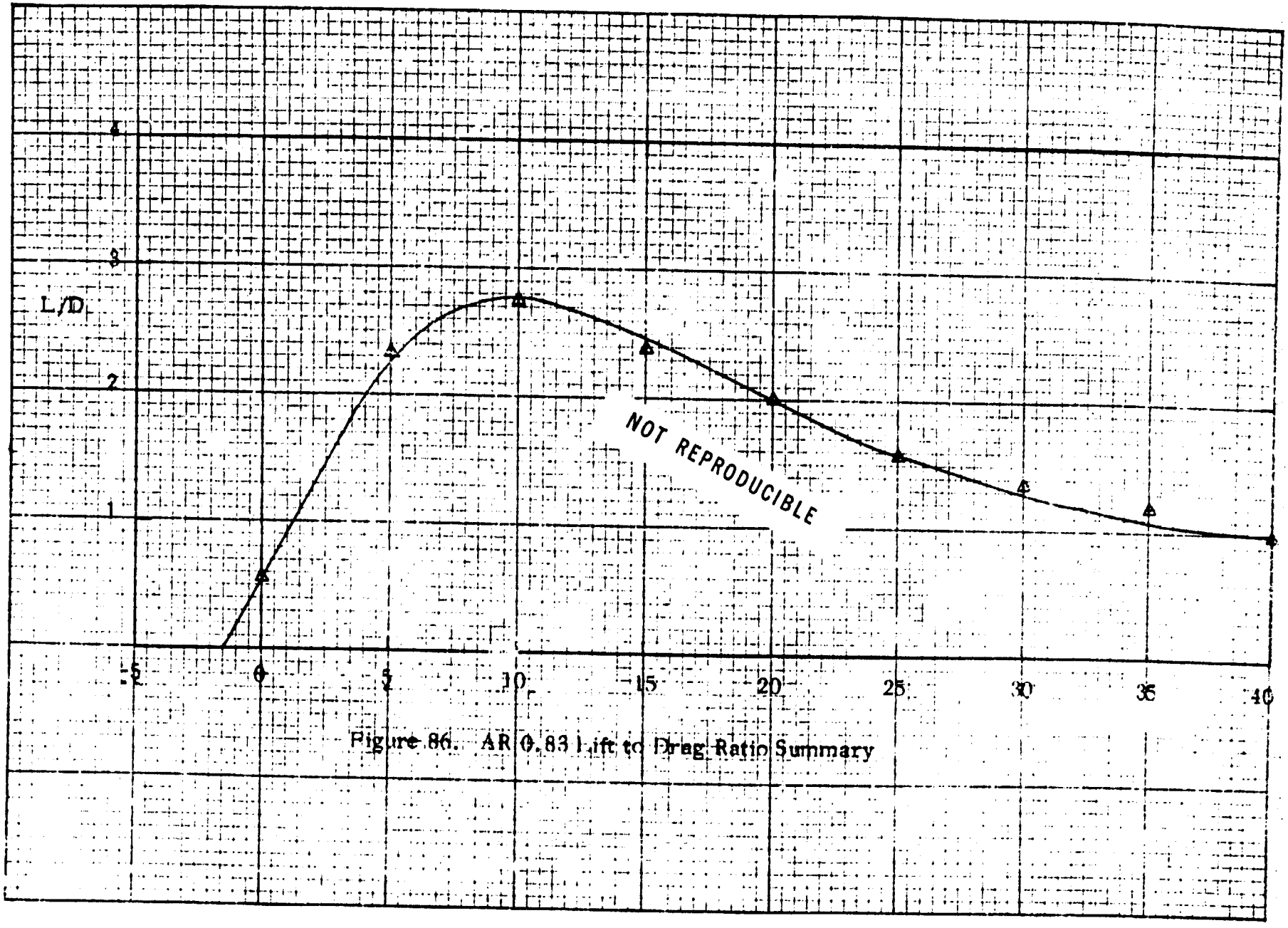

Figure 86. AR 0.83 Lift to Drag Ratio Summary

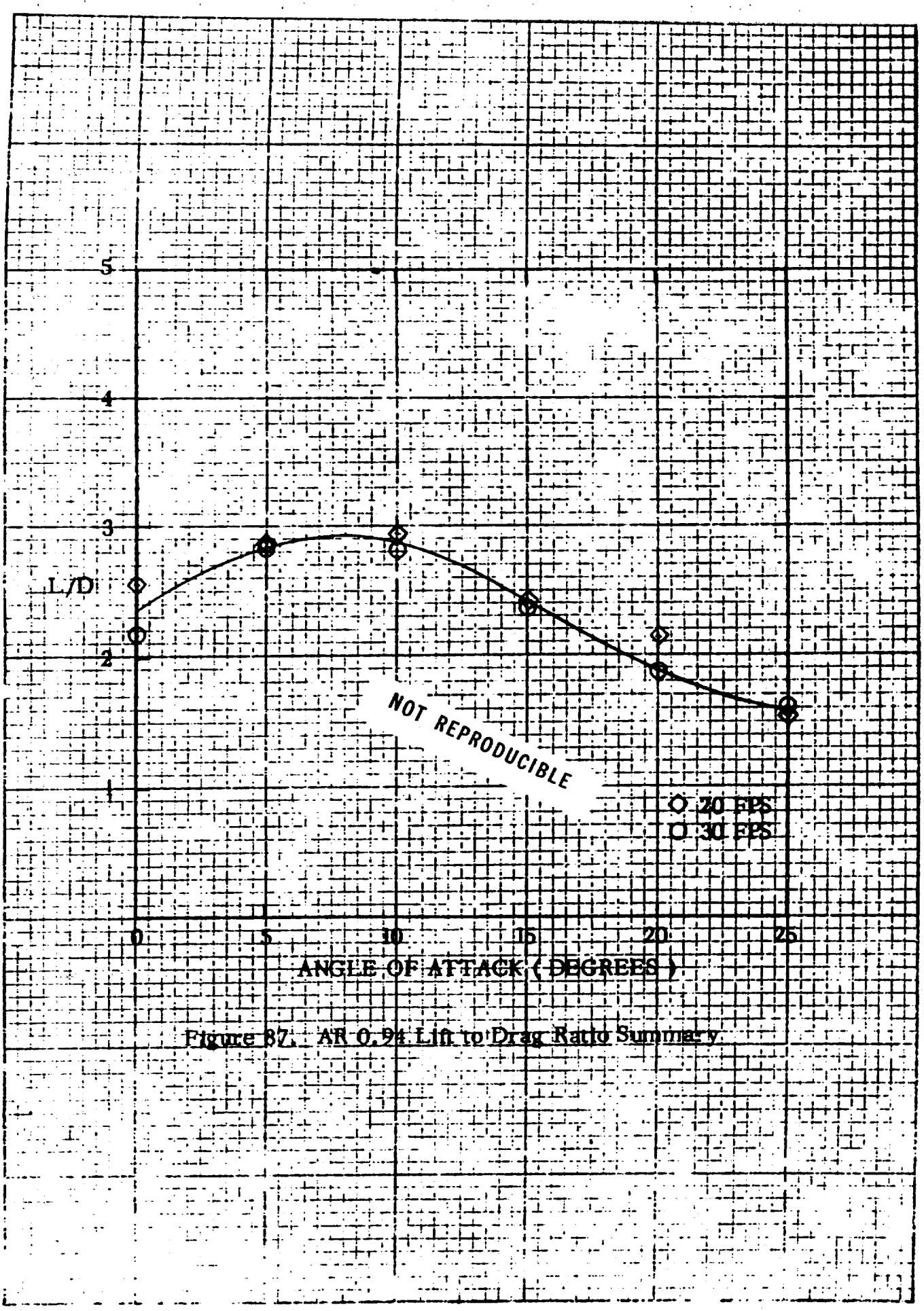

Figure 87. AR 0.94 Lift to Drag Ratio Summary

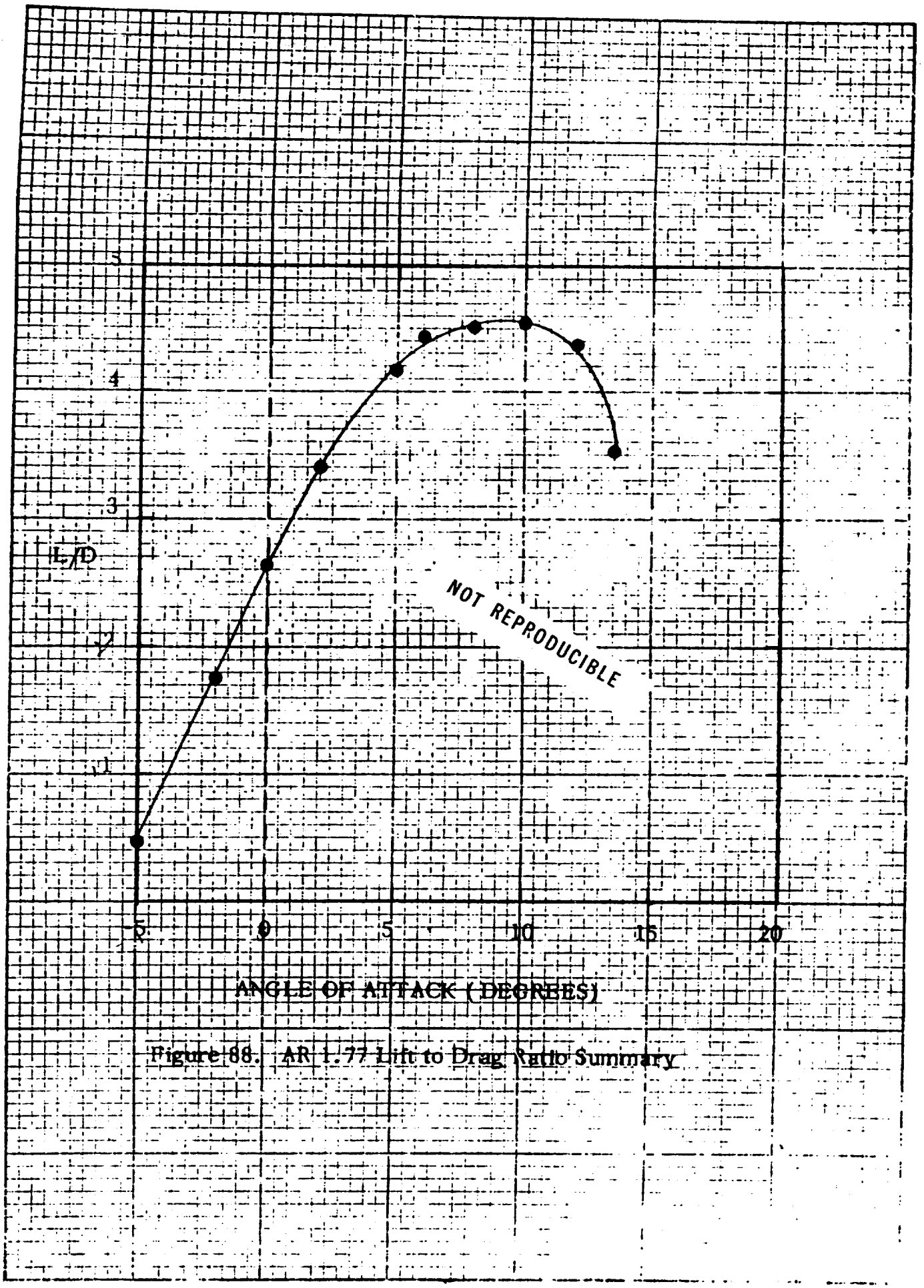

Figure 88. AR 1.77 Lift to Drag Ratio Summary

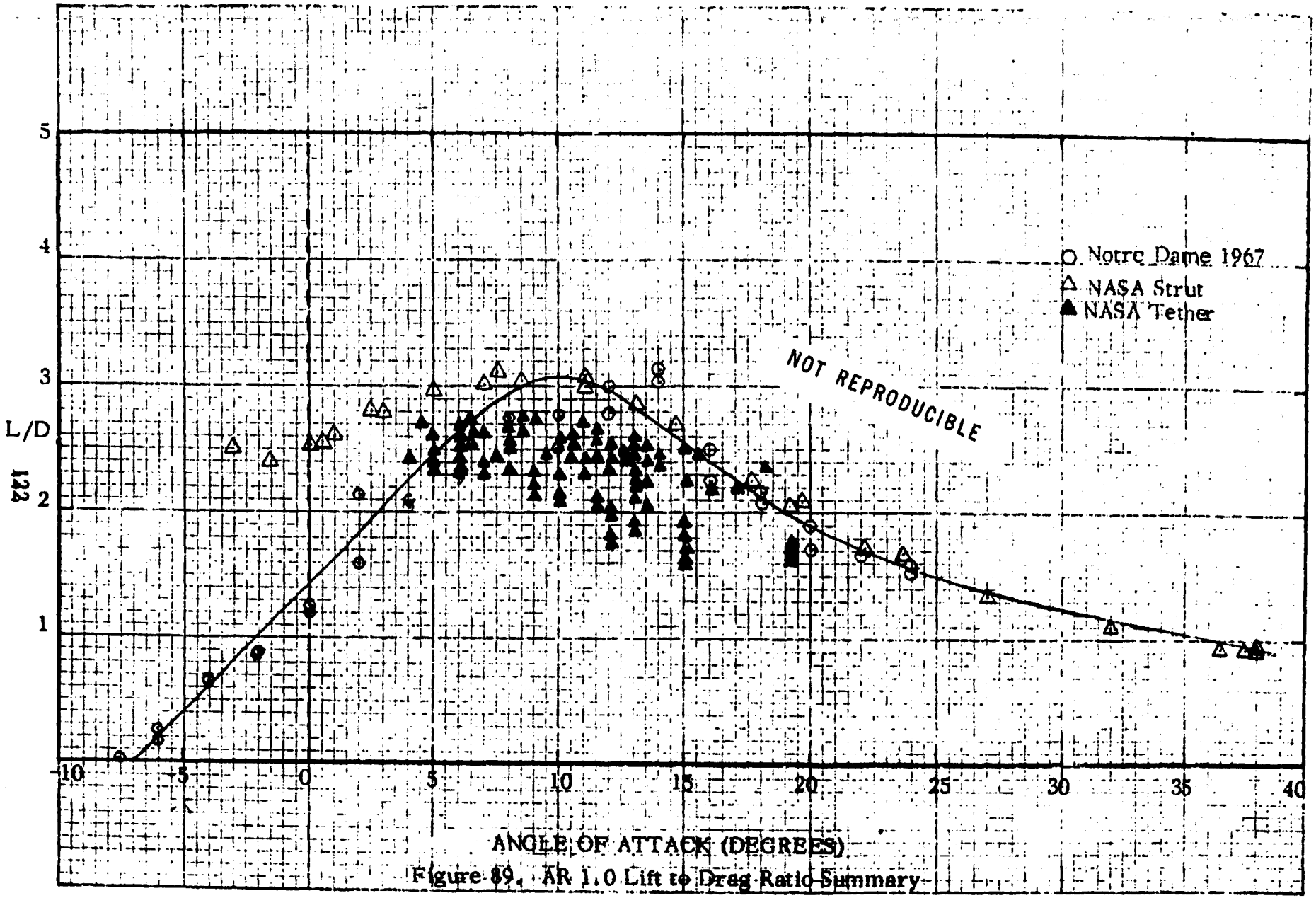

Figure 89. AR 1.0 Lift to Drag Ratio Summary

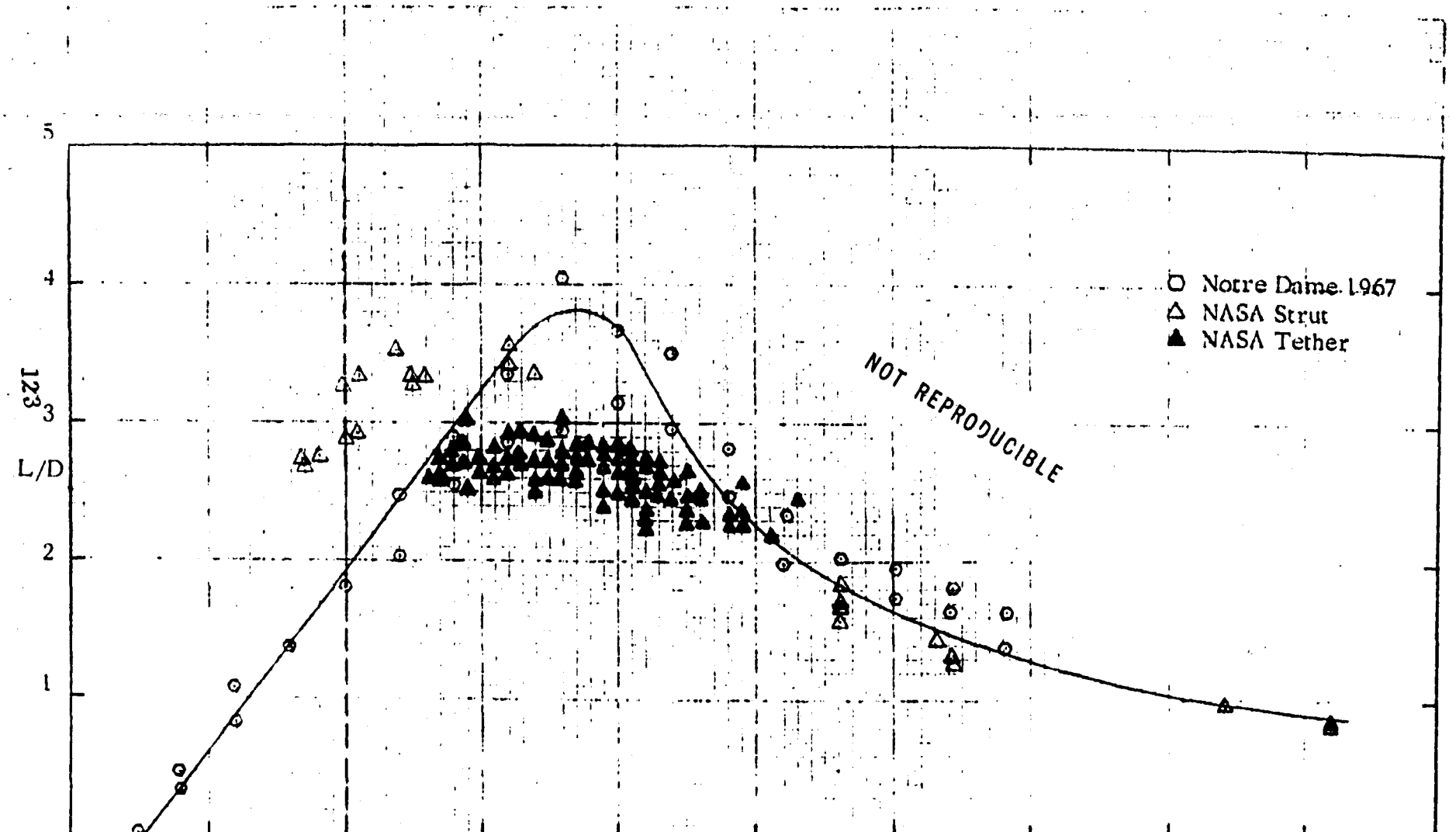

Figure 90. AR 1.5 Lift to Drag Ratio Summary

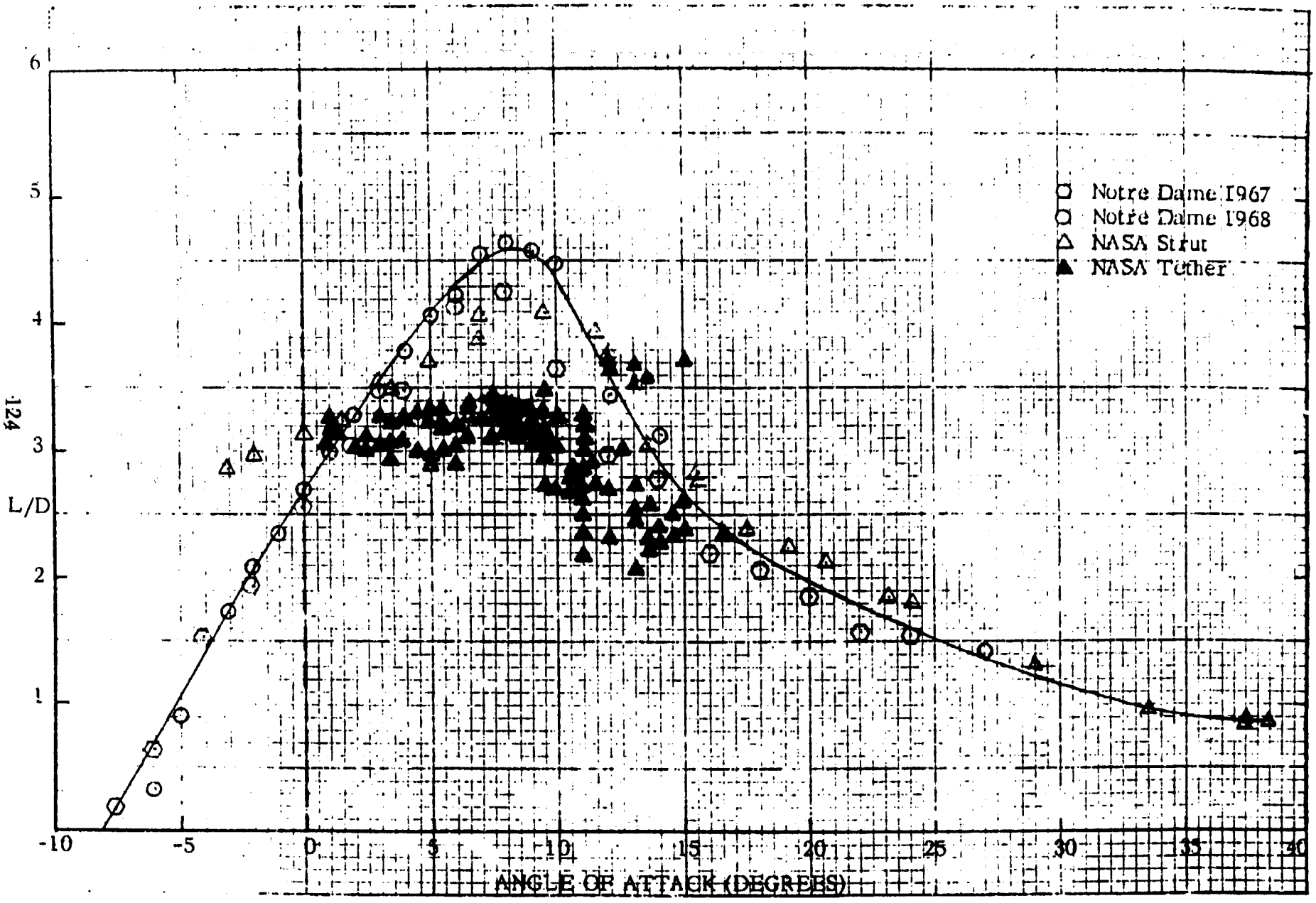

Figure 91. AR 2.0 Lift to Drag Ratio Summary

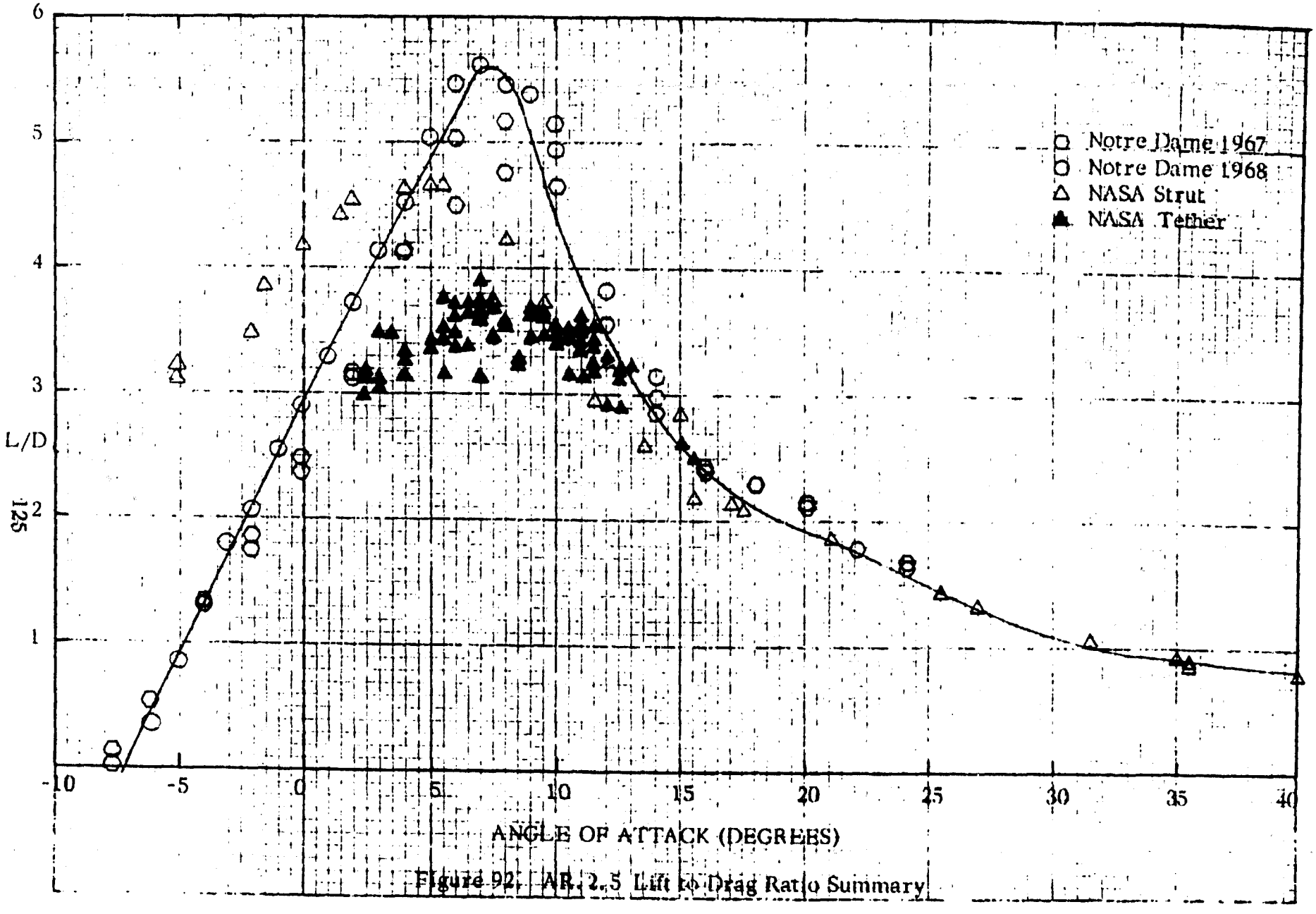

Figure 92. AR 2.5 Lift to Drag Ratio Summary

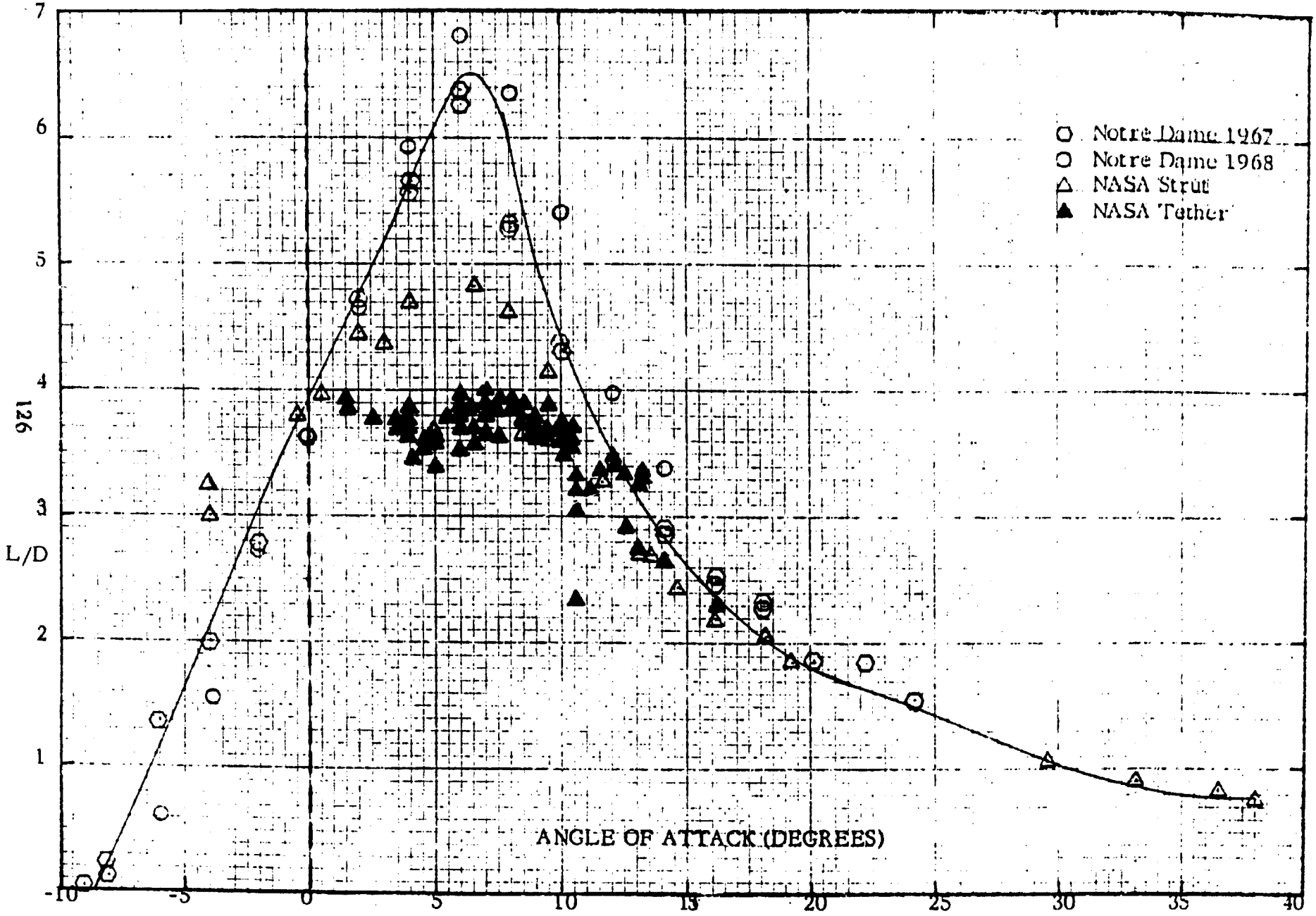

Figure 93 AR 3.0 Lift to Drag Ratio Summary

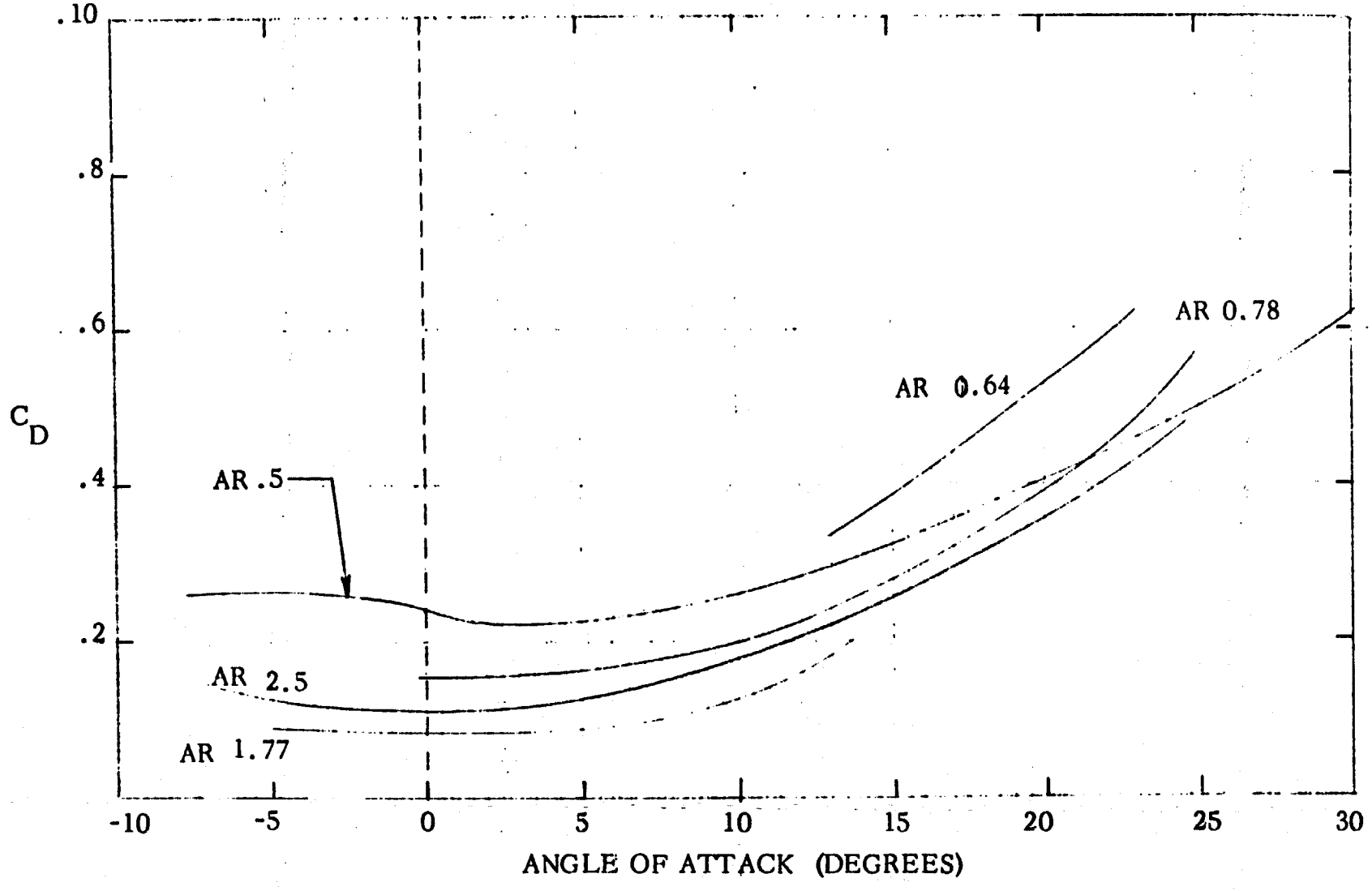

Figure 94a. Drag Coefficient: AR Summary

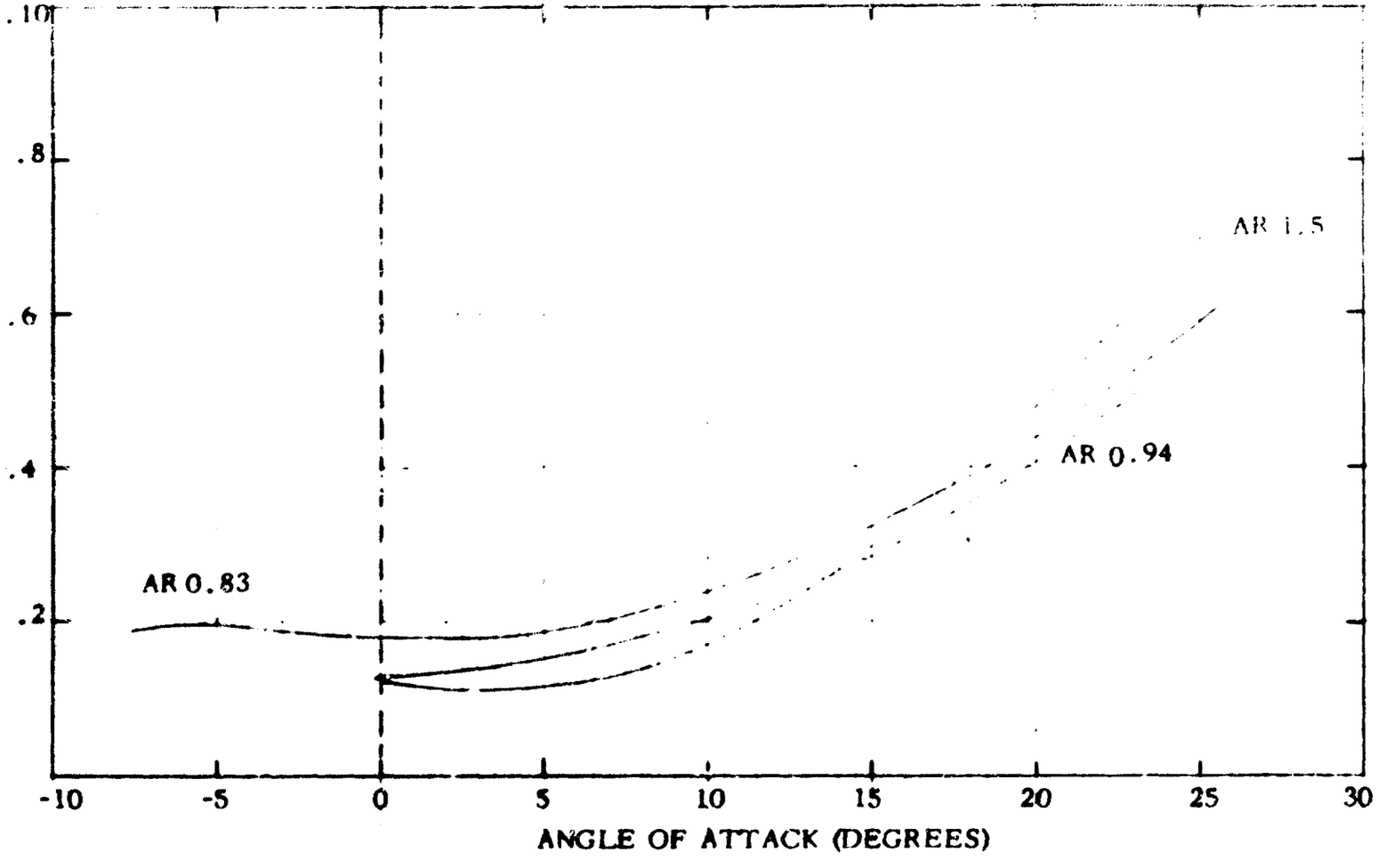

Figure 94b. Drag Coefficient: AR Summary

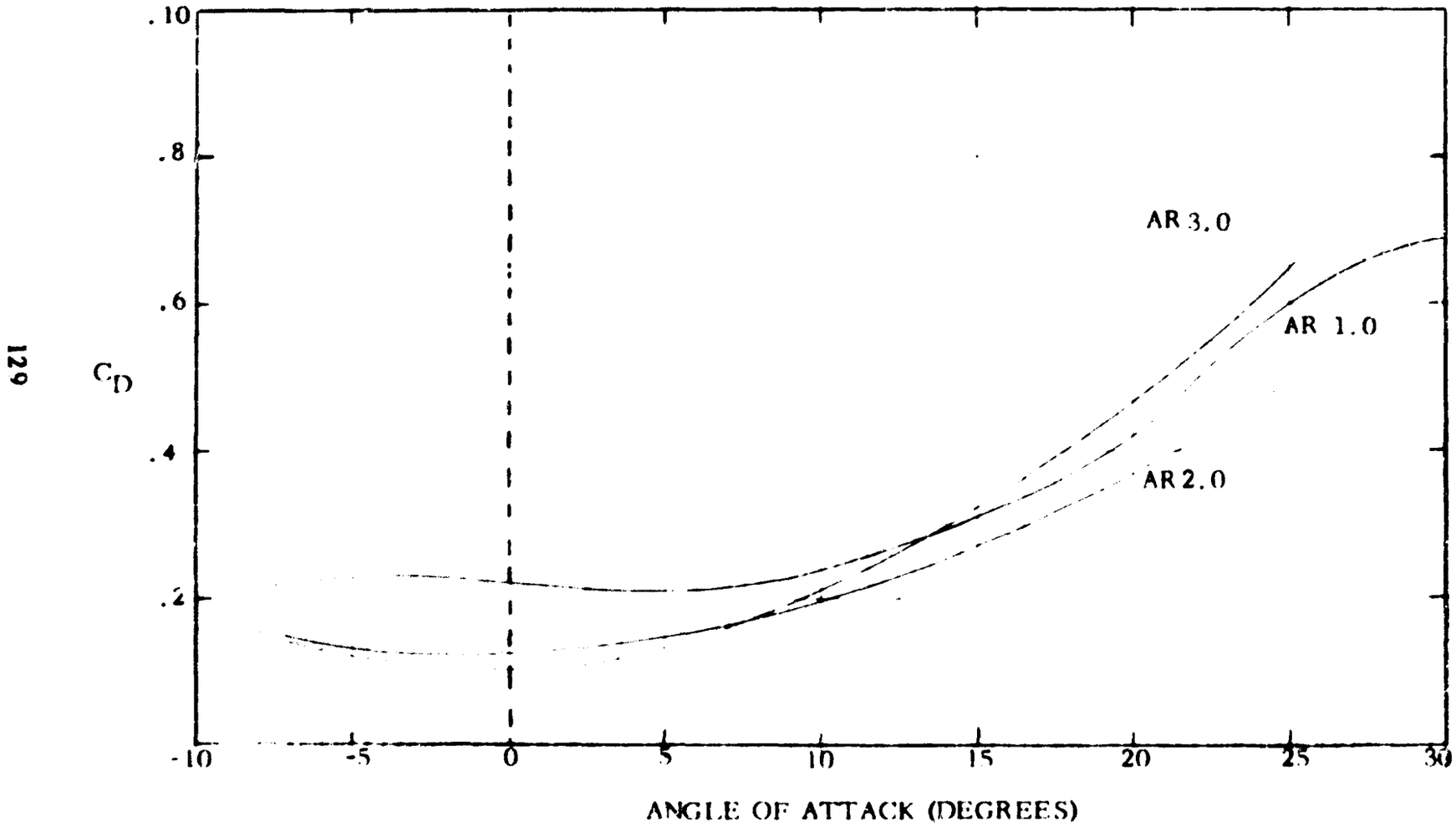

Figure 94c. Drag Coefficient: AR Summary

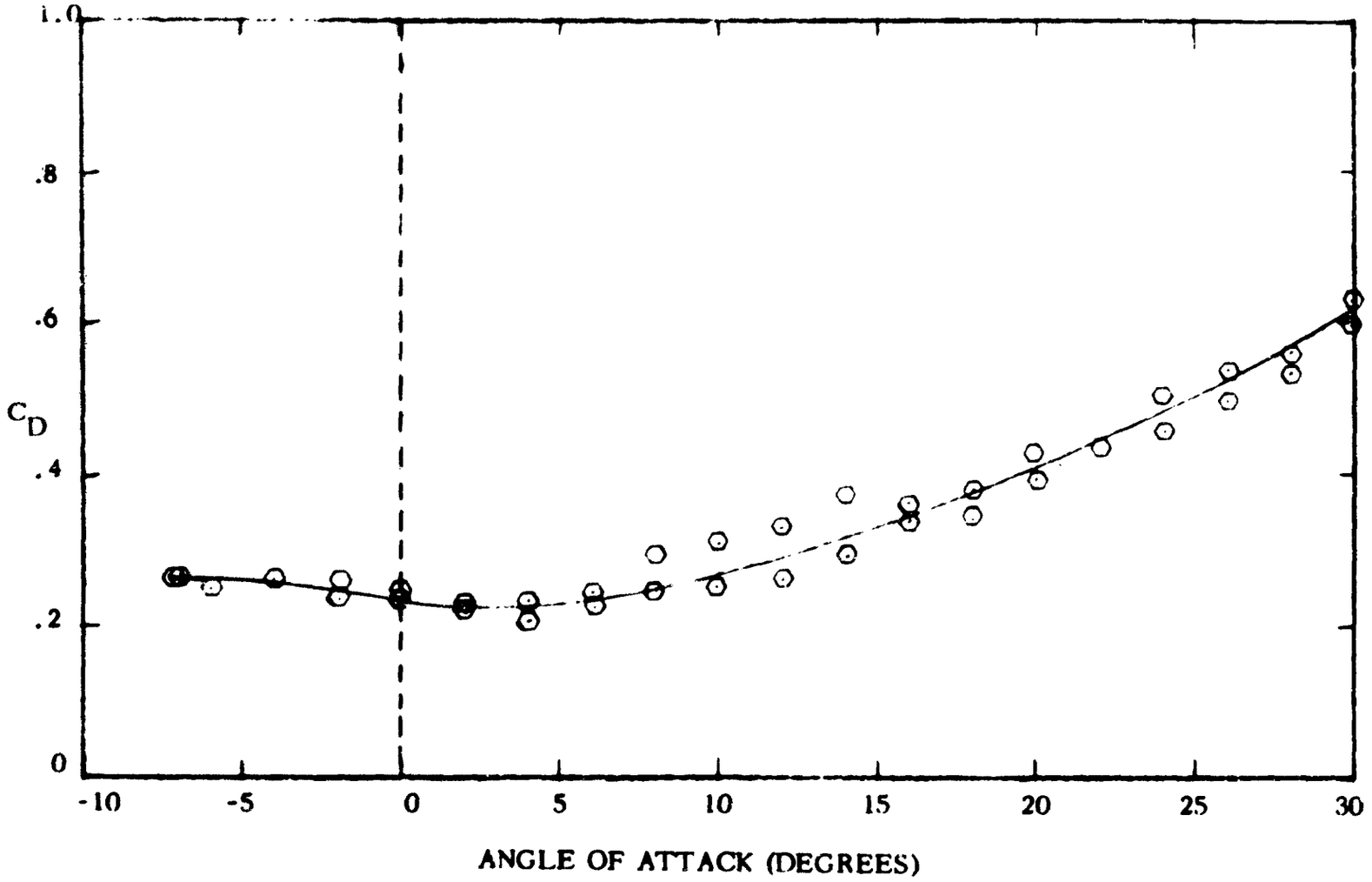

Figure 95. AR 0.5 Drag Coefficient Summary

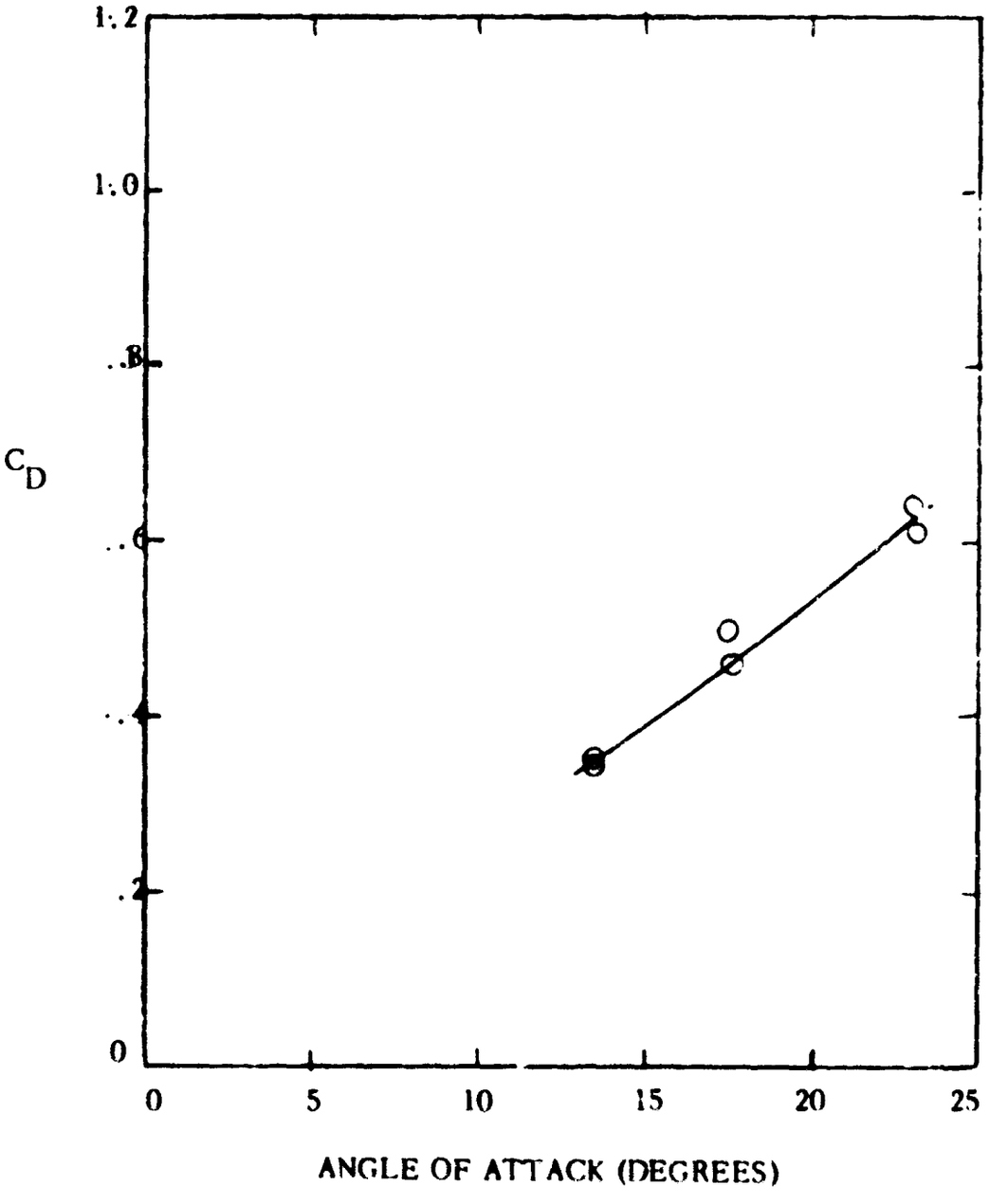

Figure 96. AR 0.64 Drag Coefficient Summary

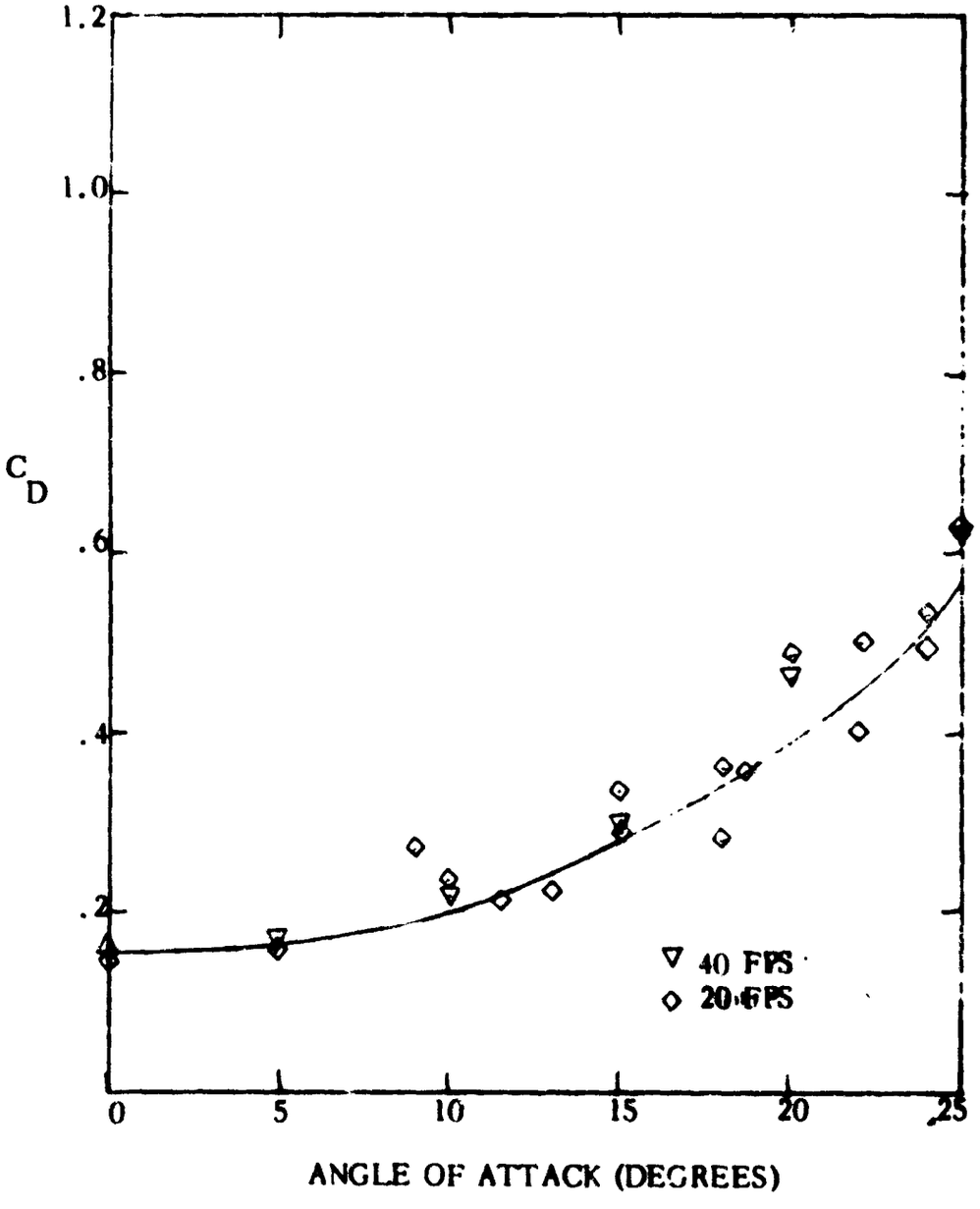

Figure 97. AR 0.78 Drag Coefficient Summary

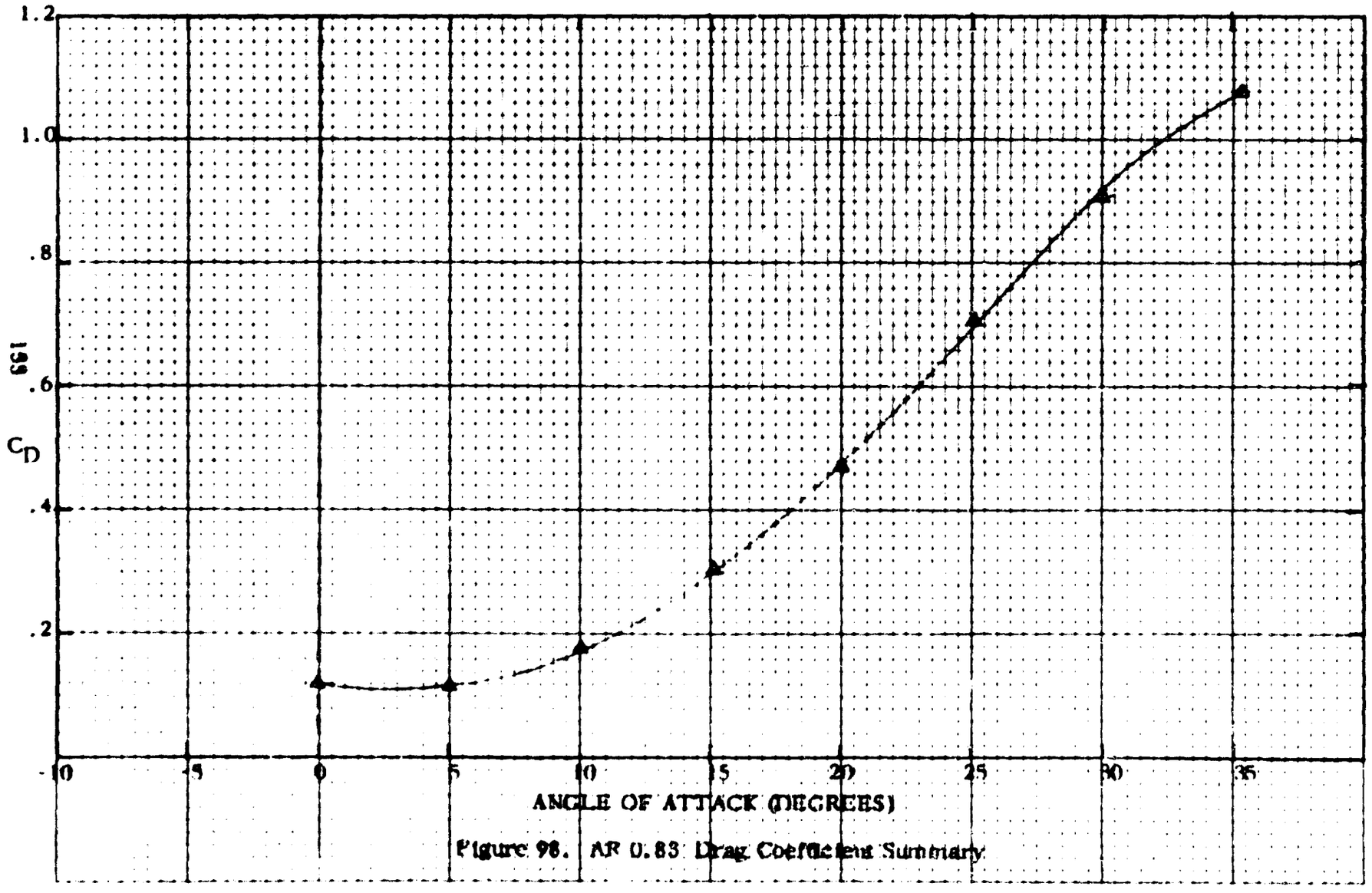

Figure 98. AR 0.83 Drag Coefficient Summary

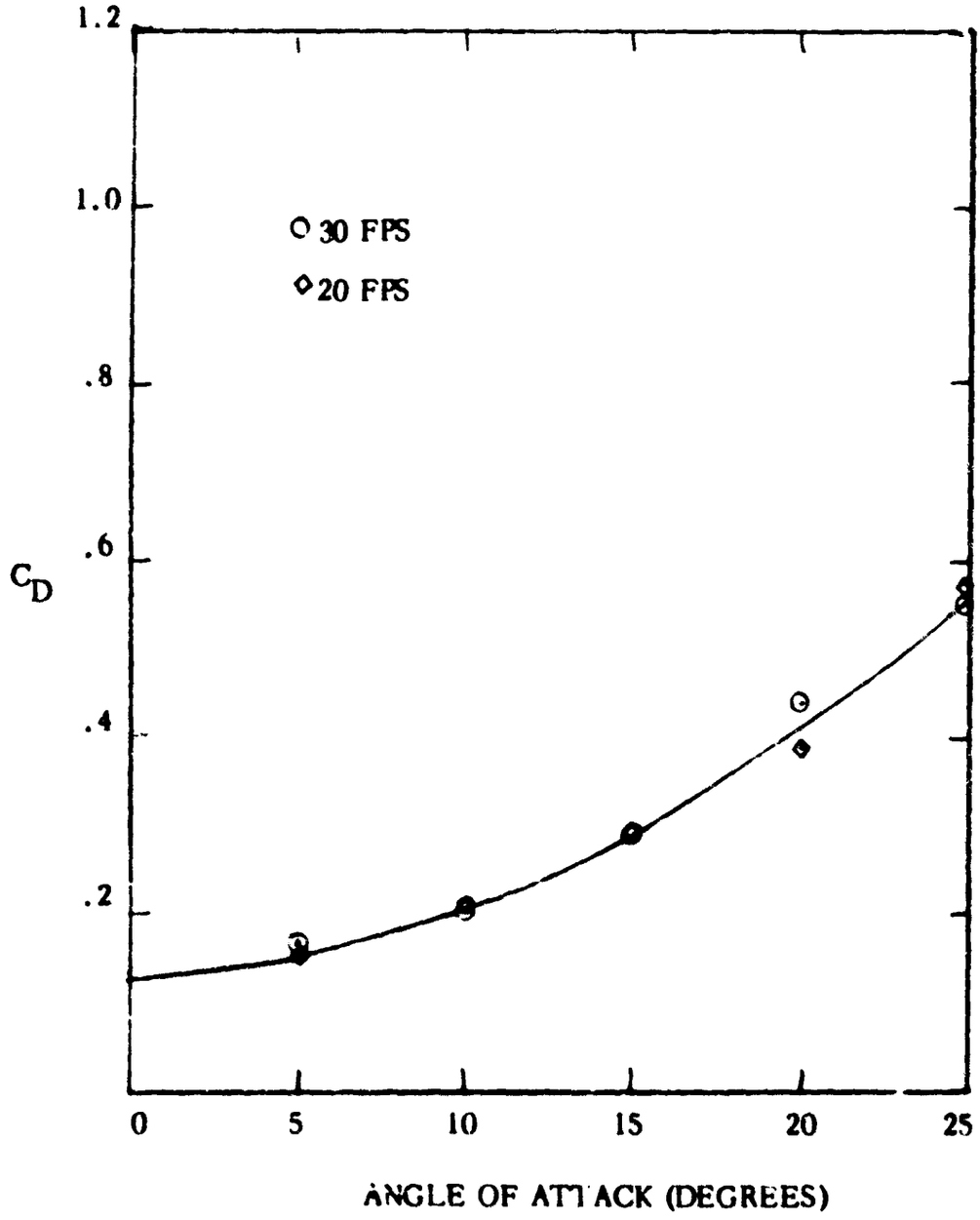

Figure 99. AR 0.94 Drag Coefficient Summary

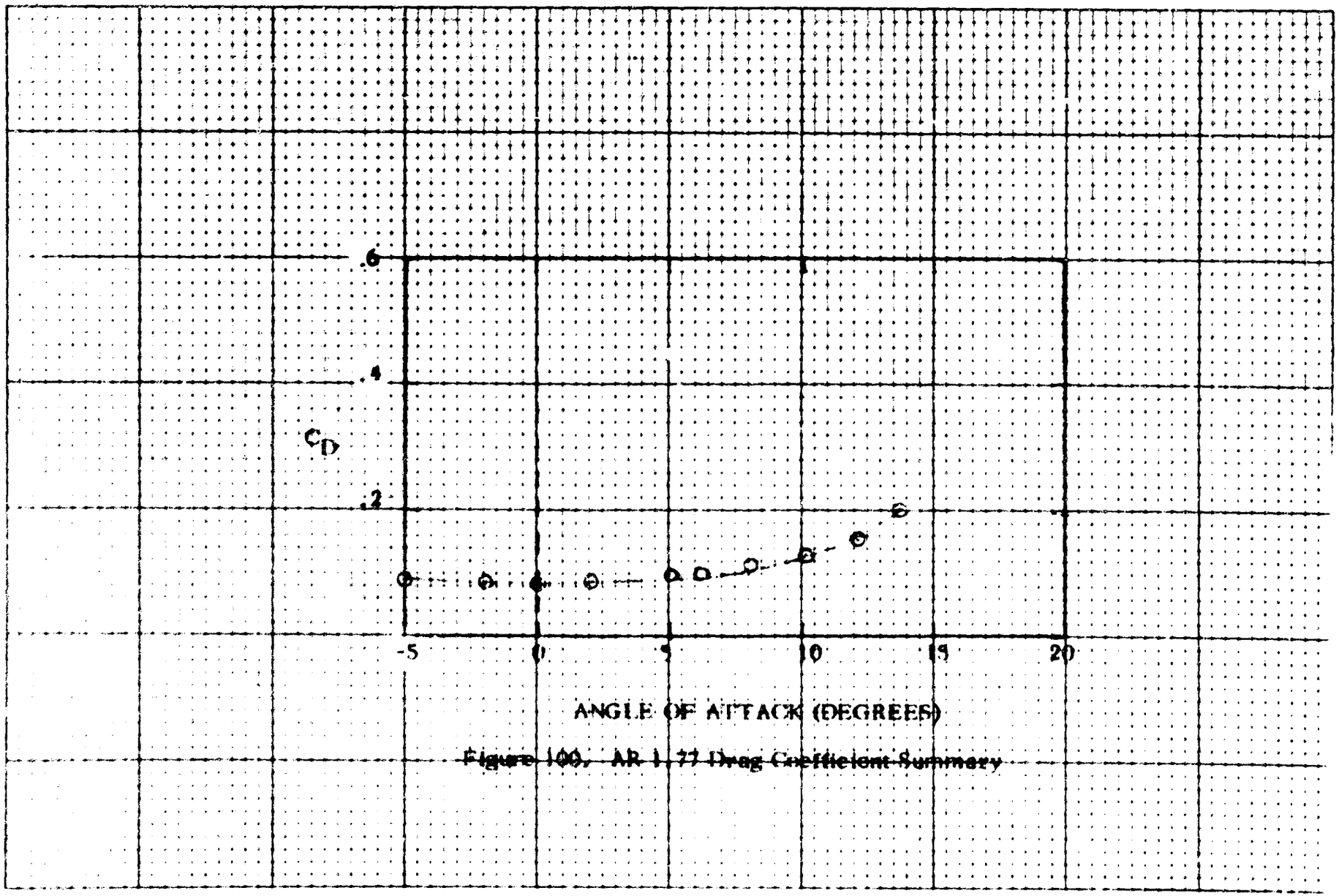

Figure 100. AR 1.77 Drag Coefficient Summary

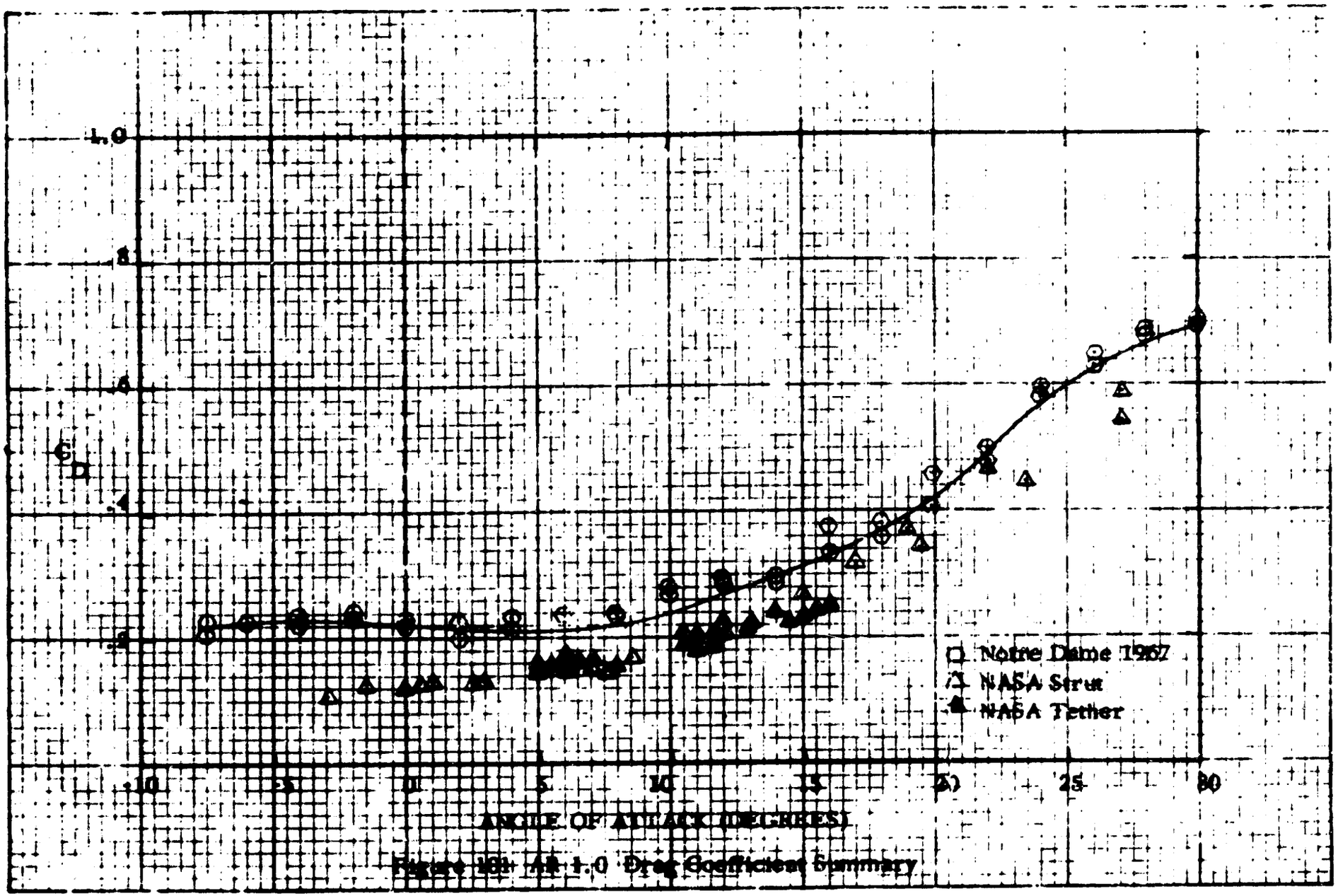

Figure 10: M_∞ 1.0 Drag Coefficient Summary

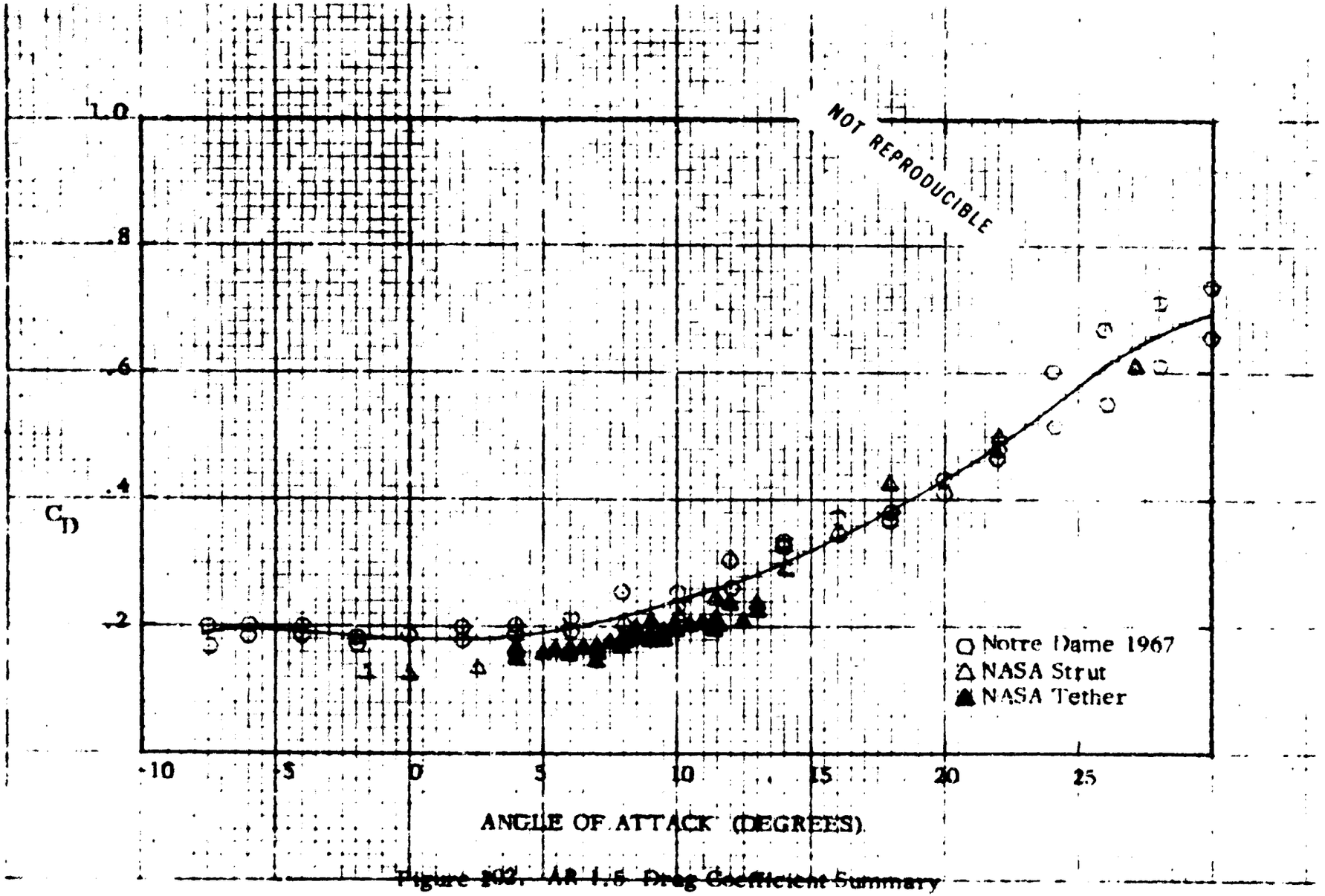

Figure 202. AR 1.5 Drag Coefficient Summary

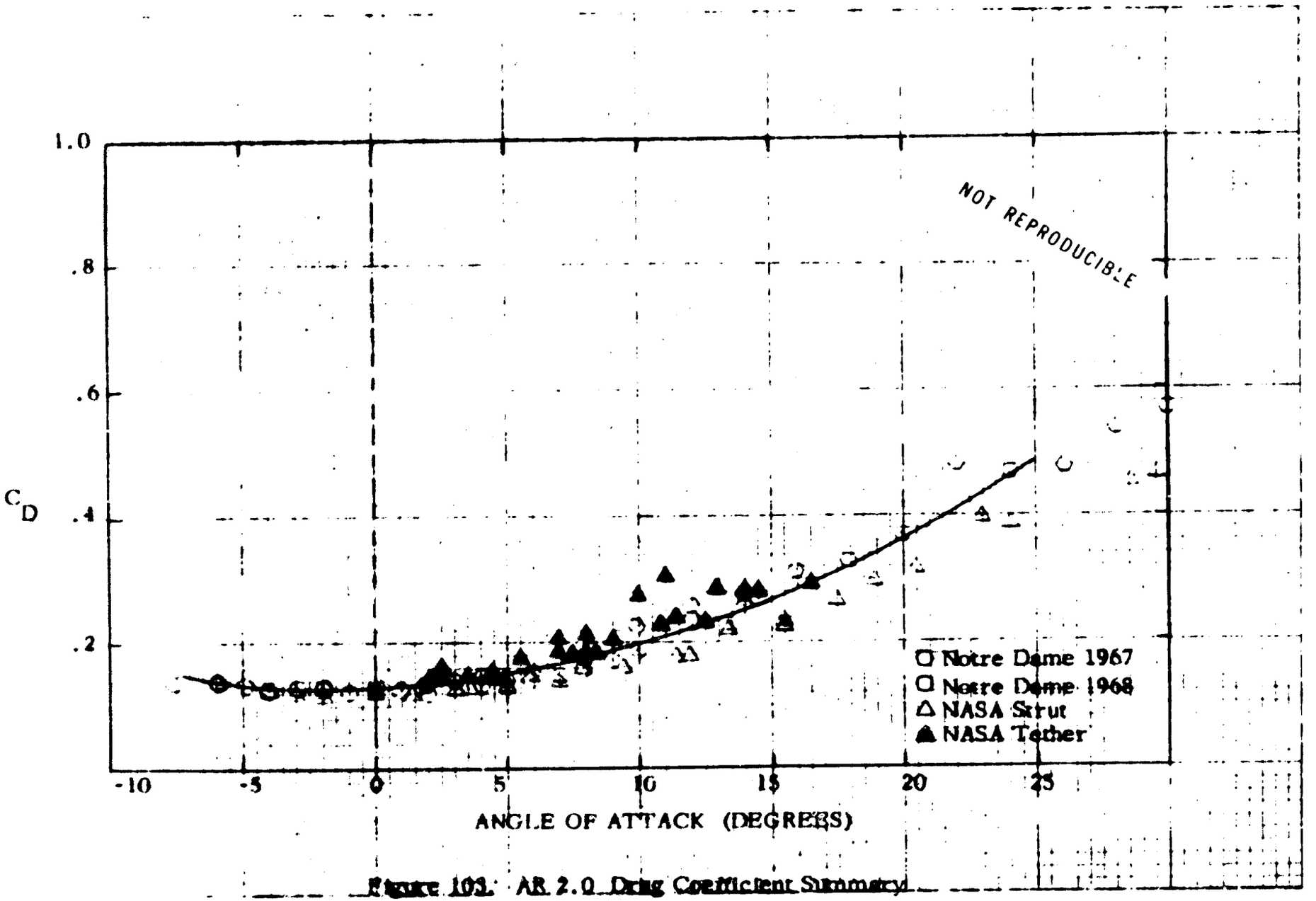

Figure 103. AR 2.0 Drag Coefficient Summary

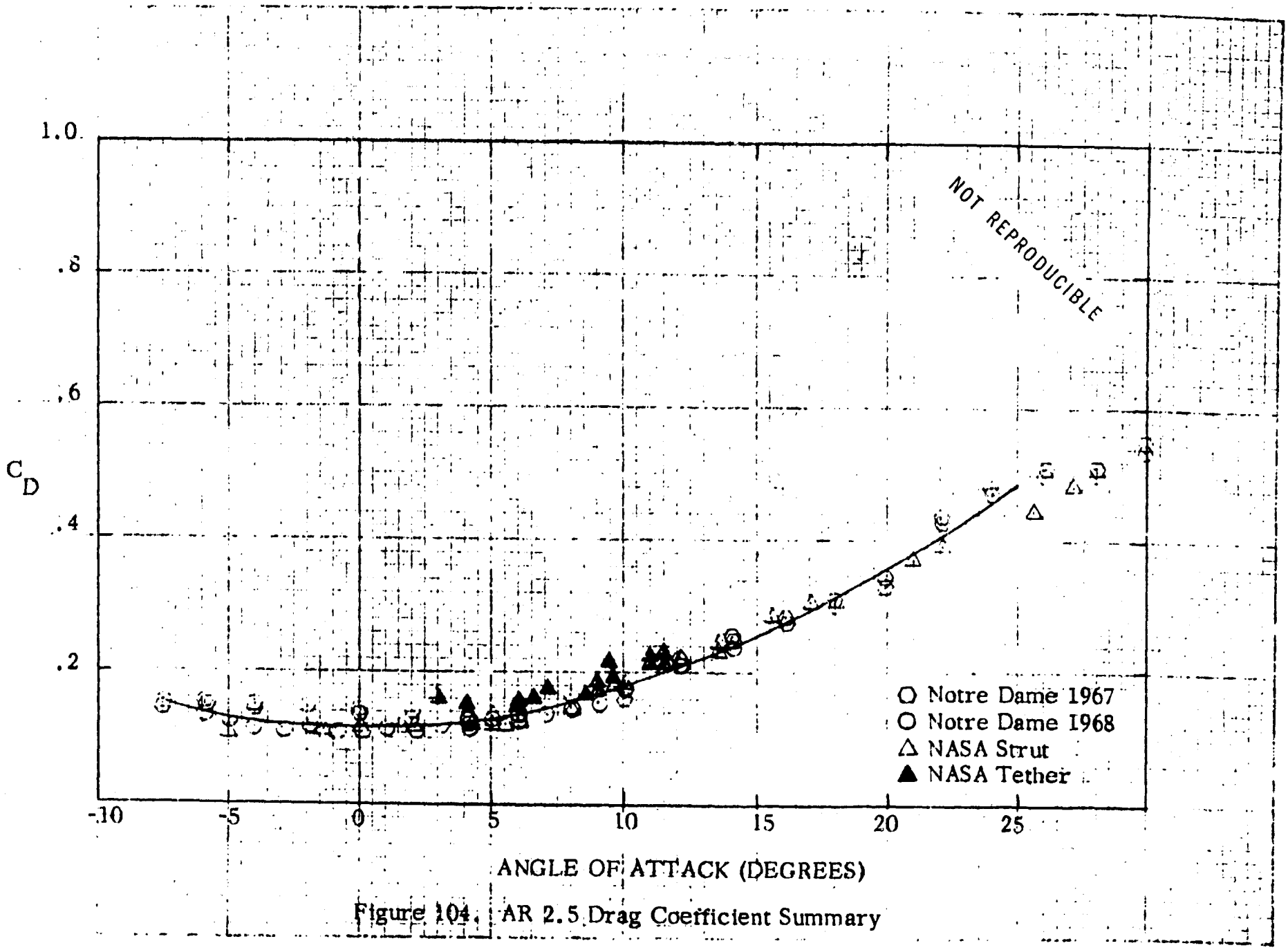

Figure 104. AR 2.5 Drag Coefficient Summary

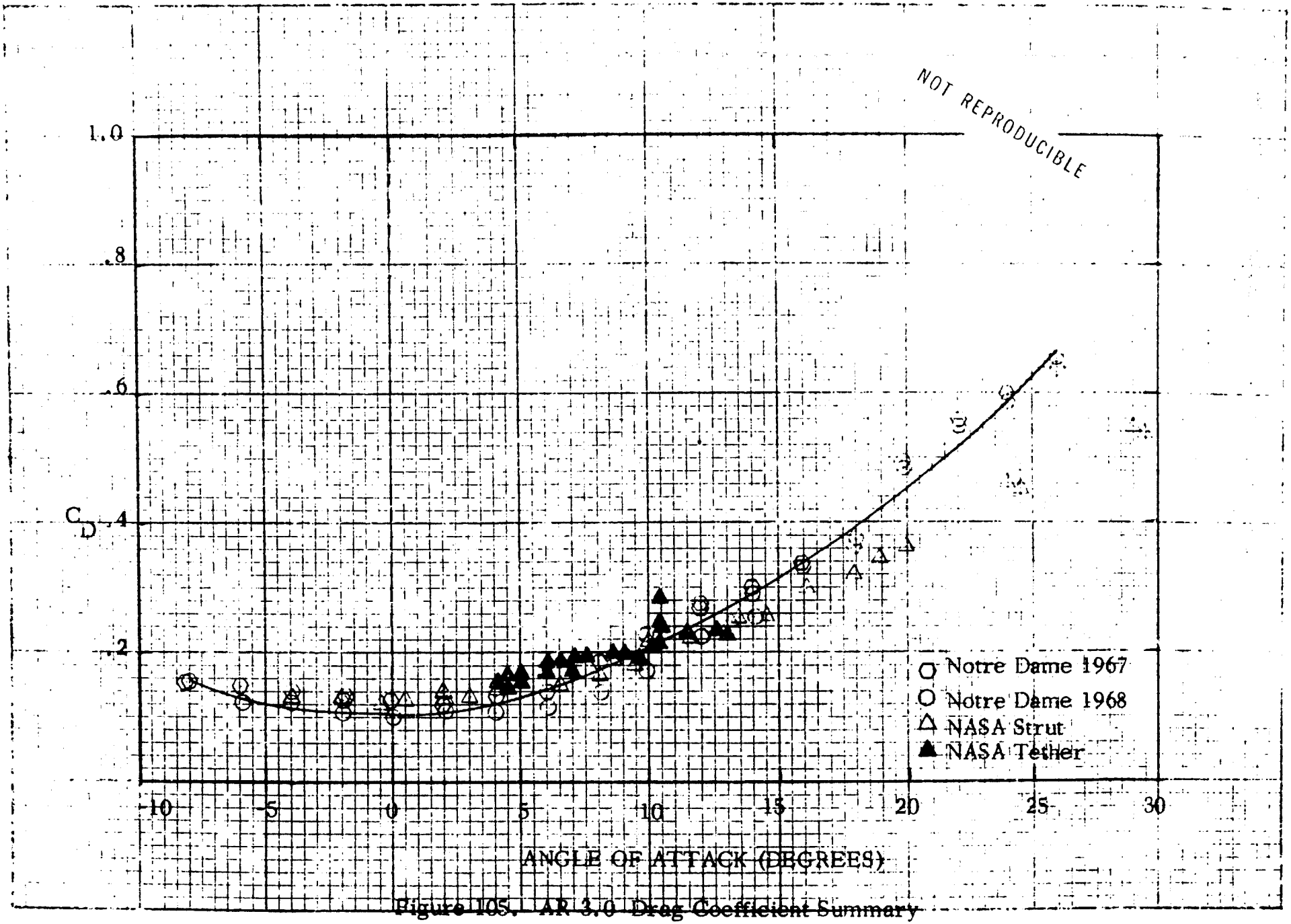

Figure 105. AR 3.0 Drag Coefficient Summary

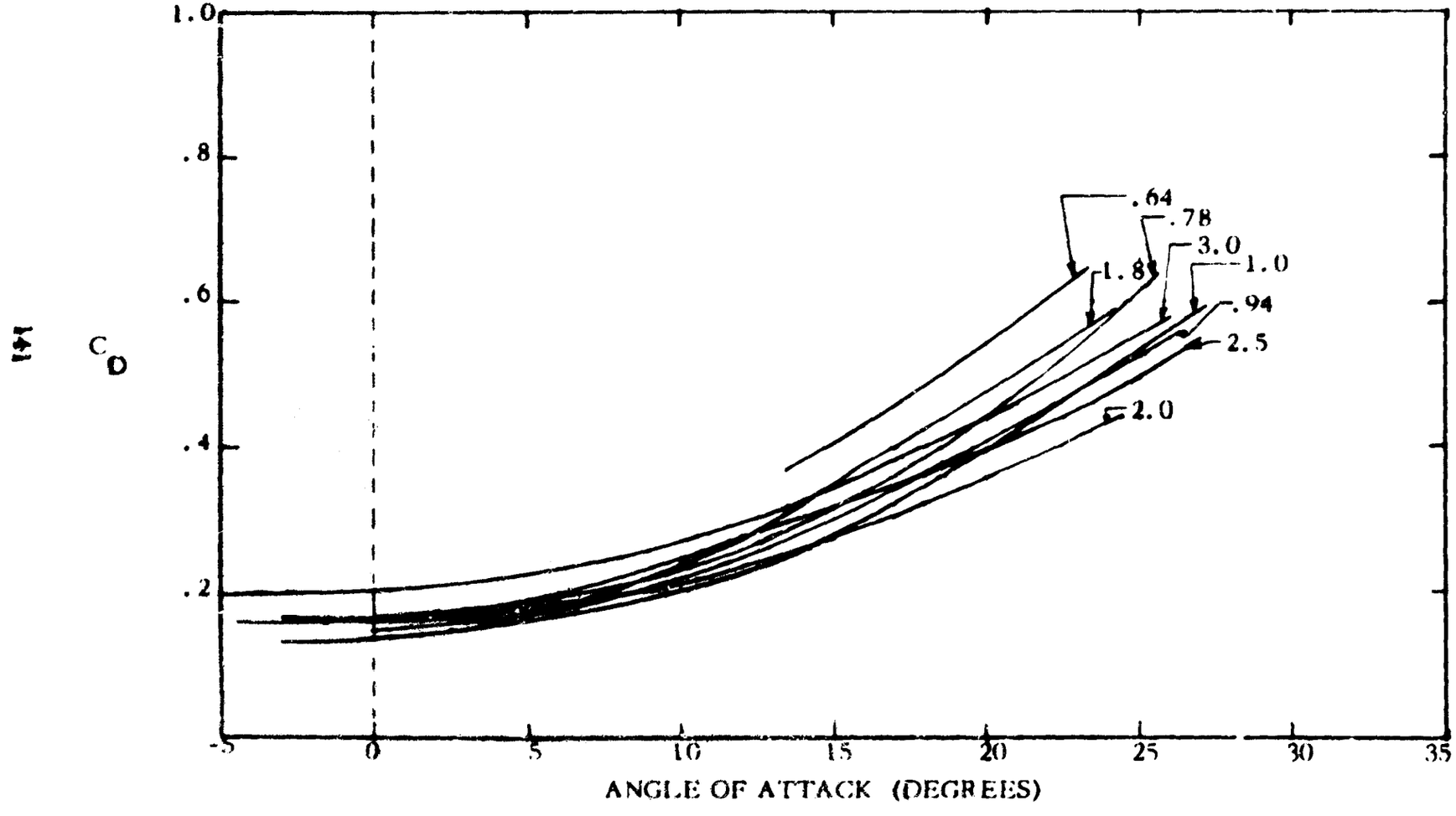

Figure 106. Drag Coefficient With Line Drag: AR Summary

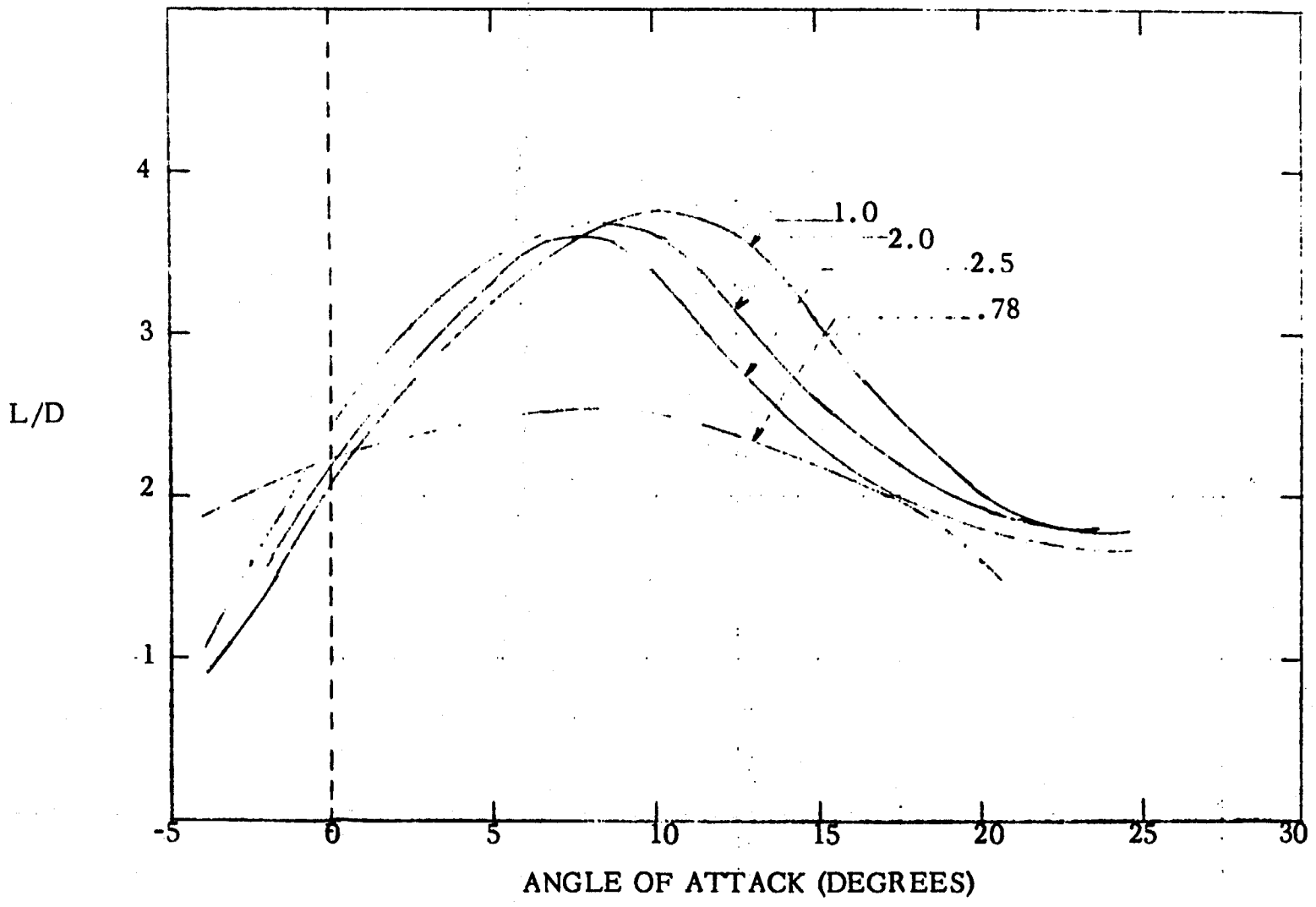

Figure 107. Lift to Drag Ratio with Line Drag: AR Summary

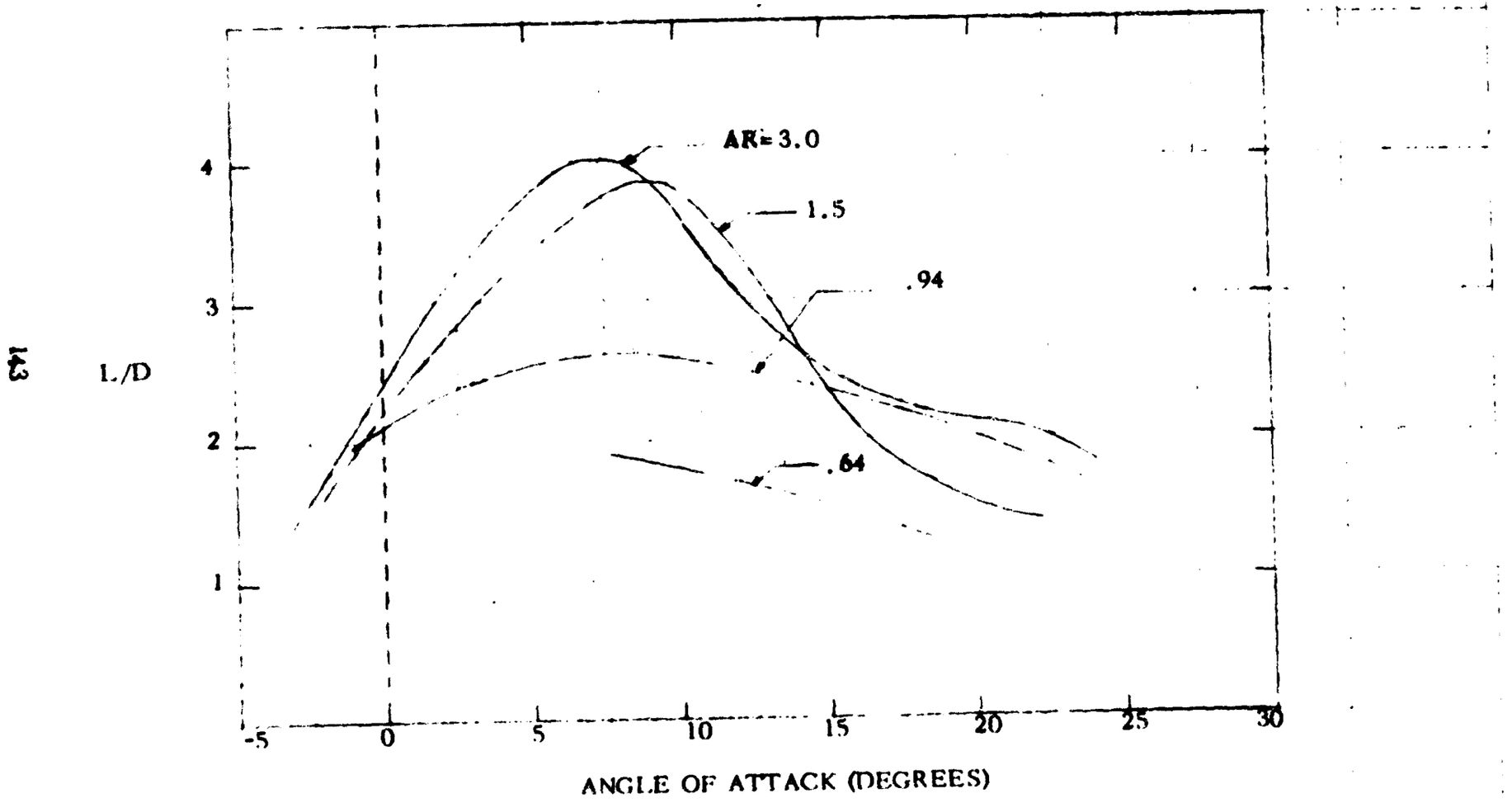

Figure 108. Lift to Drag Ratio with Line Drag: AR Summary

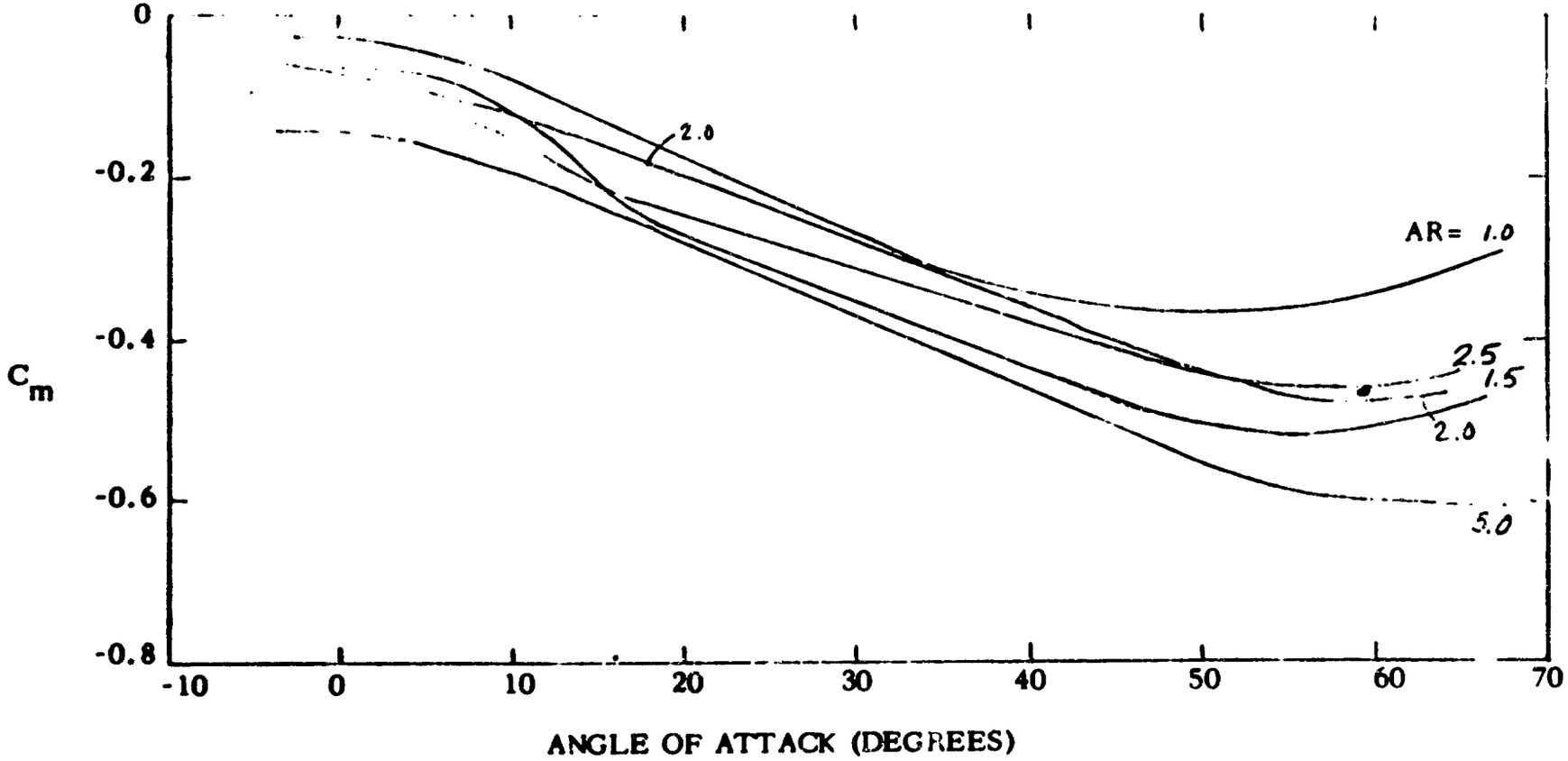

Figure 109. Cm vs α AR Summary Curves at 40 FPS.Cm at c/4.

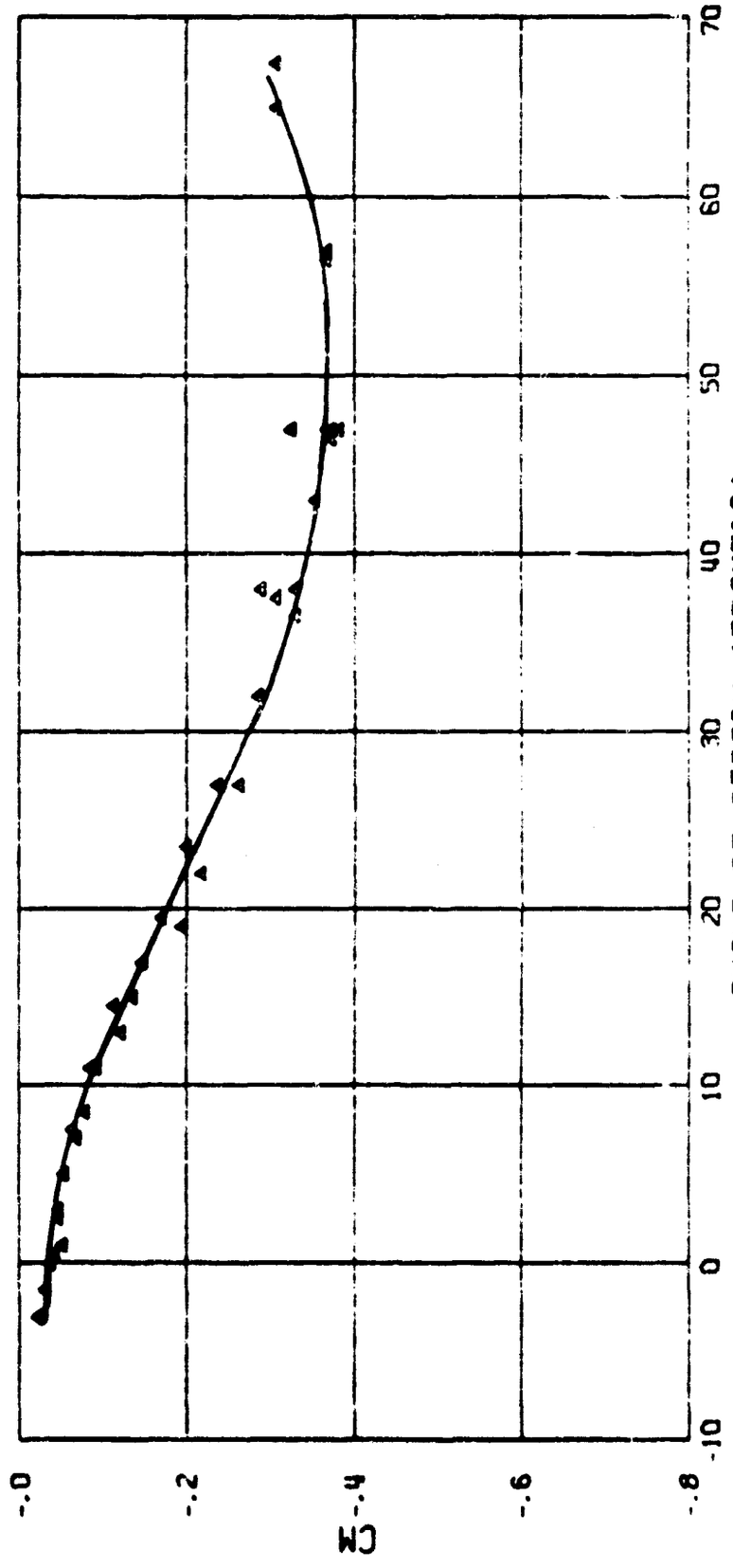

Figure 110. AR 1.0 C_m vs α

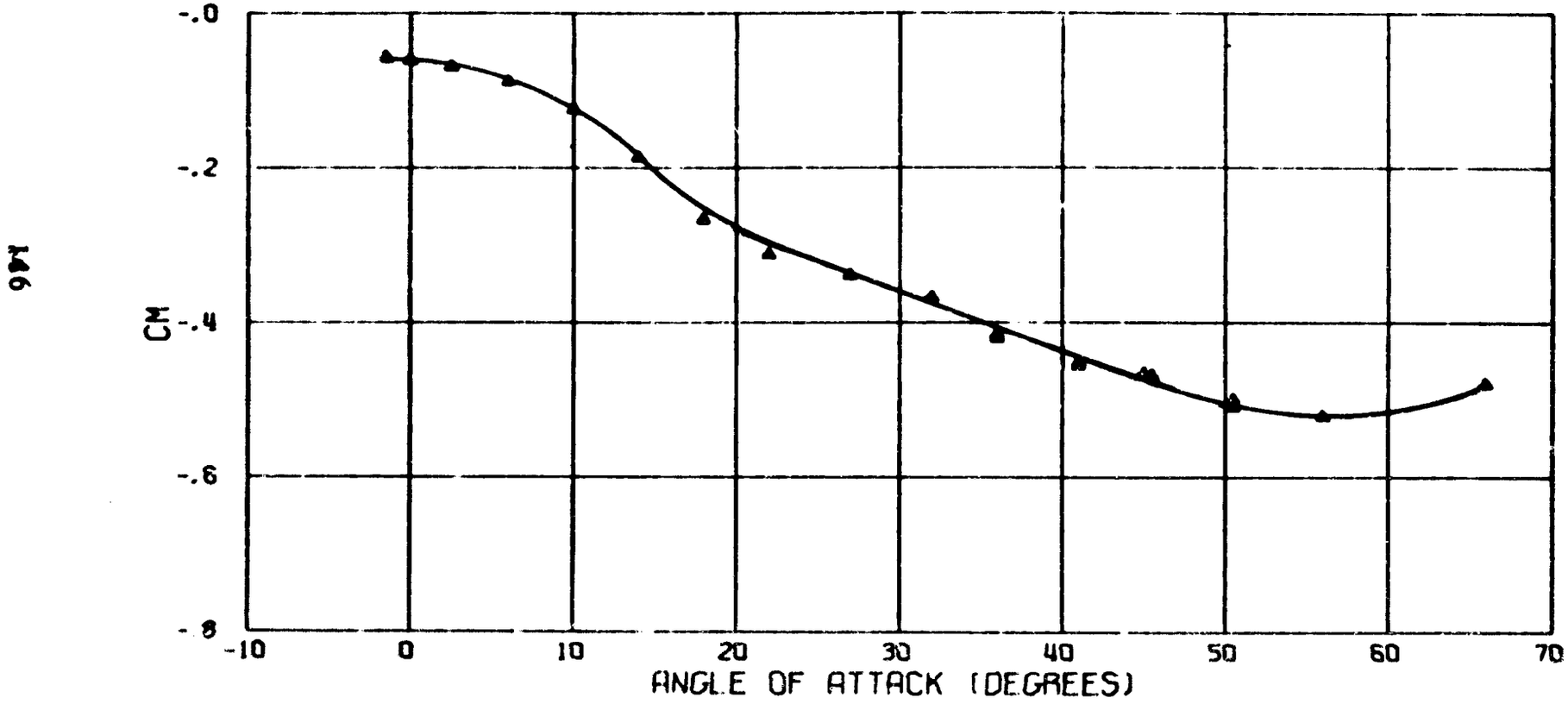

Figure 111 . AR 1.5 C_m vs α

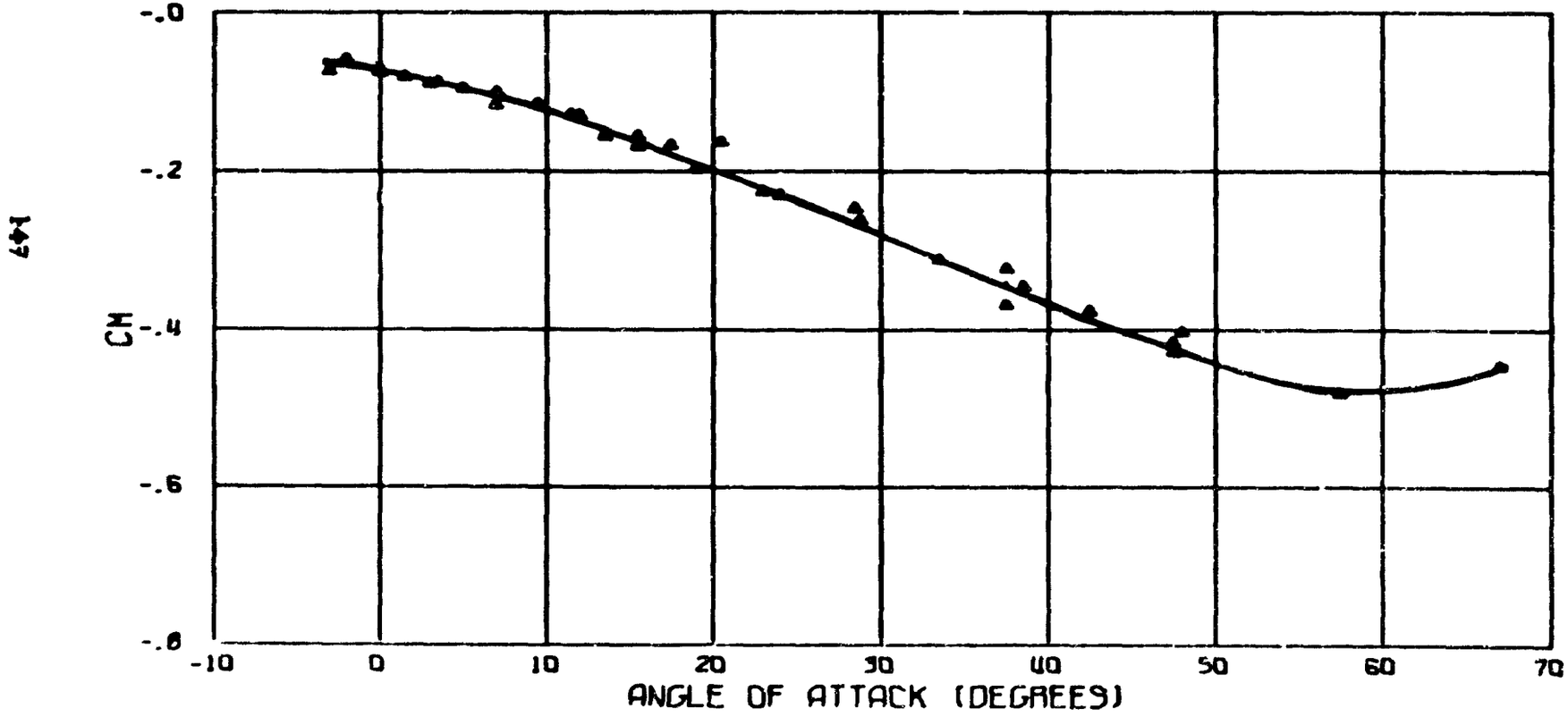

Figure 112. AR 2.0 C_m vs α

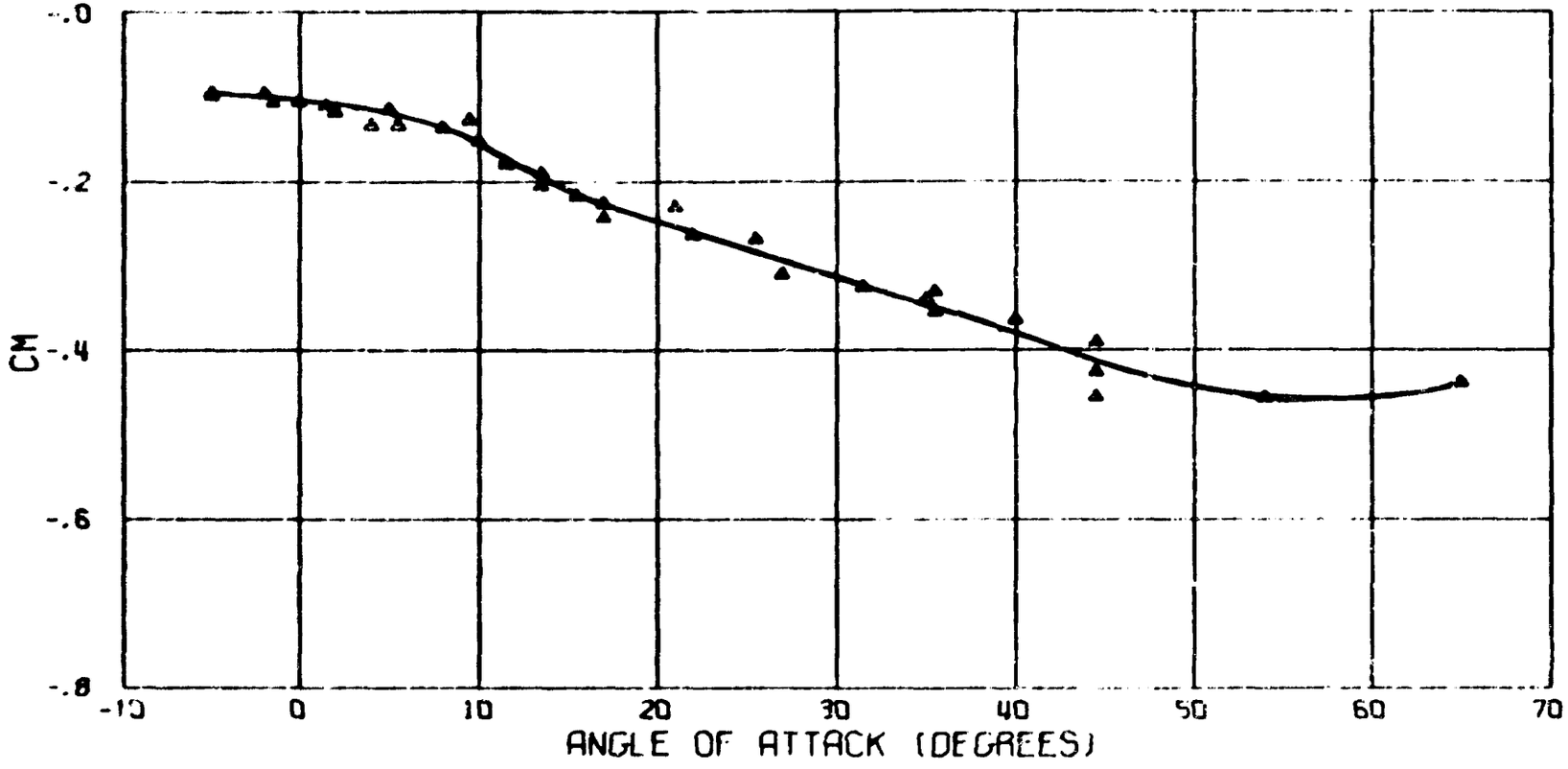

Figure 113. AR 2.5 C_m vs C_L

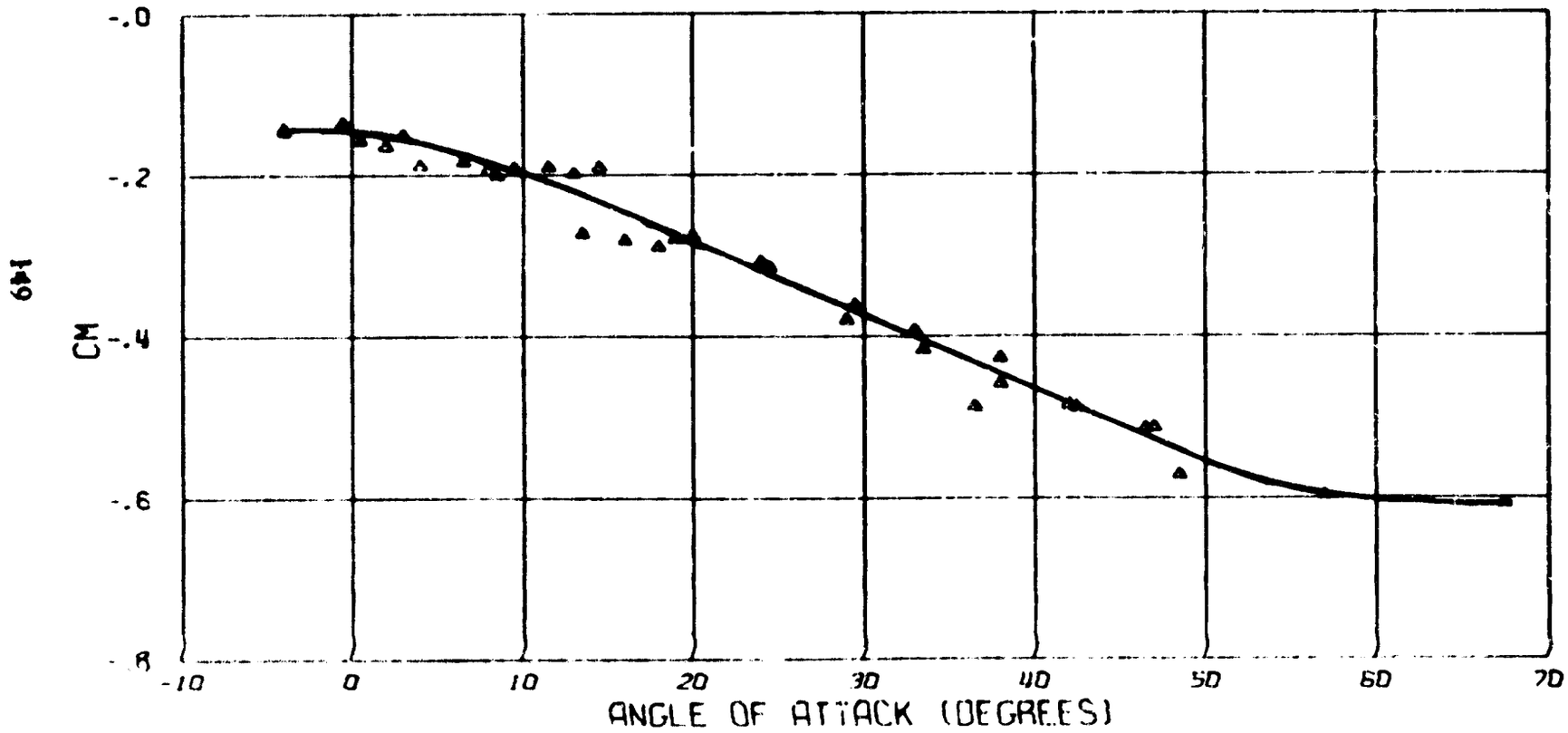

Figure 114. AR 3.0 C_m vs α

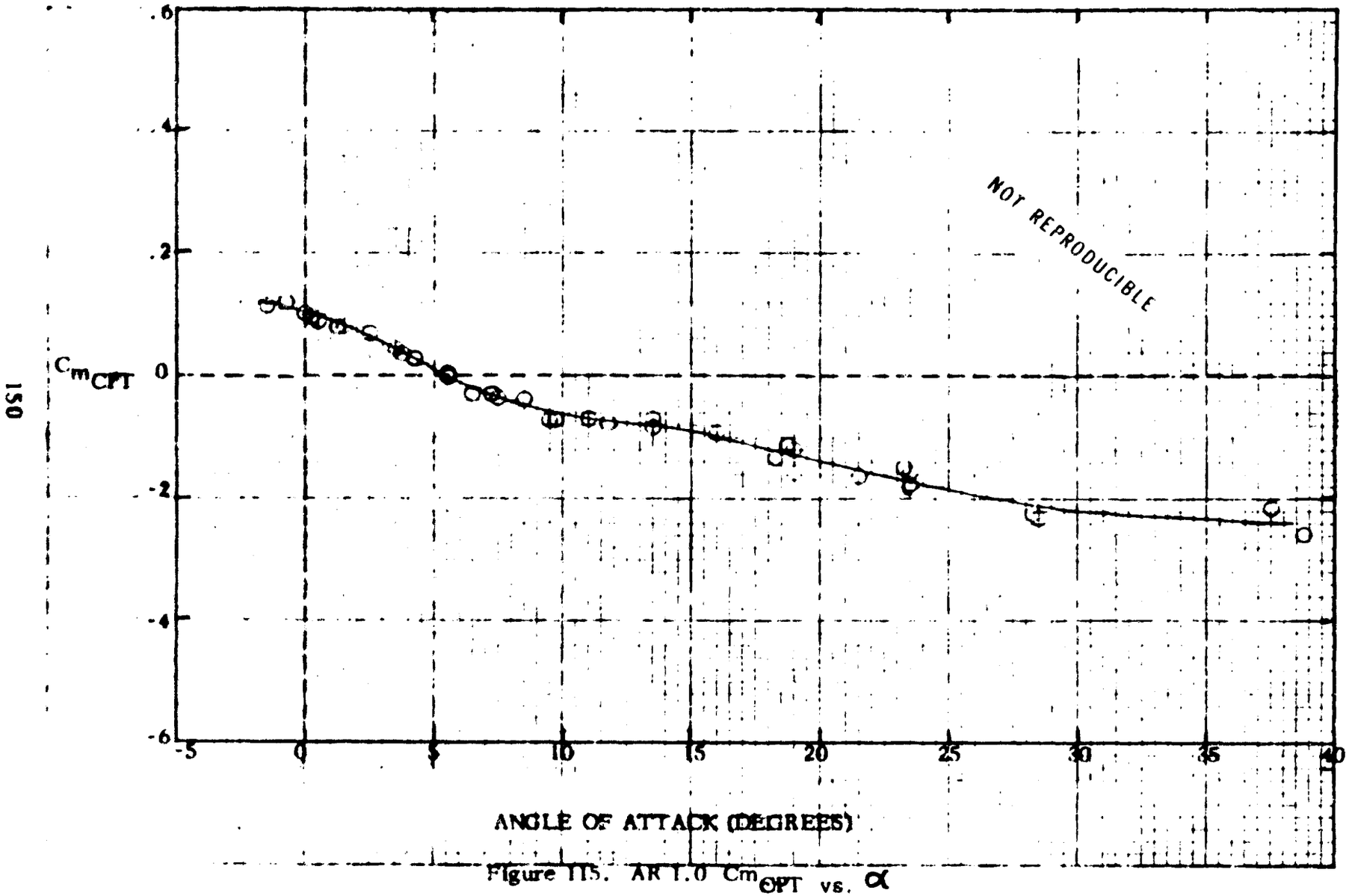

Figure 115. AR 1.0 Cm_{CPT} vs. α

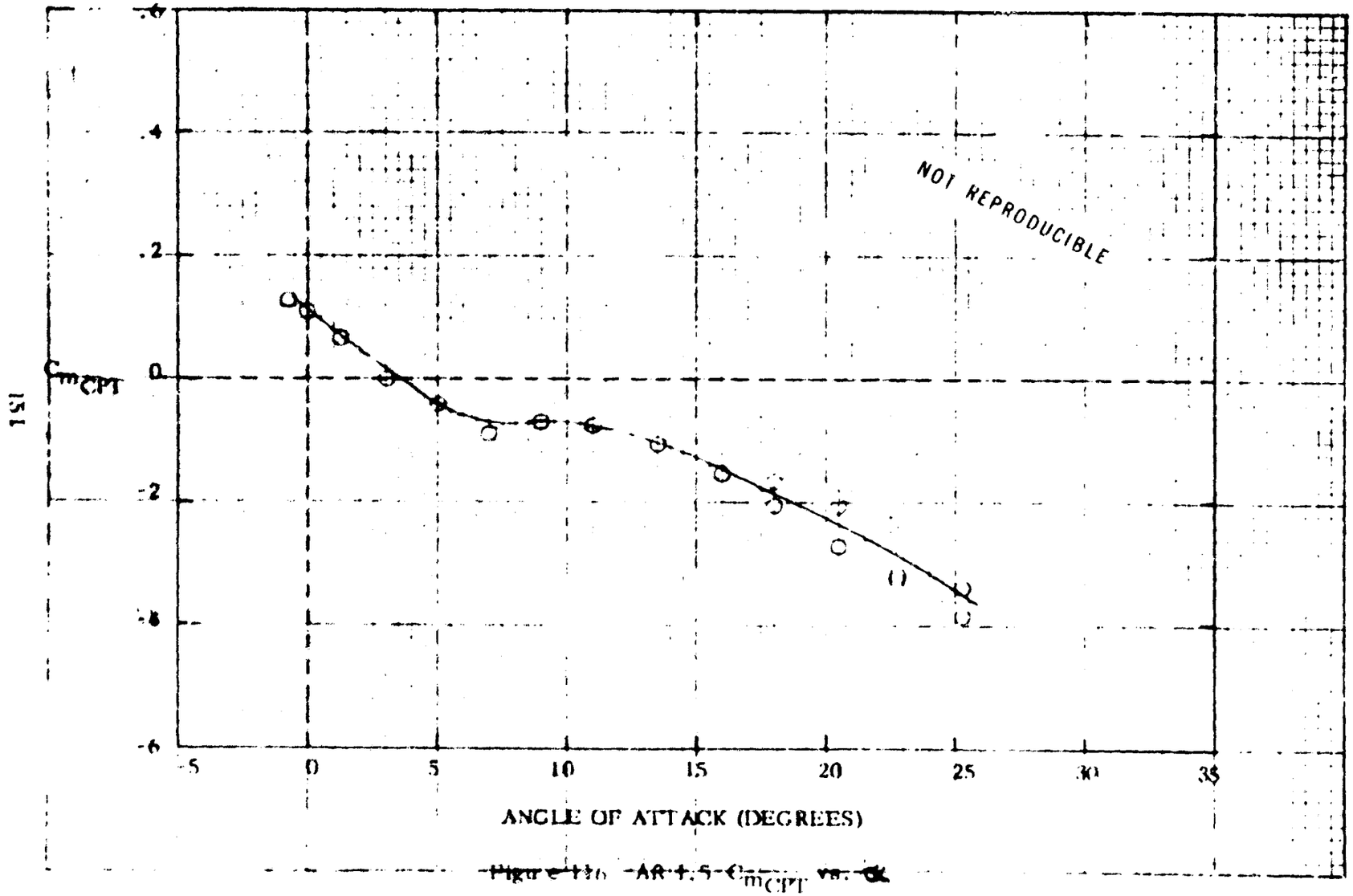

Figure 116. AR 1.5 $C_{m_{CPT}}$ vs. α

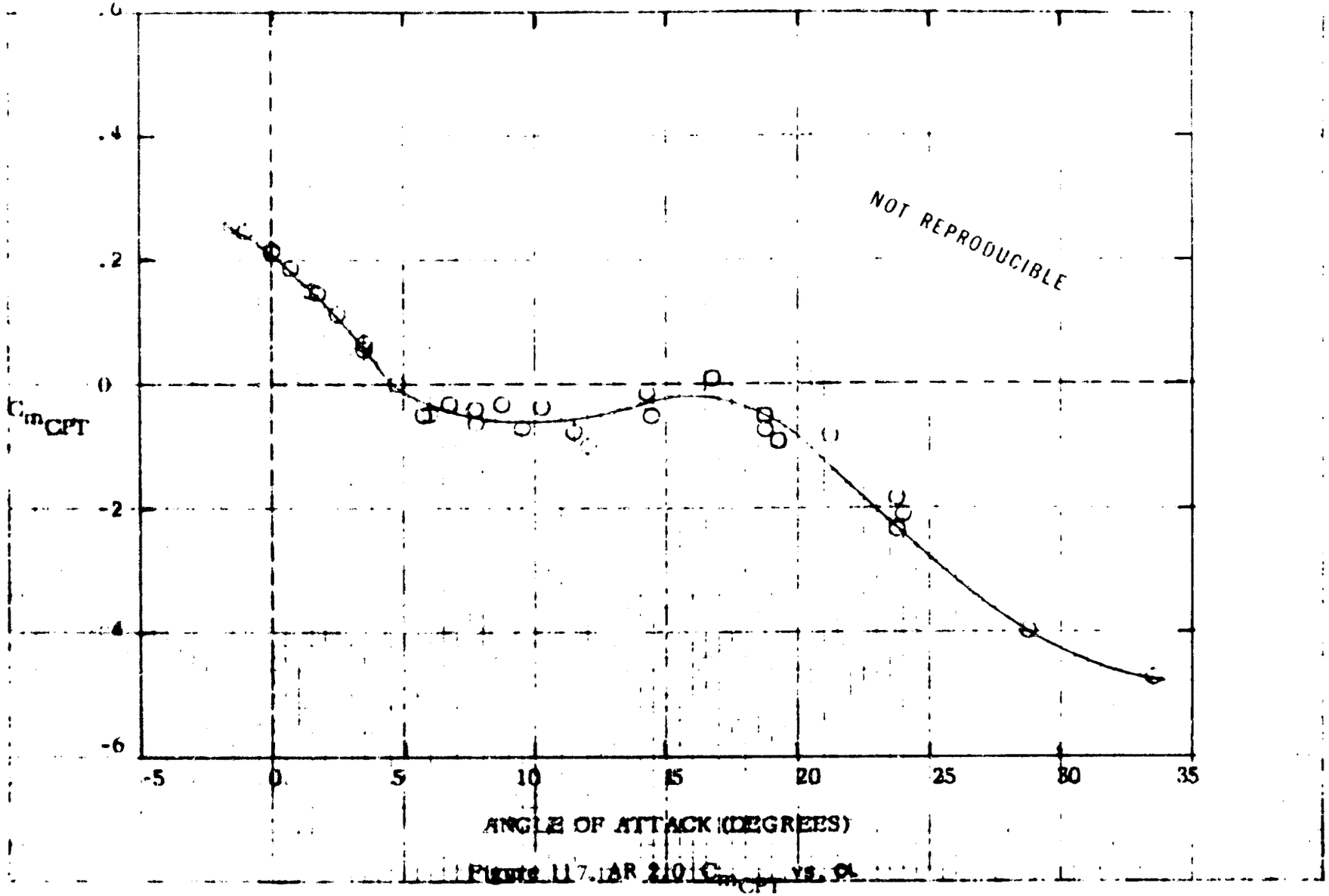

Figure 117. AR 210 $C_{m_{CPT}}$ vs. α

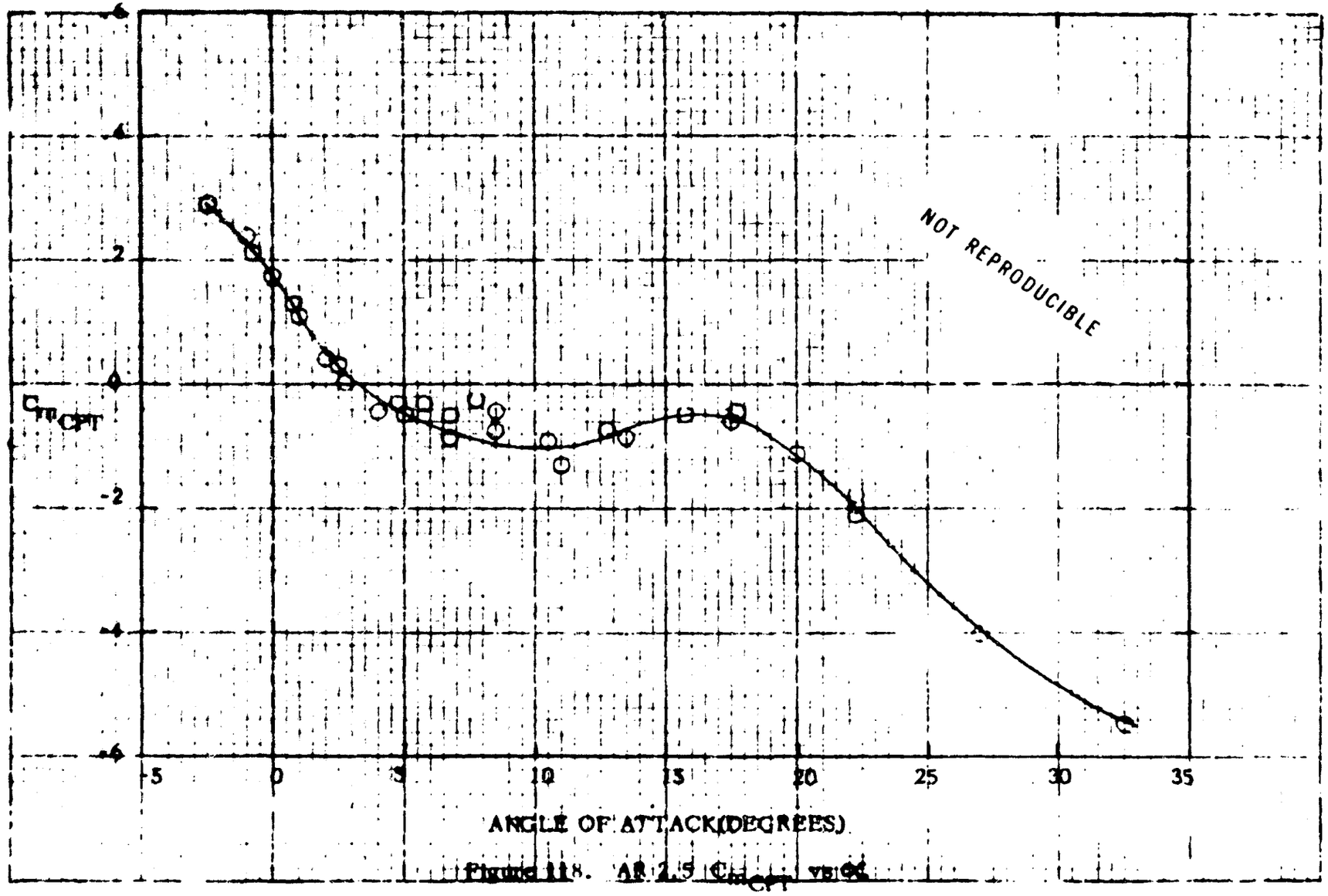

Figure 118. AR 2.5 $C_{m_{C/4_T}}$ vs α

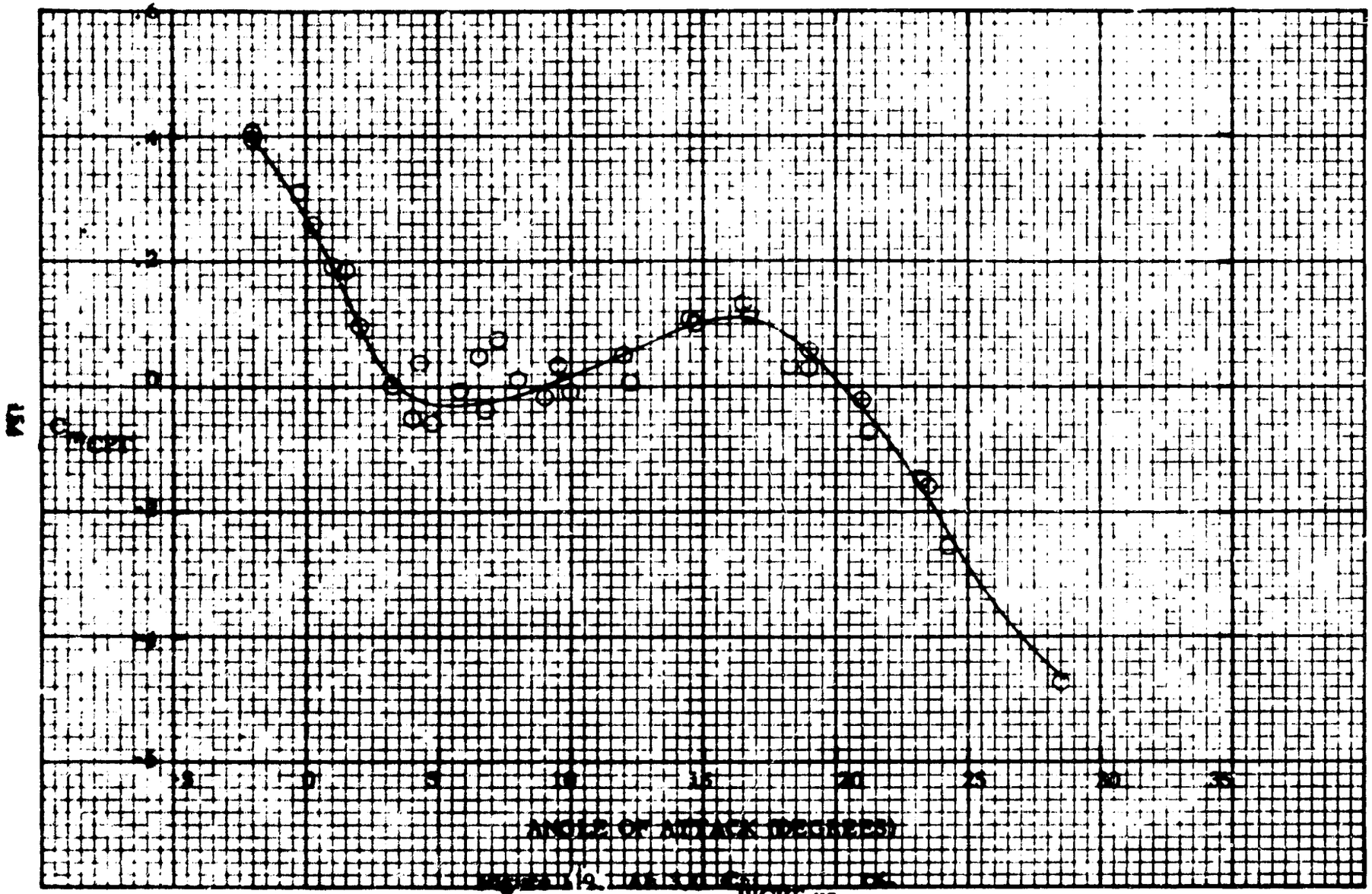

Figure 3-12. Aft Section $C_{m_{CPT}}$ vs. α

APPENDICES

APPENDICES

APPENDIX I

Transformation of Moment Coefficients About Confluence Point

The stability axes systems used in the development and presentation of the NASA Langley data and the positive direction of forces, moments, and angles are given in Figures I-1 and I-2.

As the Para-Foil moves through an air mass, forces are generated due to the dynamic reaction on the air similar to the forces associated with the wings of an airplane. These generated aerodynamic forces are known as the lift and drag forces of general airfoil theory.[12] When considered as a resultant force acting at the center of pressure varying with attitude, a moment about the lateral axis is introduced (Figure I-1). This moment is known as the pitching moment and affects the longitudinal stability of the Para-Foil.[13,14,15]

If the Para-Foil is flying directly aligned with the wind, the lift and drag are the only fluid forces generated. However, if this is not the case, additional forces are generated which act perpendicular to the lift and drag. This occurs when the relative wind is making some angle to the Para-Foil centerline (angle of sideslip, β). The resultant of these forces acting in the lateral plane is the side force, and depending upon its position and orientation with respect to the center of mass, additional moments are created. The moment tending to rotate the Para-Foil about its longitudinal axis is known as the rolling moment; about the vertical axis is known as the yawing moment (Figure I-1).[13,14,15]

The various moment coefficients are usually obtained experimentally in wind tunnel testing techniques about an arbitrary chosen reference point. Sometimes, as in the case of the Parafoil, it becomes advantageous to transfer the moment information to another point in the system (when a stability analysis of the total system is desired). For the Parafoil this point is the confluence point (CPT), that is, the point where all suspension lines are joined together and the payload is located Figure I-3.

Longitudinal Stability

The primary factor relating to longitudinal stability is the pitching moment, hence the following development outlines the derivation of the pitching moment about the CPT. To determine the pitching moment about the CPT consult Figure I-3. Summing moments about the CPT yields:

$$M_{CPT} = qSC_A \bar{z} - qSC_N x \tag{1}$$

in coefficient form:

$$cC_{M_{CPT}} = \bar{z} C_A - xC_N$$

$$= \bar{z} C_A - (\bar{x} + x_{CP}) C_N \tag{2}$$

$$= \bar{z} C_A - \bar{x} C_N - x_{CP} C_N \tag{3}$$

From Figure I-3 the following geometric relationship can be determined:

$$C_N = C_R \cos (\gamma_1 - \alpha) \tag{4}$$

with

$$cC_{m_{ref}} = - aC_R$$

$$C_R = - (\frac{c}{a}) C_{m_{ref}} \tag{5}$$

hence

$$C_N = -\left(\frac{c}{a}\right) C_{m_{ref}} \cos\left(\gamma_t - \alpha\right) \tag{6}$$

Now

$$x_{CP} = \frac{a}{\cos\left(\gamma_t - \alpha\right)} \tag{7}$$

Therefore from equations (6) and (7)

$$x_{CP} C_N = -cC_{m_{ref}} \tag{8}$$

and upon substitution of (8) into (3), results

$$cC_{m_{CPT}} = \bar{z}C_A - \bar{x}C_N + cC_{m_{ref}} \tag{9}$$

and upon division of the chord length, c, becomes

$$C_{m_{CPT}} = \frac{\bar{z}}{c} C_A - \frac{\bar{x}}{c} C_N + C_{m_{ref}} \tag{10}$$

where the independent variable is the angle of attack, α . For a given α , the coefficients C_L, C_D, and $C_{m_{ref}}$, are measured. Knowing these values, the axial force coefficient, C_A, and the normal force coefficient, C_N, are determined from the geometry of figure I-3.

$$C_A = C_R \sin\left(\gamma_t - \alpha\right) \tag{11a}$$

$$C_N = C_R \cos\left(\gamma_t - \alpha\right) \tag{11b}$$

where

$$C_R = \sqrt{C_L^2 + C_D^2} \tag{12}$$

$$\gamma_t = \arctan\left(C_D/C_L\right) \tag{13}$$

Hence, returning to equation (10) $\bar{x}$ and $\bar{z}$, the horizontal and vertical distances to the CPT from the reference point respectively, are the only remaining unknown parameters of the right hand side.

For the scope of this analysis, all tests were conducted with $\bar{z} = 1.5b$. Corresponding to this vertical distance there is only one value of $\bar{x}$ associated with a condition of longitudinal balance. This condition of longitudinal balance occurs when $C_{m_{CPT}} = 0$.[14] Imposing this condition on equation (10) and solving for $\bar{x}$ yields,

$$\bar{x} = \frac{cC_{m_{ref}} + \bar{z} \quad C_A}{C_N} \tag{14}$$

where the coefficients $C_{m_{ref}}$, C_N, and C_A are the values corresponding to the angle of attack at which C_L/C_D is a maximum. The Para-Foil is then rigged to fly at this trim angle-of-attack, which yields its best performance.

The behavior of the pitching moment about the CPT versus α will then determine the static longitudinal stability of the Para-Foil. Mathematically this corresponds to the sign and magnitude of the slope C_{m_α}, where a negative slope implies static longitudinal stability.[14]

Directional Stability

When the Para-Foil is at an angle of sideslip, ϕ, relative to its flight path, the yawing moment produced must be such as to restore it to symmetric flight. If the yawing moment coefficient is as shown in figure 1-2 the requirement for static directional stability is that the slope C_{n_ϕ} be positive.[14] Hence to determine the yawing moment about the CPT, see figure 1-4.The side force coefficient and yawing moment coefficient are measured about the reference point to be respectively, C_y and C_n. The side force coefficient acts perpendicular to the longitudinal plane which gives rise

to the yawing moment coefficient which acts in the lateral plane. Therefore, summing moments (coefficient form) about the CPT yields:

$$C_{n_{CPT}} = C_{n_{ref}} - \frac{x'}{b} C_y \quad (15)$$

where the geometry gives

$$x' = r \sin (\alpha + \epsilon) \quad (16)$$

$$r = \sqrt{\bar{x}^2 + \bar{z}^2} \quad (17)$$

$$\epsilon = \arctan (\bar{x}/\bar{z}) \quad (18)$$

Lateral Stability

When rolling oscillations occur the problem is one involving the lateral stability of the Para-Foil. If the rolling moment coefficient is as shown in figure I-2 the requirement for lateral stability is that the slope (C_{l_β}) be negative.[14] To determine the rolling moment about the CPT reference Figure I-4 The rolling moment coefficient is measured about the CPT to be $C_{\ell_{ref}}$ and acts in the vertical plane. Hence, summing moments (coefficient form) about the CPT results in:

$$C_{\ell_{CPT}} = C_{\ell_{ref}} + \frac{z'}{b} C_y \quad (19)$$

$$z' = r \cos (\alpha + \epsilon) \quad (20)$$

For a vehicle as the Para-Foil, the stability derivatives involving rolling moment and yawing moment will reflect the influence of the wing side force and sideslip characteristics to a considerable extent, whereas the pitching stability derivative depends upon the lift and drag forces. In transferring this moment information about the confluence point, the effect of the suspension lines is included. Whether or not the additional drag due to the lines produce a stabilizing or destabilizing response is still open to analysis and testing.

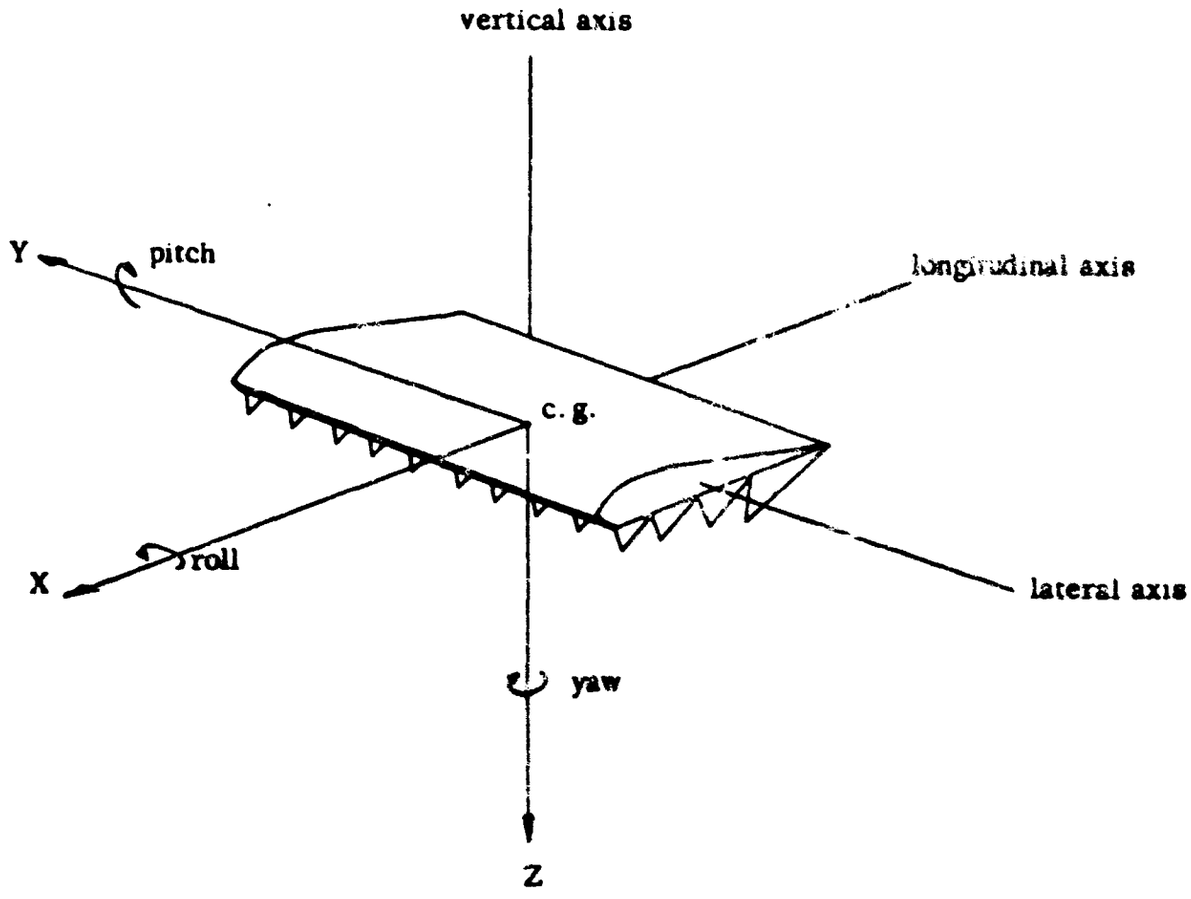

Figure I-1 Para-Foil Axis System (Body Axes)

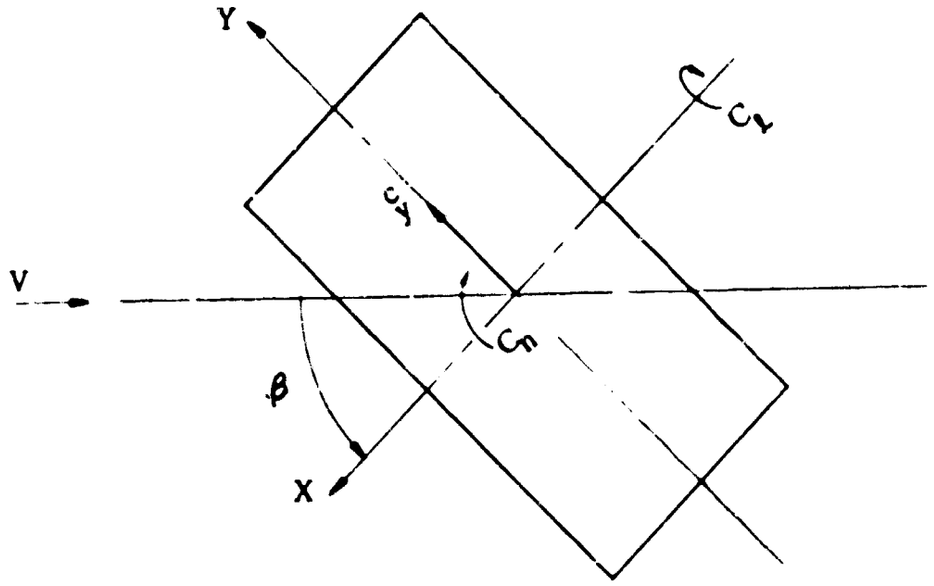

a) Directional and Lateral Forces and Moments (Pure Yaw)

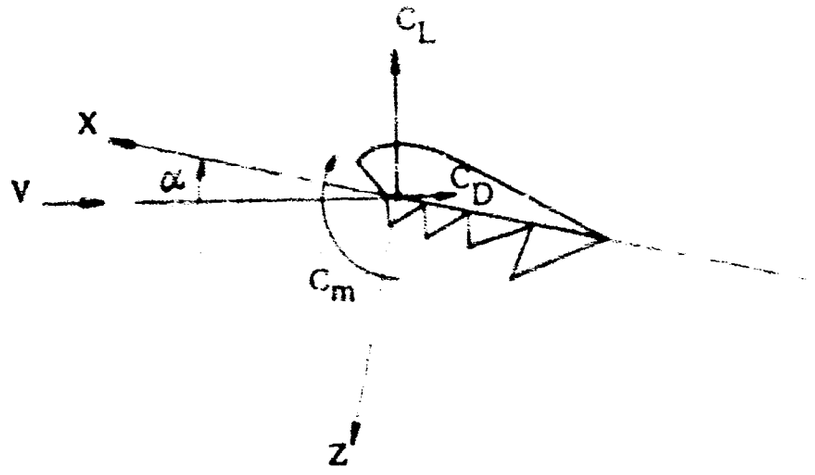

b) Longitudinal forces and moments (Pure Pitch)

Figure I-2. Axes Systems and Convention used to define positive sense of forces, moments, and angles. Longitudinal data are referred to wind axes and lateral data are referred to body axes.

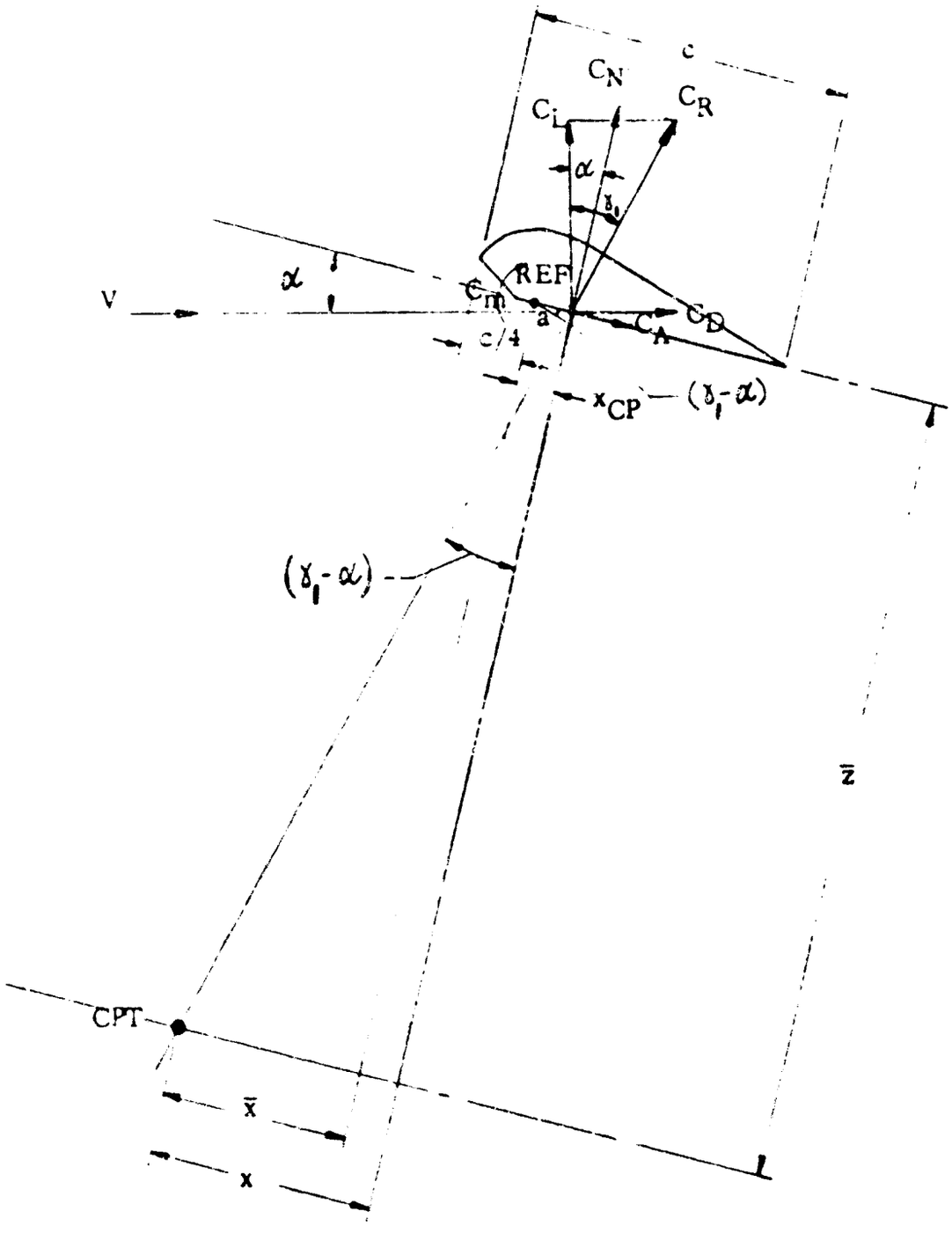

Figure 1. Longitudinal stability analysis geometry.

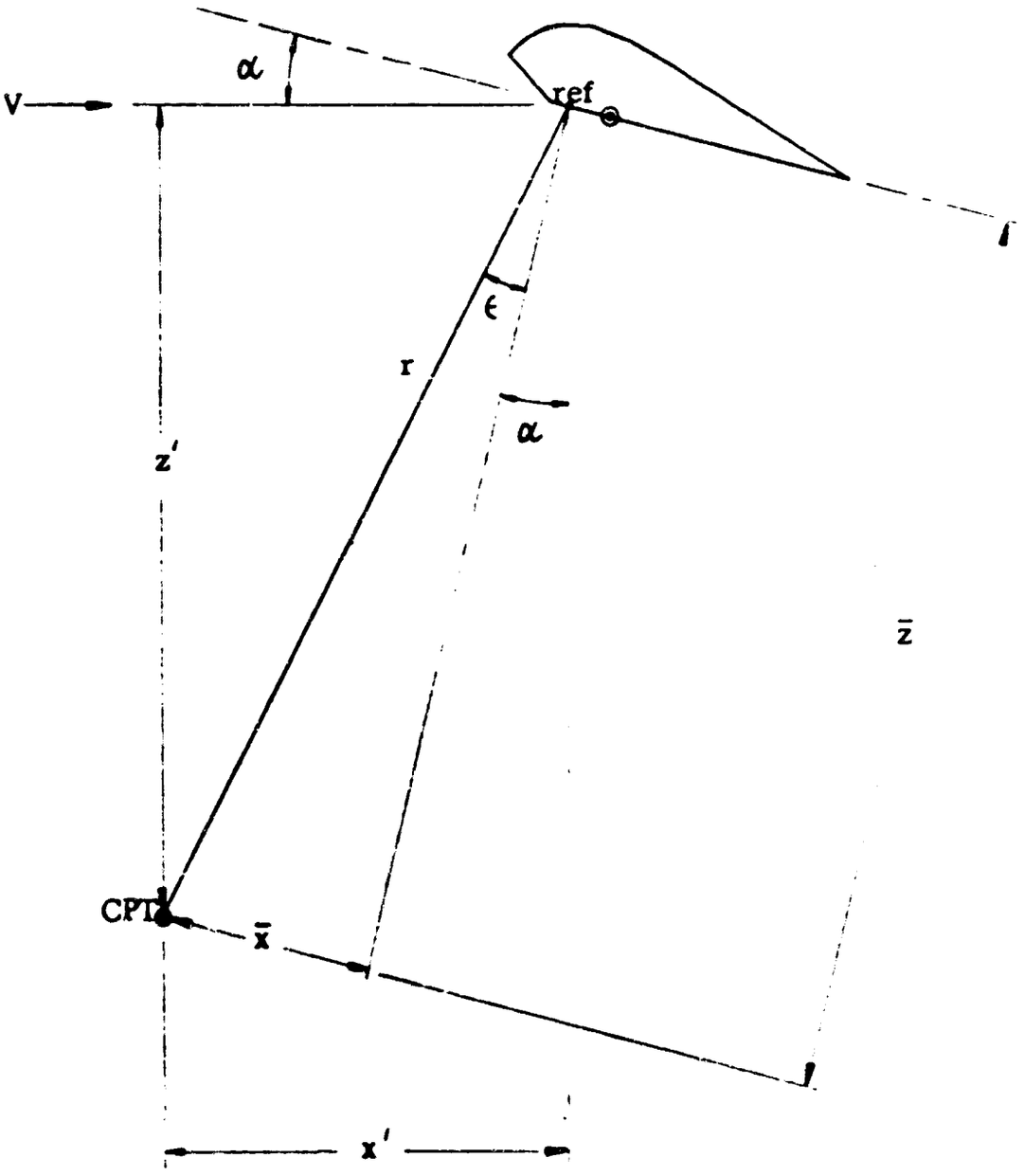

Figure I-4 Directional and Lateral Stability Analyses Geometry. Side force Acting downward at the reference.

APPENDIX II

LINE DRAG ANALYSIS - REMOVAL

NASA-Langley (Series Two): Tether Phase

The length of line exposed to the airflow was determined in the following manner. Reference Figure II-1 and Table II-1. Given the geometry in Figure II-1, h is determined accordingly:

$$h = \underline{L} \cos (\alpha + \theta_R) - (21.3 - \mathcal{f}) \tag{1}$$

Knowing h, ℓ can be determined, as follows:

$$\ell = \frac{\underline{L}\, h}{h + (21.3 - \mathcal{f})} \tag{2}$$

Assuming the air flow turns an angle of 10° and also that the incremental length, $\Delta \ell$, is perpendicular to the j-streamline,

$$\Delta \ell = x \sin 10^{\circ} \tag{3}$$

where $$x = (21.3 - \mathcal{f}) \tan (\alpha + \theta_R) \tag{4}$$

Then $(\ell + \Delta \ell)$ is the length of one of the A-suspension lines exposed to the airstream. Consulting the rigging schematic (Figures 17-21, main report) the total frontal area of all the suspension lines exposed to the airstream is:

$$S_{sus} = (n\ 375)(\ell + \Delta \ell)(dia_{375}) + (n_{550})(\ell + \Delta \ell)(dia_{550}) \tag{5}$$

Note that all the suspension line lengths exposed are assumed to be of equal length and all are assumed to be fully exposed to the airstream. All lines were also assumed not to stretch.

The control lines of each unit are joined together at a wing on each side of the Parafoil a distance ξ below the trailing edge. From these rings two primary control lines run down to the controller. Hence the frontal area of exposed control line lengths is

$$S_{cont} = (n_{cont})(\xi)(dia_{375}) + 2(2\Delta\ell)(dia_{375}) \quad (6)$$

where the distance from the ring to the j-streamline is assumed to be $(2\Delta\ell)$.

For the two guide lines a length of 300 feet per guide line was assumed exposed to the airstream. Hence the frontal area is:

$$S_{guide} = 2(30)(dia_{375}) \quad (7)$$

The total frontal area of all lines exposed to the airflow is then:

$$S_{line} = S_{sus} + S_{cont} + S_{guide} \quad (8)$$

Assuming a drag coefficient of 1.0 (from Hoerner) for the line based on the line frontal area, the drag coefficient of the line drag based on wing planform area can be computed, as follows:

$$D = q\, S_{line}\, C_{D_w} \quad (9a)$$

$$D = q\, S_{wing}\, C_{D_s} \quad (9b)$$

$$S_{line}\, C_{D_w} = S_{wing}\, C_{D_s}$$

$$C_{D_s} = \frac{S_{line}}{S_{wing}}\, C_{D_w} \quad (10)$$

The component of this drag coefficient that contributes to the drag of the system is $(C_{D_s} \cos \alpha)$ and hence this drag component was subtracted from the given data drag coefficient to yield the drag coefficient of the Parafoil

alone.

Some tests of the variable aspect ratio unit were conducted with 100 pound test line. When these situations occurred the same procedure was followed in removing the line drag, noting the diameter of 100-line to be 0.040 inches.

All computations were programmed and run on the University of Notre Dame's Univac 1107 computer.

NASA Langley (Series Two): Strut Phase

The length of line exposed to the airflow is

$$\ell = 0.339L \tag{11}$$

where L is the length given in Table II-1 and mentioned in the Tether Testing Phase. (Figure II-2)

The resulting frontal area is determined as in the preceeding tether analysis, and hence the line drag coefficients based on wing planform area are found. All computations were performed on the Univac 1107 computer.

NASA-Langley (Series One)

The length of lines exposed to the airstream was determined from the geometry of the various test configurations.[3] All lines were assumed to be fully exposed to the airstream and not to stretch. Knowing the lengths and line diameters the total frontal area of the lines was determined. In a manner similar to that of the previous section the drag coefficient of the suspension lines based on wing planform area was computed and then subtracted from the total drag yielding the drag of the Para-Foil wing only.

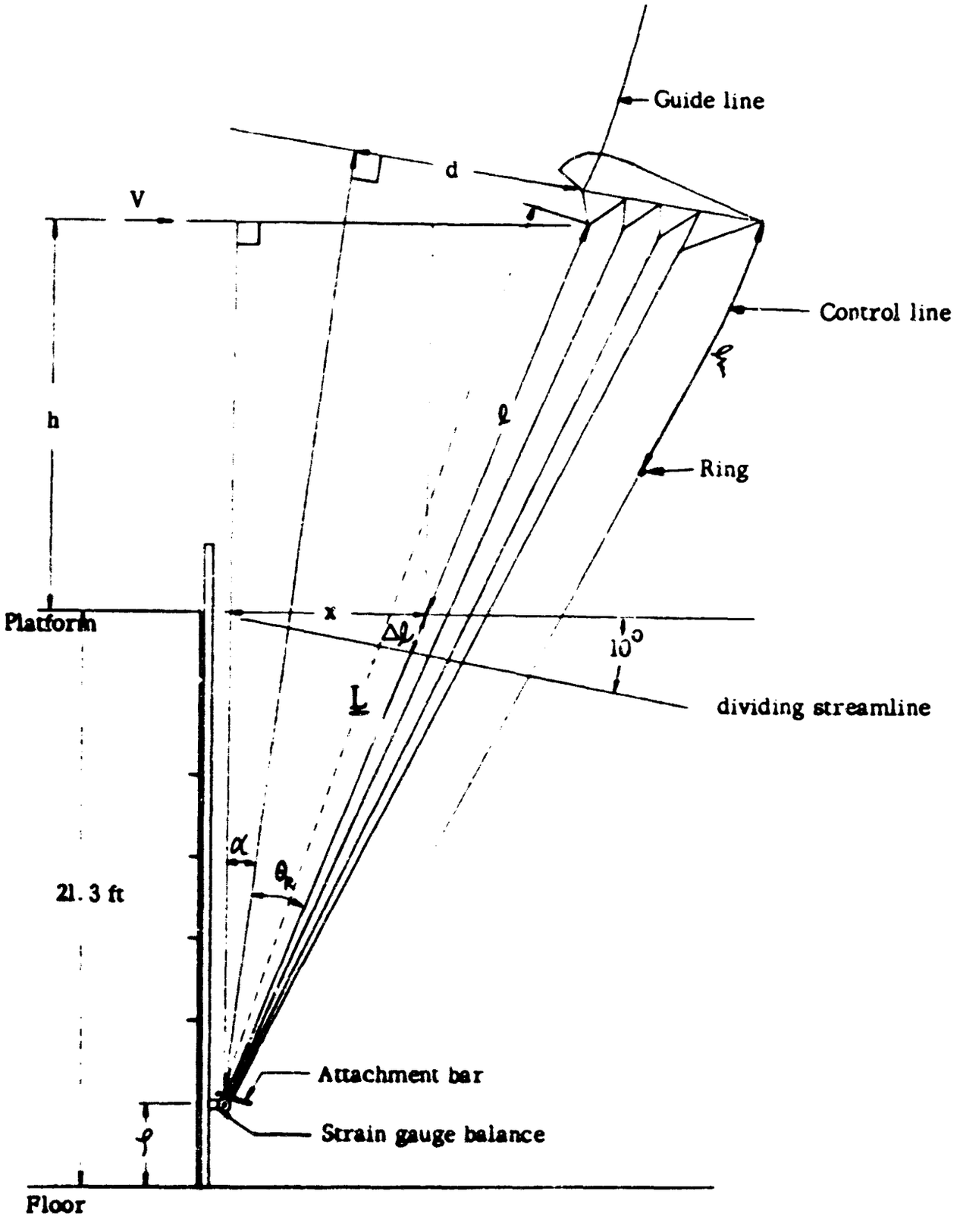

Figure II-1. Tether Testing Line Drag Determination.

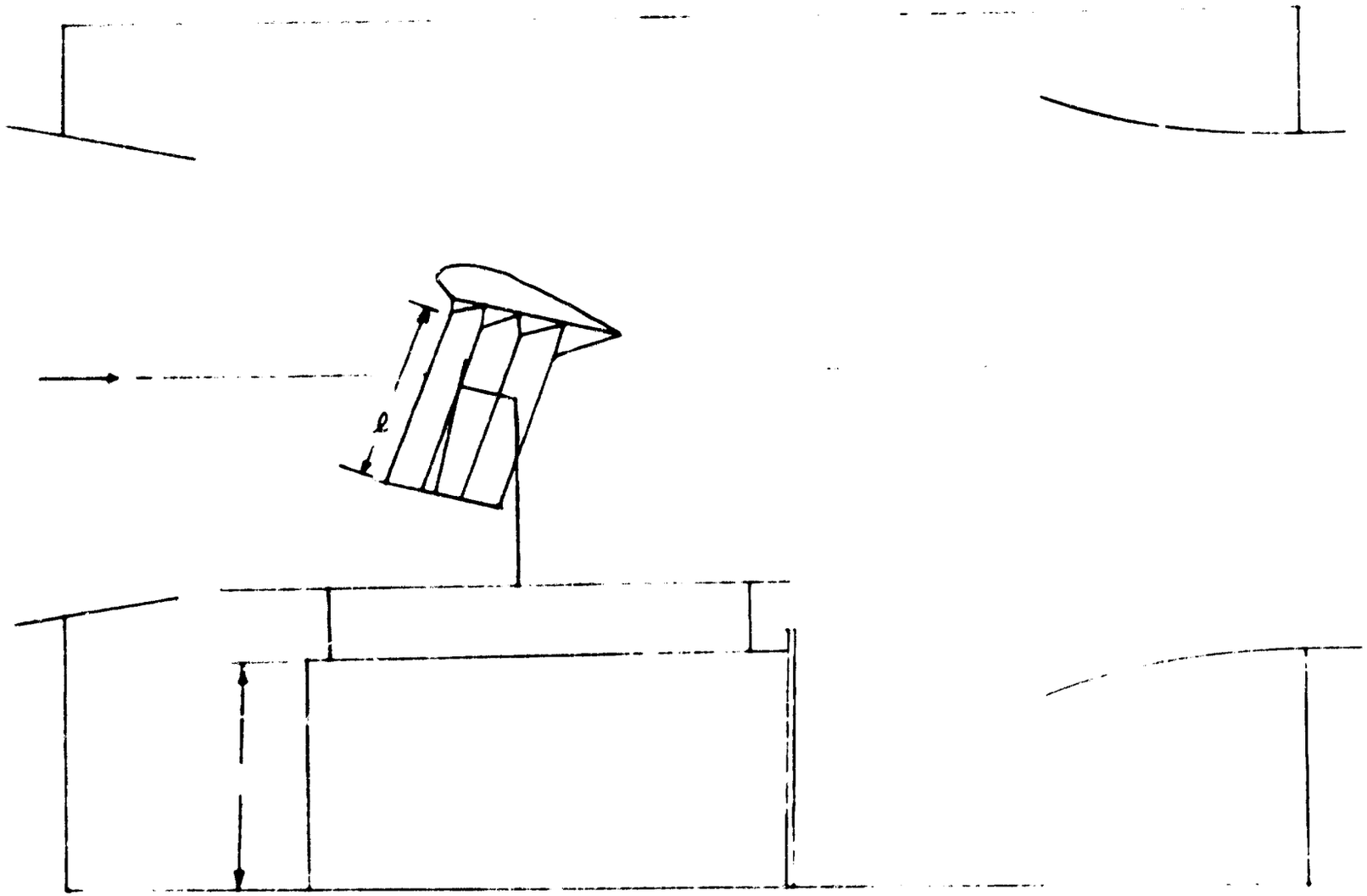

Figure II-2. Sketch of Strut Test Configuration in Langley Full Scale Tunnel

TABLE II-1

Model Description and Information

MODEL	f (in feet)	r_f (in feet)	θ_R (in degrees)	L (in feet)	DESCRIPTION
Basic AR 1.0	15	8	31	20.13	Orange w/green flares
Basic AR 1.5	12	9	26.6	23.95	White w/orange flares
Basic AR 2.0	9	10	21.8	26.84	Orange w/green flares
Basic AR 2.5	6	11	16.7	29.28	White w/orange flares
Basic AR 3.0	3	12	11.3	31.42	White w/center panel orange, alternating orange & white flares
Variable AR 3.0	3	12	11.3	31.42	green

VARIABLE	S (in feet)	# Flares	#550 lines	#375 lines	#100 lines
AR 3.0	147	13	9	4	39
AR 2.5	123	11	9	2	33
AR 2.0	87	9	9	0	27
AR 1.5	74	7	7	0	21
AR 1.0	49	5	5	0	15

APPENDIX III

LINE DRAG ANALYSIS - ADDITION

NASA - Langley (Series Two): Tether Phase

The length of line not exposed to the airstream was determined in the following manner. Reference Figure II-1 and Table II-1. Knowing the total length of the A-suspension lines ($\underline{L}$) and the length of line exposed to the airstream ($\ell + \Delta\ell$: from Appendix II), the difference yields the line not exposed to the airflow:

$$s = \underline{L} - (\ell + \Delta\ell)$$

where the same assumptions employed in Appendix II are incorporated. Hence, following the approach in Appendix II, the total frontal area of all suspension lines not exposed to the airflow is:

$$S_{\substack{\text{line} \\ \text{not} \\ \text{exposed}}} = S_{sus} + S_{cont} + S_{guide}$$

where

$$S_{sus} = S_{375} + S_{550}$$

$$= (n_{375})\,(s)\,(dia_{375}) + (n_{550})\,(s)\,(dia_{550})$$

$$S_{cont} = (2)\,(18)\,(dia_{375})$$

$$S_{guide} = 0$$

The remainder of the method is exactly similar to Appendix II but for the fact that the drag coefficient due to the unexposed lines is added to the given drag of the system.

NASA - Langley (Series Two): Strut Phase

The same procedure as Appendix II was followed except for:

$$\underline{L} - \ell = 0.661\ \underline{L}\ .$$

APPENDIX IV

NOTRE DAME MODEL

DRAG DATA CORRECTION

Upon completion of the analysis conducted in preparation for this report it was discovered that Parafoil models used in the tests conducted at Notre Dame included drag producing proturbences which were not taken into consideration in developing the drag or the lift-to-drag data. The purpose of this appendix is to present the effects of correcting the data to reflect removal of this additional drag.

Inspection of models 3 and 4 employed in the Notre Dame tests (see Table II and Figure 8) reveals that four nuts, two bolts, and aluminum flares of 24 ga. thickness were employed, the drag contributions of which were not previously taken into account. Accordingly, the incremental reduction in drag coefficient due to these proturbences is given in Figure IV-1. A new summary of the drag data for Parafoils of aspect ratios 1.0 - 3.0 is given in Figure IV-2 and a new summary for the lift to drag ratio is given in Figure IV-3.

AR	$\Sigma\Delta C_D$	ΔC_D Nuts (4)	ΔC_D Bolts (2)	ΔC_D Flares
1	.04036	.0266	.00834	.00542
1.5	.02806	.01773	.00557	.00476
2.0	.02253	.0133	.0042	.00503
2.5	.01856	.01053	.00340	.00463
3.0	.01639	.00887	.00278	.00474

NUT: C_D = .80* A = 0.283 in.^{2} (2 of this area)
A = 0.132 in.^{2} (2 of this area)

BOLT C_D = 0.80** A = .1303 in.^{2} (2 of this area)

FLARE. C_D = 0.48*** ΔA = .5250 in.^{2} (AR = 2.0)

*Fluid Dynamic Drag, Hoerner, p.5-8, Fig. 14a
**Ibid, p.5-8, Fig. 13e
***Ibid, p.5-8, Fig. 13c

Figure 7.-1. Protuberance Drag.

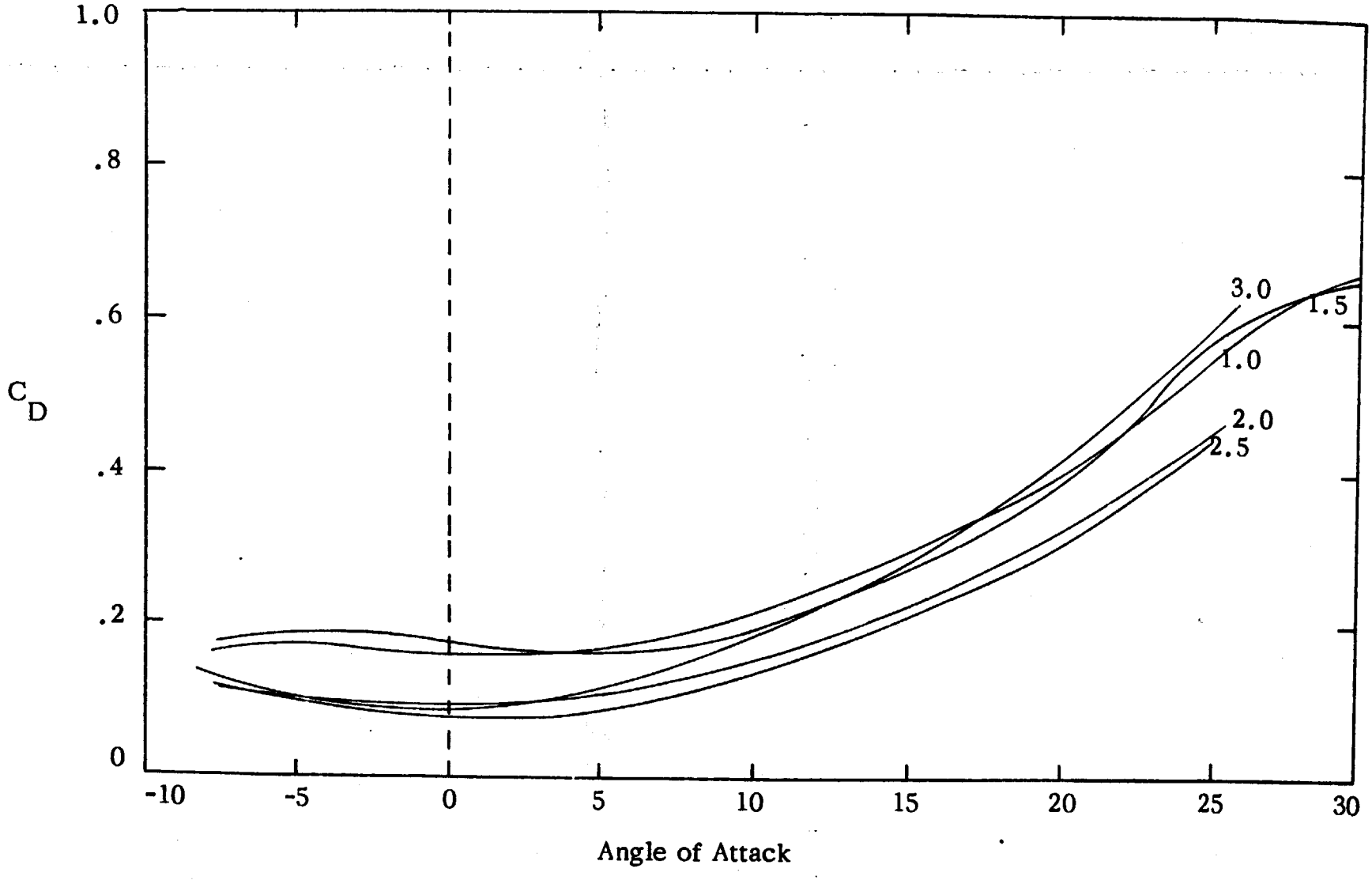

Figure IV-2. Summary of Coefficient of Drag (No Lines).

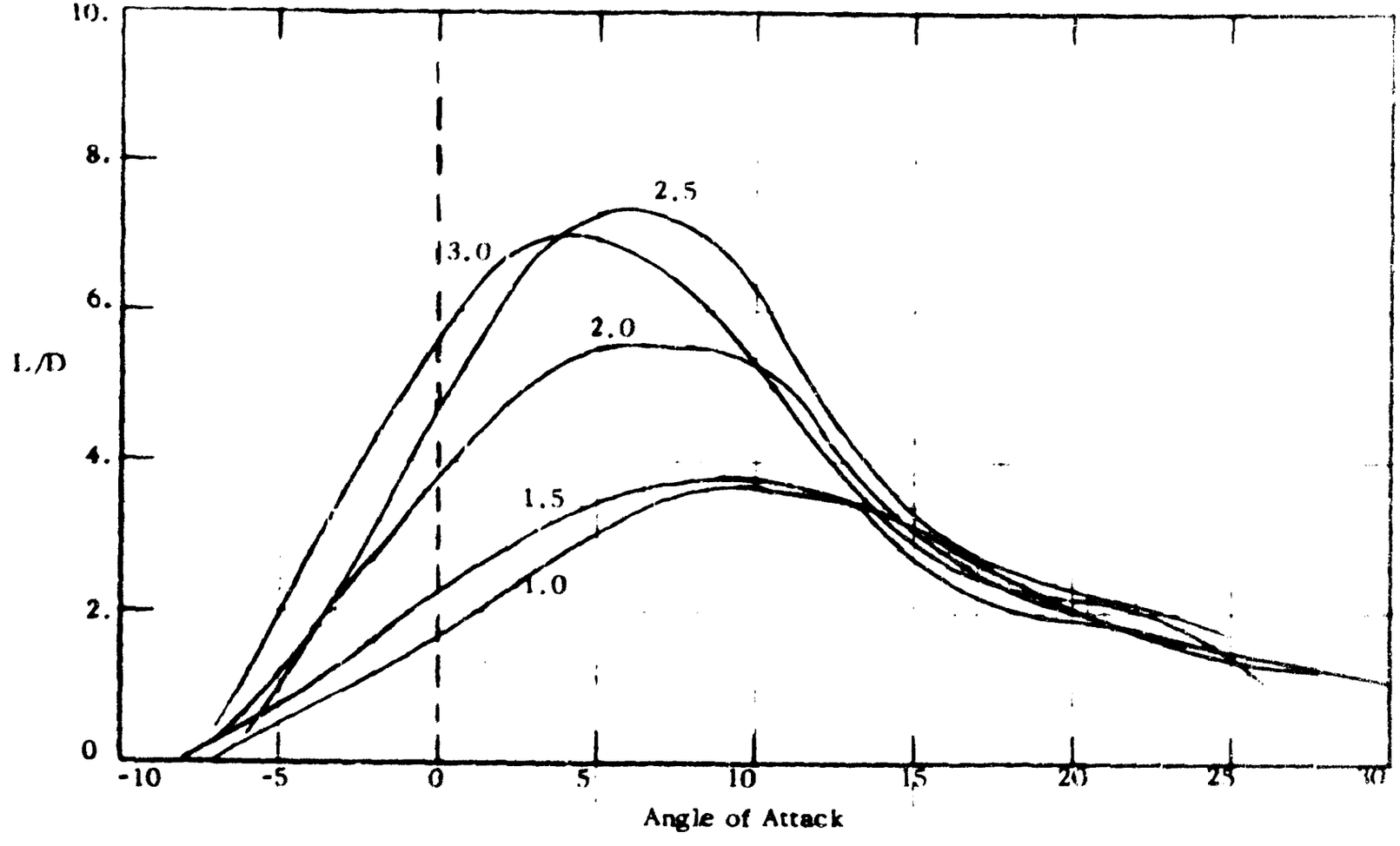

Figure IV-3. L/D Summary No Flaps.

APPENDIX V

PARAFOIL FLIGHT PERFORMANCE

The aerodynamic data for the various Parafoil designs without line drag was given in the summary Figures 69, 70, 82 and 94. Correction of these figures to reflect removal of drag due to model protuberances was presented in Appendix IV. In actual flight systems it is necessary to include drag created by lines and payload in predicting the overall system performance. The purpose of this appendix is to illustrate incorporation of line drag for a personnel size Parafoil.

In considering the additional drag due to lines, a drag coefficient of one is used as was used in Appendices II and III. Although in actual practice, the drag coefficient is less than one due to the angle of the line to the flow field, line to line interference and improved separation points a drag coefficient of one was also used in these line drag calculations for consistency.

Figure V-1 illustrates the flight configuration of lines for the standard 200 sq.ft. jump Parafoil, ND 2.0 (200). It is noted that the line diameters are all .0125 ft., and that the total length of lines are reduced by cascading the rigging. The incremental drag coefficient due to incorporation of lines is .033. Based on the figures in Appendix IV and this line drag contribution, Figure V-2 illustrates the drag coefficient for the flight configuration together with the lift coefficient and the lift to drag ratio. Figures V-3 and V-4 provide similar aerodynamic data for the AR = 2.5 and AR = 3.0 Parafoils. A summary is provided in Figure V-5.

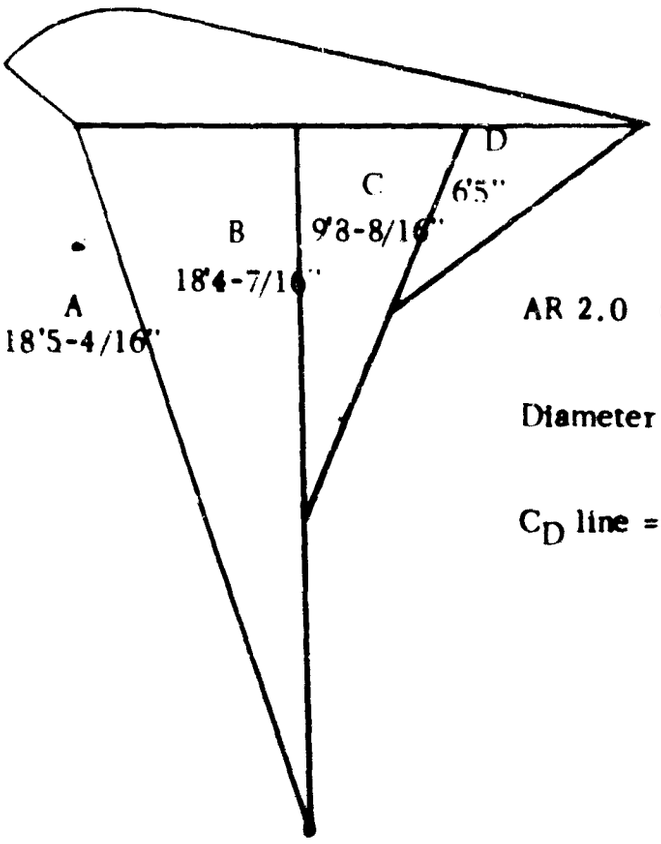

AR 2.0 (200 ft.^{2})

Diameter of line = .0125 ft.

C_D line = 1.0

Figure V-1. Line Drag Calculation AR 2.0.

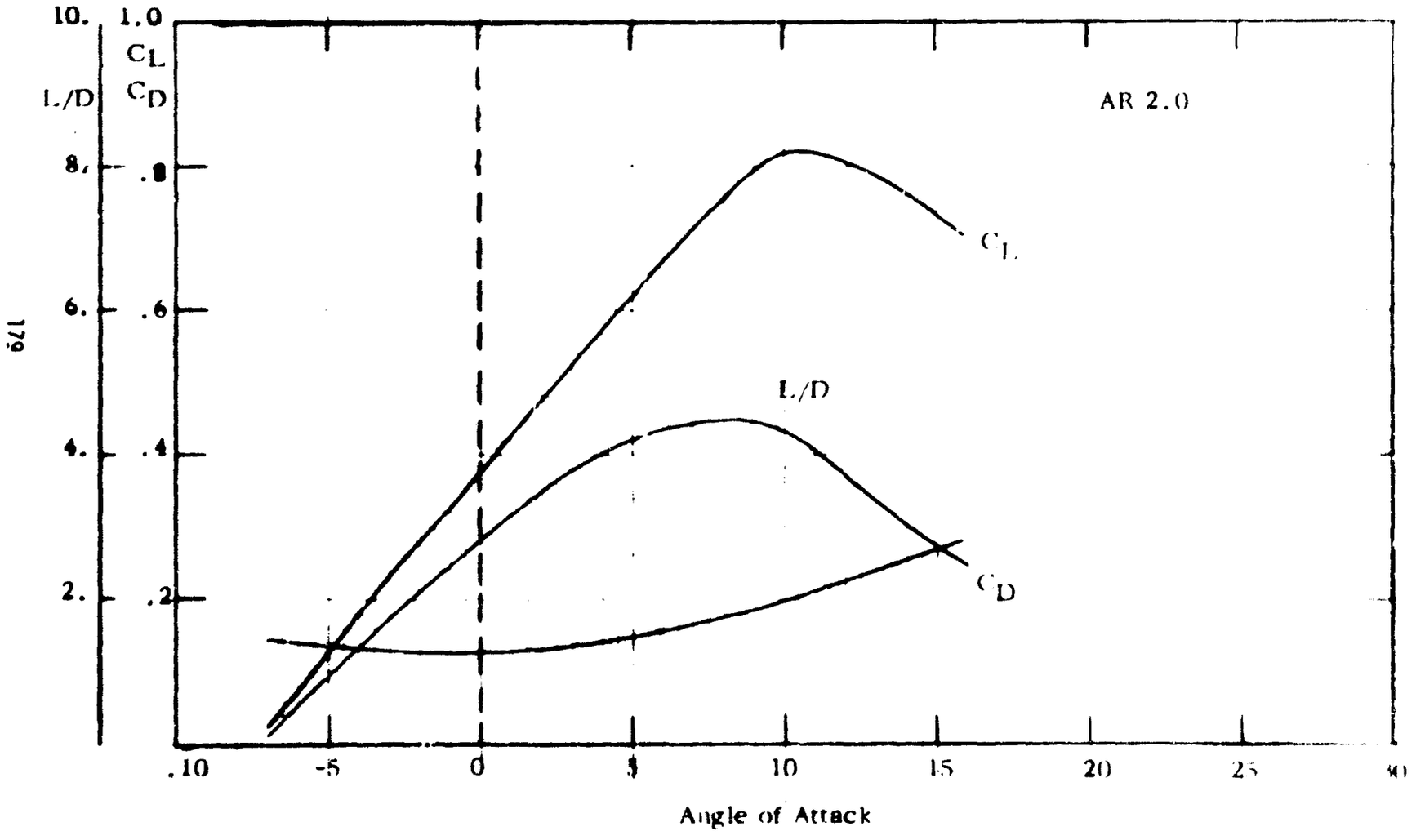

Figure 4-2. C_L, C_D and L/D for AR 2.0 With Lines.

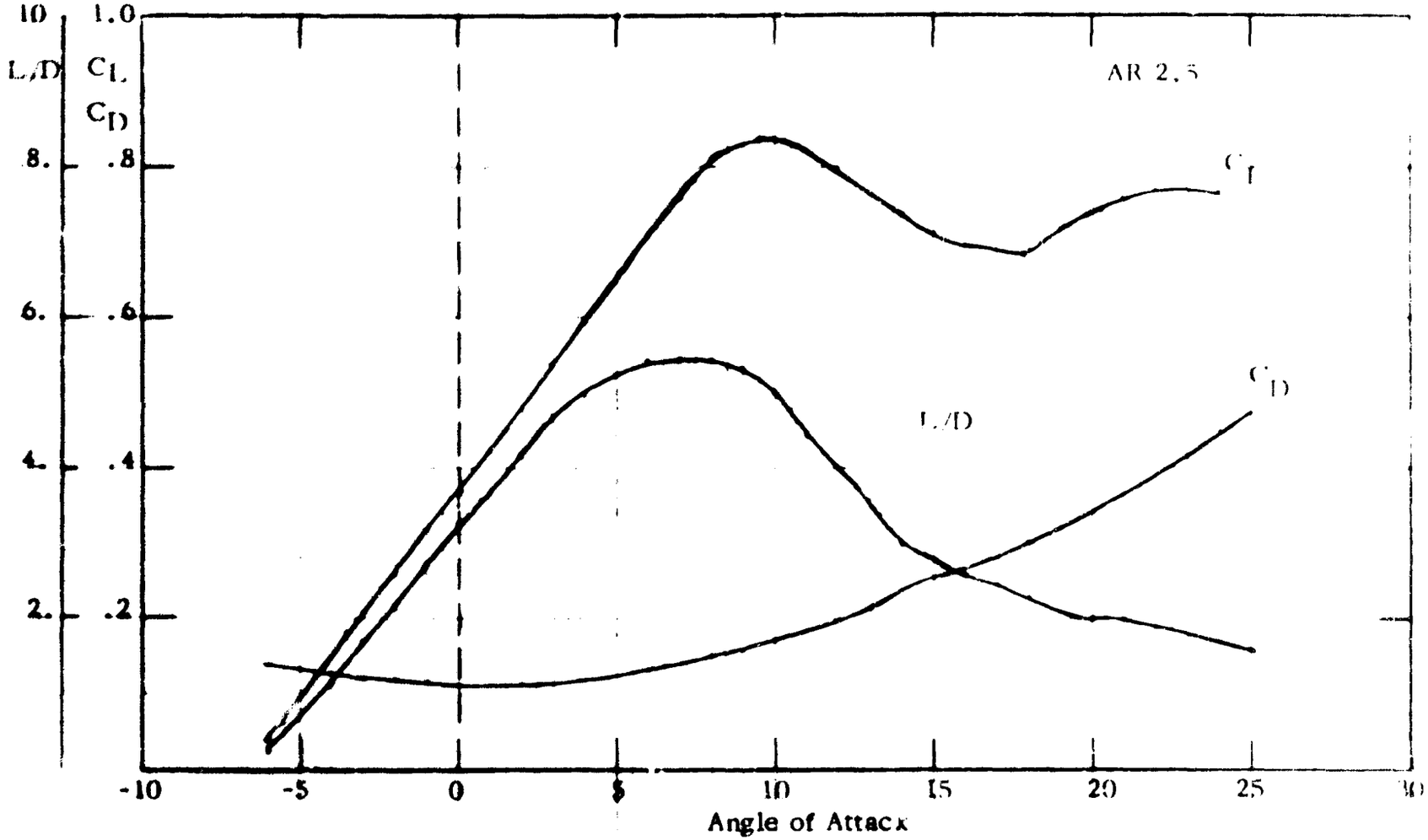

Figure V-3 C_L, C_D and L/D for AR 2.5 With Lines.

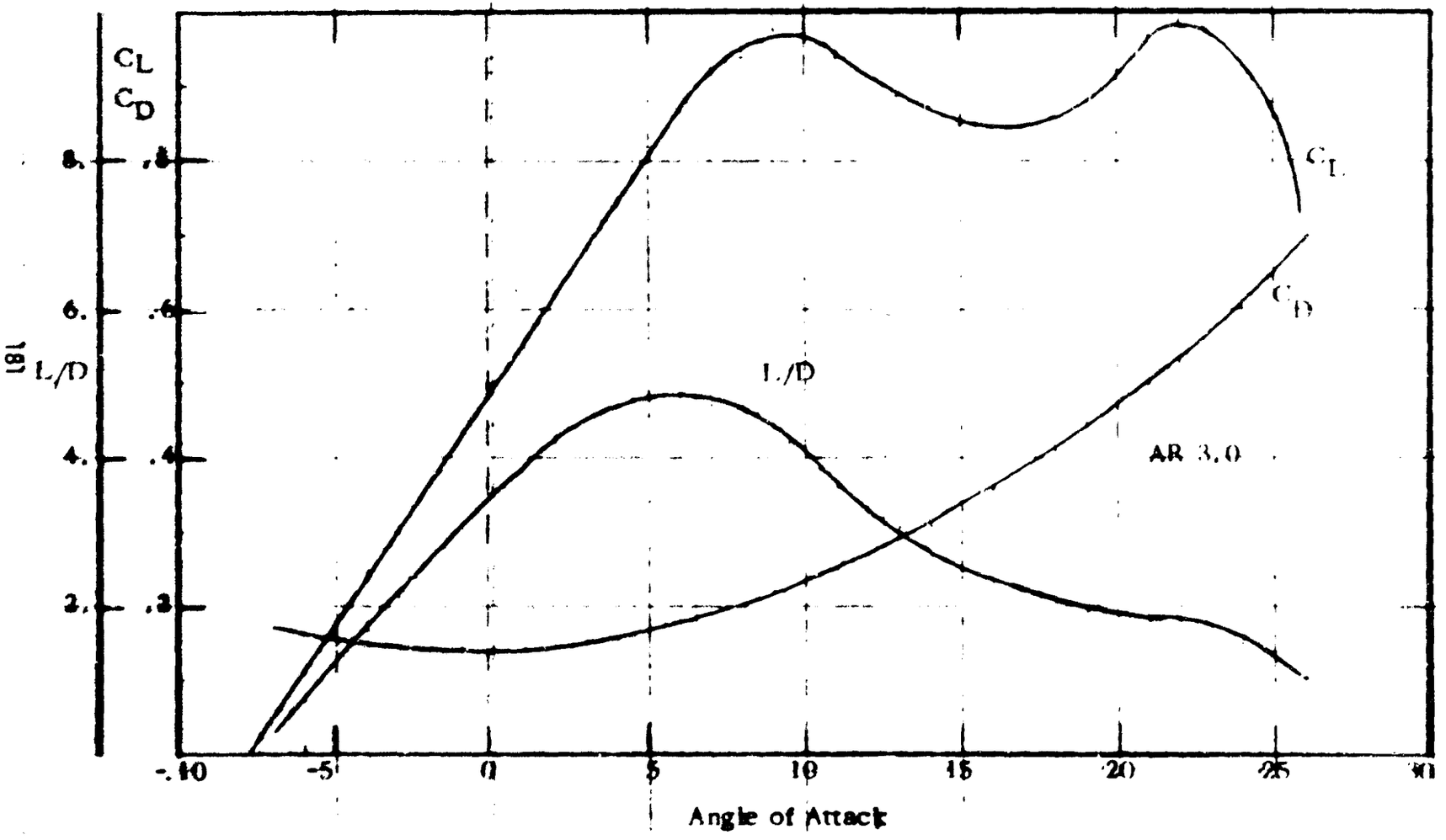

Figure V-4 . C_L , C_D and L/D for AR 3.0 With Lines.

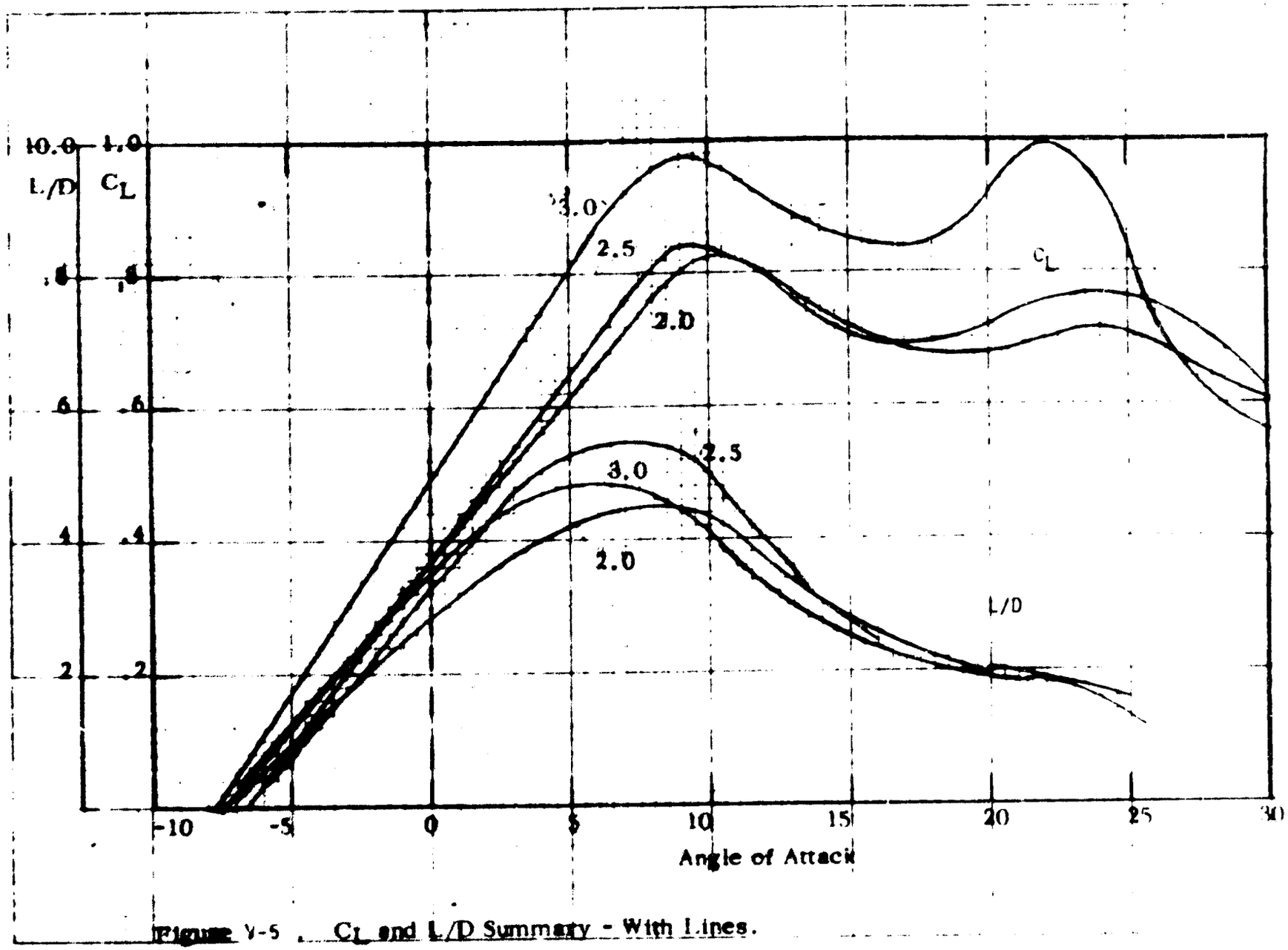

Figure V-5 . C_L and L/D Summary - With Lines.

REFERENCES

1. Nicolaides, John D., and Knapp, Charles F., A Preliminary Study of the Aerodynamic and Flight Performance of the Para-Foil, Conference on Aerodynamic Deceleration, University of Minnesota, July 8, 1965.

2. Nicolaides, John D., On the Discovery and Research of the Para-Foil, International Congress on Air Technology, Little Rock, Arkansas, November, 1965.

3. Burke, Sanger M., and Ware, George M., Static Aerodynamic Characteristics of Three Ram-Air Inflated Low Aspect Ratio Fabric Wings, Langley Research Center, Hampton, Virginia, NASA WP 264, July, 1966.

4. Pope, A., Wind Tunnel Testing, John Wiley and Sons, Inc., New York, April, 1964.

5. De France, Smith J., The NACA Full Scale Wind Tunnel, NACA Report 459, 1933.

6. Nathe, Gerald A., Knapp, Charles F., and Hall, Charles R., Wind Tunnel and Free Flight Testing of Para-Foil Model Number 125, Aero-Space Engineering Departmental Report, Notre Dame University, June, 1966.

7. Kang, W.H., On the Static Wind Tunnel Investigation of Small Para-Foil Models to Predict Flight Characteristics, Master's Thesis, Aero-Space Engineering Department, University of Notre Dame, Notre Dame, Indiana, May, 1968.

8. Walker, R.H., Static and Dynamic Characteristics of the Para-Foil as Determined from Pure Pitching Motion, Master's Thesis, Aero-Space Engineering Department, University of Notre Dame, Notre Dame, Indiana, July 1968.

9. Eikenberry, R.S., Analysis of Missile Dynamics Data, Part 1: Angular Motions, Sandia Laboratory Contractor Report, June, 1969.

10. Hoerner, S.F., Fluid Dynamic Drag, Published by author, 1965.

11. Sabersky, R.H. and Acosta, A.J., Fluid Flow, The Macmillan Co., New York, 1964, p.167.

12. Abbott, I.H., von Doenhoff, A.E., Theory of Wing Sections, Dover Publications, Inc., New York, 1959.

13. Van Deventer, C.N., An Introduction to General Aeronautics, American Technical Society, Great Britain, 1965.

14. Etkin, B., Dynamics of Flight, Stability and Control, John Wiley and Sons, Inc., New York, 1959.

15. Perkins, C.D., Hage, R.E., Airplane Performance, Stability, and Control, John Wiley and Sons, Inc., 1965.

16. By special briefings prepared for the U.S. Army, the Congress (twice), the White House, the DOD, and NASA.

17. Knapp, C.F., and Barton, W.R., Controlled Recovery of Payloads at Large Glide Distances, Using the Para-Foil. Journal of Aircraft, Vol. 5, No. 2, pp. 112-118, 1968.

18. Nicolaides, J.D., Speelman, Ralph and Menard, George, A Review of Para-Foil Programs. AIAA 2nd Aerodynamic Deceleration Systems Conference, El Centro, Calif., 23-25 Sept. 1969.